Exploring chromatin states in the Drosophila intestinal lineage

Manon Josserand

PSL UNIVERSITÉ PARIS

THÈSE DE DOCTORAT
DE L'UNIVERSITÉ PSL

Préparée à l'Institut Curie.
Ecole Doctorale ED515 Complexité du Vivant, Sorbonne Université

Exploration des états de chromatine dans le lignage intestinal chez la Drosophile

Exploring chromatin states in the *Drosophila* intestinal lineage

Supervised by Allison Bardin & Louis Gervais
Laboratoire "Cellules souches et homéostasie tissulaire"

Soutenue par
Manon JOSSERAND
Le 23 septembre 2022

Ecole doctorale n° 515
Complexité du vivant

Spécialité
Génomique, Biologie cellulaire et du développement

Composition du jury :

Charles, DURAND Professeur, IBPS Sorbonne Université	*Président*
Yad, GHAVI-HELM Chargée de recherche, IGFL	*Rapportrice*
Tony, SOUTHALL Senior Lecturer, Imperial College London	*Rapporteur*
Mounia, LAGHA Directrice de recherche, IGMM	*Examinatrice*
Céline, VALLOT Directrice de recherche, Institut Curie/PSL	*Examinatrice*
Antoine, ZALC Chargé de recherche, Institut Cochin	*Examinateur*
Allison, BARDIN Directrice de recherche, Institut Curie/PSL	*Directrice de thèse*

institutCurie | PSL

Remerciements

I would like to thank a lot of people who took part in this work in various ways. My PhD has been an incredible scientific and personal journey and the output of it went far above my expectations thanks to the support and guidance of many people along the way.

I am infinitely grateful to Allison, for her exceptional mentoring at every step of my PhD. I feel incredibly lucky to have been your student, Allison, because I learnt so much from you and you've been extremely attentive to everything I expressed. I admire your unwavering passion and enthusiasm for science as much as they have been able to boost me when I needed it. Thanks also for creating and perpetuating such a nice atmosphere in the lab and making us work together so well. Thank you for all the advice, for teaching me the secrets of good talks (the questions!), for carefully proofreading my written works and for putting me back on track when I was a bit lost.

My equal thanks go to Louis, who has been my PhD co-supervisor but more than that, my co-worker on this project. Working together as a team was great and it made me realize how much I enjoyed it. Thanks for teaching me the fly work, the DamID, and so much more. Thanks for being always available to answer my questions and to give me advice when I needed it. Also, it was always reassuring to share our doubts about the black box of bioinformatics and finally getting there together by helping each other. I hope I brought you something and that you liked our chromatin team as much as I did. Thank you so much for all your support, your kindness and for everything you bring to the lab. Thank you also, for the experiments done in the last months which were crucial to improve the story.

Although I had ups and downs, as every PhD student, I am now aware of the progress I have made as a scientist and I truly believe that it is thanks to both of you, Allison and Louis.

Then I would like to thank all the other members of the team, for scientific contributions and above all for making the lab a very supportive and great work environment. That's why I considered it as my second home and enjoyed so much my time there.

Thank you Natalia, for your precious work that has been essential for my PhD project. Thanks for all these months spent on this complicated modeling and for your determination until we got to the best model.
Thank you Marius as well, for teaching me so well the basics of bio-informatics and make me like it (I was the first surprised!). You have been an essential help and contribution to the beginning of my thesis. Louis and I are still very grateful for everything we learnt from you, which helped us to navigate through the sometimes scary world of bio-informatics. Also I will never forget your enthusiasm for science and your loud laugh (we missed it!).
Merci Marine, d'être cette personne exceptionnelle que je compte parmi mes meilleur-e-s ami-e-s. Merci de tout ce que tu apportes au labo, tes compétences, ton organisation, ton enthousiasme, ton humour, tes cadeaux, tes gâteaux, et ton aide précieuse pour les manips (les dissections… mais aussi tous les conseils techniques sur mille et une expériences !). Merci pour tout le soutien, pour les messages d'amour, pour cette amitié à laquelle je tiens tant. Je t'admire pour tout ce que tu fais et j'espère partager tout cela avec toi le plus longtemps possible.

Thank you Lara, for having been my other best friend in the lab. You are inspiring in so many ways, I admire your talent for committing yourself to many important causes and to your dreams! Thank you for all the good advice during my PhD, for your kindness and for all the wonderful moments we spent together in and out of the lab.
Kasia, thank you so much for all the constructive feedbacks you gave about my work and for the highly valuable inputs to the lab. To me you are some kind of "voice of wisdom"!
Annabelle, merci pour ta gentillesse, tes conseils, ta pédagogie quand j'étais un peu perdue sur la génétique, ta bonne humeur quotidienne et pour tout ce que tu apportes au labo. Un modèle d'organisation et de rigueur scientifique !
Thank you Hojun, for being a model of scientific rigor and commitment, and for your precious comments and questions about my work.
Merci Gwenn, pour avoir apporté une touche de folie au labo, pour tous tes rires, ton acharnement lors de nos manips de RNA FISH (l'excitation du vendredi soir au microscope !) et pour être devenue une amie géniale au quotidien. Merci de me faire tant rire, d'être la « party girl » toujours motivée pour danser n'importe où avec moi.
Merci Bénédicte d'inspirer l'équipe avec ta créativité incroyable. Merci de m'avoir aidée sur R, merci pour tes conseils relatifs aux doutes de fin de thèse, pour tous tes encouragements cette dernière année et pour nos discussions. Je suis heureuse de t'avoir eue à mes côtés ces derniers mois et je suis persuadée que tu vas beaucoup apporter au labo !
Merci Benjamin, pour avoir été un ami et un modèle de réussite au cours de cette thèse. Merci pour toutes tes contributions scientifiques, mais surtout merci d'avoir été le meilleur DJ du labo :)
Thank you Nick too, for your kindness, your bio-info tutorials, your subtle British humor and all the laughs we had with you being part of the team.
Thanks to the younger students, who brought fresh motivation to the lab and contributed to so many joyful moments. In particular, Léa, Marwa, Tania and Spyros. Spyros, don't try to copy me so much with your doubts and lack of self-confidence, you will do great ;-)

Thanks to the members of the Bellaïche and Leopold teams for the great science and all the good vibes on our "fly floor". In particular, thank you Aude for all the advice and encouragements. Thank you Victoire, my co-PhD student of the 4th floor, for the optimism and the boosts, and for sharing great moments together as well as our administrative issues. Thanks to our "fly keepers", Bénédicte and Sebastian, for allowing us to do so many experiments. Thanks to the Imaging facility and to the NGS facility, especially for helping us getting the best sequencing data when we were in trouble. Thanks to our great secretaries Isabelle and Virginie and to the whole BDD unit, for the inspiring science, and the best parties I had in these past 4,5 years.

I would also like to thank the members of my thesis committee, Bassem, Frédérique and Raphaël, for constructive feedbacks and advice during committee meetings.

Thanks to Owen Marshall for the scientific collaboration and for the very useful discussions about the chromatin state modeling.

I am also grateful to the people of the Training Unit and the LabEX for giving PhD students so many opportunities of training and preparing for the next steps of our careers. This helped me a lot to think about my future plans. Thanks to all the former and current members of ADIC, I

loved being part of it for two years and having the opportunity to contribute to young researchers' life of Institut Curie and abroad!

Merci à tous les médiateurs de la Cité des Sciences, et en particulier Benjamin, Isabelle et Lisa pour votre accueil si chaleureux dans l'équipe et pour m'avoir fait découvrir la médiation scientifique pendant 2 ans. C'était une superbe expérience et je vous remercie de tous vos efforts pour mettre en valeur et encourager les doctorants à la Cité.

Merci les Bios, pour ce lien si fort que nous avons construit pendant nos années ENS et gardé tout au long de nos chemins respectifs. Merci d'être devenus cette petite famille avec tant de souvenirs inoubliables. Partager nos galères de thèse et de perspectives de carrières est devenu notre sujet de conversation favori, et ça a toujours été rassurant de déprimer et râler ensemble, il faut bien l'avouer ! Merci Marine pour tous tes messages attentionnés et ton soutien pendant les dernières semaines d'écriture. Merci Julien et Delphine, pour tout le soutien, les conseils, pour nos racontages de vie H24 et pour m'avoir fait tant rire.

Merci à tous les amis de longue date, pour les merveilleux moments passés ensemble et indispensables à ma bonne santé mentale au milieu des moments de stress ;-) Merci de vous être toujours intéressés à mon travail (même si non, je ne fais pas vraiment une « thèse sur les mouches ») et d'avoir toujours manifesté votre soutien et votre enthousiasme pour ma thèse (meilleur public de la Cité des Sciences !). J'ai trop hâte de fêter cela avec vous.

Merci Maman, Papa, Chloé pour votre amour et votre soutien indéfectible, pour vous être toujours intéressés de près à mon travail, pour vous être adaptés à mes contraintes. Merci Maman et Chloé d'avoir été aux petits soins quand j'en avais besoin en cette fin de thèse. Et surtout, merci Papa et Maman de m'avoir donné les moyens de faire les études que je souhaitais et qui m'ont amenée jusqu'ici, et de m'avoir soutenue dans chacun de mes choix.

Enfin, merci Jason, pour tout. Merci pour ton soutien sans faille au quotidien, ta patience, pour m'avoir supportée dans les mauvais moments, pour m'avoir permis de garder un équilibre sain, pour m'avoir toujours aidée à prendre du recul, pour m'avoir tant écoutée, rassurée et surtout tant conseillée. Merci d'avoir été là à chaque fois que je t'ai demandé de l'aide, même sur des questions scientifiques ! Merci pour tout ton amour et pour la certitude que mon avenir sera à tes côtés.

TABLE OF CONTENTS

List of figures

Here are listed the figures of the Introduction. Figures of the Results are numbered separately in each Chapter of the Results section.

List of abbreviations

Appl: beta amyloid protein precursor-like
ATAC: Assay for Transposase-Accessible Chromatin
bHLH : basic-helix-loop-helix
Bib: Big brain
BlueM: Blue Mixed
BlueR: Blue Repressive
CATaDa: Chromatin Accessibility using Targeted DamID
ChIP: Chromatin Immunoprecipitation
DamID: DNA adenine methyltransferase identification
Dl: Delta
E(spl): Enhancer of split
EB: Enteroblast
EC: Enterocyte
EEP: Enteroendocrine precursor
EE: Enteroendocrine cell
EGFR: Epidermal growth factor receptor
ESC: Embryonic stem cell
Esg: Escargot
FACS: Fluorescence activated cell sorting
Fer2: 48 related 2
Fie: Fire exit
GFP: Green Fluorescent Protein
GO: Gene ontology
H1: Histone H1
Hi-C: High throughput chromosome conformation capture
HMM: Hidden Markov Model
HP1: Heterochromatin Protein 1
ISC: Intestinal stem cell
MARCM: Mosaic Analysis with a Repressible Cell Marker
NSC: Neural stem cell
Nub: Nubbin
PcG: Polycomb group
PCR: Polymerase chain reaction
Pdm2: POU domain protein 2
PH3: Phospho-Histone H3
PTM: Post-translational modification
PRC1: Polycomb Repressive Complex 1
PRC2: Polycomb Repressive Complex 2
Pros: Prospero
RNA Pol II: RNA Polymerase II
RNAi : RNA interference
Rpkm: Reads per kilobase per million mapped reads
Sens: Senseless
Sens-2: Senseless-2
Su(H): Suppressor of hairless

TAD: Topologically associated domain
TF: Transcription factor
Trr: Trithorax-related
TrxG: Trithorax group
TSS: Transcription start site
YellowW: Yellow Weak

INTRODUCTION

PREFACE

The fundamental question of how a single fertilized egg can generate a multicellular organism composed of hundreds of different cell types has been central for developmental biologists in the last century. How pluripotent stem cells differentiate and commit to distinct cell fates was first conceptualized in the "Waddington's landscape" where pluripotency is progressively lost towards the acquisition of distinct cell identities during development (Waddington, C. H., 1957). With this concept came the idea of "epigenetics" as the mechanisms underlying the interactions of the genotype with its environment to produce a phenotype during development. The concept of epigenetics was refined over the years and notably designated heritable changes in gene function not contained in the DNA sequence, such as DNA methylation. The term now commonly refers to the phenomenon causing cells with an identical genome to acquire and maintain distinct identities by expressing specific combinations of genes. While epigenetic regulation was extensively studied to better understand the basis of pluripotency and cellular identity during development, less is known about epigenetic regulation in adult tissues.

Adult stem cells are able to self-renew and to differentiate into one or several cell types, thus ensuring tissue homeostasis. Understanding the regulation of adult stem cells is crucial to have a better comprehension of uncontrolled proliferation and altered differentiation mechanisms occurring during tumorigenesis and age-dependent functional decline of tissues. In addition, adult stem cells represent a major target for therapeutic studies in the field of regenerative medicine (Ge and Fuchs, 2018). Many studies highlighted the role of epigenetic factors in stem cells and the importance of chromatin remodeling during development, which restricts the potential of cell fates (Meshorer and Misteli, 2006). Less is known about the role of chromatin organization in adult stem cell lineages, however recent findings showed that chromatin factors have key roles in the regulation of gene expression and adult stem cell proliferation, maintenance, or differentiation (Avgustinova and Benitah, 2016). Therefore, my thesis aimed to better understand what chromatin states are associated with adult stem cells and how they change during differentiation *in vivo* in an adult, homeostatic tissue. I tackled this objective by characterizing the genome-wide chromatin organization in adult stem cells and their progeny, using the *Drosophila* adult intestine as a model.

In this introduction, I will start with an overview of chromatin organization in eukaryotes and how it can regulate gene expression. In a second part, I will focus on the current

knowledge about the role of chromatin organization in stem cells and the gaps that remain to be addressed in the context of adult tissues. In the third part, I will introduce the *Drosophila* intestinal lineage as a model to address these questions.

I. An overview of chromatin organization in eukaryotes

I. A. Chromatin structure

In all eukaryotes, DNA is packed into the nucleus, a membrane-delimited organelle. Before discovering that DNA carries the genetic information and that chromosomes are the support of heritability, observations of cells and mitosis gave the first insights into the content of nuclei. The name "chromatin" was originally suggested by Walther Flemming in 1880 as he was examining cells from salamanders and noticed that substances in the nucleus could be stained with colored dyes (Flemming, 1882). In 1928, Emil Heitz distinguished two types of chromatin based on differences in staining density: the condensed "heterochromatin", and the less condensed "euchromatin" (**Fig.1**) (Heitz, 1928). Studies elucidating the underlying structure and composition of chromatin emerged later in the second half of the 20th century and opened the way to a better understanding of chromatin organization at different scales.

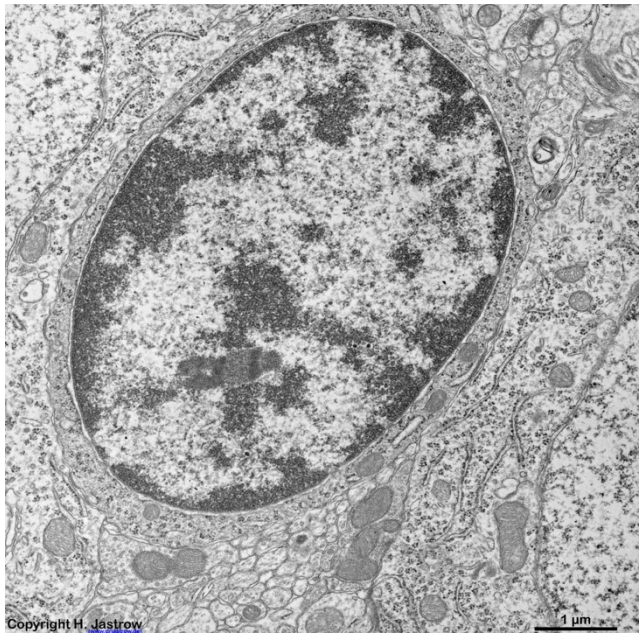

Figure 1. Heterochromatin and euchromatin.
Electron micrograph of the nucleus of a rat glial cell. Heterochromatin is darkly stained whereas euchromatin is lightly stained. Scale bar: 1 µm. Image from Dr. Jastrow's electron microscopic atlas (www.drjastrow.de) with his permission.

I.A.1. The different scales of chromatin organization

From DNA to nucleosome folding

In eukaryotes, chromatin is a complex of DNA and associated proteins found in the nucleus. Early studies in the 1970s using electron microscopy, nuclease digestion assays and crystallography identified the nucleosome as the basic subunit of chromatin (Kornberg, 1977). A nucleosome is composed of approximately 146 bp of DNA wrapped around an octamer of core histone proteins: four heterodimers of H2A/H2B, and H3 /H4 (Luger, 1997). Nucleosomes form a "beads on a string" conformation (Olins and Olins, 1974) in which they are separated by a sequence of linker DNA of variable length that is associated with Histone H1. This first level of DNA compaction can be increased by further aggregation of nucleosomes to form higher-order structures. *In vitro* studies proposed various models of nucleosome folding such as a 30 nm chromatin fiber (Dorigo et al., 2004; Finch and Klug, 1976; Robinson and Rhodes, 2006), but such regular organization could not be proven *in vivo* in human mitotic chromosomes (Eltsov et al., 2008, 2012) nor in interphase nuclei (Ou et al., 2017). Instead, it is now proposed that nucleosome folding is irregular and heterogeneous, and that it depends on different factors such as nuclear localization, chemical environment, cell cycle stage, or cell type (Strickfaden, 2021). One of the current *in vivo* models is the organization of nucleosomes into groups termed "clutches" that vary in nucleosome number and density in a cell-type specific manner (**Fig. 2**) (Ricci et al., 2015).

3D organization of the genome

With the discovery of the chromatin structure at the nanometer scale and the technical advances in molecular biology, most of chromatin research since the 1970s focused on the mechanistic aspects of chromatin in gene regulation, which I will detail in section I.B. However, more recent improvements in high-resolution microscopy and high-throughput sequencing techniques brought very important insights into the nuclear organization of chromatin, especially in *in vivo* contexts (Jerkovic´ and Cavalli, 2021).

Although the idea of distinct chromosome territories had been suggested by Boveri in 1909 (Boveri, 1909), it was only in the 1980s that their existence in the nuclear space was validated, as demonstrated by Fluorescent in Situ Hybridization (FISH) techniques that targeted human chromosomes (Lichter et al., 1988; Manuelidis, 1985; Schardin et al., 1985). Following studies showed that the chromosomal regions dense in active genes localize at the

center of the nucleus while chromosomes with less or inactive genes are found at the nuclear periphery, associated with the lamina (Bolzer et al., 2005; Croft et al., 1999). The emergence of chromosome conformation capture techniques and its derivatives such as genome-wide Hi-C in the 21st century, considerably increased our knowledge of nuclear architecture with the breakthrough discovery of Topologically Associated Domains (TADs), loops and nuclear compartments (**Fig. 2**) (Dixon et al., 2012; Lieberman-Aiden et al., 2009; Sexton et al., 2012). TADs are large genomic regions (100kb-1Mb) that physically interact more with each other than with other regions of the genome. They are delimited by boundaries often enriched in binding of the CTCF insulator protein (Dixon et al., 2012; Rao et al., 2014). The existence of TADs is conserved across species and cell types, but the exact mechanisms underlying their formation and folding are still under investigation. One mechanism is chromatin loop extrusion involving cohesin complexes (Fudenberg et al., 2016; Rao et al., 2014), as loss of cohesin leads to loop domains disappearing from genome-wide contact maps in vertebrates (Rao et al., 2017). In *Drosophila*, cohesin is not a key factor for TAD formation but has multiple roles in gene regulation (Dorsett, 2019). At the nuclear scale, Hi-C methods further identified two major compartments, A and B (Lieberman-Aiden et al., 2009) (**Fig. 2**). The A compartment is generally associated with an open chromatin state and active transcription whereas the B compartment comprises inactive sequences located at the nuclear periphery (Rao et al., 2014). These distinct properties of open and closed chromatin suggest that A and B compartments represent the euchromatic and heterochromatic parts of the genome, respectively. Therefore, these studies shed light on the highly organized folding of the genome and the subsequent multitude of potential long-range interactions.

Another recent notion that came out from collaborative work with physicists is the concept of phase separation, which is a major driver in nuclear compartmentalization (Strickfaden, 2021; Strom et al., 2017). Indeed, several membrane-less subnuclear compartments such as the nucleolus, replication foci and the pericentromeric heterochromatin form by phase separation processes that consists of multivalent interactions between macromolecules. This enables distal elements to come into close contact, the exclusion of some factors from these microenvironments, and the increase in concentration in particular molecules, thus leading to various effects on transcription and other biological processes (Hnisz et al., 2017; Strom et al., 2017).

In order to better appreciate the complexity of 3D genome organization in multiple organisms, tissues and cell types, current research in the field continues to use high-throughput sequencing, soft matter physics and imaging methods such as super resolution FISH-based techniques. To what extent chromatin architecture underlies gene regulation and cellular functions is still debated and will require the ability to integrate the outcomes of all of these recent technological improvements with the growing knowledge of biological processes.

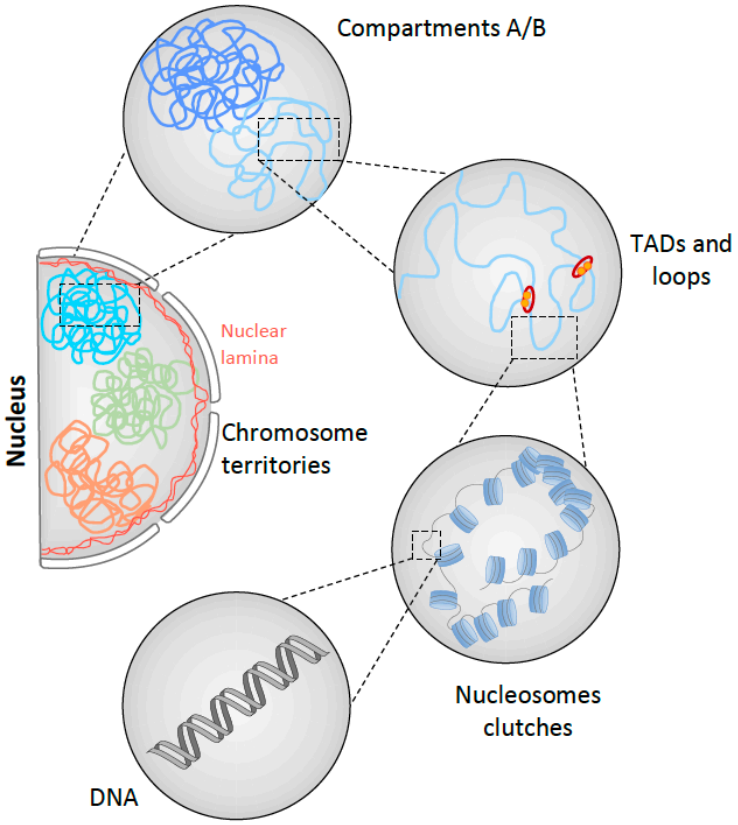

Figure 2. Chromatin organization at different scales in the nucleus.
DNA is wrapped around nucleosomes, which are arranged irregularly and can form nucleosome clutches. At a higher scale, chromatin is organized in Toplogically Associated Domains (TADs) and loops. Domains are organized in the nuclear space within compartments and chromosome territories.

I.A.2. The molecular players of chromatin structure and dynamics

At the scale of DNA and nucleosomes, the nature of the molecules that modulate chromatin structure and dynamics has been largely elucidated in the last 30 years. In particular, the discovery of histone post-translational modifications, chromatin-modifying enzymes and DNA methylation led to the concept of an “epigenetic code” that reflect the

combinatorial action of all these players to generate distinct outcomes (Turner, 2007). Thus, these variations provide an additional layer of information beyond the DNA sequence.

Histone modifications

The first description of nucleosome structure identified N-terminal histone tails that can interact with adjacent nucleosomes (Luger, 1997) and be subjected to post-translational modifications (PTMs) (Strahl and Allis, 2000). Histone PTMs were then extensively characterized, with 22 types of PTMs currently known (Bannister and Kouzarides, 2011; Kouzarides, 2007; Villaseñor and Baubec, 2021). Although most of them take place on histone tails, they can also be found in histone globular domains. The most actively studied histone PTMs include acetylation, phosphorylation, methylation, ubiquitylation, sumoylation, glycosylation and ADP-ribosylation among others. The addition of these chemical groups or proteins occurs on all histones, mostly on lysine, arginine, serine and threonine residues. They affect chromatin in two major ways: (1) by altering directly the structure of chromatin through modifications of inter-nucleosomal or DNA-histone interactions and (2) by recruiting chromatin-modifying proteins that will further alter chromatin structure (Gardner et al., 2011). In particular, chromatin remodeling enzymes rely on ATP hydrolysis energy to displace nucleosomes, such as the highly conserved SWI/SNF complex (Clapier et al., 2017; Ramachandran et al., 2003). These mechanisms therefore mediate downstream effects on several biological processes such as transcription, replication, repair or recombination. Histone acetylation on lysines is a good example of the first mechanism, as it alters the histone charge and thus weakens the DNA-histone interaction, leading to a less compact chromatin configuration (Allfrey et al., 1964; Wolffe and Hayes, 1999). This increases the access for protein machineries, consistent with histone acetylation being found mostly at enhancers and promoters and correlating with active transcription. In contrast, histone methylation illustrates well the second mechanism as it does not alter the histone charge but interacts with multiple chromatin-associated proteins through specific binding domains (Taverna et al., 2007). In addition to these modifications, canonical histones can be substituted by histone variants that differ in protein sequence and can alter chromatin structure locally (Martire and Banaszynski, 2020).

Histone modifications are reversible as they depend on the enzymatic activity of proteins commonly referred to as “writers” and “erasers”, which catalyze the deposition or

removal of PTMs, respectively (**Fig. 3**) (Bannister and Kouzarides, 2011; Gardner et al., 2011). For instance, acetylation is regulated by histone acetyltransferases (HATs) and histone deacetylases (HDACs). Histone methylation relies on various families of histone methyltransferases and demethylases that are specific to the histone, the substrate residue (lysine or arginine) but also to the level of methylation (mono/di/tri-methylation). For example, *in vitro* studies showed that the lysine demethylases containing a Jumonji domain target tri-methylated histones such as H3K9me3 and H3K36me3 (Tsukada et al., 2006), whereas the first identified demethylase LSD1 can act only on mono- and di-methylated substrates such as H3K4me1/2 (Shi et al., 2004). This difference is due to the requirement or different cofactors, and different catalytic mechanisms (Tsukada et al., 2006). In addition, proteins designated as "readers" recognize specific histone PTMs and subsequently recruit additional chromatin modifiers (**Fig. 3**). For example, bromodomains found in chromatin-remodeling complexes and transcriptional activators can bind to acetylated histones (Mujtaba et al., 2007). Extensive biochemical and genetic studies on these "writers", "erasers, and "readers" further identified numerous protein domains responsible for the recognition of amino acid residues or histone PTMs and for the recruitment of additional chromatin complexes, which gave insights into the mechanisms of establishment or remodeling of particular chromatin conformations (Chiarella et al., 2020; Gardner et al., 2011).

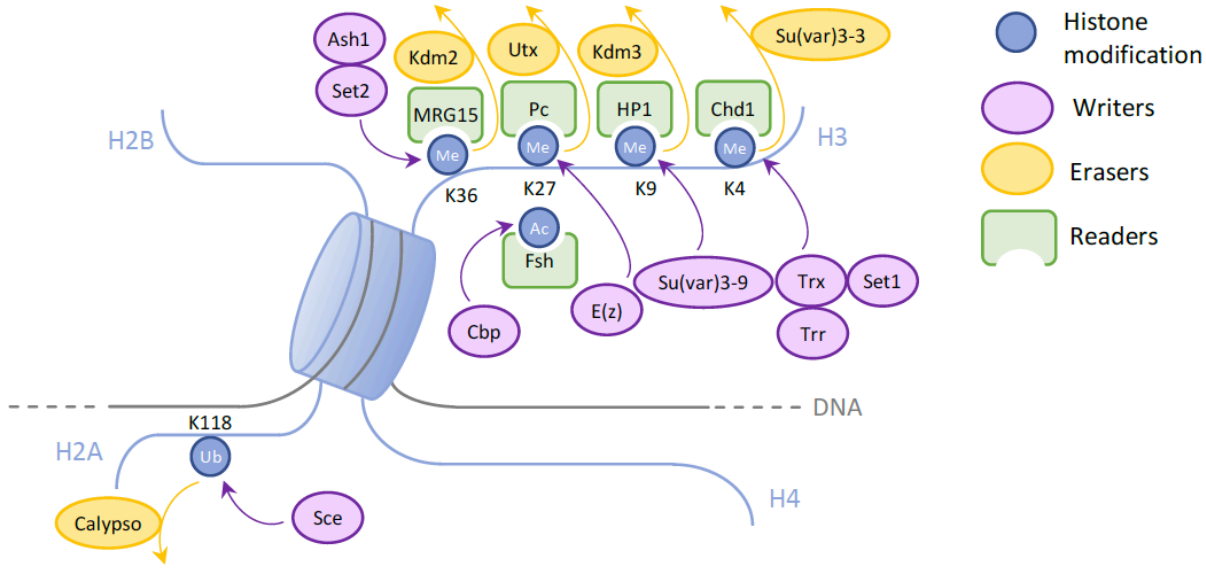

Figure 3. Histone modifications and writers, erasers, readers.
Here are shown only the main histone modifications mentioned in this work. Some histone modifications can be deposited, removed and recognized by several writers, erasers and readers, respectively. Here are presented only the most common ones. Purple arrows represent the catalytic deposition of modifications by writers, yellow arrows represent the removal of the modifications by erasers.

The interplay between different effectors of histone marks is well illustrated by H3K9me3, a mark associated with heterochromatin. Suv39H1 (Su(var)3-9 in *Drosophila*), the first identified methyltransferase, targets and methylates H3K9 through a SET catalytic domain conserved amongst N-term lysine methyltransferases (Rea et al., 2000). Heterochromatin Protein 1 (HP1), in turn, binds to H3K9me3 via its chromodomain and recruits additional Suv39H1, which methylates H3K9 in the adjacent nucleosomes. Thus, this propagates the spreading and maintains large domains of heterochromatin (Bannister et al., 2001; Lachner et al., 2001). The second most known example is the role of Polycomb Group (PcG) proteins in establishing a repressive chromatin environment (Kassis et al., 2017). PcG proteins were initially discovered for their roles in development in *Drosophila*, based on characterization of mutant phenotypes resulting from the derepression of *Hox* genes (see more details in section II). The biochemical properties of PcG proteins were discovered later and it appeared that these proteins have roles of "writers" and "readers" of histone PTMS, based on the presence of protein domains that allow these functions and interactions within the complexes. PcG proteins are organized in two main complexes, Polycomb Repressive Complex 1 and 2 (PRC1 and PRC2), but they are also found in other complexes such as dRAF, PhoRC and PR-DUB. Enhancer of zeste (E(z)), the catalytic subunit of PRC2, catalyzes the methylation of H3K27, which is bound by Pc that recruits PRC1. The PRC1 subunit Posterior sex combs (Psc) inhibits chromatin remodeling and compacts chromatin. PRC1 also catalyzes the deposition of H2AK118ub, which is thought to promote H3K27 methylation. This general model actually relies on multiple interactions between the numerous proteins of PcG complexes, which facilitate the recruitment of both PRC1 and PRC2 at Pc target regions, and further enables the stabilization and spreading of the H3K27me3-mediated heterochromatin.

Chromatin-remodeling complexes

As mentioned above, chromatin remodeling complexes are major players in chromatin structure as they can slide, exchange or eject nucleosomes. They all contain an ATPase domain that powers the moving of DNA along the histone surface, thus breaking DNA-histone contacts (Clapier et al., 2017). Extensive work in the last decade identified four families of multicomponent chromatin remodeling complexes with functional specificities: (1) imitation switch (ISWI), (2) chromodomain helicase DNA-binding (CHD), (3) switch/sucrose non-fermentable (SWI/SNF) and (4) INO80. The ISWI and CHD families are involved in nucleosome

assembly and regulate nucleosome spacing, the SWI/SNF family promotes chromatin accessibility by moving or ejecting histones, and the INO80 family catalyzes the exchange between canonical histones and histone variants. The distinct functions and specific recruitment of these remodelers rely on the presence of different protein domains that enable distinct interactions with specific histone modifications and other chromatin-modifying enzymes. Specific examples will be given in section I.B.

DNA methylation

In addition to histone methylation, DNA itself can be methylated at cytosines and adenines by DNA methyltransferases (DNMTs) (Chiarella et al., 2020). As histone PTMs, DNA methylation can be removed by a family of demethylases, the TET enzymes. DNA methylation is found mostly at CG dinucleotides in vertebrates and is associated with gene repression. Of note, bacteria have abundant adenine methylation, which is rare in eukaryotes (Ratel et al., 2006). In mammals, DNA methylation has major roles during gametogenesis and early embryogenesis. However, DNA methylation is not conserved across all eukaryotes and is notably nearly undetectable in *Drosophila* (Lyko et al., 2000). Therefore, it is likely that gene repression in species without DNA methylation relies on other epigenetic mechanisms.

A combinatorial code to generate distinct outcomes

Importantly, these epigenetic marks often act in concert. One histone modification can be bound by several proteins, and chromatin-associated proteins can write, remove or recognize several histone modifications. This results in some modifications influencing the deposition or recognition of other modifications in the same nucleosome or in adjacent nucleosomes (Gardner et al., 2011). This “crosstalk” can generate feedback and feed-forward loops, hence reinforcing and propagating specific chromatin signatures. Overall, these multiple interactions lead to many possible combinatorial patterns that add another layer of complexity to the downstream biological outcomes of chromatin structure, in particular the regulation of transcription.

I. B. Chromatin structure and regulation of transcription

How does chromatin structure at different scales influence transcription? It has been proposed for a long time that euchromatin is associated with active transcription whereas

heterochromatin correlates with inactive genes. Extensive studies in the last 50 years gave a more accurate picture of the chromatin features underlying this correlation. In particular, differences in DNA accessibility levels, histone modification profiles, binding of specific proteins and nuclear localization correlate with distinct transcriptional states that I will describe in more detail below.

I.B.1. DNA accessibility determinants

Transcription is initiated by RNA polymerase along with transcription factors and co-activators that target promoters and enhance transcription rates, respectively. In animals, RNA Pol II produces messenger RNAs and microRNAs, RNA Pol I synthesizes ribosomal RNAs, and RNA Pol III synthesize ribosomal RNAs, transfer RNAs and other small RNAs. Transcription initiation is highly dependent on DNA accessibility at promoters for the transcription machinery (Klemm et al., 2019; Serebreni and Stark, 2021). Genome-wide profiling of DNA accessibility by DNaseI-seq in the human genome notably showed that 94% of transcription factor binding sites, as defined by ChIP-seq peaks fall within open chromatin (Thurman et al., 2012). Consistent with this, active regulatory sequences are depleted for nucleosomes, which represent a barrier to DNA-transcription factor interaction, and therefore, to transcription initiation (Kornberg and Lorch, 2020; Lee et al., 2004). Nucleosome occupancy and dynamics rely strongly on the binding of the linker Histone H1, which is required for chromatin compaction *in vitro* and *in vivo* (Bednar et al., 1998; Finch and Klug, 1976; Fyodorov et al., 2017). Although H1 is widely distributed throughout the genome, it is enriched in heterochromatin and mostly associated with repressed genes while depleted at promoters of actively transcribed genes (Nalabothula et al., 2014). H1 function is widely conserved across species, but the sequences of particular H1 domains differ between variants and species (Fyodorov et al., 2017). In *Drosophila*, it was shown that H1 participates in heterochromatin establishment by recruiting Su(var)3-9 and mediating H3K9 methylation in nucleosomes (Lu et al., 2013). The combined action of H1 and H3K9me3 thus promotes silencing of genes located in heterochromatin, in particular transposable elements. H1 physical interaction with PIWI proteins and HP1 also promotes heterochromatin formation and TE repression (Fyodorov et al., 2017; Iwasaki et al., 2016). Moreover, interaction between H1 and H3K27me were shown *in vitro* and in human cancer cells, where H1 stimulates PRC2 activity while H3K27me3 promotes H1 occupancy, thus reinforcing silencing effects via a positive feedback

loop (Fan et al., 2005; Kim et al., 2015). H1 can also prevent the binding of chromatin-modifying proteins that deposit active marks and it competes with the HMGD1 protein that enhances chromatin accessibility (Fyodorov et al., 2017; Nalabothula et al., 2014). Therefore, the role of H1 in limiting DNA accessibility and subsequent transcription in heterochromatic regions is well established, but only more recent *in vivo* studies gave the first insight into H1's roles in regulating the expression of genes with specific biological functions. In particular, H1 depletion in mammalian embryonic stem cells does not affect global transcription but rather the expression of specific genes (both upregulated and downregulated) and it reduces nucleosome spacing locally (Fan et al., 2005). Other studies in human cancer cells and mouse hematopoietic cells demonstrated that H1 depletion leads to altered chromatin accessibility, H3K27me3 decrease, H3K36me3 increase and derepression of genes located in decompacted regions as a direct consequence of these chromatin changes (Torres et al., 2016; Willcockson et al., 2020; Yusufova et al., 2021). Thus, beyond H1 roles in chromatin compaction in heterochromatin, it is likely that H1 also influences transcription locally in more specific ways.

What are the drivers of nucleosome dynamics and variations in chromatin accessibility? First, it was proposed that some transcription factors have a “pioneering” activity capable of destabilizing nucleosomes in compacted chromatin (Zaret and Carroll, 2011). They target specific sites prior to the binding of other factors and initiate chromatin structure changes (**Fig. 4**). Studies on FoxA protein family identified the mechanisms underlying this ability to overcome the nucleosome barrier (Cirillo et al., 2002; Iwafuchi-Doi, 2019; Zaret and Carroll, 2011). FoxA pioneer factors contain a “winged helix” domain similar to that of linker histones, allowing them to bind nucleosomal DNA. They can further displace nucleosomes to open chromatin locally, thus creating a permissive state for the recruitment of chromatin remodelers and transcription factors. In *Drosophila*, Zelda, Grainyhead and GAGA factor were categorized as pioneer factors for their ability to bind nucleosomal DNA and increase chromatin accessibility at their sites (Chetverina et al., 2021; Foo et al., 2014; Jacobs et al., 2018). However, as for some other mammalian pioneer factors, it is still unclear whether they open chromatin themselves or instead rely on the recruitment of chromatin remodelers to perform these chromatin changes (Iwafuchi-Doi, 2019; Klemm et al., 2019). For instance, the pluripotency factor OCT4 requires the recruitment of BRG1/BRM, a catalytic subunit of the SWI/SNF complex, to increase chromatin accessibility at its target sites (King and Klose, 2017).

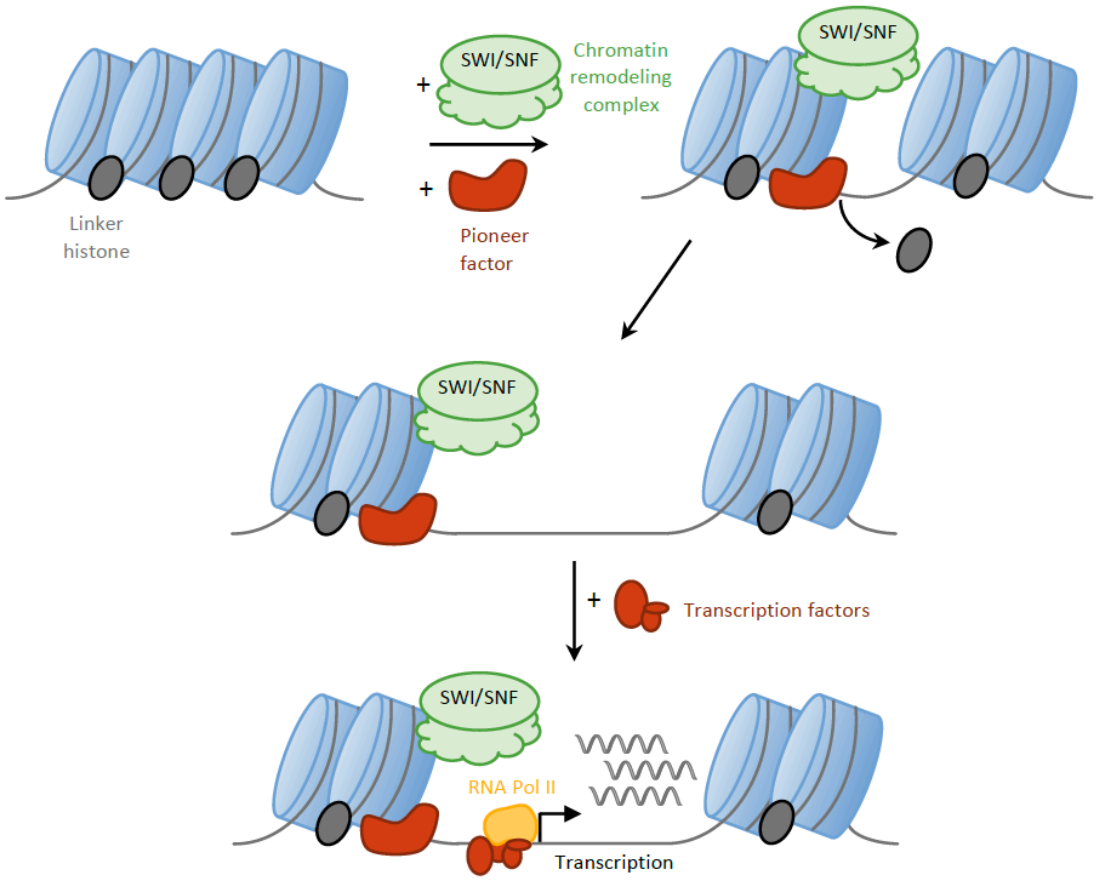

Figure 4. Modulation of DNA accessibility by linker histones, pioneer factors and chromatin-remodeling complexes.

In this model, pioneer factors target nucleosomes and open chromatin by displacing nucleosomes and/or recruiting chromatin remodeling complexes. This results in an increase of nucleosome spacing and allows the recruitment of transcription factors, which in turns enables transcription.

More generally, mechanisms of nucleosome moving or eviction to facilitate transcription factor binding mostly rely on enzymes of the SWI/SNF family (Clapier et al., 2017; Ramachandran et al., 2003) (**Fig. 4**). For instance, RSC (remodels structure of chromatin), a member of the SWI/SNF family, is recruited at promoters and mediates nucleosome positioning to increase promoter accessibility (Kubik et al., 2018). Importantly, a study investigating the function of ISWI and SWI/SNF in mouse ESCs showed that chromatin remodeling proteins selectively recruit ISWI-specific and SWI/SNF-specific sets of transcription factors, suggesting that they do not only create a chromatin environment suitable for the binding of any transcription factor, but also provide specificity (Barisic et al., 2019). Furthermore, studies in yeast showed that chromatin remodelers such as Chd1 and Swi/Snf can regulate transcription by displacing nucleosomes during the elongation process (Schwabish and Struhl, 2007, 2003), which also requires the histone chaperone FACT

(Orphanides et al., 1998). Importantly, chromatin remodelers of the ISWI and CHD families can also promote gene silencing through regulation of nucleosome spacing (Clapier et al., 2017). In summary, the accessibility of DNA for active transcription depends on the dynamic interplay between multiple linker histones, chromatin remodelers and transcription factors.

I.B.2. Histone modifications and transcription

As described in part A, histone modifications establish a variety of chromatin environments, through direct alteration of chromatin structure or recruitment of modifying enzymes, which results in regulation of DNA-templated tasks such as transcription. Therefore, histone modifications correlate with either gene activation or repression (**Fig. 4**) (Kouzarides, 2007). However, it also became clear in the last decades that the potential to activate or inhibit transcription is context-dependent and that histone modifications are not always predictive of a particular transcriptional state. I will discuss these limits in the next section (B.3).

Globally, active transcription correlates with (1) high levels of histone acetylation and (2) high levels of methylation of H3K4, H3K36 and H3K79. Acetylated histones and H3K4me3 are enriched at transcription start sites whereas H3K36me3 is associated with transcription elongation. Histone acetylation influences nucleosome dynamics and likely increases DNA accessibility, but is also recognized by bromodomains found in HATs and SWI/SNF complexes (Mujtaba et al., 2007). Similarly, H3K4 and H3K36 methylation mediates transcription activation by recruiting chromatin-modifying proteins, which, in turn, recruit or interact with downstream factors to orchestrate the different steps of transcription. Furthermore, high levels of H3K4me1 and H3K27ac are found at active enhancers, which are binding platforms for transcription factors and coactivators (Calo and Wysocka, 2013; Heintzman et al., 2009). In contrast, H3K9 and H3K27 methylation are enriched in heterochromatin and thus correlate with transcriptional repression via the recruitment of HP1 and PRC1/2 respectively, and the subsequent mechanisms explained in part I.A.2.

I.B.3. Limits of the "histone code" model

Although chromatin marks described above usually correlate with active or repressive transcription, the view of the histone code model has been challenged by several examples. For instance, H3K9me2/3 has been found associated with coding regions of actively transcribed genes on mammalian cells, together with the binding of the HP1γ isoform through

its physical association with the phosphorylated form of RNA Pol II (Vakoc et al., 2005). HP1 association with a subset of active genes located in euchromatin was also reported in *Drosophila* and uncovered HP1 roles in the positive regulation of transcription, thus revealing context-dependent roles for HP1 (De Lucia et al., 2005; Eissenberg and Elgin, 2014; de Wit et al., 2007). Moreover, the idea that histone marks are not always instructive of the transcriptional outcome was supported by findings about histone mark-independent functions of chromatin-modifying enzymes. For example, lack of H2Aub in *Drosophila* does not prevent PcG mediated repression at PRC1 canonical target genes (Pengelly et al., 2015). In addition, several chromatin-modifying enzymes have non-catalytic functions (Morgan and Shilatifard, 2020). For instance, the SET domain of the H3K4 methyltransferase Set1 is dispensable for embryonic stem cell (ESC) self-renewal whereas the full protein is essential for ESC viability (Sze et al., 2017). Another limit of the histone code model appeared with the discovery of bivalent domains in mouse embryonic stem cells, which carry both active and repressive marks (H3K4me3 and H3K27me3) (Azuara et al., 2006; Bernstein et al., 2006; Mikkelsen et al., 2007). It was further showed that H3K4me3 and H3K27me3 physically co-exist in a single nucleosome, though not on the same histone tail (Voigt et al., 2012). Coexistence of these two marks with two predicted opposite outputs was associated with low expression or silencing of developmental transcription factor-encoding genes. Upon differentiation, only one mark is conserved, and it was proposed that some genes are in a "poised" state to enable rapid activation during later developmental stages. Bivalent domains were then found in other mammalian cell types at promoters and enhancers, but their functional relevance in differentiation is now debated (Shah et al., 2021). In *Drosophila*, the existence of bivalent domains has been rarely observed and often attributed to heterogeneity in the cell populations profiled, but a recent study found evidence of bivalency at several Polycomb-target genes in *Drosophila* embryos (Akmammedov et al., 2019).

I.B.4. The role of higher-order chromatin organization in transcription

Beyond the local chromatin structure, higher-order organization of chromatin can also influence transcription. In particular, the presence of loop domains brings promoters in close contact with distal enhancers. These promoter-enhancer interactions can lead to gene activation or repression, by bringing transcription factors and chromatin-modifying proteins to the targeted promoters. For instance, the interaction of *even-skipped* enhancers with their

target promoter was historically studied in the *Drosophila* embryo through *lacZ* reporter expression after the insertion of insulators and spacers (Cai and Levine, 1995). Improvements in live imaging allowed a better spatial and temporal characterization of this long-range interaction and its effects on transcription (Chen et al., 2018a). A recent technique, Hi-M, also uses live imaging to describe 3D chromatin organization simultaneously with the detection of transcriptional activity (Cardozo Gizzi et al., 2019). Using Hi-C techniques, it was shown in mammals that the disruption of TADs through structural rearrangements affects gene expression, which can lead to developmental defects (Lupiáñez et al., 2015; Serebreni and Stark, 2021; Vos, 2021). However, mis-expression of genes upon TAD loss through CTCF or cohesin depletion is overall limited (Nora et al., 2017; Rao et al., 2017). In *Drosophila*, the use of balancer chromosomes to induce structural rearrangements had limited effects on gene expression despite major changes in TAD organization (Ghavi-Helm et al., 2019). Therefore, the precise role of TADs in mediating misappropriate enhancer-promoter interactions and subsequent gene expression changes is still debated. Spatial localization of chromosomes in the nucleus can also affect transcription, as suggested by the association of inactive genes with the nuclear lamina (Pickersgill et al., 2006). Indeed, artificial tethering of genes to the nuclear lamina can lead to their repression (Reddy et al., 2008), whereas depletion of B-type lamin upregulates lamina-bound gene clusters (Shevelyov et al., 2009). Therefore, the organization of the genome in the nuclear space can influence the transcription of genes, through localization in particular chromatin environments or interactions with distal elements.

I.B.5. Emerging view of the complexity of chromatin states

In summary, the different scales of chromatin organization have multiple effects on gene transcription. Although chromatin accessibility is required for transcription initiation, it is not sufficient to dictate gene activation, which relies on multiple interactions between histone modifications, chromatin-modifying enzymes and transcription factors. In addition, long-range interactions with distal regulatory elements add another layer of complexity to gene regulation. The increasing number of studies generating genome-wide maps of chromatin features led to the view that chromatin states are defined by combinations of multiple chromatin marks, which, in turn, favor specific transcriptional outcomes and the subsequent downstream biological processes.

I. C. Chromatin state modeling

Chromatin state definition in this study

During my PhD, I used a chromatin state modeling approach to define and characterize chromatin states in the *Drosophila* intestinal lineage. Therefore, the term "chromatin state" will refer to "a specific combination of chromatin marks" in the rest of this manuscript. "Chromatin marks" refers to histone modifications and binding of chromatin-associated proteins. I will detail below the approaches that have been used to model chromatin states.

I.C.1. Genome-wide protein profiling techniques

The development and improvement of protein profiling technologies coupled with next-generation sequencing have greatly expanded the possibilities of identifying the genomic binding sites of numerous proteins such as modified histones, chromatin-modifying proteins and transcription factors (Klein and Hainer, 2019). Here, I will briefly describe ChIP-seq and DamID, which have been used to generate genome-wide binding maps of various proteins to further integrate these for chromatin state modeling.

ChIP-seq is based on chromatin immunoprecipitation (ChIP), which consists of crosslinking of proteins with DNA, DNA fragmentation by sonication and immunoprecipitation of DNA-bound protein complexes using a specific antibody for the protein of interest (**Fig. 5**). Crosslinks are then reversed, and co-precipitated DNA fragments are purified for subsequent sequencing (Barski et al., 2007).

In DamID (DNA adenine methyltransferase identification), the tethering of the Dam-methyltransferase from *E.coli* to a protein of interest allows methylation of adenine on GATC sites surrounding the binding sites of the protein of interest (**Fig. 5**). Methylated GATC sites can thereby be detected via enzymatic digestion and whole genome sequencing (Steensel and Henikoff, 2000). A main advantage of DamID over ChIP-seq is that it does not require an antibody to profile the protein of interest. It relies instead on the expression of the Dam-protein fused construct, which determines chromatin binding sites *in vivo* without cell purification. On the other hand, ChIP-seq gives a more precise spatial resolution than DamID, which is limited by the distribution of GATC sites in the genome. However, comparison with ChIP-seq data showed that DamID is robust, reproducible and sensitive and has a broad range of applications (Aughey et al., 2019).

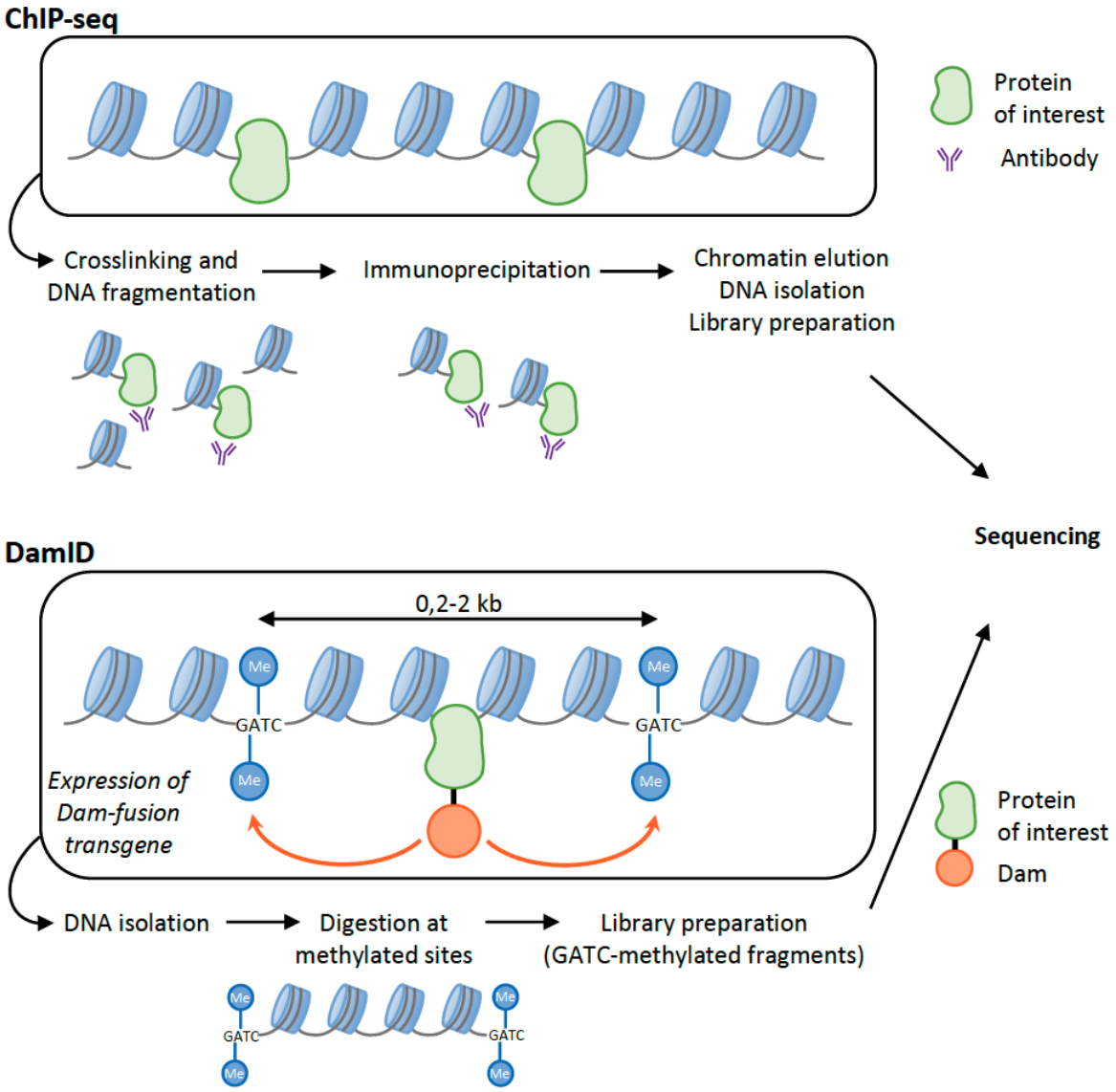

Figure 5. DamID and ChIP-seq to determine genome-wide binding of proteins.

ChIP-seq relies on immunoprecipitation of DNA bound by the protein of interest, whereas DamID allows the detection of methylated sites around the binding sites of the protein of interest. See more details in the text.

I.C.2 Hidden Markov Model to define chromatin states

Hidden Markov Models (HMM) were shown to be suitable for the definition and description of chromatin states (Hamada et al., 2015). Thus, they have been used in several studies and in my PhD project. A Markov model is a system with several states and probabilities to transition from one sate to another (or to go back to the same state). In a Hidden Markov Model, states are unknown (hidden) but generated by observations with some emission probability (**Fig. 6**). The use of machine learning enables to predict a sequence of (hidden) states from a sequence of observations. In the context of chromatin states, the

observations are the combinations of binding signal of the profiled proteins at each genomic locus, and the modeling output is a sequence of chromatin states along the genome. The emission probabilities are the frequencies with which a protein binding signal is observed in each state and the transition probabilities reflect the spatial relationships between neighboring positions in the genome (Ernst and Kellis, 2010; Filion et al., 2010; Kharchenko et al., 2011). Therefore, HMM allows to capture the diversity of combinations of binding profiles and to map them along the genome.

Figure 6. Chromatin state modeling with HMM.
Modeling allows to predict a sequence of chromatin states from a sequence of observed events. Arrows represent the transitions probabilities between transitions (y) and the emission probabilities that reflect the

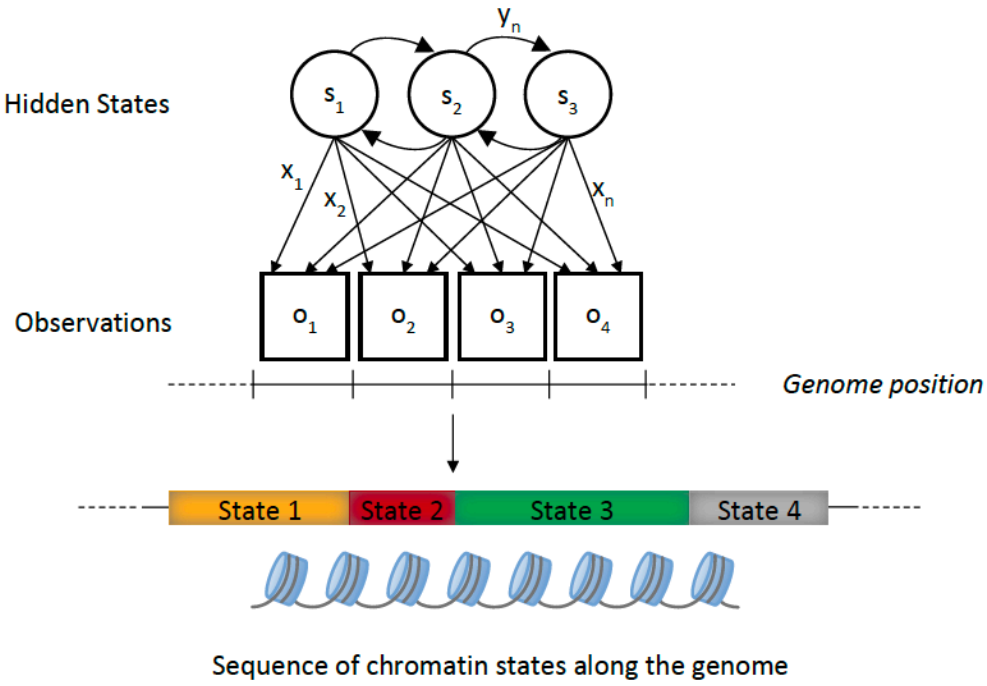

frequency of observations in each state. s_n: chromatin states, o_n: binding intensities of proteins, x_n: emission probabilities, y_n: transition probabilities between states.

I.C.3. Chromatin state models reveal new chromatin signatures

HMM-based chromatin state modeling approaches considered either the binding intensities of chromatin marks, or employed a binarization approach based on the presence/absence of each mark within a state at a specific genomic location. This second method was used to define chromatin states in the human genome based on genome-wide occupancy of 38 different histone marks, histone variant H2AZ, RNA Pol II and CTCF obtained by ChIP-seq (Ernst and Kellis, 2010). In this model, the 51 states were grouped and biologically

interpreted relative to genomic and genic features: “promoter”, “transcribed”, “active intergenic”, “repressive”, “repetitive”.

Around the same time, two studies used an HMM approach to characterize the chromatin landscape of the *Drosophila* genome in embryonic cell lines (Filion et al., 2010; Kharchenko et al., 2011). In Kharchenko et al., nine chromatin states captured the diversity of 18 histone modifications patterns (**Fig. 7A**). These states were functionally described in regard of genomic features and transcriptional states, as what was done in Ernst and Kellis’ work. In particular, they highlighted distinct chromatin signatures associated with active genes depending on genic features such as gene length, exon content, or function. In Filion et al., chromatin state modeling was based on the DamID profiling of 53 chromatin-associated proteins (**Fig. 7B**). The combinations of the 53 binding profiles clustered into five groups, named as the “five chromatin colors”: Blue, Green, Black, Red and Yellow. Unlike the other models described above, the initial segmentation into five states was only data-driven and based on PCA analysis, regardless of genome annotations. Beyond the classical view of euchromatin and heterochromatin, this study showed that chromatin states could be reduced to five major states which faithfully recapitulate the information obtained from the 53 protein binding profiles. In particular, the authors identified two distinct types of active chromatin (Red and Yellow), and three types of repressive chromatin (Blue, Green and Black). The Green chromatin reflects the constitutive heterochromatin enriched in HP1 whereas the Blue chromatin is characterized by the enrichment in Polycomb proteins. The Black chromatin is a previously uncharacterized repressive state covering half of the genome and lacking the classic chromatin factors associated with transcriptional repression. It is instead enriched in structural components of chromatin such as H1 and D1 chromosomal protein, and Lamin. The Red and Yellow states are both associated with transcriptionally active chromatin but they mark different types of genes. Broadly expressed and housekeeping genes are found in Yellow chromatin whereas genes with more restricted expression patterns and functions are found in Red chromatin. Moreover, only the Yellow chromatin is enriched in MRG15 and H3K36me3, which are markers of elongating transcription. The Red chromatin is instead enriched in chromatin-modifying proteins and in particular Brahma, the key catalytic subunit of the SWI/SNF remodeling complex. It was further showed that these five chromatin types can be approximated by the binding of five proteins that are highly enriched in each type: MRG15, Brahma, HP1, H1 and Polycomb (Filion et al., 2010).

Taken together, these studies describing chromatin states highlighted the importance of considering combinations of chromatin marks and their genome-wide distribution rather than individual marks to make accurate genome annotations. In particular, these reductionist approaches allow to interpret large datasets by pointing out the most relevant chromatin features coming from these data. These models also proved to be powerful tools to predict regulatory elements and biological functions.

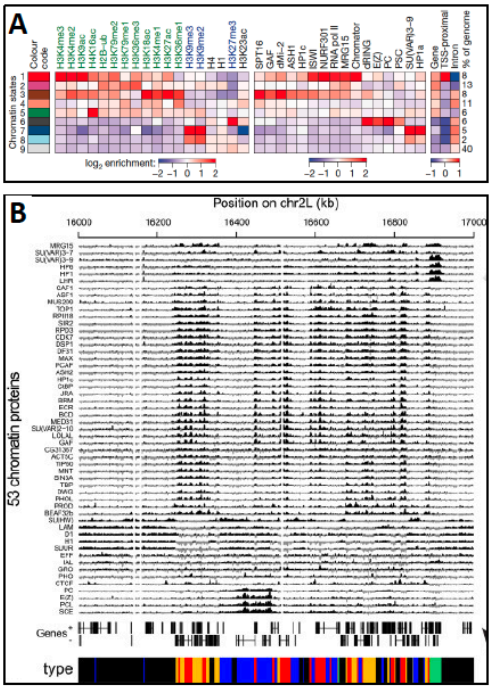

Figure 7. Examples of chromatin state models of the *Drosophila* genome (Kharchenko et al., 2011) and (Filion et al., 2010).
A: 9-state model in S2 and BG3 cells from (Kharchenko et al 2010). Each row is a state and the color scale represents the enrichment in chromatin marks (first panel). The second panels represent the enrichment of chromosomal proteins. The third panel shows the enrichment of genomic features in each state. Reprinted by permission from Springer Nature Customer Service Centre GmbH: Springer Nature, NATURE. Copyright Nature Publishing Group, a division of Macmillan Publishers Limited. **B**: Chromatin state map (bottom) on a portion of chromosome 2L in a 5-state model in Kc167 cells from (Filion et al 2010). The model was fitted from the binding profiles of 53 chromatin proteins. Copyright Elsevier (2010).

II. The role of chromatin organization in the regulation of stem cells and differentiation

II. A. Chromatin dynamics in development

In the first part of this introduction, I gave an overview of chromatin organization at different scales in eukaryotic cells, and how this chromatin structure influences transcription. Direct observations using microscopy followed by genome-wide profiling of chromatin marks highlighted differences in chromatin organization between cell types, in particular in the context of development. Significant knowledge about the role of chromatin organization in stem cells was initially gained from studies on mammalian embryonic stem cells (ESCs), which provided an easy way to observe chromatin organization at different scales and to study the roles of chromatin factors in pluripotency and differentiation (Schlesinger and Meshorer, 2019). In this part, I will highlight the main chromatin differences between embryonic pluripotent stem cells and differentiated cells, before giving an overview of how this chromatin remodeling occurs in various *in vivo* developmental contexts.

II.A.1. Chromatin features of embryonic pluripotent stem cells

Nuclear organization: an open chromatin structure

Early studies using microscopy revealed morphological differences between nuclei from embryonic stem cells and nuclei from differentiated cells. Several lines of evidence showed a more open chromatin in pluripotent stem cells compared to differentiated cells. For instance, electron microscopy revealed that nuclei of human and mouse ESCs display a regular granular chromatin whereas it becomes more heterogeneous and condensed in differentiated cells (Efroni et al., 2008; Park et al., 2004). This structural transition was also observed in the early mouse embryo, where chromatin compaction and concentration at the nuclear envelope occurs as cells become restricted to specific lineages (Ahmed et al., 2010). Consistent with this, HP1 and H3K9me3 staining is diffuse in ESCs whereas it appears in discrete foci in differentiated cells (**Fig. 8**) (Meshorer et al., 2006). In addition, the localization of centromeres changes upon differentiation, since in ESCs they are found less at the nuclear periphery compared to differentiated cells (Wiblin et al., 2005). Relocation of pluripotency genes such as *NANOG* and *OCT4* was also observed, with *NANOG* found more at the nuclear periphery and *OCT4* undergoing a local reorganization at the scale of its chromosome territory (Wiblin

et al., 2005). Another feature of ESCs is the absence of lamin A, while lamins B/C are expressed at high levels but form a less-organized and more dynamic structure than in differentiated cells (Bhattacharya et al., 2009; Constantinescu et al., 2006; Melcer et al., 2012). Consistent with this, it was shown that lamin A contributes more to nucleus stiffness than lamin B (Lammerding et al., 2006). A study using super-resolution microscopy (STORM) found that nucleosome "clutches" were less abundant and smaller in mouse ESCs than in differentiated neural precursor cells (Ricci et al., 2015). Larger clutches in differentiated cells also correlated with heterochromatin marked by high levels of H1 and lower levels of RNA polymerase II (Ricci et al., 2015). In addition to these morphological properties of the nuclear architecture, accessibility profiling techniques indicated that chromatin was globally more accessible in ESCs than in differentiated cells (Schlesinger and Meshorer, 2019), partly mediated by the binding of HMGN1 and Atad2 to nucleosomes (Deng et al., 2013; Morozumi et al., 2016). Experiments of fluorescence recovery after photobleaching (FRAP) revealed that a fraction of chromatin structural proteins such as lamins, HP1 and core and linker histones are loosely bound to chromatin and highly dynamic in the nucleus of ESCs, whereas they do not display this mobility in differentiated cells (Bhattacharya et al., 2009; Melcer et al., 2012; Meshorer et al., 2006). Therefore, ESCs display a specific nuclear architecture consistent with a more open chromatin than in differentiated cells, which was suggested to be important for the pluripotent state.

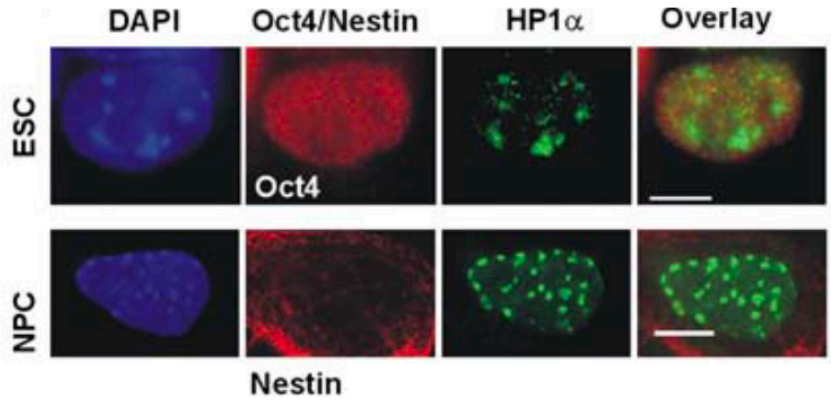

Figure 8. Chromatin structure differences between embryonic stem cells (ESC) and neural progenitor cells (NPC) from (Meshorer et al., 2006).
Immunostainings for DAPI, the ESC marker Oct4, the NPC marker Nestin and HP1α. Scale bar: 5µm. Copyright Elsevier (2006).

Chromatin marks in ESCs

Consistent with their open chromatin structure, ESCs were found to have high levels of histone acetylation on H3 and H4, which decrease upon differentiation (Azuara et al., 2006; Efroni et al., 2008; Krejčí et al., 2009; Meshorer et al., 2006). In contrast, differentiation is characterized by an enrichment and an expansion of repressive marks, in particular H3K9 methylation, as previously mentioned based on immunostainings and later confirmed by ChIP-seq (Hawkins et al., 2010; Meshorer et al., 2006; Wen et al., 2009). Low levels of H3K9 methylation are important for preserving ESC self-renewal, as depletion of the H3K9 demethylases Jmjd1a and Jmjd2c lead to ES cell differentiation as a result of the downregulation of ESC-specific regulators (Loh et al., 2007). Furthermore, ESCs display differences in the distribution of DNA methylation, with an enrichment outside of CpG islands which is not observed in differentiated cells (Hawkins et al., 2010; Lister et al., 2009). Globally, these results indicated that ESCs are enriched in active chromatin marks and depleted of repressive marks compared to differentiated cells. This correlates with high transcriptional activity in ESCs, which was suggested to allow a high level of plasticity, thus ensuring a large potential to differentiate (Efroni et al., 2008). However, lineage-specific genes must be silenced or expressed at very low levels to prevent premature differentiation. This is achieved by binding of PRC1 and PRC2 complexes, consistent with the presence of H3K27me3 at these genes (Boyer et al., 2006; Lee et al., 2006). Loss of the PRC2 subunit Eed causes derepression of developmental regulators that are normally activated upon differentiation (Boyer et al., 2006). Moreover, a subset of Polycomb-target genes is also bound by the pluripotency factors OCT4, NANOG and SOX2, suggesting an interplay between these transcription factors and Polycomb group proteins to maintain the pluripotent state.

Roles of chromatin modifying proteins in ESCs

To maintain the chromatin hallmarks of ESCs, chromatin modifying proteins are required to establish and maintain the histone marks mentioned above, but also to ensure the chromatin organization at the scale of the nucleosomes. Several chromatin remodelers were identified for their specific roles in ESCs (Gaspar-Maia et al., 2011). In addition, chromatin-remodeling factors have higher levels of expression in ESCs than in differentiated cells, both at the transcript and protein levels (Efroni et al., 2008; Kurisaki et al., 2005). For instance, the

SWI/SNF complex esBAF is unique to ESCs and its catalytic subunit BRG1 is downregulated upon differentiation. EsBAF is required for ESC self-renewal and interacts with OCT4 to regulate genes promoting pluripotency (Ho et al., 2009; King and Klose, 2017). The remodeler Chd1, which is associated with actively transcribed regions of the genome, is essential to maintain the open chromatin of ESCs and their pluripotent state (Gaspar-Maia et al., 2009). Loss of ChD1 notably causes ESC to lose their ability to differentiate into primitive endoderm. Another example is the role of the nucleosome-remodeling and histone deacetylation (NuRD) complex in the regulation of the ESC differentiation potential (Gaspar-Maia et al., 2011; Kaji et al., 2006). In particular, the subunit Mbd3 is required to silence specific lineage genes in order to ensure proper cell fate specification when differentiation is induced (Kaji et al., 2006). Importantly, studies investigating the mechanisms that enable reprogramming somatic cells to induced pluripotent stem cells (iPSCs) brought new insight into the chromatin organization underlying pluripotency (Gaspar-Maia et al., 2011). Indeed, reprogramming requires large chromatin remodeling and several screens for factors that improve reprogramming helped to identify chromatin regulators associated with the pluripotent state of ESCs (Gaspar-Maia et al., 2011; Singhal et al., 2010)

Therefore, *in vitro* chromatin studies revealed major differences between the chromatin organization of ESCs and differentiated cells. These changes occur at different scales, and several lines of evidence suggest that chromatin-associated proteins play important roles in this chromatin remodeling.

II.A.2. The functional roles of chromatin-associated factors in development

The observations of chromatin remodeling upon cell differentiation and the growing knowledge about the chromatin-associated proteins that establish and maintain distinct chromatin states led developmental biologists to examine the functional consequences of chromatin factor depletion during development. Numerous *in vivo* studies in various model organisms revealed that many chromatin-associated proteins are required for proper embryonic development and specification of distinct lineages (Ho and Crabtree, 2010).

Among the most studied chromatin factor roles in development are the Polycomb group (PcG) and Trithorax group (TrxG) proteins, which are major repressors and activators of transcription, respectively (Kassis et al., 2017). As previously mentioned, PcG proteins were discovered based on mutant phenotypes in *Drosophila* development caused by *Hox* gene

derepression. On the other hand, screens for mutations that suppressed PcG mutant phenotypes in flies led to the identification of the TrxG proteins as positive regulators of *Hox* genes. TrxG proteins include various chromatin modifying proteins such as the H3K4 methyltransferases Trx and Ash2 (found in COMPASS complexes), the H3K36 methyltransferase Ash1 and the H3K27 acetyltransferase Cbp. TrxG proteins also comprise chromatin remodeling complexes of the SWI/SNF family (BAP and PBAP) and the CHD family protein Kismet. PcG and TrxG proteins are conserved in metazoans, including mammals where they also have key roles in embryonic development (Grossniklaus and Paro, 2014; Kingston and Tamkun, 2014).

Roles of PcG proteins in development

In *Drosophila*, mutations in PcG components cause homeotic transformations due to ectopic expression of *Hox* genes after establishment of embryonic segmentation. Such homeotic changes are also observed in mice mutant for the PRC1 subunit Phc2, which have skeletal malformations (Isono et al., 2005). Mutations in other core subunits of PRC1 and PRC2 frequently result in embryonic lethality. For instance, mouse embryos lacking Ring1b (PRC1) fail to develop further than the gastrulation stage (Voncken et al., 2003). The PRC1 component Bmi-1 is also required for complete embryonic development but at later stages (Lugt et al., 1994). Mice mutant for core subunits of PRC2 also fail to develop normally and display homeotic phenotypes (Grossniklaus and Paro, 2014; Piunti and Shilatifard, 2021). These results are consistent with those obtained in ESCs, where depletion of PcG proteins usually do not affect self-renewal but leads to differentiation defects (Boyer et al., 2006; Lee et al., 2006). Importantly, many non-canonical components of PRC1 and PRC2 have been identified and characterized in both vertebrates and invertebrates, and their assembly in additional complex variants can greatly vary between cell types and stages of development. These non-canonical complexes generate distinct and more specific outcomes in terms of lineage specification and regulation (Piunti and Shilatifard, 2021).

Roles of TrxG proteins in development

As mentioned above, TrxG proteins also play key roles in *Drosophila* embryonic development by maintaining active transcription of *Hox* genes in appropriate segments (Kassis et al., 2017; Kingston and Tamkun, 2014). This role is conserved in mammals, where the *trx*

ortholog *MLL1* is also required for proper mouse development through regulation of *Hox* genes (Yu et al., 1995). Extensive characterization of individual TrxG proteins demonstrated their crucial roles in developmental processes (Cenik and Shilatifard, 2021). Mutations in proteins of the BAF and PBAF complexes (BAP and PBAP in *Drosophila*) cause a wide range of developmental defects, some of which are specific to tissues or developmental stages. This is partly due to the evolution of the subunit composition of complexes during development (Cenik and Shilatifard, 2021; Staahl et al., 2013). For instance, neural progenitors express the npBAF complex which differs in subunit composition compared to the esBAF complex expressed in ESCs and to the nBAF complex expressed in neurons (Staahl et al., 2013). This precise complex composition is essential for correct neurogenesis (Lessard et al., 2007). Another example of a TrxG chromatin remodeling enzyme playing a key role in development is CHD7, found mutated in the human CHARGE syndrome, which consists of multiple congenital defects (Vissers et al., 2004). Mice lacking Chd7 show embryonic lethality with defects in several developing tissues, partially recapitulating the CHARGE syndrome (Hurd et al., 2007). Further studies showed that Chd7 is essential for neural development through regulation of transcription of neuronal genes (Bajpai et al., 2010; Feng et al., 2017). Chd7 is found at active enhancers and H3K4me3 sites, it is required to maintain an open chromatin and it can both activate or repress transcription of tissue-specific genes during differentiation (Feng et al., 2017; Schnetz et al., 2009, 2010). In *Drosophila*, the Chd7 ortholog Kismet stimulates transcription elongation and counteracts PcG-mediated H3K27 methylation by recruiting the histone methyltransferases ASH1 and TRX (Srinivasan et al., 2008). Our lab also showed that Kismet is required to limit intestinal stem cell proliferation (Gervais et al., 2019). Details are in Chapter 2 of the Results section.

Roles of other chromatin factors in development

In addition to PcG and TrxG proteins, many other chromatin remodeling enzymes have key roles in development (Ho and Crabtree, 2010), such as several components of the ISWI family. In *Drosophila*, *ISWI* null mutants are embryonic lethal and ISWI is particularly required for oogenesis (Deuring et al., 2000). Similarly, the mammalian ISWI ATPase Snf2h is essential for early mouse development (Stopka and Skoultchi, 2003). Another example is BTPF, a subunit of the NURF complex, which is required for mouse post-implantation development.

BPTF is essential for proper formation of endoderm, mesoderm and ectoderm lineages through regulation of specific developmental genes (Landry et al., 2008).

In summary, functional studies investigating the role of chromatin-modifying proteins in development highlighted their essential requirement in major developmental processes. These factors, by modulating the transcription of key developmental genes, influence cellular processes such as self-renewal and differentiation, demonstrating the importance of chromatin remodeling occurring during development. Another layer of complexity emerges from the context-dependent and combinatorial functions of chromatin-associated proteins, and recent improvements in genome-wide mapping techniques are now providing more insight into these specific functions and how they contribute to the global chromatin landscape changes occurring during development.

II.A.3. Chromatin landscape changes during development

The last 15 years have been marked by a significant and fast evolution of sequencing techniques, which allowed the production of numerous genome-wide maps of various genomic elements and subsequent identification of regulatory elements of the genome. In particular, the profiling of histone modifications, chromatin-binding proteins, chromatin accessibility and transcription factors in different cell types and at different stages of development gave new insight into the chromatin landscape changes occurring upon differentiation. For instance, genome-wide ChIP-seq maps of several histone marks and RNA Pol II in mouse ESCs, neural progenitors and embryonic fibroblasts enabled to better identify the genes marked by H3K4me3 and H3K27me3 and how this correlated with their expression in specific tissues, with a focus on bivalent promoters (Mikkelsen et al., 2007). This notably demonstrated that these histone marks were reflecting the active, repressed or poised state of tissue-specific genes, thus providing information about their lineage potential. Mapping chromatin accessibility across early developmental stages in the mouse embryo also showed that pluripotency is characterized by a broad permissive state until gastrulation. It also identified the genomic regulatory regions that modulate the emergence of lineage-specific patterns when the three germ layers are specified (Argelaguet et al., 2019; Wu et al., 2016). Chromatin accessibility profiling of embryonic $Oct4^{+}$ cranial cells also revealed similarities with epiblast stem cells, demonstrating the occurrence of *in vivo* reprogramming during neural

crest development (Zalc et al., 2021). In another study, the respective roles of PRC1 and PRC2 were investigated by integrating single-cell RNA-seq from post-implantation wild-type and mutant mouse embryos, which revealed the predominant contribution of PRC2 to early lineage restriction and gave a more accurate temporal resolution of PRC2 function (Grosswendt et al., 2020). Moreover, such genome-wide mapping of chromatin marks allowed a finer characterization of enhancers, whose chromatin features are highly cell-type specific (Heintzman et al., 2009). Indeed, "poised" enhancers found in mouse and human ESCs are marked by H3K4me1, H3K27me3 and PRC2 binding but lack H3K27ac, that is found only at active enhancers in a cell-type specific manner (Creyghton et al., 2010; Rada-Iglesias et al., 2011). These poised enhancers drive transcription activation of key developmental genes during differentiation, concomitantly with a loss of H3K27me3 and a gain of H3K27ac.

The integration and interpretation of many other genomic studies was also facilitated by collaborative efforts such as the ENCODE project that pools experimental datasets to make it a wide resource for a better comprehension of the organization and function of genomes in various organisms (ENCODE Project Consortium, 2004; Ho et al., 2014; Moore et al., 2020; The modENCODE Consortium et al., 2010). For instance, this allowed the generation of chromatin state maps in *Drosophila* and human cell lines mentioned in part I.C (Ernst and Kellis, 2010; Kharchenko et al., 2011). Chromatin state modeling was also recently performed on mouse fetal development at seven time points, integrating transcriptomes, profiling of eight histone marks, chromatin accessibility profiles and DNA methylation profiles from up to 12 different tissues (Gorkin et al., 2020; van der Velde et al., 2021). These very wide resources gave an overview of the tissue-specific and stage-specific changes of epigenomes and highlighted the predominant variations observed at enhancers and bivalent promoters. In *Drosophila*, integration of 300 ChIP-seq maps of chromatin marks and transcription factors at different stages of development also highlighted the dynamics of chromatin features at promoters and enhancers (Nègre et al., 2011).

Importantly, although these studies confirmed the idea that chromatin is broadly open in embryonic pluripotent stem cells and acquire restricted patterns of repressive marks during development, they especially improved the spatial and temporal resolution of these chromatin landscape changes during development, revealing intermediate states characterized by complex combinations of chromatin marks. These studies also enabled the prediction of new regulatory elements. Nevertheless, the dynamics of chromatin states during

development was mostly examined at regulatory elements such as enhancers, promoters, or heterochromatin and did not explore in detail the association of specific chromatin states with gene function. This alternative approach was used to describe the chromatin state changes during neural development in *Drosophila*, based on the DamID mapping of RNA Pol II, Brahma, Polycomb, HP1 and H1 in neural stem cells, larval immature neurons and adult mature neurons (Marshall and Brand, 2017). Using a HMM approach, the authors observed chromatin states similar to the five chromatin colors described in embryonic cells (Filion et al., 2010) and additional states reflecting "mixed" configurations with both active and repressive chromatin proteins ("TrxG mixed", "PcG mixed", "TrxG repressive"). This work revealed chromatin transitions associated with particular categories of genes upon differentiation. For instance, neural stem cell genes are silenced in the HP1-enriched chromatin in neurons while neuronal genes are found in the Black or TrxG repressive chromatin before transitioning to active states upon differentiation. Therefore, the authors propose the involvement of other chromatin states in gene regulation during development, beyond the view of the predominant role of PcG and TrxG proteins in cell fate acquisition (Marshall and Brand, 2017).

In summary, the complementarity of functional and descriptive studies provided strong evidence of chromatin remodeling occurring during development, in various organisms and tissues. While current research is still unravelling the relevance of chromatin state changes associated with cell differentiation during development, much less is known about such chromatin changes in the context of adult tissues.

II. B. Chromatin organization in adult tissues

Adult tissue homeostasis relies on resident adult stem cells, which are able to self-renew and differentiate into one or several cell types. The equilibrium between these two processes must be tightly regulated to avoid tumorigenesis, premature aging or impaired tissue function. In addition, the ability of adult stem cells to replenish a tissue after damage makes them a major therapeutic target in regenerative medicine (Ge and Fuchs, 2018). In the last 50 years, adult stem cells have been identified in many tissues in various model organisms using techniques such as cell transplantation and lineage tracing. Given the evidence of the role of chromatin organization and dynamics during cellular differentiation in the context of development, many questions emerged regarding the role of chromatin organization in adult

stem cell properties. What is the chromatin landscape of adult stem cells and their progeny? How does the chromatin landscape affect cell fate decisions? What are the consequences of disrupting chromatin regulators on tissue homeostasis? To answer these questions, the development of *in vivo* models is necessary to gain insights into the regulatory networks maintaining tissue homeostasis in physiological conditions and in response to environmental signals. The ability to target specific tissues and cell types without affecting development has been technically challenging, but the improvements of genetic and genomic tools now allow us to gain more insight into the roles of chromatin organization and function in adult stem cell lineages. Here, I will highlight recent findings about the functional roles of chromatin regulators in adult tissues, the genome-wide mapping of chromatin landscapes and the interrogations that remain to be addressed.

II.B.1. Functional roles of chromatin regulators in adult tissues

Several chromatin-associated factors have key roles in the regulation of gene expression and adult stem cell proliferation, maintenance or differentiation (Adam and Fuchs, 2016; Avgustinova and Benitah, 2016). In particular, genes impacting chromatin organization are frequently mutated in pathological contexts such as human tumors (Flavahan et al., 2017). Indeed, mutations in chromatin regulators can lead to oncogene activation or tumor suppressor silencing, thus driving tumor initiation or progression. For instance, mutations in SWI/SNF genes are found in ≈20% of human cancers (Kadoch et al., 2013). Other TrxG proteins such as the methyltransferase MLL1 are essential for mammalian hematopoietic stem cell self-renewal and lineage differentiation, with MLL1 depletion leading to bone marrow failure (Jude et al., 2007; McMahon et al., 2007). PcG proteins also have important roles in the hematopoietic system. Several lymphomas harbor gain of function mutations in EZH2, thus preventing differentiation of B cells (Kim and Roberts, 2016; Morin et al., 2010). On the other hand, inactivation of EZH2 can also cause misexpression of many genes and become tumorigenic in some contexts such as what is found in leukemias. The PRC1 subunit BMI1 promotes stem cell self-renewal in the hematopoietic system, the muscle and the mammary gland, notably via repression of cell cycle regulators (Jacobs et al., 1999; Park et al., 2003; Pietersen et al., 2008; Robson et al., 2011). In the adult mammalian brain, the chromatin remodeler Chd7 is required for neurogenesis (Feng et al., 2013) but also for the survival and differentiation of oligodendrocyte precursors (Marie et al., 2018). Overall, these and other

functional studies demonstrated the importance of various chromatin-associated factors in adult tissues. However, the effects of altering chromatin regulators depend strongly on the factor considered and vary from negligible defects to stem cell loss or premature differentiation (Avgustinova and Benitah, 2016). The mechanisms causing these phenotypes are still unclear and require a better identification of the chromatin organization and gene expression changes in these particular contexts.

II.B.2. Genome-wide chromatin landscapes of adult tissues

As in developmental contexts, genome-wide profiling of chromatin marks is required to better understand the chromatin landscape of adult stem cells and their progeny. Such studies using ChIP-seq of histone marks were carried out notably in the mouse epidermal and intestinal epithelia, which are fast-renewing tissues. Given the numerous phenotypes associated with perturbations of PcG and TrxG proteins in both embryonic and adult tissues, most studies initially focused on the profiling of H3K27me3 and H3K4me3 patterns. In hair follicle stem cells, H3K27me3 marks skin differentiation genes and key regulators of other tissues fate, whereas H3K4me3 marks stemness genes (Lien et al., 2011). Upon lineage commitment, differentiation genes lose H3K27me3 while stemness genes acquire this repressive mark (**Fig. 9**). PcG-target genes are upregulated upon depletion of PRC2 in the whole skin, but this does not drive premature differentiation (Ezhkova et al., 2011; Lien et al., 2011). Instead, hair follicle stem cell display hypoproliferation due to deregulation of cell cycle genes, as shown in the context of Bmi-1 loss in other adult tissues. In the adult intestine, stem cells and terminally differentiated cells display similar profiles of H3K27me3, and PRC2 has a limited role in silencing differentiation genes in intestinal stem cells (ISCs) (Jadhav et al., 2016). Moreover, the effects of H3K27me3 loss on gene expression seem to be more dependent on H3K4me3 levels at promoters that are co-occupied by this active mark (Jadhav et al., 2016, 2020). Another report identified changes in the distribution of H3K4me3, H3K27ac and histone variant H2A.Z upon ISC to enterocyte differentiation, including at genes whose expression is increased in enterocytes (Kazakevych et al., 2017).

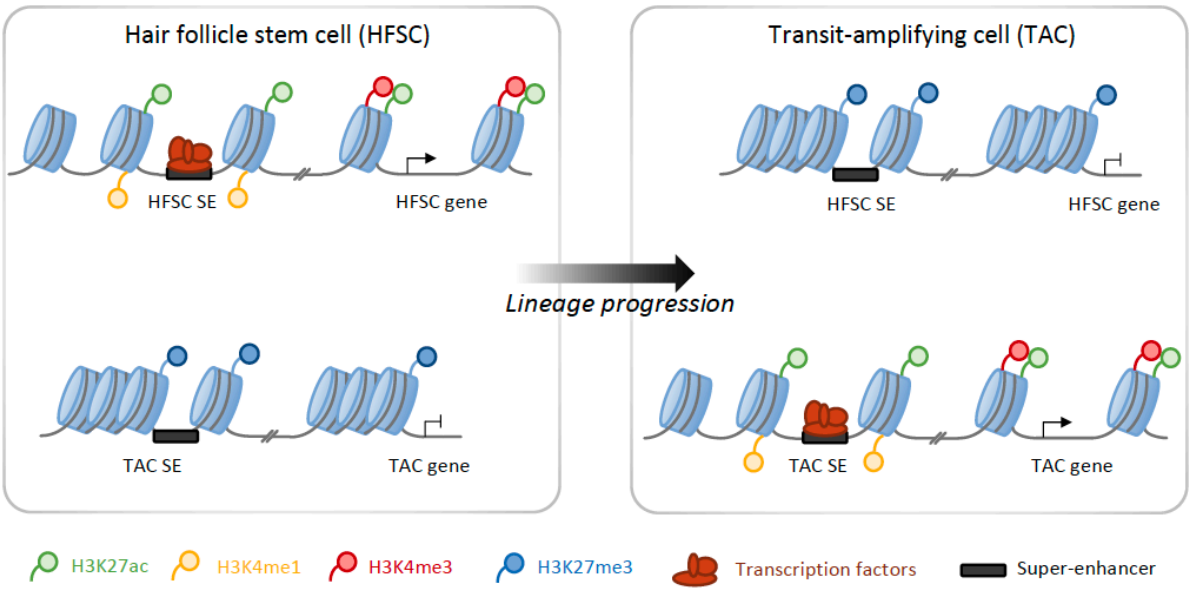

Figure 9. Model of chromatin remodeling during lineage progression in the adult hair follicle.
Summary of chromatin changes observed between adult hair follicle stem cells (HFSC) and their progeny, the transit-amplifying cells (TACs). Cell type-specific super-enhancers (SE) and promoters undergo chromatin changes upon lineage progression. HFSC SE lose H3K27ac and H3K4me1 and gain H3K27me3. HFSC genes lose H3K4me3 and gain H3K27me3 at their promoters. TAC SE and TAC genes undergo the reciprocal chromatin changes.

Other studies in the skin and intestine investigated the contribution of enhancers to cell identity in adult stem cells and their progeny. In particular, dense clusters of transcription factor binding sites called “super-enhancers” undergo chromatin changes upon lineage progression and in response to environmental cues in the hair follicle (**Fig. 9**) (Adam et al., 2015; Hnisz et al., 2013). More specifically, hair follicle stem cell super-enhancers lose H3K27ac and gain H3K27me3 in committed progenitors (TACs) and reciprocally, likely mediated by the pioneer factor SOX9. These and later findings highlighted an important regulatory role of cell type-specific enhancers, together with the combinatorial action of transcription factors, in governing lineage decisions in the hair follicle (Adam et al., 2015, 2020). In contrast, in the intestine, putative active enhancers defined by H3K4me2 and H3K27ac in progenitor cells of the enterocyte or secretory lineage show a large overlap and have similar chromatin accessibility (Kim et al., 2014). As these sites are also marked by H3K4me2 in intestinal stem cells, the authors suggested that the chromatin remains broadly permissive in stem cells and both types of committed progenitors, and that cell type

specification relies mostly on the binding of cell-type specific transcription factors at enhancers. Consistent with this, deletion of the secretory-specific transcription factor Atoh1 was sufficient to induce cell fate conversion towards the enterocyte lineage (Kim et al., 2014). However, later studies report that the secretory lineage has a chromatin landscape that significantly differs from that in the enterocyte lineage and in undifferentiated cells. In particular, secretory-specific enhancers were identified (Jadhav et al., 2017), and chromatin accessibility changes between intestinal stem cells, secretory cells and enterocytes were found at cell type-specific transcription factor binding sites (Raab et al., 2019). These conflicting studies can be explained partly by the technical challenge of isolating pure cell type-specific populations from the intestine.

Overall, these studies in the adult hair follicle and intestine highlighted the idea that chromatin regulators such as PcG proteins reinforce or stabilize cellular identity, whose establishment relies more on the chromatin state of enhancers and specific combinations of transcription factors. In addition, genome-wide mapping of chromatin marks enabled the prediction and validation of new regulatory elements controlling cell differentiation. However, several gaps remain to be filled to gain a better knowledge of chromatin states in adult tissues.

II.B.3. Gaps in the field

Here, I will present the main questions that have not been addressed yet in the descriptive and functional studies investigating chromatin regulation in adult tissues. First, only a subset of chromatin marks has been examined, thus hindering a more accurate description of the global chromatin landscape in adult stem cells and their progeny. As explained in part I.C, chromatin state modeling taking into account combinations of chromatin marks can overcome this limitation. Chromatin state modeling in the *Drosophila* developing brain suggested previously uncharacterized contributions of HP1-enriched chromatin and H1-enriched Black chromatin to the regulation of neural stem cell differentiation (Marshall and Brand, 2017). Therefore, it is possible that these chromatin states have similar roles in adult stem cell lineages. Moreover, recent studies revealed roles of Histone H1 in adult hematopoietic cells (Willcockson et al., 2020; Yusufova et al., 2021). H1 mutations are frequent in B cell lymphomas, where chromatin decompaction causes derepression of stem cell genes (Yusufova et al., 2021). These findings reinforce the interest of exploring the function of various chromatin-associated proteins in specific cell types.

A second limitation in the description of chromatin states in adult lineages is the difficulty to isolate specific cell types, due to the lack of cell-type specific markers or to the limited amount or certain populations of cells. Previous studies integrating numerous chromatin marks in the frame of the ENCODE project allowed the identification of chromatin state differences between tissues, but similar characterization within each particular lineage is missing. Mapping chromatin states in one type of adult stem cell and in its progeny would give more insight into the process of stem cell differentiation in this homeostatic context. Recently developed single-cell approaches, such as single-cell ChIP-seq or single-cell CUT&Tag, are also likely to address this question (Grosselin et al., 2019; Kaya-Okur et al., 2019). Furthermore, there is growing evidence that chromatin remodeling plays key roles in response to injury in adult tissues (Adam and Fuchs, 2016; Saxena and Shivdasani, 2020). Therefore, an accurate characterization of chromatin states could also allow a better understanding of the mechanisms underlying plasticity of adult stem cells and differentiated cells.

Finally, descriptive and functional studies need to be combined to better understand the role of chromatin organization and dynamics in adult tissues. In particular, to what extent chromatin states are instructive in the regulation of gene expression and subsequent cellular processes remains unclear, as exemplified by the variety of phenotypes associated with the loss of PcG proteins.

Therefore, my thesis aimed to characterize chromatin states in stem cells and their progeny *in vivo* in an adult homeostatic tissue. To achieve this objective, I used the *Drosophila* adult intestine as a model, that I present hereafter.

III. The *Drosophila* intestinal lineage: a model to study chromatin organization in an adult tissue

III. A. A powerful *in vivo* model to study adult stem cell biology

Drosophila has always been an important model organism for genetic studies, as it enabled breakthrough discoveries in many biological processes, from embryonic development to organ physiology. In particular, the *Drosophila* intestine is a simple system where properties of adult tissues can be investigated. Both in mammals and in *Drosophila*, lineage tracing studies demonstrated that the intestine is a constantly self-renewing tissue that can regenerate rapidly in response to environmental cues such as physical, chemical, or infectious stress due to activity of intestinal stem cells (Barker et al., 2007; Gervais and Bardin, 2017; Micchelli and Perrimon, 2006; Ohlstein and Spradling, 2006). The *Drosophila* intestine is composed of the foregut, midgut and hindgut, from anterior to posterior. Most focus has been done on the midgut, which is the equivalent of the mammalian small intestine. It has a simple structure, contains several thousands of intestinal stem cells (ISCs) and is suitable for the use of a wide range of genetic tools. Therefore, the Bardin lab has been using the *Drosophila* midgut as an *in vivo* model to study the cellular biology of adult stem cells and how they ensure tissue homeostasis.

III. B. Structure and cell type composition of the *Drosophila* midgut

III.B.1. General structure of the midgut

The *Drosophila* midgut is composed of a pseudostratified epithelium surrounded by visceral muscles, enteric neurons and trachea. The midgut is compartmentalized into six major regions (R0-R6) that differ in terms of morphology, function, and genetic properties (Buchon et al., 2013; Marianes and Spradling, 2013). For instance, the middle R3 region is acidic, it contains specialized copper cells, and expresses specific subsets of genes involved in digestion.

III.B.2. Cell types of the midgut

The midgut epithelium is maintained by ISCs, which are scattered along the basal surface (Micchelli and Perrimon, 2006; Ohlstein and Spradling, 2006). ISCs are multipotent and mostly divide asymmetrically to self-renew and give rise to two types of precursor cells, the enteroblasts (EBs) or the enteroendocrine precursors (EEP) (**Fig. 10**). Unlike the transit-

amplifying progenitors present in the mammalian ISC lineage, EBs do not proliferate but directly differentiate into enterocytes (ECs). EEPs divide once and differentiate to generate the second type of differentiated cells of the midgut, the enteroendocrine cells (EEs) (Chen et al., 2018b; He et al., 2018; Zeng and Hou, 2015). ECs are large polyploid cells that represent ~80% of intestinal differentiated cells and whose primary function is to absorb and metabolize nutrients. EEs are diploid cells with small nuclei and have multiple roles such as peptide hormone secretion and nutritional status sensing (Amcheslavsky et al., 2014a; Scopelliti et al., 2014).

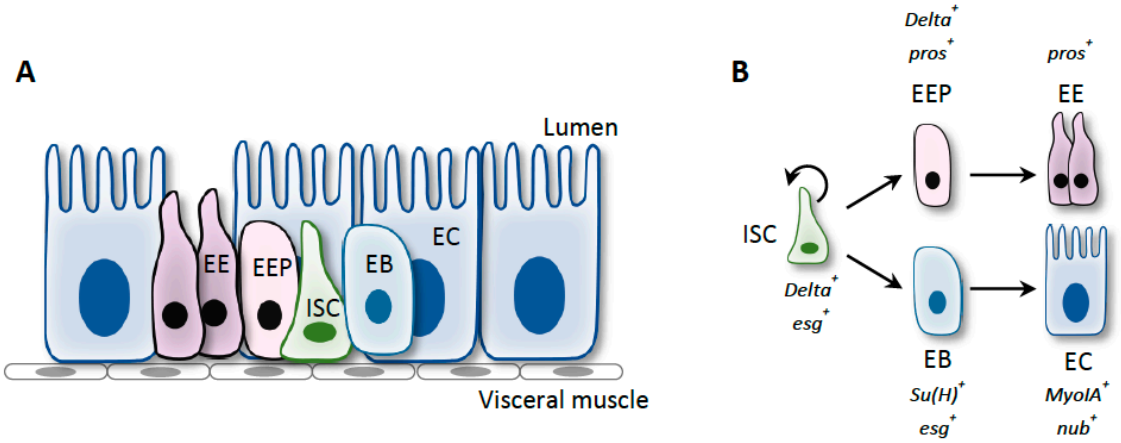

Figure 10. Organization and lineage of the *Drosophila* midgut epithelium.
A: Organization of the midgut epithelium. **B**: Cell types of the midgut with their specific markers (in italic). ISCs divide asymmetrically, giving rise to one ISC (self-renewal) and one EB or EEP. EBs differentiate into ECs. EEPs divide to give rise to EEs. ISC: intestinal stem cell, EB: enteroblast, EC: enterocyte, EEP; enteroendocrine precursor, EE: enteroendocrine cell.

Cell-type specific markers allowed a finer characterization of these cell types, notably based on their transcriptome and on their localization in the midgut. Bulk RNA-seq on FACS-sorted populations of cell types gave more insights into the gene expression differences between ISCs, EBs, ECs and EEs (Dutta et al., 2015). Genes highly expressed in ISCs are enriched for functions related to the cell cycle and stem cell proliferation, EE-high genes encode components of neuropeptide signaling pathways, and EC-high genes comprise digestive enzymes such as serine endopeptidases and proteases. Comparison of transcription levels between cell types also identified new markers and candidates for cell-type specific functions (Dutta et al., 2015). Region-specific bulk RNA-seq further revealed differences in the transcriptomes of each cell type depending on the region, consistently with previously reported differences in the properties and abundance of ISCs along the midgut (Marianes and

Spradling, 2013). Nevertheless, the main cell types described above are found throughout all the midgut, with the same general properties.

The recent advances in single-cell technologies were used to better define the diversity of midgut cell types (Guo et al., 2019; Hung et al., 2020). Gene expression profiling of individual cells revealed that ECs and EEs cluster into distinct subtypes characterized by specific gene signatures and regional differences (Hung et al., 2020). For instance, ECs can be distinguished based on the type of metabolic and immune genes that they express, while EE subtypes differ by the expression of distinct combinations of hormone peptides. EE diversity was further explored in a single-cell study focused on EEs only, shedding light on the combinations of peptide hormones that define 10 EE subtypes (Guo et al., 2019). These EE subtypes are spatially restricted along the midgut and specified by 14 transcription factors that form a "TF combinatorial code" (Guo et al., 2019). These two single-cell transcriptome studies also identified new transcription factors regulating the acquisition of cell identity of midgut cell types and subtypes, based on their enrichment in particular clusters or on the presence of binding sites in the regulatory regions of the genes defining the cellular subtypes. In addition, these datasets identified the molecular markers of intermediate states of EE and EC differentiation. I will detail in the section below insights from these papers and a previous body of literature on the regulation of cell fate decisions in the intestinal lineage.

III. C. Control of cell fate decisions and ISC activity in the *Drosophila* midgut

III.C.1. Cell fate decisions in the intestinal lineage

How are the different cell types specified and maintained in the intestinal lineage? Primary lineage decisions depend strongly on Notch signaling, a conserved pathway involved in multiple cell differentiation processes during development and in adult tissues including the mouse and zebrafish intestines (Fre et al., 2011). Loss of *Notch* in ISCs causes ISC and EE accumulation, showing that Notch signaling is required to limit ISC proliferation, inhibits EE fate acquisition, and promotes the EC fate (Micchelli and Perrimon, 2006; Ohlstein and Spradling, 2006). The Notch ligand Delta is expressed in ISCs, and high levels of Notch signaling in EBs after stem cell division promotes the EC fate through activation of Notch targets including the bHLH E(spl) transcription factors (**Fig. 11**) (Bardin et al., 2010). While it was initially proposed that low Notch levels in EB would promote the EE fate (Guo and Ohlstein, 2015), immunostainings and single-cell analyses have given evidence for the existence of

enteroendocrine precursor cells (EEPs) expressing both *Delta* and *prospero*, a marker of EEs (Chen et al., 2018b; He et al., 2018; Hung et al., 2020; Zeng and Hou, 2015). The current proposed model is that ISCs are likely primed towards either the EC or EE fate, by low *Notch* expression or *scute* expression, respectively (Boumard and Bardin, 2021). However, the precise mechanisms underlying ISC priming towards different cell fates remains not fully elucidated.

Beyond the role of Notch/Delta signaling in early cell fate decisions, many functional studies identified transcription factors and some examples of post-transcriptional regulation involved in terminal cell differentiation of ECs and EEs (**Fig. 11**). For instance, EB-specific expression of *klumpfuss* (*klu*) maintains the EC fate by repressing EE fate genes (Hung et al., 2020; Korzelius et al., 2019). In addition, *Sox100B* and its downstream target *Sox21a* promote EB differentiation to EC, notably by upregulating the EC marker *nubbin* (*nub/Pdm1*) in homeostasis or during tissue repair after injury (Chen et al., 2016; Jin et al., 2020; Meng et al., 2020; Zhai et al., 2015, 2017). The transcription factor GATAe also acts downstream of Sox21a to regulate EB differentiation (Okumura et al., 2016; Zhai et al., 2017). Interestingly, EBs can delay their terminal differentiation into ECs depending on local cues and Notch signaling. While the transcription factor Escargot (Esg) prevents EC differentiation, the zinc finger transcription factor Zfh2 supports the growth and morphological changes that accompany EB activation, and expression of the microRNA *miR-8* can trigger terminal differentiation to EC (Antonello et al., 2015; Korzelius et al., 2014; Villa et al., 2019). Another level of regulation was observed in ISCs and EBs with the finding of P-bodies that prevent mRNAs of lowly transcribed differentiation genes such as *nubbin* to be translated, in order to maintain progenitors (Buddika et al., 2021).

As previously mentioned, *scute* plays a role in priming ISCs towards the EE fate. A positive feedback loop involving the protein Phyllopod (Phyl) promotes *scute* expression which in turn controls *prospero* expression that induces EE differentiation (Li et al., 2017; Yin and Xi, 2018). In addition, other factors have been shown to influence this process. For example, Numb is required for EE differentiation through inhibition of Notch signaling (Sallé et al., 2017). The ion channel Piezo, expressed in EEPs, regulates EE differentiation through mechanical sensing and regulation of calcium levels (He et al., 2018). Finally, Slit/Robo signaling negatively regulates EE fate commitment (Biteau and Jasper, 2014). The single-cell transcriptome analysis of EEs previously mentioned also better characterized the EE subtype

specification into two major EE classes upon EEP division and terminal differentiation (Guo et al., 2019). Class I EEs expressing Allatostatin C (AstC) rely on *Ptx1* whereas class II EEs expressing Tachykinin (Tk) are specified by *mirror*, and Notch signaling in EEPs is required for this cell fate decision.

In summary, cell fate decisions in the intestinal lineage are controlled by the Notch signaling pathway and a set of transcription factors as well as post-transcriptional regulation.

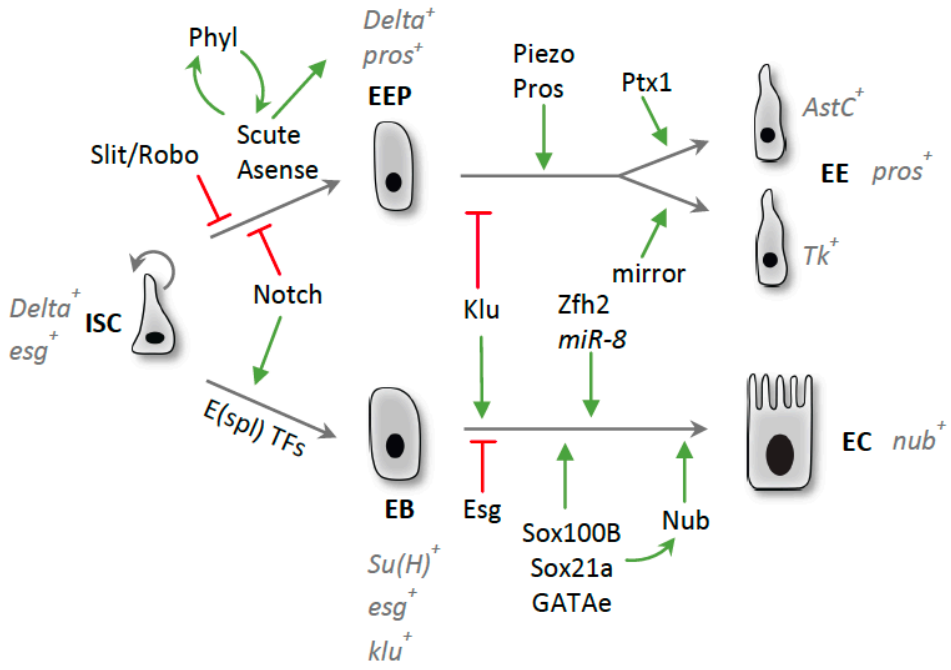

Figure 11. Control of cell fate decisions in the intestinal lineage.
Here are shown the main transcripton factors and signaling pathways regulating ISC differentiation towards the EE or EC lineage. See details in the text.

III.C.2. Control of ISC activity

The identification of ISCs in the *Drosophila* midgut was followed by many functional studies focused on the intrinsic and extrinsic signals that control ISC proliferation and differentiation, both in homeostasis and in response to various stress conditions. The EGFR and Jak-Stat pathways are responsible for the main mitogenic signals inducing ISC division during homeostasis and upon injury (Biteau and Jasper, 2011; Buchon et al., 2010; Jiang et al., 2009). Additional signaling pathways such as Hippo, BMP, Wnt/Wg, Hedgehog and JNK control proliferation and differentiation in stress conditions or during aging (Gervais and Bardin, 2017; Jiang et al., 2016; Miguel-Aliaga et al., 2018). Interaction between all these pathways is not well understood but several reports reveal that they can have common targets such as the transcription factors Sox100B, Sox21a, dMyc, Fos and genes involved in cell cycle and cell

growth, as they are upregulated during tissue regeneration (Biteau and Jasper, 2011; Jin et al., 2020; Meng and Biteau, 2015; Ren et al., 2013). Other transcription factors play key roles in the regulation of ISC stem cell maintenance and proliferation. During homeostasis, Hairless and Daughterless maintain ISC fate through interplay with Notch target genes (Bardin et al., 2010). Escargot also maintains stemness by repressing differentiation genes (Korzelius et al., 2014). Sox100B, Sox21a and Ets21c act downstream of various pathways to promote ISC proliferation after stress (Jin et al., 2020; Meng and Biteau, 2015; Mundorf et al., 2019). In contrast, Lola restricts ISC proliferation downstream of the Hippo/Wts pathway by repressing mitotic genes (Hao et al., 2020). Other types of factors like the RNA-binding protein Spen and the adenosine receptor (AdoR) also regulate ISC proliferation (Andriatsilavo et al., 2018; Xu et al., 2020). In addition, non-autonomous signals coming from intestinal cells or from other tissues such as hormones, reactive oxygen species and septate junctions modulate ISC proliferation (reviewed in (Boumard and Bardin, 2021)). Overall, midgut homeostasis requires a precise regulation of ISC activity and cell fate acquisition. This implies multiple transcription factors and signaling pathways, which are activated in response to tissue needs.

III. D. A good model to study chromatin organization

The regulation of ISC activity has been described mostly at the transcriptional level. In contrast, the role of chromatin organization in this lineage remains to be addressed. However, several chromatin-modifying proteins were shown to be involved in ISC activity and cell fate decisions or maintenance of cell identity (**Fig. 12**).

III.D.1. Chromatin factors involved in ISC activity

The protein Scrawny, a H2B ubiquitin protease, was shown to be required for the maintenance of ISCs (Buszczak et al., 2009). In particular, *scny* mutations cause loss of ISCs in the midgut, likely due to an upregulation of Notch target genes leading to premature differentiation. Two components of the SWI/SNF complex, Osa and Brahma, play various roles in the lineage. Osa binds to the promoters of *Delta* and *asense* to promote differentiation into ECs and EEs, respectively (Zeng et al., 2013). Brahma is required for EC differentiation, but also for ISC proliferation in both normal conditions and during stress-induced regeneration (Jin et al., 2013). One study showed that Atac2, a component of a histone acetyltransferase complex, promotes ISC differentiation (Ma et al., 2013). Another HAT subunit, Nipped-A, regulates

global acetylation levels in ISCs and maintains their proliferation during aging and in response to damage (Tauc et al., 2017). Moreover, a role for the zinc-finger protein Charlatan (Chn) in maintaining ISC division was reported, where *chn* knockdown also affects HP1 nuclear distribution and H3 acetylation levels (Amcheslavsky et al., 2014b). It was proposed that Chn maintains a chromatin structure in ISCs compatible with cell division. Furthermore, through a genetic screen, our lab has also identified the conserved chromatin remodeler Kismet/CHD7/CHD8 and the histone methyltransferase Trr/MLL3/4 as regulators of ISC proliferation (Gervais et al., 2019). More details are presented in Chapter 2 of the Results section. Finally, a recent study suggested a role for PcG proteins in priming progenitors towards the EE fate, as *Polycomb* or *E(z)* knockdown cause reduced commitment to the EE lineage (Tauc et al., 2021). Thus, these findings show that chromatin factors with distinct functions in chromatin structure are important for the *Drosophila* intestinal homeostasis.

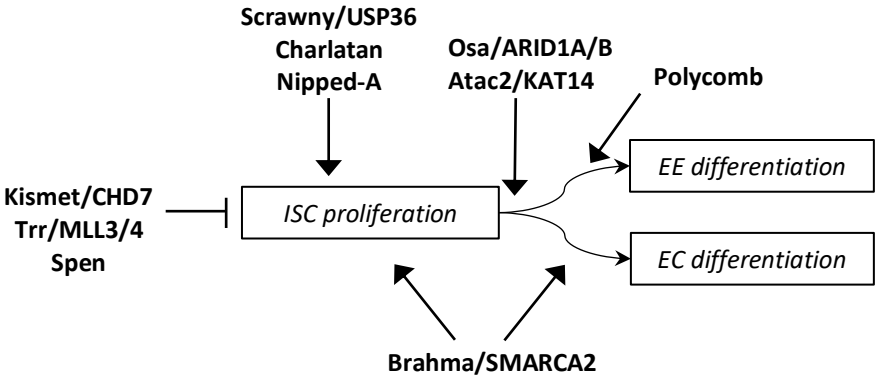

Figure 12. Summary of the action of chromatin-associated factors on ISC proliferation and differentiation. See details in the text.

III.D.2. Chromatin organization in midgut differentiated cells

Recent studies shed light on the role of chromatin organization in preserving EC identity. First, the transcription factor Hey maintains the nuclear organization of EC through regulation of nuclear lamins (Flint Brodsly et al., 2019). Upon Hey inactivation in ECs, *nubbin* expression is reduced while the ISC marker *Delta* is ectopically expressed, and the global EC gene signature is downregulated. Moreover, the EC nuclear organization is impaired and the expression of the EC-specific lamin, LamC, is reduced while the ISC-enriched LamDm0 levels are increased, which likely mediate the transcriptional changes causing loss of EC identity. Similarly, the Nonstop identity complex (NIC) including a deubiquitinase safeguards EC

identity by maintaining an EC gene signature, likely through promoting chromatin accessibility at these genes (Erez et al., 2021).

Therefore, the chromatin organization in differentiated ECs seems important to preserve their identity. As ECs are polyploid cells, it is possible that their chromatin organization is established and maintained through mechanisms specific for polyploid cells, which would explain why depletion of Hey and NIC do not affect EE identity in these two studies. Further work will be needed to decipher the precise mechanisms underlying these phenotypes and to determine if other factors could play similar roles in the maintenance of EE chromatin organization and identity.

III.D.3. The need for a genome-wide characterization of chromatin organization in the intestinal lineage

Overall, the specific phenotypes observed upon depletion of several chromatin-associated factors in the midgut highlight their importance in the regulation of the intestinal lineage and demonstrate that the midgut is a very good model to investigate the role of chromatin organization *in vivo* in an adult tissue. In addition, profiling of chromatin accessibility using CATaDa in ISCs, EBs and ECs revealed chromatin remodeling upon ISC to EC differentiation (Aughey et al., 2018). However, an integrated view of how chromatin factors change the chromatin organization and affect the transcription of specific genes is lacking. Moreover, chromatin factors can mediate chromatin changes widely over the genome, and they often act in concert, which makes the interpretation of their specific roles difficult in functional studies. Therefore, in my PhD I explored the chromatin landscape of the intestinal lineage more globally, by characterizing chromatin states at the genome-wide scale.

IV. Objectives of my PhD

In this introduction, I covered the large principles of chromatin organization and how it changes during development. Chromatin state changes during development have been explored in various systems and is still an active field of research. However, there is a lack of knowledge about chromatin states in adult tissues. Recent studies gave some insight into chromatin changes associated with lineage specification in homeostasis but there is no

description of cell-type specific chromatin states at the genome-wide scale. Therefore, in my PhD I had three main objectives:

1. Define chromatin organization in adult stem cells and their progeny.
2. Determine the chromatin state transitions associated with stem cell differentiation.
3. Test the relevance of chromatin state changes on lineage specification and cell state.

I tackled these aims by determining the cell-type specific genome-wide binding of 5 chromatin-associated proteins in ISCs, EBs, ECs and EEs, followed by chromatin state modeling using an HMM approach. This allowed me to determine the chromatin state changes occurring upon differentiation and gave a better understanding of the regulation of cell type specification in the lineage. Then, I tested the biological relevance of these chromatin states by using functional genetics and genomics to investigate the consequences of depleting H1 and HP1 proteins. These results are presented in Chapter 1 and partly in Chapter 2. I also performed genetic experiments to test the role of candidate factors in the regulation of the intestinal lineage, presented in Chapter 3.

RESULTS

Overview

I will present the Results in three chapters. The **first chapter** is the main work of my PhD that will be used as a basis for a paper to submit soon. The **second chapter** is a paper published in 2019 (Gervais et al., 2019) to which I contributed with the results obtained during my Master 2 internship and the beginning of my PhD. The **third chapter** presents part of the work I did during my PhD but will not go into a paper. In this part I explored the role of candidate genes in the intestinal lineage, selected based on results that I obtained in the second chapter.

Chapter 1: Chromatin state transitions in the *Drosophila* intestinal lineage reveals principles of cell type specification

In this Chapter, I will present the main results of my PhD work. In this part, I defined and characterized chromatin states in the intestinal lineage, and then studied the chromatin state transitions occurring during differentiation. Moreover, I investigated the roles of HP1 and H1 in ISCs/EBs on chromatin accessibility, transcription and tissue homeostasis.

These results are the outcome of a collaborative effort between Louis Gervais, Natalia Rubanova and myself. Louis Gervais made an important contribution on this work. In particular, we worked together on the validation of chromatin state modeling and he helped with the characterization of chromatin states. He also performed the CATaDa analyses based on the DamID data I generated. He carried out the ATAC-seq experiments and did the subsequent bio-informatic analyses. Finally, he also performed part of the genetic experiments on H1 and HP1. Natalia Rubanova, bio-informatician in the team, performed the chromatin state modeling, based on scripts developed by our collaborator Owen Marshall. She adapted and improved part of the scripts and carried out additional analyses not presented in this work but which helped to validate the output of our modeling.

Chromatin state transitions in the *Drosophila* intestinal lineage reveals principles of cell type specification

Manon Josserand[1], Natalia Rubanova[1], Marine Stefanutti[1], Virginie Raynal[2], Owen Marshall[3], Nicolas Servant[4], Louis Gervais[1], Allison J. Bardin[1].

[1] Institut Curie, PSL Research University, CNRS UMR 3215, INSERM U934, Stem Cells and Tissue Homeostasis Group, 75248 Paris, France.

[2] ICGex Next-Generation Sequencing platform, Institut Curie, PSL Research University, 75005 Paris, France.

[3] Menzies Institute for Medical Research, University of Tasmania, Australia

[4] Institut Curie Bioinformatics core facility, PSL Research University, INSERM U900, MINES ParisTech, Paris 75005, France.

INTRODUCTION

Adult stem cells ensure tissue homeostasis through self-renewal and differentiation into the resident cell types of a tissue. Understanding the regulation of adult stem cell activity is crucial to have a better comprehension of uncontrolled proliferation and altered differentiation mechanisms occurring during tumorigenesis and age-dependent functional decline of tissues. Growing evidence supports the importance of chromatin organization in the regulation of adult stem cell proliferation, maintenance or differentiation (Avgustinova and Benitah, 2016). Accordingly, genes impacting chromatin organization are frequently mutated in pathological contexts such as human tumors (Flavahan et al., 2017). Studies in embryonic stem cells and in various *in vivo* developmental contexts have extensively described the roles of chromatin-associated factors in stem cells and development (Gaspar-Maia et al., 2011; Ho and Crabtree, 2010; Meshorer and Misteli, 2006). In addition, genome-wide profiling of histone modifications and chromatin accessibility greatly improved our understanding of the chromatin remodeling occurring during development (Argelaguet et al., 2019; Mikkelsen et al., 2007; Wu et al., 2016). Indeed, distinct chromatin states are established during cell lineage differentiation and act to limit the developmental potential of differentiated cells. However, the chromatin changes associated with stem cell differentiation during tissue homeostasis remain poorly elucidated.

Here, we use the *Drosophila* adult intestine (midgut) as a model to address this question. The midgut is a constantly self-renewing tissue that can regenerate rapidly in response to

environmental cues due to activity of intestinal stem cells (ISCs) (Gervais and Bardin, 2017; Jiang et al., 2016; Micchelli and Perrimon, 2006; Ohlstein and Spradling, 2006). ISC divisions can give rise to two types of intermediate progenitors, the enteroblasts (EBs) or the enteroendocrine precursors (EEPs) (**Fig. 1A**). EBs differentiate into enterocytes (ECs), while EEPs divide and differentiate to produce enteroendocrine cells (EEs). While *Drosophila* intestinal lineage has been widely used to study the regulation of stem cell proliferation and cell fate specification at the transcriptional level (Boumard and Bardin, 2021), less is known about the chromatin organization of ISCs and their progeny. We and others have provided evidence of roles of conserved chromatin factors in controlling ISC proliferation and differentiation, highlighting their importance in the regulation of the intestinal lineage (Amcheslavsky et al., 2014b; Andriatsilavo et al., 2018; Buszczak et al., 2009; Erez et al., 2021; Flint Brodsly et al., 2019; Gervais et al., 2019; Jin et al., 2013; Ma et al., 2013; Tauc et al., 2017, 2021; Zeng et al., 2013). Despite these studies, an understanding of the chromatin organization in the lineage at the genome-wide scale is lacking.

Chromatin studies in adult tissues such as the mouse intestine and skin have focused on profiling a subset of chromatin associated marks, including the histone modifications H3K27me3, H3K4me, and H3K27ac. These studies notably highlighted chromatin changes at enhancers during cell type specification (Adam et al., 2015; Jadhav et al., 2016, 2017; Kazakevych et al., 2017; Lien et al., 2011; Raab et al., 2019). However, it became evident in the last ten years that chromatin states are defined by the combinations of multiple chromatin marks, beyond the classical view of euchromatin and heterochromatin. In the last ten years, chromatin state modeling approaches allowed a more accurate description of chromatin landscapes in various genomes, including those of humans and flies (Ernst and Kellis, 2010; Filion et al., 2010; Ho et al., 2014; Kharchenko et al., 2011). In *Drosophila* cultured cells, a model of five main chromatin types was described based on the combinations of the binding profiles of 53 chromatin-associated proteins (Filion et al., 2010). Chromatin state modeling is now used to better characterize chromatin remodeling during development by integrating genome-wide maps of chromatin features across developmental stages in various tissues (Gorkin et al., 2020; Marshall and Brand, 2017; Nègre et al., 2011; van der Velde et al., 2021). However, combinatorial chromatin states have not been described in adult stem cells and their progeny. Here, we take advantage of the well-characterized *Drosophila* intestinal lineage to profile in a cell-type specific manner the binding sites of five chromatin-associated proteins

that are representative of the previously described five major types of chromatin (Filion et al., 2010): RNA Pol II and Brahma for active chromatin states, Polycomb, HP1a and H1 for repressive chromatin states. Subsequent cell type-specific chromatin state modeling allowed us to identify the chromatin state transitions associated with cell type specification during tissue homeostasis, thus revealing principles of cell type specification in this adult tissue. We further explored the effect of genetic perturbation of HP1 and H1 on chromatin accessibility, transcription and tissue homeostasis and uncovered a role for H1 in priming ISCs towards the EE fate.

RESULTS

Cell-type specific profiling of chromatin-associated factors in intestinal stem cells and their progeny

Functional studies of chromatin-associated factors demonstrated the importance of chromatin organization in the adult *Drosophila* intestinal lineage, but a genome-wide understanding of cell type-specific chromatin states is lacking so far. In order to characterize chromatin states in adult intestinal stem cells and their progeny in the context of homeostasis, we generated whole-genome binding maps for the core subunit of RNA Polymerase II, Brahma, Polycomb, HP1a (hereafter referred to as HP1) and Histone H1 in ISCs, EBs, EEs, and ECs. To do so, we used the Targeted DamID technique that results in GAL4 driven low-level expression of transgenic Dam lines (Marshall et al., 2016; Southall et al., 2013). Cell type-specific expression of previously generated UAS-Dam constructs (Marshall and Brand, 2017) was achieved using well-known specific drivers for midgut cell types (**Fig. 1A-C**).

Overall, the binding profiles of the 5 proteins had general features conserved in all midgut cell types and consistent with their properties in other tissues (**Fig. 1D-E, S1A-C**). At the whole-genome scale, HP1 was found to be highly enriched around centromeres and on chromosome 4, known to be heterochromatic (**Fig. 1D, S1A**). In addition, Polycomb was enriched at *Hox* gene clusters, consistently with these genes being silenced by Polycomb Group proteins (**Fig. 1E**). RNA Pol II and Brahma were enriched at 5'UTRs (**Fig. S1B**), mostly bound to actively transcribed regions of the genome and negatively correlated with H1, which was found at silent genes (**Fig S1B-C**).

Despite a global similarity of the binding patterns of the 5 proteins across intestinal cell types, significant differences existed at specific regions and at the gene-scale. In particular, we

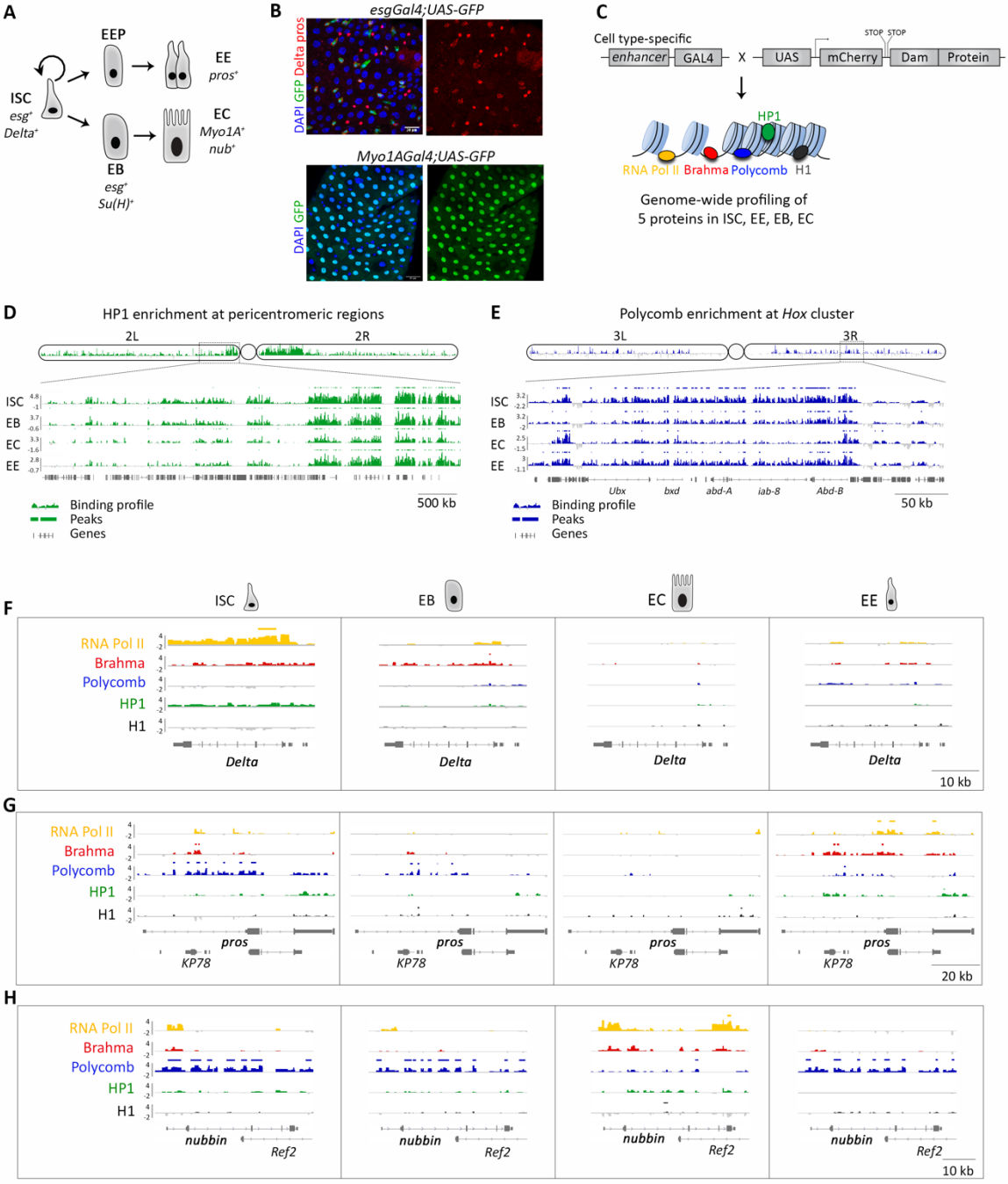

Figure 1. Cell-type specific profiling of chromatin-associated factors in the intestinal lineage.
A. Cell types of the intestinal lineage and their specific markers (in italic). ISCs divide asymmetrically, giving rise to one ISC (self-renewal) and one EB or EEP. The EBs differentiates into an EC, the EEP divides to produce two EEs. **B.** Representatives images of midguts. Top: GFP staining marks esg+ ISCs and EBs, Delta marks ISCs only (cytosplamic red), pros marks EEs (nuclear red). Bottom: GFP staining marks Myo1A+ ECs. Nuclei are stained with DAPI. Scale bars: 20 µm. **C.** Experimental setup of Targetd DamID. Flies with cell type-specific drivers were crossed with flies carrying a Dam-Protein fusion transgene to allow the genome-wide profiling of chromatin proteins in ISC, EE, EB, and EC. **D.** Overview of HP1 DamID binding profile on chromosome 2 in ISCs. The framed region shows HP1 enrichment (profile and significant peaks) in a pericentromeric region in the four cell types. **E**. Overview of Polycomb DamID binding profile on chromosome 3 in ISCs. The framed region shows Polycomb enrichment (profile and significant peaks) at *Hox* genes region in the four cell types. **F-H**: DamID binding profiles and significant peaks of RNA Pol II, Brahma, Polycomb, HP1 and H1 in the four cell types at cell type specific-genes: *Delta* for ISCs (**F**), *pros* for EEs (**G**), *nubbin* for ECs (**H**).

examined the chromatin environment of genes known to be important for stem cell maintenance or differentiation in the intestinal lineage. Consistent with the known ISC-specific expression of *Delta*, ISCs, but not other cells in the lineage showed RNA Pol II binding throughout *Delta*, which also had some Brahma and HP1 binding in ISCs (**Fig 1F**). The EE-specific gene, *prospero,* was bound by the repressive Polycomb protein in ISCs and became significantly marked by RNA Pol II and Brahma in EEs (**Fig. 1G**). Similarly, the EC-specific gene *nubbin (Pdm1)* had Polycomb enrichment in ISCs, kept many peaks of Polycomb in EBs and EEs, and lost most of Polycomb binding in ECs accompanied with expansion of RNA Pol II and Brahma binding (**Fig. 1H**). Therefore, these examples of stem cell and lineage genes displayed combinations of proteins that varied between cell types, suggesting transitions in the chromatin organization at specific genes upon differentiation, as illustrated by different combinations of chromatin-associated factors.

Chromatin state modeling allows a genome-wide characterization of seven major chromatin states in the midgut

Next, we wanted to better understand the chromatin changes associated with adult stem cell differentiation by comparing the chromatin organization in ISCs and in their progeny. In particular, we aimed to identify the main chromatin state transitions occurring upon intestinal stem cell lineage differentiation and the genes undergoing these transitions in order to gain insight into the regulatory programs that maintain tissue homeostasis. Cell-type specific chromatin states in adult tissues undergoing homeostatic renewal have been addressed by examining either chromatin accessibility, such as in the mammalian hematopoietic system (Martin et al., 2021), or common histone marks (H3K4me2/3, H3K27ac, H3K27me3) like in the mouse skin and intestine (Jadhav et al., 2016, 2017; Kim et al., 2014; Lien et al., 2011). However, to our knowledge, chromatin state modeling integrating combinations of different epigenetic marks was done only in cultured cell lines or in contexts of development, not in a homeostatic adult tissue.

We thus defined genome-wide chromatin states by using Hidden Markov Modelling (HMM) to capture the diversity of the observed protein binding combinations obtained by Targeted DamID. For each cell type, a 35-state HMM was fit, in which the 35 states further clustered into seven major groups that separated into distinct regions in PCA space (**Fig. 2A-B**). These seven major chromatin states recapitulating the data in ISCs, EBs, EEs and ECs,

named as seven colors, were used for further analyses (**Fig. 2C**). Genome-wide maps of chromatin states were then generated (**Fig. 2D, Fig S2A**).

We identified two distinct active states similar to the previously described Yellow and Red chromatin types (Filion et al., 2010). The Yellow state was enriched in RNA Pol II binding but also showed Brahma and HP1 binding, though was strongly depleted for Polycomb and H1 (**Fig. 2A**). The Red state was more enriched in Brahma and also frequently included HP1 and Polycomb binding. The model detected the three repressive states defined in (Filion et al., 2010), here named as the Blue Repressive (BlueR), Green and Black states enriched in Polycomb, HP1 and H1 binding respectively (**Fig. 2A**). In addition to these five states, our model detected two states that we defined as "intermediate", as they displayed features of both active or repressive chromatin states. First, there was another Polycomb-enriched state that was also defined by RNA Pol II and Brahma binding, hence named "Blue Mixed" (BlueM) (**Fig. 2A**). Second, we identified the "Yellow Weak" state that was similar to the Yellow state in terms of genomic coverage (**Fig. 2E, S2B**) and depletion of Polycomb binding (**Fig. 2A**), but with a much lower enrichment of RNA Pol II binding. Therefore, the HMM approach provided an accurate description of the combinatorial patterns that define the seven major chromatin states.

Chromatin state genomic coverage

In order to better define these seven chromatin states in midgut cell types, we examined the distribution of chromatin states at genomic features, which was globally similar between the cell types (**Fig. 2E, S2B**). Even though the Yellow and Red states were both enriched in 5'UTRs, the Yellow chromatin was predominantly enriched at exons and 3'UTRs whereas the Red chromatin was enriched at introns. Strikingly, 60% of the YellowW state was found at exons, a feature known to be associated with H3K36me3 and the Yellow chromatin as initially described (Delandre and Marshall, 2019; Filion et al., 2010; Kharchenko et al., 2011; Kolasinska-Zwierz et al., 2009). In contrast, the BlueR, Green and Black states covered large portions of intergenic regions, that represented 35 to 46% of each state coverage **(Fig. 2E, S2B**). Thus, the genomic coverage of chromatin state revealed some of their specific features, and notably highlighted differences between the Yellow, Red and YellowW states.

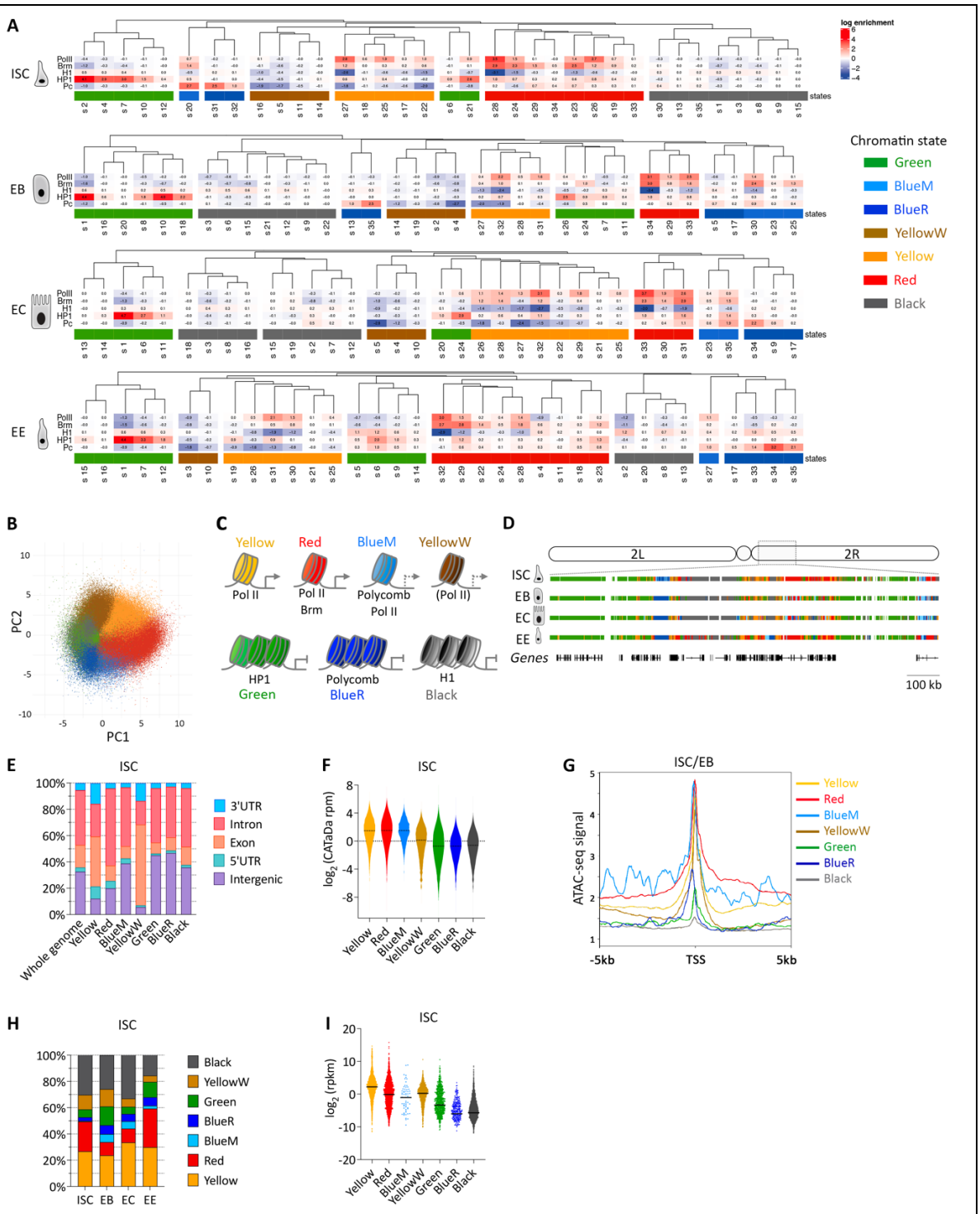

Figure 2. Chromatin state modeling reveals seven major chromatin states in the midgut.
A. HMM-fitted 35-state model for each midgut cell type. The color scale represents the mean binding intensity of proteins in each state. States were automatically clustered into seven major chromatin states (color bars) based on similarities in protein binding intensities and on transition probabilities between neighboring states. State numbers do not correspond between cell types. **B.** PCA plot of all GATC sites across cell types with their corresponding chromatin state as a color. **C.** Scheme representing the seven major chromatin states interpreted as active (Yellow, Red), intermediate (BlueM, YellowW) and repressive (Green, BlueR, Black). Proteins enriched in each state are indicated. **D.** Chromatin state maps in the four cell types on a portion of chromosome 2R, near the centromere. **E.** Genome-wide distribution of chromatin states in ISCs relative to genomic features. **F.** Chromatin accessibility levels as defined by CATaDa in each chromatin state in ISCs. **G.** Chromatin accessibility levels as defined by ATAC-seq in ISC/EB at the TSS of all genes, grouped by chromatin state. **H.** Distribution of all genes in chromatin states in ISCs. **I.** Transcript levels of the genes found in each chromatin state in ISCs.

Chromatin states and chromatin accessibility

In order to assess the relationship between chromatin accessibility and the chromatin states defined above, both CATaDa (Chromatin Accessibility profiling using Targeted DamID) (Aughey et al., 2018) and ATAC-seq were used. CATaDa uses the binding profile of untethered Dam when expressed alone, which reflects accessible regions of the genome. This allowed us to obtain chromatin accessibility levels for each cell type and to examine their correlation with chromatin states (**Fig. 2F, S2C**). We also profiled chromatin accessibility using ATAC-seq on FACS-sorted ISCs/EBs using the *esgGal4*^{ts} driver. The Yellow and Red states displayed the highest values of accessibility whereas the Green, BlueR and Black states had the lowest values, consistent with our categorization of active and repressive states (**Fig. 2F, G**). The BlueM state showed average accessibility levels comparable to the ones in Yellow or Red, suggesting that it is likely a permissive state despite its enrichment in Polycomb binding. Furthermore, the chromatin accessibility around TSS of genes in ISCs/EBs as depicted by our ATAC-seq experiment exhibited lower enrichment at TSS located in repressive states than in active and intermediate states (**Fig. 2G**). Therefore, the average chromatin accessibility correlated well with our categorization of active and repressive states, and showed that intermediate states likely reflect open chromatin states.

Chromatin states at genes

Next, we investigated the relationship between chromatin states and the genes covered by these states. To facilitate analyses, one single chromatin state was assigned to each gene based on the predominant state covering the gene. 60 to 80% of genes were found in the Yellow, Red and Black states while the BlueM and BlueR states covered relatively few genes (**Fig. 2H**). Despite a large genomic coverage **(Fig. S2A, S2E**), the Green state marked only 5 to 14% of all genes, consistent with heterochromatic regions being poor in genes.

Cell-type specific RNA-seq data was then integrated (Dutta et al., 2015) to compare chromatin states at genes with their respective expression levels in the four cell types. Consistent with our classification of Yellow and Red as active states, these were mostly associated with actively transcribed genes ($\log_2$(rpkm)>0) (**Fig. 2I, S2D**). Of note, genes marked by the Red state showed a wider range of transcription levels in ISCs and EEs compared to EBs and ECs (**Fig. 2I, S2D**). Therefore, although the Red state correlated with genes that are on average expressed, it was also found at genes with low transcription, particularly in ISCs and

EEs. Genes marked by the YellowW state displayed on average lower transcript levels than genes marked by the Yellow state, hence the name "Yellow Weak". Consistent with our definition of repressive states, the Green, BlueR and Black genic coverage was mostly associated with lowly-transcribed genes (**Fig. 2I, S2D**).

To determine the type of genes found in each state, we performed gene ontology enrichment analysis on the genes marked by each state in each cell type. Common terms were consistent with those previously described (Filion et al., 2010; Marshall and Brand, 2017): housekeeping functions in Yellow and YellowW, response to stimulus and signaling in Red, developmental terms in BlueM and BlueR, and nervous system functions in Black.

Overall, our genome-wide characterization of chromatin states in the intestinal lineage highlighted the general features of the distinct chromatin types that are conserved among midgut cell types. However, comparing the genomic coverage of the 7 chromatin states between cells of the lineage (ISC vs EB, EB vs EC and ISC vs EE) revealed that 32% to 36% of the genome underwent chromatin state transitions during the differentiation process, while the remaining 63%-68% were static, unchanging within the lineage (**Fig. S2E**).

Genes undergo lineage-specific chromatin state transitions upon differentiation

We then wanted to understand better the dynamic chromatin changes occurring upon ISC differentiation to EE or EC lineages as well as identify static chromatin domains that are unaltered during differentiation. We hypothesized that distinct chromatin state transitions may mark different classes of genes undergoing altered transcription throughout the differentiation process. We, therefore, focused on chromatin states specifically at genes based on our assignment of chromatin states to genes in each cell type as described above. Overall, 61% of all genes underwent at least one chromatin state change upon ISC differentiation, whereas 39% of genes remained marked by the same chromatin state in the four cell types, with many genes remaining in the Yellow or Black states (**Fig. 3A-B, 3E**).

Interestingly, EE vs EC lineage-specific differences were apparent when considering the major chromatin state transitions occurring at genes during differentiation. For example, the number of genes in the active Red state in ISCs was reduced upon EC differentiation (**Fig. 3A, 3B-B'**). Strikingly, 67 % of the genes that exited the Red state in ECs remained in the Red state in EEs (**Fig. 3B'**). Overall, active states of genes were more conserved during ISC to EE differentiation than during ISC to EC differentiation (**Fig. 3C**).

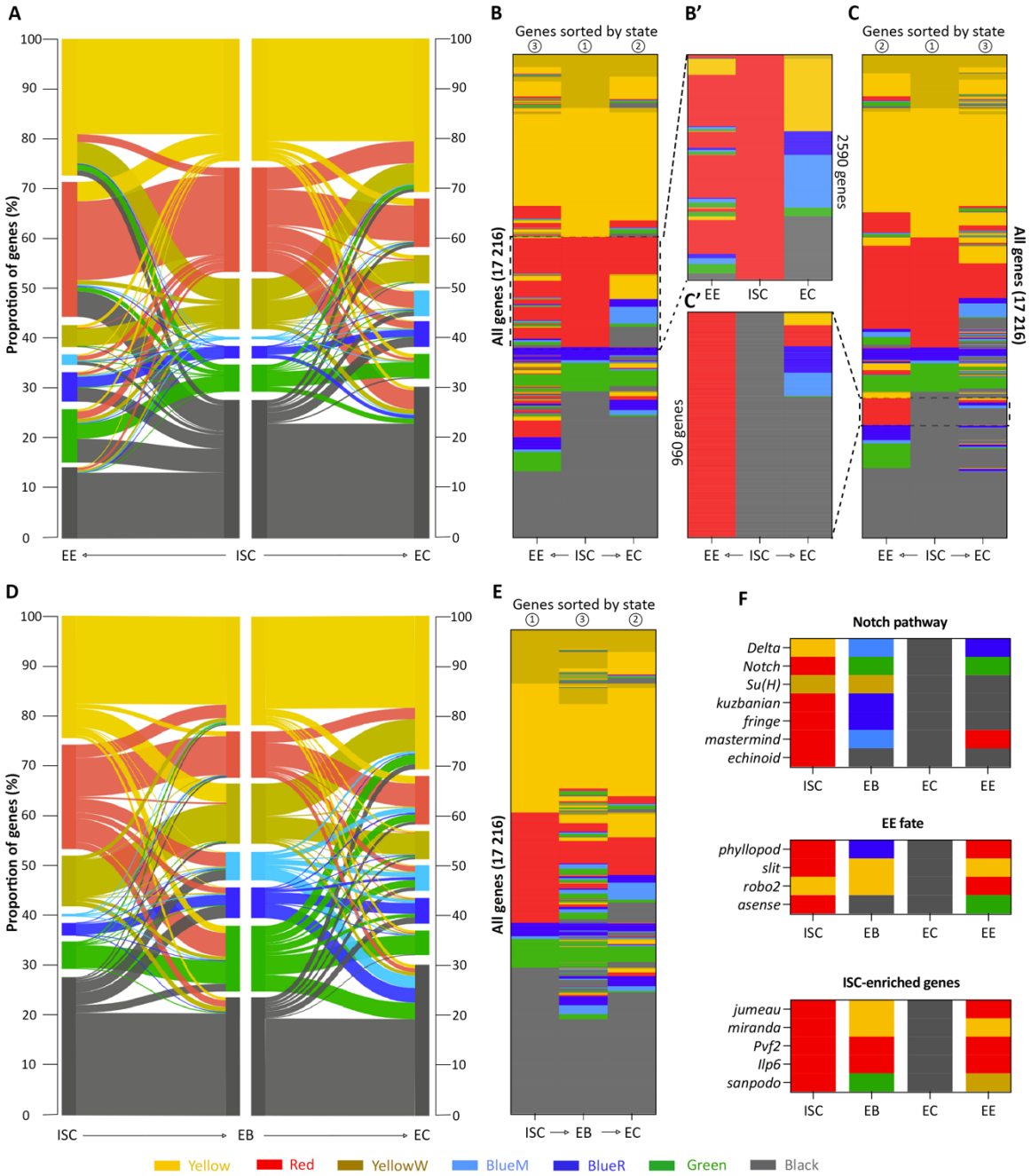

Figure 3. Lineage-specific chromatin state transitions at genes upon ISC differentiation.
A. Chromatin state transitions between ISCs and ECs, ISCs and EEs. Boxes on the sides of each plot represent the proportion of genes marked by each chromatin state. The flows represent the proportion of genes undergoing chromatin state transitions from one state to another between cell types. **B-C**. Colored maps of genes in chromatin states in ISCs, ECs and EEs. Each row is a gene with its corresponding chromatin state in each cell type. Genes are sorted by chromatin state, in the order indicated by the numbers above the map: ISC, EC, EE in (**B**), ISC, EE, EC in (**C**). **B'** and **C'** are enlarged zooms of the framed regions in **B** and **C**, respectively. **D.** Chromatin state transitions between ISCs and EBs, EBs and ECs. **E.** Colored maps of genes in chromatin states in ISCs, EBs and ECs. **F.** Chromatin states of subsets of genes enriched in ISCs or with important functions in ISC differentiation, showing lineage-specific and intermediate transitions upon differentiation.

In contrast to EC cells, the Red state was expanded in EEs compared to ISCs: a large proportion of genes marked by the repressive Black state in ISCs acquired the Red state during differentiation to EE cells (**Fig. 3A, 3C-C'**). This transition was correlated with a significant increase in the mean rpkm of RNA of these genes from ISCs to EEs (**Fig. S3A**). Among these genes following the Black to Red transition in EEs, 598 (62%) remained in Black in ECs (**Fig. 3C'**). Additionally, the data indicated that chromatin transitions also occur between repressive states, such as from Black to Green (**Fig. 3A, 3C**). Thus, while EEs share more genes with ISCs in active states, ECs have more genes in common with ISCs in repressive states (**Fig. 3A-B**).

Next, we further explored the chromatin changes occurring upon EC differentiation by examining chromatin states in EBs, the precursors of ECs (**Fig. 3D**). Surprisingly, we observed several major intermediate transitions. Notably, our data revealed that genes undergoing the transition from the Red active state in ISCs to repressive states (Black, BlueM or BlueR) in ECs passed through other intermediate states in EBs, most prominently the HP1-enriched Green state (**Fig. 3E**). Interestingly, genes important for ISC differentiation, such as components of the *Notch* pathway, followed intermediate chromatin transitions, going from active or intermediate states in ISCs to the Black state in ECs (**Fig. 3F**). This was also observed for genes playing a role in ISC to EE differentiation, like *phyl*, *slit*, *robo2* and *ase* (**Fig. 3F,** "EE fate"), as well as for several ISC-enriched genes. These ISC-enriched genes, whose transcript levels are reduced in ECs and EEs based on rpkm (Dutta et al., 2015), were still found in active states in EE cells (**Fig. 3F**). This suggests that decreasing the expression of these genes in EEs did not require a repressive chromatin state. We also noticed that genes of the *E(spl)* complex, which are downstream targets of Notch signaling important in the lineage, were found in the Red active state in ISCs but in inactive Polycomb-enriched states (BlueR or BlueM) in ECs (**Fig. S3B**). Moreover, these genes often passed through the HP1-associated Green state in EBs and were found in the Green state in EEs (**Fig. S3B**).

Therefore, these results highlight that genes undergo major chromatin state changes that are distinct upon differentiation to EC or EE lineages, indicating that they are regulated in different ways depending on cell fate determination. The fact that key regulators of ISC differentiation are subjected to distinct chromatin state transitions suggest that these differences of chromatin organization between the EC and EE lineages might be critical for cell fate decisions.

Physiology-related genes are marked by the Black state in ISCs

Next, we further explored the chromatin state transitions occurring at genes which become activated during differentiation. We reasoned that these genes likely undergo transitions from repressive states in ISCs to active states in EEs or ECs. Therefore, we examined in more detail the genes marked by the inactive (Black, Green and BlueR) states in ISCs and found in the active (Yellow and Red) states in EEs/ECs (**Fig. 4A, 4C**).

In order to identify potential differences in the categories of genes marked by each repressive state, we performed GO analysis on the genes following the transitions "Black to active", "Green to active" and "BlueR to active" separately. For the "Black to active" transition upon EE differentiation, we found a significant enrichment in GO categories related to the EE-specific neuropeptide hormone production and signaling as well as ion transport (**Fig. 4B**). In contrast, there was no significant enrichment for the genes following the "Green to active" or "BlueR to active" transitions. We then wondered if the genes following a "Black to active" transition upon EC differentiation would be enriched for EC-specific functions. GO analysis resulted in significant enrichment of "long-chain fatty acid metabolic process" (**Fig. 4D**). To further test the notion that gut metabolic genes may specifically undergo a Black to active transition, 226 midgut-enriched digestive enzymes (Lemaitre and Miguel-Aliaga, 2013) were assessed and indeed, a major type of transition was "Black to Red" (**Fig. 4E**). In addition, many of these enzymes appear already expressed at high levels in ISCs in RNA-seq data (Dutta et al., 2015), and these remain in Red or Yellow states throughout differentiation (**Fig 4E**). Together, these results show that genes underlying the physiological functions of differentiated cells mostly undergo a chromatin state transition from the repressive Black state to an active state upon their activation. In line with these data, the genes undergoing the Black to active transition upon EE or EC differentiation had a significant increase in their RNA levels, based on the published RNA-seq data (**Fig. 4F-G**).

We then explored the relationship between the "Black to active (Yellow/Red)" chromatin state transition and chromatin accessibility by integrating our ATAC-seq data from ISCs/EBs. We compared the chromatin accessibility around the TSS of different classes of genes: (1) genes marked by the Black state in all cell types ("Black stable"), (2) genes following the transition "Black to active" upon differentiation to EEs, and (3) the transition "Black to active" in ECs (**Fig. 4H**). Interestingly, we found that the TSS of genes that will become marked

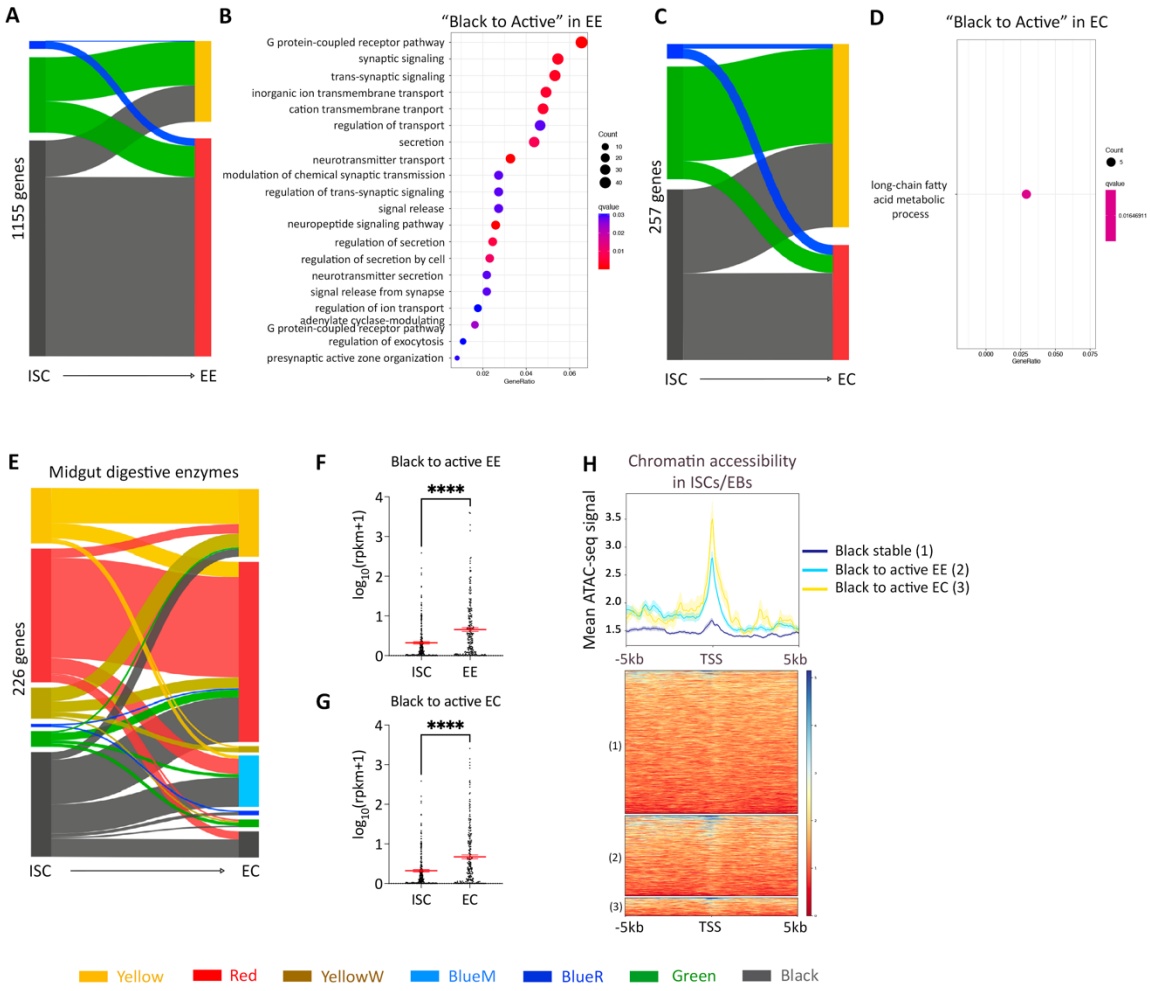

Figure 4. Physiology-related genes undergo a "Black to active" transition upon their activation.
A. Chromatin states transitions of genes marked by a repressive state in ISCs and an active state in EEs. **B.** GO terms enriched in the genes undergoing the Black to active transition in EEs. **C.** Chromatin states transitions of genes marked by a repressive state in ISCs and an active state in ECs. **D.** GO term enriched in the genes undergoing the Black to active transition in ECs. **E.** Chromatin state transitions of genes encoding midgut digestive enzymes upon EC differentiation. **F-G.** Transcript levels of genes undergoing the Black to active transition in EEs (**F**) and in ECs (**G**). Significance was assessed with a match-paired Wilcoxon test. Mean values in red, error bars are SEM, **** for p<0.0001. **H.** Chromatin accessibility levels as defined by ATAC-seq in ISCs/EBs at the TSS of genes remaining in the Black state or undergoing the Black to active transition upon differentiation.

by active states in differentiated cells were more accessible in ISCs/EBs than the genes remaining permanently in the Black state. This suggests that in ISCs, the transcriptional program of differentiated cells is likely primed for activation. The differential accessibility between class (1) and classes (2)/(3) genes suggests that, although these genes are all in the same chromatin state as defined in our model, additional regulation plays roles to fine-tune the chromatin accessibility required for future transcription of these genes upon differentiation.

Regulation of stem cell and lineage transcription factors involves the Polycomb-enriched Blue Mixed and Blue Repressive states

Next, we explored the chromatin states of transcription factor-encoding genes, using a list of 885 annotated transcription factors from the GLAD database (Hu et al., 2015). While no major difference was found between ISC-, EB-, EC-, and EE-cell types, genes encoding transcription factors were enriched in the Polycomb-enriched BlueR state compared to the distribution of all genes in chromatin states (**Fig. 5A**). While 43% of these TFs remained in the same chromatin state in all cell types, we examined the TFs that underwent chromatin changes during differentiation. First, several TFs known for their essential role in the regulation of ISCs (*esg*, *wor*, *Sox100B*, *Ets21c*, *klu*) were found in active states in ISCs and/or EB cells and were marked by the BlueR or BlueM state in ECs (**Fig. 5B**). This trend was also found with numerous genes of the *E(spl)* complex (**Fig. S3B**). However in EEs, repression of stem cell-specific transcription factors correlated with either the BlueR or the Red state, supporting the idea of different modes of chromatin regulation depending on the lineage.

Strikingly, the primary TFs controlling the ISC lineage were marked by BlueR in ISCs and transitioned to active Red or Yellow states during EE or EC differentiation. These include *nubbin* important for EC specification and *prospero, mirror* and *Pox neuro* important within the EE lineage (**Fig. 5C**). Therefore, our data suggest that Polycomb-enriched chromatin states mark transcription factors that are important for the regulation of the intestinal lineage that need to be turned on or off upon differentiation. To further test the functional relevance of Polycomb-mediated silencing in ISCs for repression of lineage TF genes, we compared chromatin states in ISCs with the differential accessible regions and deregulated genes in Pc knockdown context using published data (Tauc et al., 2021) (**Fig. S4**). Although chromatin accessibility was overall little affected in Pc knockdown condition, more accessible regions ("Gain") and the most upregulated genes upon Pc RNAi were mainly in the BlueR and Black states (**Fig. S4A-C**), consistent with a role for Pc in maintaining a repressive chromatin state. However, *prospero*, *mirror*, *Pox neuro* and *nubbin* were not upregulated in Pc knockdown context, suggesting that Pc binding at these genes is a mark of their repressive state but is not instructive *per se* for the initiation of the maintenance of their repression.

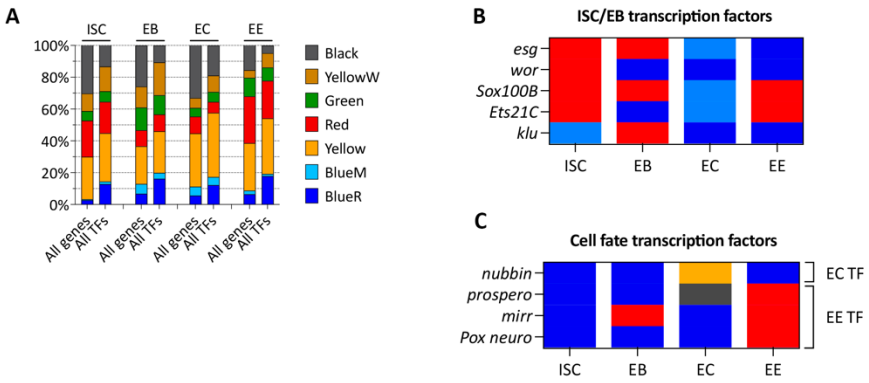

Figure 5. Regulation of stem cell and lineage transcription factors involved the Polycomb-enriched Blue chromatin states.
A. Distribution of 885 genes encoding transcription factors in chromatin states in each cell type, compared with the distribution of all genes. **B-C.** Chromatin states of subsets of TF-encoding genes with important functions in ISC regulation (**B**) or in cell fate specification (**C**).

HP1 is required for ISC proliferation and proper expression of translation-related genes

HP1 was initially known for its predominant role in heterochromatin formation and maintenance and gene silencing. However, further studies showed that HP1 plays roles in both activation and repression of gene expression in a context-dependent manner (Schoelz and Riddle, 2022). Indeed, HP1 is also found at euchromatic regions that are transcriptionally active, but the underlying mechanisms of HP1 role in transcriptional activation remain poorly understood.

Our chromatin state modeling in the intestinal lineage showed that HP1 was strongly enriched in the Green state, which was involved in chromatin state transitions associated with stem cell genes. HP1 binding was also present in the Red and Yellow active states (**Fig. 2A**), which prompted us to explore further the role of HP1 in the intestinal lineage. We thus investigated how loss of HP1 in ISCs and EBs changes chromatin accessibility and gene expression and impacts tissue homeostasis. To this aim, we performed ATAC-seq and RNA-seq on FACS-sorted population of ISCs and EBs from control guts or guts expressing RNAi against HP1 in ISCs/EBs for 4 days (**Fig. 6A**). To better understand the relationship between HP1 function, gene expression changes and chromatin state transitions in the lineage, we integrated the cell type-specific chromatin states with ATAC-seq and RNA-seq analyses.

HP1 knockdown led to differential accessibility of 106 regions (peaks) with 92 peaks significantly more accessible (“gain”) and 14 peaks becoming less accessible (“loss”) in comparison to the control condition (**Fig. 6B**). Chromatin accessibility gain occurred mostly in

intergenic portions of the genome, at the pericentromeric regions marked by the Green state in ISCs and EBs (**Fig. 6B-D, S5A**). This indicated a role for HP1 in maintaining a condensed chromatin in these regions while not having a strong impact on the Green regions covering the euchromatic genome. The few genomic regions that were less accessible upon HP1 knockdown were found predominantly in the Red state in ISCs and in various chromatin states in EBs, which could reflect direct or indirect effects (**Fig. 6B, 6D**). Therefore, HP1 loss in ISCs/EBs altered chromatin accessibility locally, mostly in pericentromeric heterochromatin.

Despite the few changes in chromatin accessibility, HP1 knockdown led to 683 upregulated genes and 686 downregulated genes in RNA-seq analysis (**Fig. 6E, Table S1**). 86% of deregulated genes showed mild transcription changes, with a $\log_2$ fold-change comprised between -1 and 1 (**Fig. 6E-G**). The most deregulated genes ($\log_2$(fold-change)>|2|) were found in the Black, Green, Red and BlueM states in ISCs and EBs (**Fig. 6F-G**), suggesting that the consequences of HP1 loss on transcription were greater for genes in these chromatin states. Interestingly, 56% of downregulated genes were marked by a Yellow chromatin state in ISCs (**Fig. 6H**) and did not undergo any chromatin transition during differentiation (**Fig. S5B**). As these genes were often bound by HP1 in ISCs and EBs, HP1 binding may play an active role in promoting their expression, consistent with HP1 enrichment in the Yellow state. Of note, in contrast to changes in chromatin accessibility peaks, altered gene expression upon HP1 knockdown was found distributed widely in the genome (**Fig. S5C**). While some regulation is likely indirect, we favor the hypothesis that HP1 has more subtle roles in gene expression in the euchromatic regions that are independent of its role in chromatin compaction at heterochromatic regions.

Next, we asked what were the consequences on tissue homeostasis of heterochromatin alteration and gene expression changes caused by HP1 loss. We thus assessed the effect of HP1 knockdown on ISC regulation. In guts expressing HP1 RNAi in ISCs/EBs for 10 days, there was a significant decrease of *esg*$^+$ cell numbers accompanied with a decrease of PH3$^+$ cells (**Fig. 6I-6L**). While in control guts, *esg*$^+$ cells were usually found as “nests” of either single cells, doublets or small clones, there was a significant increase in the proportion of single *esg*$^+$ cells in HP1 knockdown context, consistent with a reduction in stem cell proliferation (**Fig. 6M-N**).

These results indicated that HP1 was required for ISC division. To investigate whether HP1 loss causes differentiation defects, we generated MARCM clones expressing HP1 RNAi for 10 days. Clone size was significantly decreased in HP1-knockdown clones with less *Delta+* ISCs

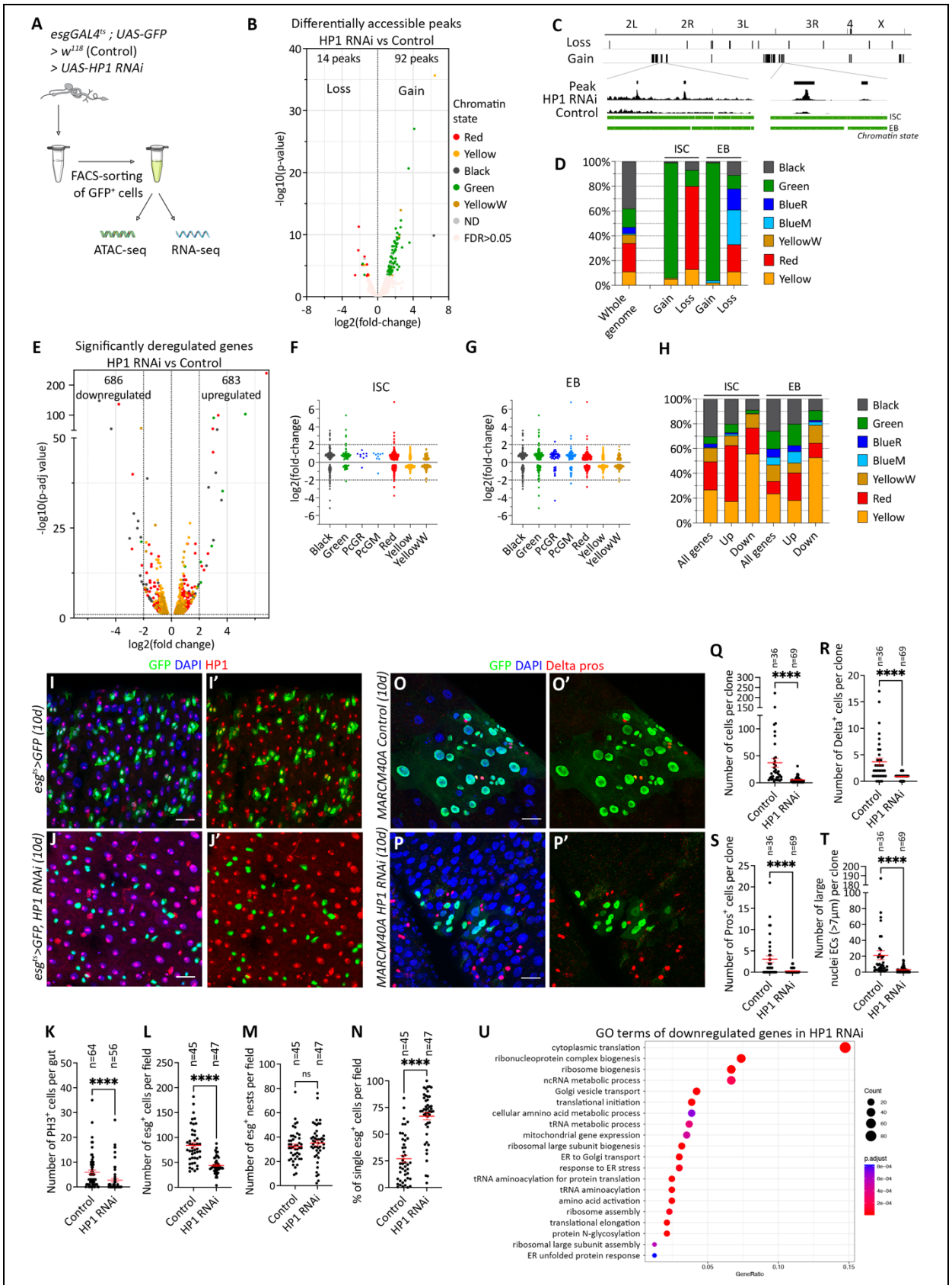

Figure 6. HP1 knockdown alters chromatin accessibility, transcription and ISC homeostasis.
A. Experimental setup to isolate ISCs and EBs for ATAC-seq and RNA-seq. **B**. Volcano plot of more (Gain) or less (Loss) accessible peaks in HP1 RNAi compared to the control condition. **C.** Genome-wide distribution of significant differentially accessible peaks, with zooms of regions with peaks of gained accessibility in HP1 RNAi compared to control. These regions are marked by the Green state in ISCs/EBs. **D.** Chromatin states of the significant

differentially accessible peaks in HP1 RNAi, compared to the chromatin state distribution in the whole genome. **E**. Volcano plot of significantly deregulated genes in HP1 RNAi compared to the control condition. The color of the dots is the chromatin state of the corresponding gene in ISCs. **F-G.** Chromatin states of deregulated genes in ISCs (**F**) and EBs (**G**). **H.** Distribution of upregulated and downregulated genes in chromatin states in ISCs and EBs, compared to the distribution of all genes in chromatin states. **I-J.** Midguts immunostained for GFP, HP1 and DAPI in control (**I**) and ISC/EB-specific HP1 RNAi (**J**) conditions after 10 days of RNAi induction. **K.** Quantification of $PH3^+$ cells per gut. **L-N.** Quantification of (I-J). For each midgut, images were taken for five fields corresponding to five different regions (n=number of fields). Esg^+ cells were quantified as the number of esg^+ cells per field (**L**), the number of esg^+ nests (nest = an isolated esg^+ cell or a group of adjacent esg^+ cells) (**M**) and the number of single esg^+ cells (single = isolated esg^+ cell) (**N**). **O-P.** Control clones (**O**) and HP1-RNAi expressing clones (**P**) in midguts immunostained for GFP, Delta (membrane), Pros (nuclear) and DAPI after 10 days of RNAi induction. **Q-T**. Quantifications of the number of cells per clone (**Q**), number of ISCs ($Delta^+$) per clone (**R**), number of EEs ($Pros^+$) per clone (**S**), number of ECs (large nuclei) per clone (**T**). **U.** GO terms enriched in genes downregulated in HP1 RNAi.
Significance was assessed with a two-tailed Mann-Whitney test. Mean values in red, error bars are SEM. ns for non-significant, **** for $p<0.0001$. Scale bars, 20 µm.

per clone (**Fig. 6O-R**), and the numbers of both EEs and ECs were reduced compared to control clones (**Fig. 6S-T**). Thus, upon loss of HP1, ISCs divide less, though can produce reduced numbers of the different intestinal cell types.

We wondered what could be responsible for this phenotype and therefore examined in more detail the function of deregulated genes in HP1 knockdown. We found that downregulated genes were strongly enriched in GO terms related to translation, nucleic acid metabolism and energetic metabolism (**Fig. 6U, Table S2**). Indeed, many genes encoding ribosomal proteins, that are very highly expressed in all intestinal cell types and found in the Yellow state, were expressed at lower levels upon HP1 knockdown in ISCs and EBs. This suggests a global deregulation of translation processes, which could cause the observed ISC proliferation defect. Moreover, *Notch*, *Delta* and two *E(spl)* genes were upregulated, which could also affect ISC behavior.

Together, these results show that HP1 has various functions in ISCs/EBs. While it is required for maintaining heterochromatin at pericentromeric regions, it is also necessary for proper expression of many genes with cellular metabolic functions. Moreover, HP1 is necessary to maintain ISC division. Further work will be needed to test the function of HP1 in regulating translation and how this could mediate the regulation of ISC activity.

Histone H1 role in EE fate priming and control of ISC proliferation

Histone H1 has been shown to be important for nucleosome compaction and heterochromatin formation in *Drosophila* embryonic tissues (Hu et al., 2018; Lu et al., 2009, 2013; Willcockson et al., 2020). In the adult intestine, our chromatin state modeling approach

showed that H1 was enriched in the Black state, which covers a large portion of the genome. The Black state was also associated with dynamic chromatin changes occurring at many genes with key functions in cell fate determination and intestinal physiology. H1 binding was also found in the Green state, consistent with its known functions in heterochromatin establishment (Lu et al., 2009, 2013). We thus hypothesized that, as for HP1, the depletion of H1 in ISCs and EBs could alter chromatin accessibility, transcription, and tissue homeostasis.

The knockdown of H1 for 4 days resulted in relatively few changes to chromatin accessibility in the population of ISCs and EBs (**Fig. 7A**). We note, however, that RNAi depletion of H1 for 7 days resulted in only a partial loss of H1 protein (**Fig. S6B-D**). More open ATAC-seq peaks were found predominantly in the Green and Black states while less accessible regions were located mostly in the Red state in ISCs and in various states in EBs (**Fig. 7B**). Unlike HP1, more accessible regions were widely distributed along the genome (**Fig S6A**).

Despite the mild effect on chromatin accessibility, H1 knockdown in ISCs and EBs caused the upregulation of 356 genes and downregulation of 421 genes (**Fig. 7C, Table S3**). First, 65,7% (23 genes) of the most upregulated genes (log_2(fold-change>2) were found either in the Black or Green states in ISCs/EBs (**Fig. 7D-E, Table S3**) and had very low expression levels in all 4 cell types based on published RNA-seq data (Dutta et al., 2015) (**Fig. 7F**). This is consistent with the possibility that H1 has a role in maintaining the repression of these genes in the intestine and with perturbation of Black and Green states enriched in Histone H1. In addition, 21 upregulated genes were part of the "Black to Active" chromatin transition category defined above whose expression levels increase in differentiated cells. These included some EC-metabolic genes (*Jon44E*, *Jon65Aii*, *CG33966*, *CG4653*) as well as EE-specific genes (*Syn2*, *TrissinR*, *dysc*, *Mip*) (**Fig. 7F**). These 21 genes were not found in the vicinity of differentially accessible peaks. Therefore, H1 seems to be required to maintain the silencing of a subset of genes in ISCs and EBs, though independently of changes in chromatin accessibility detected by ATAC-seq. Furthermore, a majority of upregulated genes (200 genes, 56%) were in the Red, Yellow or YellowW states in ISCs/EBs (**Fig. 7D-E, 7G**). Lack of H1 binding in these states suggests that the observed gene upregulation likely occurred through indirect effects.

On the other hand, 28% of downregulated genes were in the Black state in ISCs and EBs, suggesting that H1 could also be required for the expression of these genes (**Fig. 7G**). Surprisingly, gene ontology analysis enrichment on all downregulated genes revealed a strong enrichment for neuropeptide secretion and signaling functions, characteristic of the EE

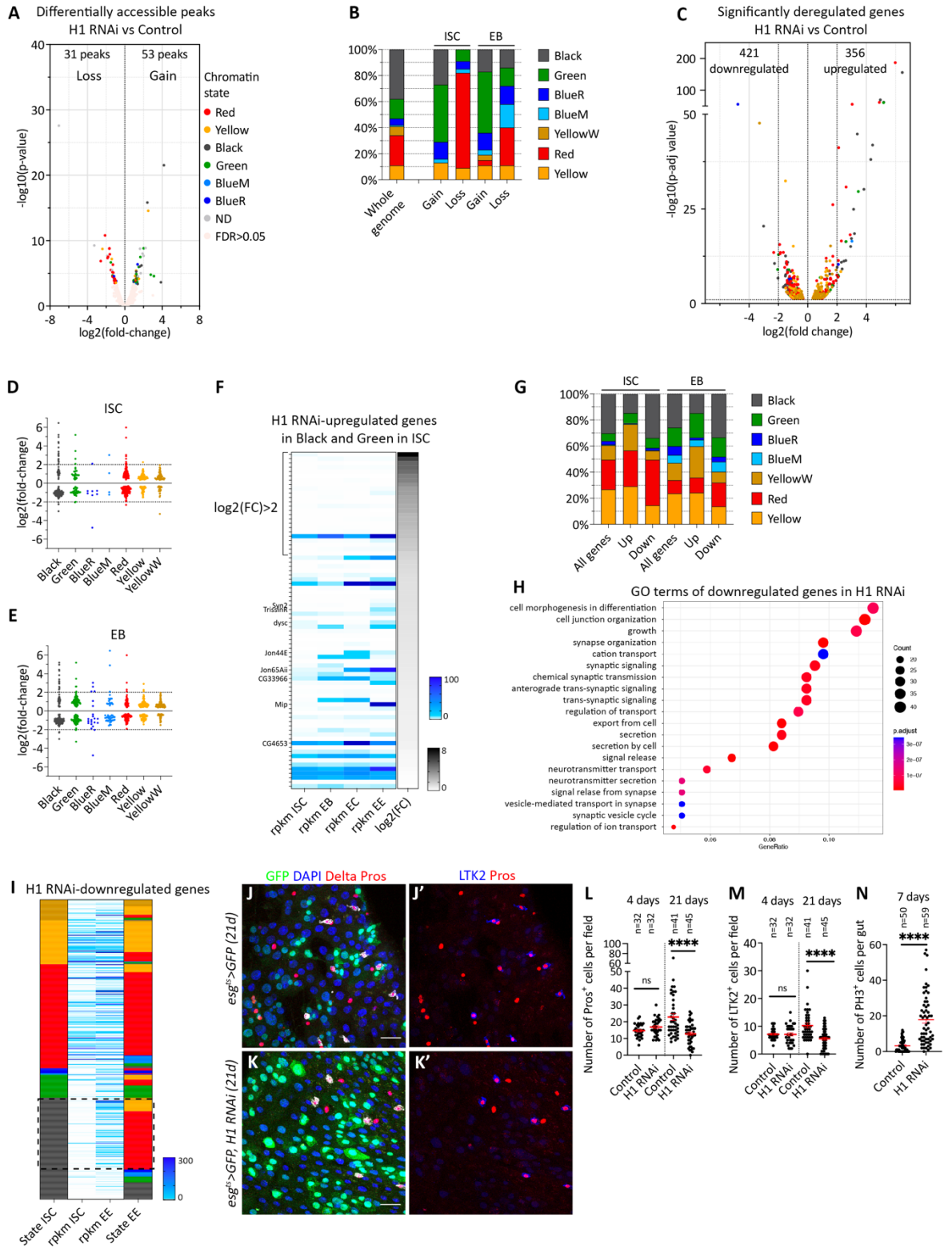

Figure 7. H1 knockdown alters the transcription of EE-identity genes and ISC priming towards the EE fate.
A. Volcano plot of more (Gain) or less (Loss) accessible peaks in H1 RNAi compared to the control condition. **B.** Chromatin states of the significant differentially accessible peaks in H1 RNAi, compared to the chromatin state distribution in the whole genome. **C**. Volcano plot of significantly deregulated genes in H1 RNAi compared to the control condition. The color of the dots is the chromatin state of the corresponding gene in ISCs. **D-E.** Chromatin states of deregulated genes in ISCs (**D**) and EBs (**E**). **F.** Transcript levels of H1 RNAi-upregulated genes which are in the Black and Green states in ISCs. Genes are sorted by decreasing log2(fold-change) of transcription in H1 RNAi

compared to the control condition. **G.** Distribution of upregulated and downregulated genes in chromatin states in ISCs and EBs, compared to the distribution of all genes in chromatin states. **H.** GO terms enriched in genes downregulated in H1 RNAi. **I.** Chromatin state and transcript levels of H1 RNAi-downregulated genes in ISCs and EEs. The framed region highlights genes undergoing the Black to active transition and a transcription increase upon ISC to EE differentiation. **J-K.** Midguts immunostained for GFP, Pros, LTK2 and DAPI in control (**J**) and ISC/EB-specific H1 RNAi conditions (**K**) after 21 days of RNAi induction. **L-M.** Quantification of (J-K) at 4 days and 21 days of RNAi induction. For each midgut, images were taken for five fields corresponding to five different regions. Number of $Pros^+$ cells (**L**) and $LTK2^+$ cells (**M**) was quantified in each image. **N.** Quantification of $PH3^+$ cells after 7 days of RNAi induction. Significance was assessed with a two-tailed Mann-Whitney test. Mean values in red, error bars are SEM. ns for non-significant, **** for p<0.0001. Scale bars, 20 µm.

transcriptional program and metabolic function (**Fig. 7H, Table S4**). Indeed, 68% of the downregulated genes in ISCs/EBs upon H1 knockdown are genes known to increase expression upon ISC to EE lineage differentiation, and 31% of these genes are associated with a chromatin state transition from Black in ISCs to Red in EEs for (**Fig. 7I**). Transcription factors involved in EE fate such as *prospero* and *mirror* were also found downregulated. Therefore, despite low expression of EE-identity associated genes in ISCs/EBs during homeostasis, H1 knockdown caused a striking global downregulation of this category of genes.

We thus asked whether H1 in ISCs/EBs may promote EE differentiation in the lineage. The number of $Pros^+$ cells in midguts expressing H1 RNAi in ISCs/EBs after 4 days or 21 days of induction. The number of $Pros^+$ cells and Tachykinin ($LTK2^+$) was significantly reduced compared to control guts after 21 days of RNAi induction, though not at 4 days, a timepoint at which EE cells would not yet have undergone turnover (**Fig. 7J-M**). In addition, we observed more dividing cells in H1 RNAi than in controls after 7 days of RNAi expression (**Fig. 7N**) and an increase in *esg>GFP+* cell numbers (**Fig. S6B-C, S6E**). Taken together, these results show that H1 is required for maintaining basal levels of ISC proliferation and for EE differentiation by priming ISCs towards the EE fate, likely through direct or indirect mechanisms of transcription regulation of EE-identity genes.

DISCUSSION

In this study, we investigated the chromatin state transitions occurring during differentiation in the *Drosophila* intestinal lineage. By generating cell-type specific chromatin state maps, we highlighted the major chromatin state changes followed by functionally relevant groups of genes such as stem cell-associated genes, cell fate regulators and physiology-related genes.

Modeling chromatin states in a tissue with two types of differentiated cells revealed lineage-specific transitions, suggesting distinct chromatin remodeling events depending on cell fate commitment towards the EE or EC lineage. More specifically, a large proportion of genes marked by the Red active state in ISCs remains in Red in EEs while they are found in other states in ECs. In particular, several ISC-enriched genes and genes encoding transcription factors regulating ISC differentiation follow a decrease of transcription upon differentiation, which correlates with an active to repressive transition in ECs but not in EEs. These examples suggest that in EEs, many genes are located in a permissive state, and that their transcriptional state might rely more on the recruitment of transcriptional activators or repressors. This might be less true for ECs, since the same examples are found in repressive states in ECs, in particular in the Black state. Why these "stem cell genes" are regulated in different ways upon EE or EC differentiation remains an open question. Of note, the major, lineage-specific chromatin changes described here were also observed at the genome-wide scale, suggesting that this chromatin remodeling is not limited to genes. This observation suggests that part of the genome is organized in different ways in EEs and ECs. Interestingly, in the developing brain, neuronal differentiation is marked by chromatin changes that seem similar to those we find during ISC to EE differentiation. For instance, there is a decrease in the number of genes marked by the Black state and an increase of genes marked by the "TrxG" and "HP1" states, which are equivalent to the Red and Green states in our data (Marshall and Brand, 2017). Moreover, several genes expressed in neural stem cells such as *ase*, *dpn*, *E(spl)m7* and *E(spl)mdelta* follow similar transitions from TrxG to HP1 states upon neuronal differentiation and EE differentiation, whereas these genes are found in the BlueR or Black states in ECs in our data. Neurons and EEs share part of their transcriptional programs, since EEs express many genes involved in neuropeptide and neurotransmitter secretion, as well as transcription factors that regulate the expression of these neuropeptide genes (Guo et al., 2019; Li et al., 2020; Veenstra et al., 2008). Our study suggests similarities in the chromatin organization of EEs and neurons, and in the chromatin changes occurring during neuronal and EE differentiation. In the mammalian intestine, the secretory lineage differs from the ISCs by changes in chromatin accessibility and histone modifications at cell-type specific enhancers (Jadhav et al., 2017; Raab et al., 2019). It is possible that such changes at enhancers, not investigated here, occur in the *Drosophila* EE cells.

Our data showed that transcription factors with important roles in the regulation of the intestinal lineage are marked by Polycomb-enriched Blue Mixed or Blue Repressive states. Polycomb-mediated repression of differentiation genes has been extensively characterized in embryonic stem cells, but whether it represents a specific chromatin feature of these genes in adult stem cells remains unclear. In this work, the BlueR state marks genes encoding the major cell fate regulators of EC and EE lineages in ISCs. However, it was recently shown that loss of Polycomb in ISCs does not lead to derepression of these genes, arguing against an instructive role in repression of these genes (Tauc et al., 2021). Surprisingly, the authors found instead that several genes involved in early cell fate decisions towards the EE fate were downregulated in Polycomb knockdown context, consistent with a slight decrease in the number of $Pros^{+}$ EEs in the midguts expressing *E(z)* or *Polycomb* RNAi in ISCs and their progeny. These genes were not marked by a Polycomb-enriched state or bound by Polycomb in our data, suggesting indirect regulation. A recent study testing the role of PRC2 in quiescent hair follicle stem cells (qHFSCs) showed that it was dispensable for maintaining qHFSC identity despite changes in their transcriptome, thus arguing against an instructive role in preventing premature activation or differentiation of adult stem cells (Flora et al., 2021). Thus, our data and other studies suggest that, despite being markers of important cell fate regulator genes, Polycomb Group protein function in adult stem cells remains uncertain.

Most chromatin studies in adult stem cell lineages such as the mouse intestine or skin focused on H3K27me3, H3K4me3 and H3K27ac profiles in stem cells and their progeny. Here, our chromatin state modeling approach allowed us to explore other types of chromatin and notably revealed new insight into the functional relevance of the H1-enriched Black state. In particular, we identified the “Black to active” transition as the predominant type of “repressive to active” transition, during both EE and EC differentiation. We found that genes marked by this transition are enriched in terms related to the physiological functions of differentiated cells. In the developing brain, it was also shown that genes that become active during neuronal differentiation are marked by the Black state in neural stem cells (Marshall and Brand, 2017). Given the previously mentioned similarities between neurons and EEs, gene silencing in the Black state could be seen as a feature of neuronal genes. However, the fact that many genes involved in the EC-specific metabolism were also silenced in the Black state leads us to propose it as a general signature of physiology-related genes in ISCs and possibly other adult lineages. This finding raises many questions. How does this “Black to active”

chromatin state transition occur upon differentiation? How are EC and EE-specific genes targeted for activation? Given that the Black state represents a compacted chromatin without histone modifications, we hypothesize that transcription factors might have a primary role in this regulation.

We further explored the functional relevance of chromatin states in the intestinal lineage by investigating the effect HP1 and H1 knockdown on chromatin accessibility, transcription and tissue homeostasis. We showed that HP1 knockdown in ISCs/EBs had various effects, that illustrate well the versatility of HP1 roles. Beyond HP1 requirement to maintain chromatin compaction in heterochromatic regions, our data suggest that HP1 function in transcription regulation may be independent of chromatin accessibility. Deregulated genes in HP1 knockdown were half upregulated and half-downregulated, consistent with previous studies showing both upregulation and downregulation of genes in *Drosophila* cell lines, embryos and larvae mutant for HP1 (Cryderman et al., 2005; De Lucia et al., 2005; Lee et al., 2013; Park et al., 2019). Whether deregulated genes are a direct or indirect effect of HP1 loss is not well understood, but it has been proposed that HP1 facilitates transcription elongation (Lin et al., 2008; Piacentini et al., 2009). At the tissue level, our data show that HP1 knockdown led to a decrease of ISC proliferation. Previous work reported cell cycle alteration in cultured cells and during embryogenesis, concomitant with deregulation of cell cycle genes (De Lucia et al., 2005; Park et al., 2019). Here, we instead found a strong enrichment of genes encoding ribosomal proteins and other factors involved in translation among the downregulated genes. This enrichment was also reported in HP1-deficent embryos (Park et al., 2019). We hypothesize that defects in translation and other metabolic processes could explain the ISC proliferation defect. Interestingly, a recent study showed that knockdown of HP1c, another isoform of HP1 mostly found at euchromatin (Schoelz and Riddle, 2022), promotes ISC to EC differentiation, likely through upregulation of several Notch target genes (Sun et al., 2021). Our RNA-seq analysis showed upregulation of *Notch*, *Delta*, and two *E(spl)* genes, suggesting redundant roles of HP1 and HP1c in controlling Notch signaling. As *Notch* and *E(spl)m7* are found in the Green state in EBs in our data, it is possible that HP1 has a direct role in their regulation.

Finally, our study uncovered a role for Histone H1 in EE fate priming. H1 knockdown in ISCs/EBs had little effect on chromatin accessibility as assessed by ATAC-seq. However, our RNA-seq analysis revealed that H1 is required for the basal expression of a large subset of

genes that are very characteristic of the EE transcriptional program. Many of these genes are following the "Black to active" transition previously identified. We further showed that H1 is required in ISCs/EBs to produce normal numbers of EEs in the midgut. Thus, we propose that H1 has a role in priming ISCs towards the EE fate, likely facilitating their future activation upon differentiation. This finding raises many questions regarding the mechanism through which H1 could mediate this function. Does H1 maintain a chromatin structure that allows low or stochastic transcription at these EE-identity genes? Does it require an interaction with other chromatin-associated proteins? Does H1 limit the access to transcriptional repressors that specifically target EE genes? Another intriguing question is why EC-identity genes are not downregulated in the same way upon H1 knockdown. Therefore, our characterization of H1 role in ISCs/EBs revealed a previously uncharacterized role for H1 in regulating cell fate decisions in an adult tissue. Interestingly, it was shown in the *Drosophila* adult ovary that H1 maintains germline stem cells, likely by preventing premature differentiation (Sun et al., 2015). This contrasts with our results but implies that H1 may have complex roles in other adult stem cell lineages, thus opening the path to future studies.

Overall, our characterization of chromatin state transitions in the *Drosophila* intestinal lineage *in vivo* unveils new insight into the modes of regulation of genes that are critical for stem cell activity and differentiation in the lineage, as well as physiology-related genes specific of midgut terminally differentiated cells. Our data provides a large resource for investigating further aspects of chromatin regulation in this adult homeostatic tissue as well as in other contexts such as environmental stress and disease.

MATERIALS AND METHODS

Fly stocks

The following fly stocks were used in this work: *esgGAL4 UAS-GFP;Su(H)GBE-GAL80 tubGAL80^{ts}* (Wang et al., 2014a), *esgGAL4;tubGAL80^{ts} UAS-GFP* (*esg^{ts}*) (Jiang et al., 2009), *Su(H)GBE-GAL4 UAS-GFP;tubGAL80^{ts}* (Zeng et al., 2010), *MyoIAGAL4;tubGAL80^{ts} UAS-GFP* (Jiang et al., 2009), *GAL4prosVoila tubGAL80^{ts}* (Balakireva et al., 1998). For DamID experiments, fly lines were the following: *UAS-LT3-NDam*, *UAS-LT3-NDam-RpII215*, *UAS-LT3-Dam-Brm*, *UAS-LT3-Dam-Pc*, *UAS-LT3-Dam-HP1*, *UAS-LT3-Dam-H1* (Marshall and Brand, 2017). For RNA-seq and ATAC-seq experiments, the following lines were used: *His1 RNAi*

(31617-R3) from the NIG Fly stock center (Kyoto), *HP1 RNAi* (VDRC31994) from the Vienna Drosophila RNAi Center (VDRC), w^{118} (gift from M. McVey).

Targeted DamID

Library preparation

Expression of *UAS-Dam*, *UAS-Dam-RpII215*, *UAS-Dam-Brm*, *UAS-Dam-HP1*, *UAS-Dam-H1*, and *UAS-Dam-Pc* was targeted to specific cell types using GAL4 driver lines. ISC-specific expression was achieved with the *esgGAL4* driver, combined with EB-specific expression of the inhibitor of GAL4, GAL80 (Su(H)GBE-GAL80). *Su(H)GBE-GAL4* was used for EB-specific expression, *Myo1AGAL4* for ECs and *GAL4prosVoila* for EEs. Crosses and their offspring were kept at 18°C to allow the expression of the temperature sensitive $GAL80^{ts}$ protein and therefore control temporally the expression of UAS-Dam constructs in ISCs. 2-3 day-old female flies with the correct genotype were shifted to 29°C (GAL80 restrictive temperature) for 1 day to induce Dam and Dam-fusion transgenes expression. For each experiment and replicate, 60 guts were dissected in PBS and immediately frozen in dry ice. Three biological replicates were realized for each experiment. Following tissue dissociation, genomic DNA was extracted from the guts with and digested with DpnI to cut at GATC methylated sites. DNA was purified and ligated with PCR adaptors specific to methylated fragments, before digestion with DpnII and PCR amplification. Then, DNA samples were purified and sonicated to reduce the fragment size to approximately 300 bp, followed by Alw1 digestion in order to remove DamID adaptors and initial GATC sequences. Digested DNA was purified with magnetic Seramag beads and end-repaired, adenylated and ligated with Illumina TruSeq adaptors. Samples were subsequently cleaned twice with Seramag beads and enriched by 6 cycles of PCR, and cleaned again with Seramag beads.

Sequencing and data analysis

Samples were sequenced by a HiSeq 2500 (rapid run) to generate 50 bp single-end reads. The damidseq_pipeline script was used to align the NGS reads on the Drosophila reference genome and normalize them (log2 ratio of Dam-fusion/Dam alone) (Marshall and Brand, 2015). Correlations between the ratio files were calculated with the Pearson's method. Replicates that correlated less than 0.8 with other replicates were discarded, leading to two or three replicates per experiment, that were averaged for further processing. Significant

peaks were obtained by processing the ratio files with find_peaks. Scripts can be found at https://github.com/owenjm. All analyses were performed in the Galaxy server and the visualization of alignments was performed using the IGV software.

CATaDa analysis

Chromatin accessibility profiling was performed using Dam-only reference sequences generated for Targeted DamID (3 replicates per cell type). Fastq files were processed for CATaDa as described in (Aughey et al., 2018). Reads were aligned to the Drosophila melanogaster reference genome version 6 and assigned to bins delimited by GATC sites using damidseq_pipeline_output_Dam-only_data. Peaks were called and mapped to genes, using Peak_Calling_for_CATaDa Perl program (FDR<0,01) and a consensus peak list was determined between each replicate. Scripts for CATaDa can be found at https://github.com/tonysouthall.

Chromatin state modeling

The log2 ratio files obtained from the damidseq-pipeline for the five proteins in begraph format were averaged and scaled by the standard deviation as proposed in (Marshall and Brand, 2017). HMM modeling was performed using Universal Chromatin HMM script version 0.9.10. HMM models were fitted to chromosomes 2L and 2R with a maximum of 2000 iterations and 10 random initializations. Models with 5-40 states were fitted independently for each cell type, in order to allow the detection of chromatin state differences between cell types. Next, Viterbi paths were calculated for the whole genome for each model. Mean binding intensities of an HMM state for each protein were calculated by averaging the binding intensities of the protein for all GATC fragments that were assigned the HMM state. These mean binding intensities were plotted on the heatmaps. HMM states were clustered based on their transition probabilities, and the clustering dendrogram was cut into 8 clusters. Each cluster was then assigned a chromatin state based on the strongest Pearson correlation between the mean binding intensities of the cluster and the predefined intensities for 7 chromatin states (data provided by Owen Marshall). Lastly, simplified Viterbi paths for the assigned chromatin states were created. Manual adjustments were performed to correct some group mis-assignments. The best model for each cell type was chosen by controlling the Akaike information criterion (AIC) and manually inspecting the clustering dendrogram. The best fitting model was the one with 35 states. Calculations of genome coverage and

intersections with other datasets were performed using BEDtools in Galaxy (https://usegalaxy.eu/). The karyotype view in Fig. S2 was generated using the R package karyoploteR.

Each gene was assigned single chromatin state based on the prevalent state covering the gene length. Chromatin state transition plots were generated using SankeyMATIC (https://sankeymatic.com/). Cell-type specific RNA-seq data published in Dutta et al. can be found on (http://flygutseq.buchonlab.com/). On the graphs presented in Fig. 2 and Fig. S2, null values of rpkm were excluded for easier visualization. The list of gene-encoding transcription factors comes from https://www.flyrnai.org/tools/glad/web/. Gene Ontology enrichment analysis was carried out using the R Studio packages clusterprofiler and enrichGO (https://www.rstudio.com/products/rpackages/). All graphs were generated using Prism 9.

RNA-seq

RNA isolation

3-day old female flies with *esg^{ts} UAS-GFP* (control) or *esg^{ts} UAS-GFP UAS-H1 RNAi*, or *esg^{ts} UAS-GFP UAS-HP1 RNAi* were kept at 18°C for 2 days and shifted to 29°C for 4 days on poor food to induce RNAi expression. For each replicate, 70 guts (control and H1 RNAi) or 100 guts (HP1 RNAi) were dissected in cold PBS, dissociated in elastase and FACS-sorted to isolated GFP^{+} cells (ISCs and EBs). RNA isolation and purification was then performed with the Arcturus PicoPure RNA Isolation kit (Thermofisher) as described in (Dutta et al., 2013).

Sequencing and data analysis

RNA libraries were prepared with the Illumina Stranded mRNA Prep kit by the NGS facility of the Institut Curie. Libraries were sequenced by a NovaSeq (Illumina, S1 flow cell) to generate 100-bp paired-end reads. FastQ files were generated with bcl2Fastq, demultiplexed and trimmed to remove adaptors using the Raw-QC and RNA-seq analysis pipelines. Reads were aligned to the Drosophila reference genome (dm6) to generate raw counts tables. Differential expression analysis was carried out with DESeq2 in Galaxy. Genes were filtered for p-adjusted value<0.05 to be considered as significantly deregulated genes. List of genes were further analyzed in Excel.

ATAC-seq

DNA tagmentation and isolation

3-day old female flies with *esg^{ts} UAS-GFP* (control) or *esg^{ts} UAS-GFP UAS-H1 RNAi*, or *esg^{ts} UAS-GFP UAS-HP1 RNAi* were kept at 18°C for 2 days and shifted to 29°C for 4 days on poor food to induce RNAi expression. ISCs and EBs were sorted by FACS similarly as for RNA-Seq. ATAC-seq protocol was adapted to the fly intestine from (Buenrostro et al., 2015). For each replicate, we collected a minimum of 50-100,000 GFP^{+} progenitor cells. Sorted cells were washed in cold PBS and spun down at 4°C. The pellets were suspended in transposition mix (25 µL of TD buffer, 22.5 µL of water and 2.5 µL of Tn5 transposase (Illumina, #FC-121-1030) and incubated at 37 °C for 30 min. The Tagmented DNA was then purified using the Qiagen Minelute Cleanup Kit (Cat #28204). Purified transposed samples were amplified by PCR using the NebNext Hi-Fi 2× PCR Master Mix (New England Biolabs Cat #M0541S) and Illumina Nextera DNA Unique Dual Indexes. Determination of the cycle number at which each sample produced 25% of maximum fluorescent intensity was determined by qPCR. Amplified libraries were then purified using Qiagen PCR Cleanup Kit and AMPure XP beads for double size selection. Library yield was assessed using the Qubit dsDNA HS assay kit (Thermo Fisher) while library quality and molarity calculation were determined using Agilent Bioanalyzer high sensitivity DNA kits.

Sequencing and data analysis

Libraries were pooled and sequenced on Illumina NovaSeq to generate 50 bp paired-end reads. Raw reads were trimmed for adapters using trimgalore and aligned to the *Drosophila* melanogaster reference genome (dm6) using bowtie2. Duplicated reads were removed from the aligned results with Picard, and filtered to discard low mapping quality reads <20, aligned to mitochondrial chromosome reads as well as singleton reads. Only valid pairs were considered. Read shifting was applied to account for Tn5 insertions (+ strand reads adjusted by 4 bp, and - strand reads adjusted by -5bp). Peaks were called using MACS2 and Narrow peaks with q<0.01 were reported. Peak sets per conditions (control, H1 RNAi and HP1 RNAi) were obtained using bedtools Multiple Intersect between replicates. Differential peaks analysis between conditions was performed with DiffBind with significance set at FDR < 0.05. Peak Annotation was performed with ChIPseeker with TSS region defined at -3kb to +3kb and all genes within the 10kb distance are reported for each peak. Metaplots were produced using deepTools plotHeatmap in Galaxy.

H1 and HP1 RNAi experiments

For quantification of $PH3^+$ cells, esg^+ cells and $Pros^+$ cells, 3-day old female flies with *esg^{ts} UAS-GFP* (control) or *esg^{ts} UAS-GFP UAS-H1 RNAi*, or *esg^{ts} UAS-GFP UAS-HP1 RNAi* were kept at 18°C for 2 days and shifted to 29°C for 4 days, 10 days, or 21 days to induce RNAi expression. Mitotic clones expressing HP1 RNAi were generated with the Mosaic Analysis with Repressible Cell Marker (MARCM) technique. The following stocks were used : *yw [hs-Flp]1.22 p[Tub-FRT-Gal4] p[UAS-nlsGFP]/(FM6); P{tubP-GAL80}LL10* and *;FRT40A/FRT40A;MKRS/TM6B*. 3-day old female flies were maintained at 25°C, heat-shocked at 36.5°C for 35 min to induce clones and dissected 10 days after heat-shock.

Immunostainings

Flies were dissected in PBS 1X to isolate whole guts associated with Malpighian tubules. Guts were fixated in 4% PFA for 2 hours, rinsed in PBT (PBS 1X, 0,1% Triton-X 100) and then cut at the anterior and posterior sides in order to keep midguts only. Midguts were incubated in 50% glycerol/PBS 1X for 30 min to make waste exit, rinsed in PBT and incubated with primary antibodies overnight at 4°C. Then, midguts were rinsed with PBT and incubated with secondary antibodies for 3 hours at room temperature. Next, they were washed in PBT and incubated with DAPI (1:1000,) for 5 min and equilibrated in 50% glycerol/PBS 1X before being mounted on slides.

The following primary antibodies were used: mouse anti-Delta (1:2000, DSHB C594.9B), rabbit anti-pH3 (1:2000, Millipore), chicken anti-GFP (1:1000, Invitrogen), mouse anti-Prospero (1:2000, DHSB), mouse anti-H1 (1:300, ActiveMotif), mouse anti-HP1 (1:500, DHSB).

Imaging and quantifications

Imaging was conducted using a Zeiss LSM900 confocal microscope and the ZEN software at the Curie Institute imaging facility (PICT). Images were acquired with a 40X oil objective. For stack images, z-step was set at 1 to 1.5 µm. Quantifications of $PH3^+$ cells were done with a Leica epifluorescence microscope. Image analysis was performed using Fiji software followed by image assembly using Adobe Photoshop.

Statistical analyses were performed in Prism using the two-tailed Mann-Whitney test or Wilcoxon test. Significant values were reported as ns for non-significant, * for $p<0.05$, ** for $p<0.01$, *** for $p<0.001$ and **** for $p<0.0001$.

Author contributions

M.J, L.G and A.J.B designed the study and analyzed the data. M.J performed genetic experiments, DamID, and RNA-seq experiments. L.G. performed genetic experiments, ATAC-seq experiments, and analyses. M.S. helped with RNA-seq and ATAC-seq experiments. V.R. optimized RNA-seq protocols. N.R., supervised by N.S, and using the scripts of O.M., performed the chromatin state modeling. M.J, L.G and A.J.B wrote the manuscript.

SUPPLEMENTARY FIGURES

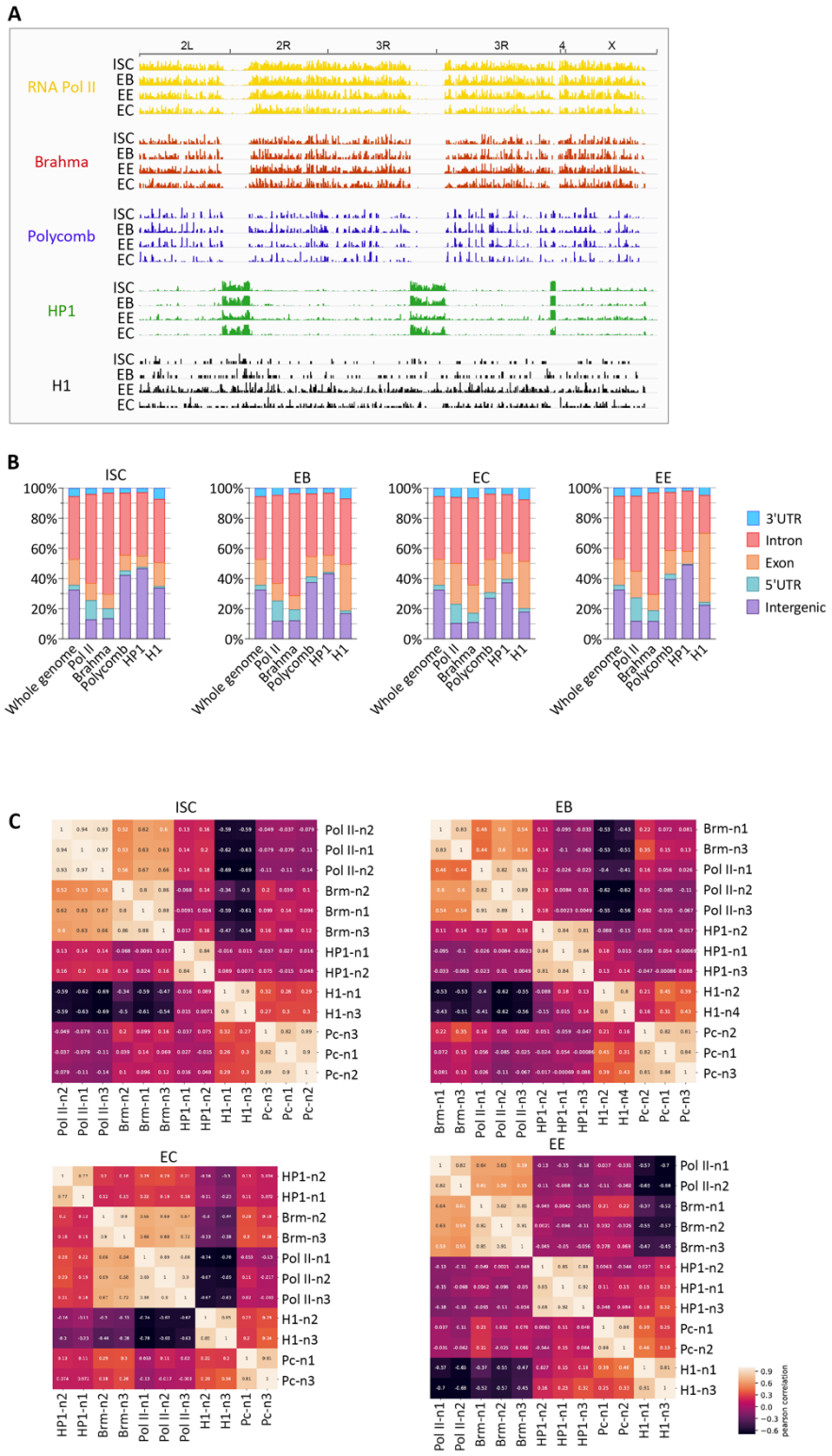

Figure S1. Characterization of RNA Pol II, Brahma, Polycomb, HP1 and H1 genome-wide binding profiles in midgut cell types.

A. Genome-wide overview of RNA Pol II, Brahma, Polycomb, HP1 and H1 binding profiles in the four midgut cell types. **B.** Genome-wide distribution of the five protein binding sites relative to genomic features. **C.** Pearson's correlation between biological replicates (n) and between the five proteins in each cell type.

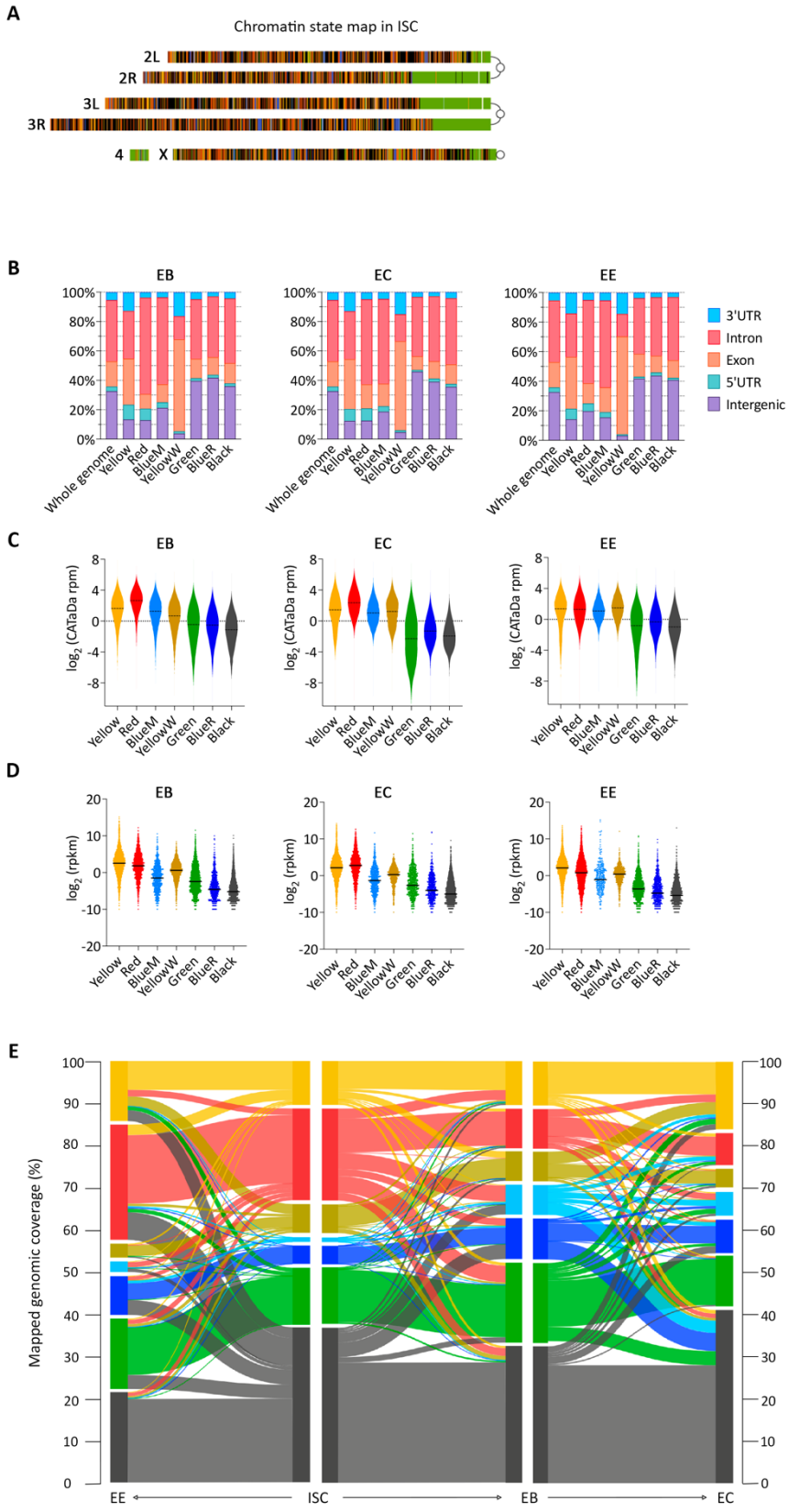

Figure S2. Genome-wide characterization of chromatin states in the midgut.
A. Genome-wide chromatin state map in ISCs. **B.** Genome-wide distribution of chromatin states in EBs, ECs and EEs relative to genomic features. **C.** Chromatin accessibility levels as defined by CATaDa in each chromatin state in EBs, ECs and EEs. **D.** Transcript levels of the genes found in each chromatin state in EBs, ECs and EEs. **E.** Changes in genome-wide coverage by chromatin states between ISCs and EBs, EBs and ECs, ISCs and EEs. Boxes on the

sides of each plot represent the proportion of the genome covered by each chromatin state. The flows represent the proportion of the genome undergoing chromatin state transitions from one state to another between cell types.

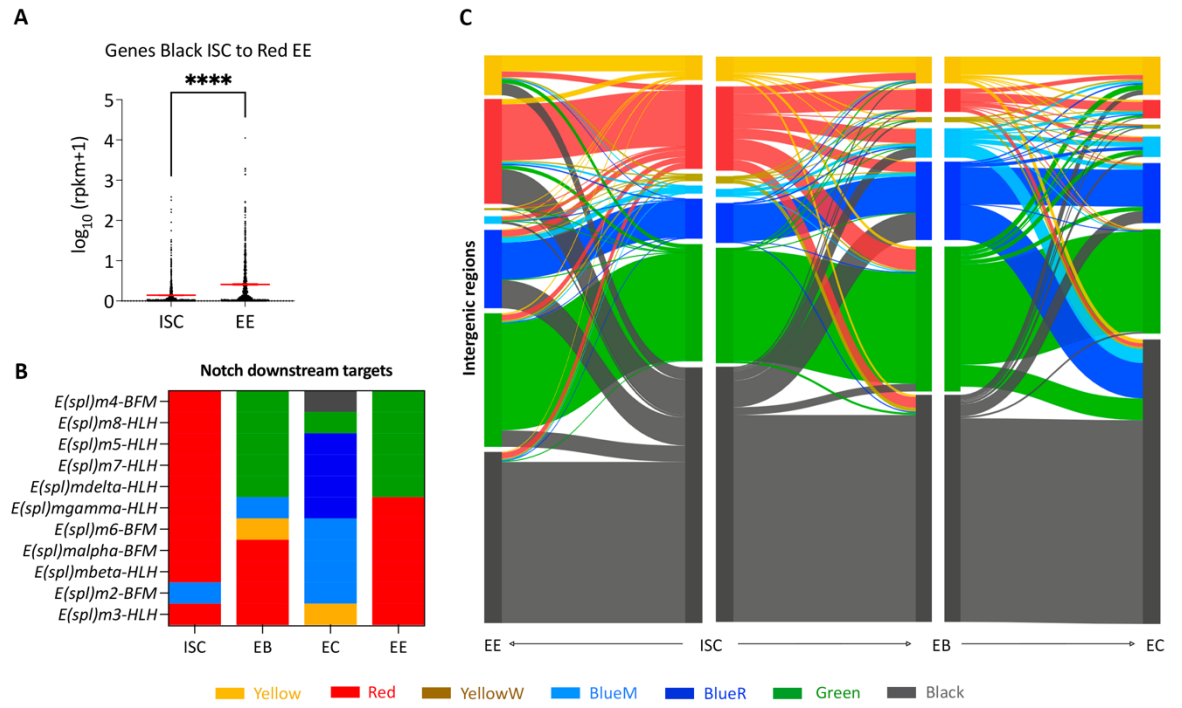

Figure S3. Characterization of genes undergoing lineage-specific chromatin state transitions.
A. Transcript levels of genes marked by the Black state in ISCs and Red state in EEs increase upon ISC to EE differentiation. Significance was assessed with a match-paired Wilcoxon test. Mean values in red, error bars are SEM, **** for p<0.0001. **B.** Chromatin states of E(spl) genes, showing EC and EE-specific chromatin state transitions upon differentiation.

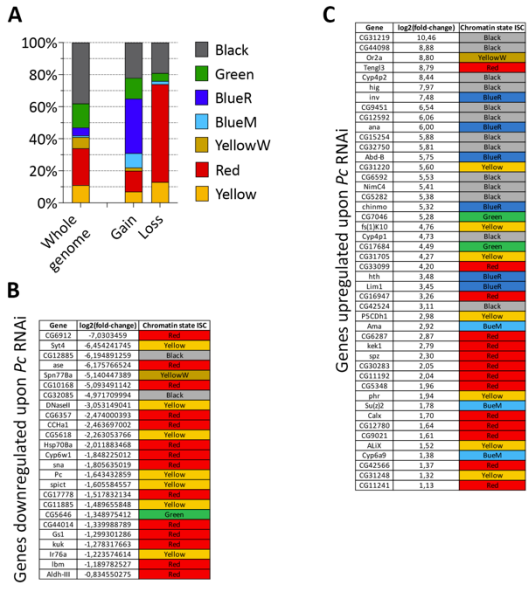

Figure S4. Chromatin states of differentially accessible regions and deregulated genes upon Polycomb knockdown.
A. Chromatin states of more (Gain) or less (Loss) accessible regions upon Polycomb RNAi, compared to the chromatin state distribution in the whole genome. **B-C.** Chromatin states of downregulated (**B**) and upregulated (**C**) genes upon Polycomb RNAi.

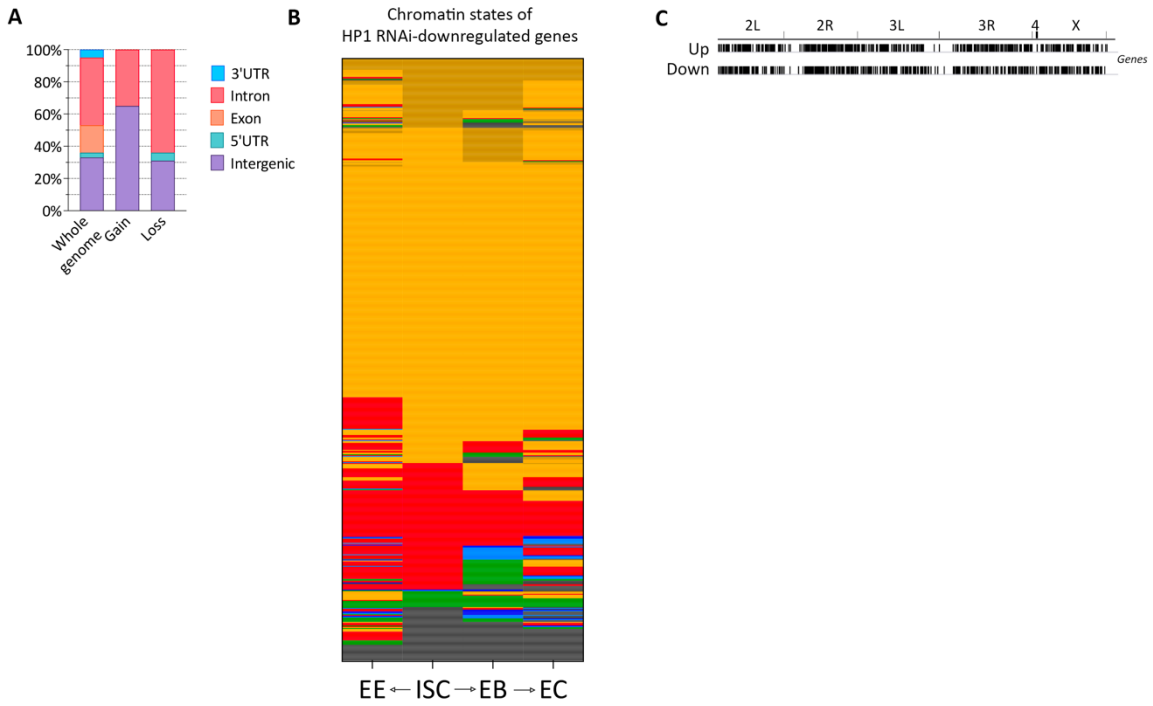

Figure S5. Characterization of differentially accessible regions and deregulated genes upon HP1 knockdown. **A.** Distribution of more (Gain) or less (Loss) accessible regions upon HP1 RNAi relative to genomic features. **B**. HP1 RNAi-deregulated genes are mostly in the Yellow state in all midgut cell types. **C.** Genome-wide distribution of upregulated and downregulated genes in HP1 RNAi.

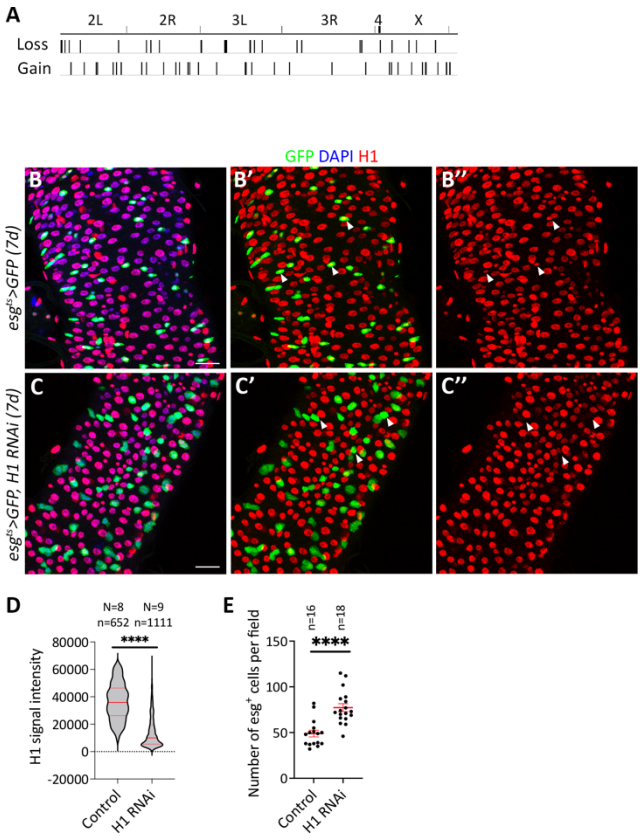

Figure S6. Characterization of differentially accessible regions and ISC proliferation upon H1 knockdown.
A. Genome-wide distribution of significant differentially accessible peaks in H1 RNAi compared to control condition. **B-C.** Midguts immunostained for GFP, H1 and DAPI in control (**B**) and ISC/EB-specific H1 RNAi (**C**) conditions after 7 days of RNAi induction. Arrowheads show esg$^+$ cells with complete or partial depletion of H1 staining (**B",C"**). **D.** Quantification of H1 staining in esg$^+$ cells (N=number of guts, n=number of cells). Signal intensity was measured on z-projections. **E.** Quantification of (B-C). For each midgut, images were taken for two fields corresponding to a posterior and an anterior region of the midgut (n=number of fields). Significance was assessed with a two-tailed Mann-Whitney test. Mean values in red, error bars are SEM. ns for non-significant, **** for p<0.0001. Scale bars, 20 µm.

Table S1. Deregulated genes upon HP1 knockdown.
https://www.dropbox.com/s/ygca3t7xd8dhdl8/Table%20S6%20HP1%20RNAi%20genes.pdf?dl=0

Table S2. GO terms enriched in downregulated genes upon HP1 knockdown.

GO ID	Description	qvalue	Count
GO:0002181	cytoplasmic translation	1.05555947687502e-73	84
GO:0006413	translational initiation	7.94088248543471e-10	22
GO:0042254	ribosome biogenesis	3.35897900522456e-09	38
GO:0042273	ribosomal large subunit biogenesis	1.1696510158062e-07	18
GO:0022613	ribonucleoprotein complex biogenesis	1.66143432376838e-07	42
GO:0006418	tRNA aminoacylation for protein translation	2.4770031264452e-07	14
GO:0043039	tRNA aminoacylation	7.047896206389e-07	14
GO:0043038	amino acid activation	8.95212168236966e-07	14
GO:0006414	translational elongation	4.69395000977408e-06	12
GO:0006888	endoplasmic reticulum to Golgi vesicle-mediated transport	5.1521196775101e-06	17
GO:0006487	protein N-linked glycosylation	5.67609921346647e-06	12
GO:0048193	Golgi vesicle transport	1.27005890969198e-05	24
GO:0034976	response to endoplasmic reticulum stress	5.39399088414721e-05	17
GO:0042255	ribosome assembly	5.39399088414721e-05	13
GO:0034660	ncRNA metabolic process	0.000197567579005508	38
GO:0006399	tRNA metabolic process	0.000322843313917276	21
GO:0140053	mitochondrial gene expression	0.000439054249682042	20
GO:0000027	ribosomal large subunit assembly	0.000530220000034135	7
GO:0006520	cellular amino acid metabolic process	0.000643485121296353	22
GO:0030968	endoplasmic reticulum unfolded protein response	0.000777410037316038	7
GO:0009145	purine nucleoside triphosphate biosynthetic process	0.000940889451260856	9
GO:0009205	purine ribonucleoside triphosphate metabolic process	0.000940889451260856	9
GO:0009206	purine ribonucleoside triphosphate biosynthetic process	0.000940889451260856	9
GO:0009144	purine nucleoside triphosphate metabolic process	0.00120107370343026	9
GO:0009225	nucleotide-sugar metabolic process	0.00130656081537345	6
GO:0009199	ribonucleoside triphosphate metabolic process	0.00183007954487357	9
GO:0009201	ribonucleoside triphosphate biosynthetic process	0.00183007954487357	9
GO:0006900	vesicle budding from membrane	0.00194825426881612	7
GO:0006754	ATP biosynthetic process	0.00197665544579958	8
GO:0046034	ATP metabolic process	0.00220720175125061	19
GO:0055086	nucleobase-containing small molecule metabolic process	0.00224313038691874	29
GO:0019752	carboxylic acid metabolic process	0.00234101899280362	36
GO:0043436	oxoacid metabolic process	0.00240583023770043	36
GO:1901137	carbohydrate derivative biosynthetic process	0.0024350202709065	31
GO:0032543	mitochondrial translation	0.00244506896224426	16
GO:0045333	cellular respiration	0.00244506896224426	18
GO:0042274	ribosomal small subunit biogenesis	0.00266132486449344	12
GO:0009142	nucleoside triphosphate biosynthetic process	0.00270714588043382	9
GO:0006082	organic acid metabolic process	0.00270959989434211	36
GO:0035966	response to topologically incorrect protein	0.0027207704651386	11
GO:0015980	energy derivation by oxidation of organic compounds	0.00279524651878421	21
GO:0015985	energy coupled proton transport, down electrochemical gradient	0.00353238593629322	7
GO:0015986	ATP synthesis coupled proton transport	0.00353238593629322	7
GO:0006486	protein glycosylation	0.00397092053692197	15
GO:0043413	macromolecule glycosylation	0.00397092053692197	15
GO:0022618	ribonucleoprotein complex assembly	0.00415361234993009	17
GO:0009141	nucleoside triphosphate metabolic process	0.00415361234993009	9
GO:0002183	cytoplasmic translational initiation	0.00415361234993009	6

Table S3. Deregulated genes upon H1 knockdown.
https://www.dropbox.com/s/s4duo92ur5ni642/Table%20S7%20H1%20RNAi%20genes.pdf?dl=0

Table S4. GO terms enriched in downregulated genes upon H1 knockdown.

GO ID	Description	qvalue	Count
GO:0034330	cell junction organization	2.98243904798857e-09	40
GO:0023061	signal release	3.540733775246e-09	24
GO:0050808	synapse organization	3.540733775246e-09	35
GO:0140352	export from cell	1.0683485528236e-08	30
GO:0043269	regulation of ion transport	1.52824521545643e-08	17
GO:0032940	secretion by cell	1.52824521545643e-08	29
GO:0099536	synaptic signaling	2.28702592573954e-08	34
GO:0046903	secretion	2.28702592573954e-08	30
GO:0007268	chemical synaptic transmission	2.79868599657393e-08	33
GO:0098916	anterograde trans-synaptic signaling	2.79868599657393e-08	33
GO:0099537	trans-synaptic signaling	3.02851980340991e-08	33
GO:0006836	neurotransmitter transport	3.82599563107171e-08	21
GO:0040007	growth	6.54104590248672e-08	39
GO:0051049	regulation of transport	6.54104590248672e-08	32
GO:0000904	cell morphogenesis involved in differentiation	7.67252683482003e-08	41
GO:0007269	neurotransmitter secretion	1.14786120625058e-07	18
GO:0099643	signal release from synapse	1.14786120625058e-07	18
GO:0099003	vesicle-mediated transport in synapse	2.70450108482594e-07	18
GO:0099504	synaptic vesicle cycle	2.70450108482594e-07	18
GO:0006812	cation transport	2.72581001860621e-07	35
GO:0045055	regulated exocytosis	4.18212556492015e-07	14
GO:0001505	regulation of neurotransmitter levels	4.96947868480571e-07	18
GO:0015837	amine transport	9.18799184060463e-07	8
GO:0048589	developmental growth	1.02623446774893e-06	33
GO:0048667	cell morphogenesis involved in neuron differentiation	1.21695119241297e-06	36
GO:0048812	neuron projection morphogenesis	1.58840591740326e-06	36
GO:0048858	cell projection morphogenesis	1.66418415732389e-06	36
GO:0120039	plasma membrane bounded cell projection morphoger	1.66418415732389e-06	36
GO:0007186	G protein-coupled receptor signaling pathway	1.79556054504436e-06	25
GO:0006887	exocytosis	2.35097503376502e-06	16
GO:0032990	cell part morphogenesis	2.415417947013e-06	36
GO:0031175	neuron projection development	3.13778029402761e-06	37
GO:0051046	regulation of secretion	3.30030508639432e-06	16
GO:0007611	learning or memory	4.66463851496399e-06	20
GO:0007409	axonogenesis	4.70621808160776e-06	29
GO:0050890	cognition	4.88421422612177e-06	20
GO:0061564	axon development	1.03352700461906e-05	29
GO:1903530	regulation of secretion by cell	1.03352700461906e-05	15
GO:0015872	dopamine transport	1.26013536697012e-05	6
GO:0051937	catecholamine transport	1.26013536697012e-05	6
GO:0015844	monoamine transport	2.28453740906451e-05	6
GO:0017156	calcium-ion regulated exocytosis	2.28453740906451e-05	6
GO:0051952	regulation of amine transport	2.28453740906451e-05	6
GO:0007617	mating behavior	3.09177142522626e-05	16
GO:0016079	synaptic vesicle exocytosis	3.35985955413506e-05	11
GO:0034329	cell junction assembly	5.17408856328206e-05	22
GO:0040008	regulation of growth	5.21485916117935e-05	26
GO:0030537	larval behavior	7.03619455869649e-05	10
GO:0030001	metal ion transport	7.44084059810438e-05	23
GO:0010959	regulation of metal ion transport	8.17808983250387e-05	10
GO:0019098	reproductive behavior	8.56142986642248e-05	16
GO:0007619	courtship behavior	8.75211508994051e-05	12
GO:0006935	chemotaxis	9.81983306425968e-05	24
GO:0007411	axon guidance	0.000108037013394487	23
GO:0007416	synapse assembly	0.000121496083432694	18

GO:0006813	potassium ion transport	0.000143271801516489	11
GO:0007618	mating	0.000165130130437758	16
GO:0034220	ion transmembrane transport	0.000165130130437758	27
GO:0097485	neuron projection guidance	0.000165397506328428	23
GO:0008345	larval locomotory behavior	0.000167243984079574	8
GO:0042391	regulation of membrane potential	0.000169151253343365	12
GO:0042330	taxis	0.00019290769511769	26
GO:0098662	inorganic cation transmembrane transport	0.000198419603333148	22
GO:0071805	potassium ion transmembrane transport	0.000253093861179699	10
GO:0051050	positive regulation of transport	0.000349946279323109	16
GO:0098660	inorganic ion transmembrane transport	0.000403330421197045	23
GO:0050803	regulation of synapse structure or activity	0.000403330421197045	18
GO:0006869	lipid transport	0.000403330421197045	12
GO:1904062	regulation of cation transmembrane transport	0.000431533402477694	8
GO:0120035	regulation of plasma membrane bounded cell projectio	0.000480615950955067	15
GO:0030865	cortical cytoskeleton organization	0.000480615950955067	10
GO:0098655	cation transmembrane transport	0.000543785215099629	22
GO:0050804	modulation of chemical synaptic transmission	0.000543785215099629	15
GO:0099177	regulation of trans-synaptic signaling	0.000543785215099629	15
GO:0048638	regulation of developmental growth	0.000549075959220634	20
GO:1903305	regulation of regulated secretory pathway	0.000573669790524049	5
GO:0031344	regulation of cell projection organization	0.000617873596920397	15
GO:0007274	neuromuscular synaptic transmission	0.000659438759937692	11
GO:0034765	regulation of ion transmembrane transport	0.000659438759937692	8
GO:0070588	calcium ion transmembrane transport	0.000659438759937692	8
GO:0007626	locomotory behavior	0.000739062090507826	17
GO:0034762	regulation of transmembrane transport	0.000769736475788836	8
GO:0071248	cellular response to metal ion	0.000796822179286057	5
GO:0007528	neuromuscular junction development	0.000820074296878441	17
GO:0010975	regulation of neuron projection development	0.000852240601682748	12
GO:0007613	memory	0.00112708420462012	13
GO:0048469	cell maturation	0.00150036535507892	16
GO:2001257	regulation of cation channel activity	0.00153011393142196	6
GO:0051260	protein homooligomerization	0.00153797686182508	5
GO:0008045	motor neuron axon guidance	0.00153797686182508	10
GO:0007188	adenylate cyclase-modulating G protein-coupled recep	0.00153797686182508	9
GO:0022898	regulation of transmembrane transporter activity	0.00153797686182508	7
GO:0032409	regulation of transporter activity	0.00153797686182508	7
GO:0032412	regulation of ion transmembrane transporter activity	0.00153797686182508	7
GO:0071695	anatomical structure maturation	0.00157444445545563	16
GO:0022603	regulation of anatomical structure morphogenesis	0.00166639976791591	16
GO:0009583	detection of light stimulus	0.00187884460146148	9
GO:0051240	positive regulation of multicellular organismal process	0.0018831659862576	17
GO:0007266	Rho protein signal transduction	0.00209536274326795	7
GO:0035220	wing disc development	0.00220469833987336	25
GO:0006816	calcium ion transport	0.0023105234829352	9
GO:0021700	developmental maturation	0.00243448850835447	17
GO:0051924	regulation of calcium ion transport	0.00243448850835447	5
GO:0071241	cellular response to inorganic substance	0.00243448850835447	5
GO:1990709	presynaptic active zone organization	0.00243448850835447	5
GO:0007612	learning	0.00243448850835447	9
GO:0007264	small GTPase mediated signal transduction	0.00243448850835447	15
GO:0015850	organic hydroxy compound transport	0.00243448850835447	6
GO:0009581	detection of external stimulus	0.00243448850835447	10
GO:0009582	detection of abiotic stimulus	0.00243448850835447	10
GO:0043624	cellular protein complex disassembly	0.00266780367529598	8

GO:0051259	protein complex oligomerization	0.00302531595090113	5
GO:0007189	adenylate cyclase-activating G protein-coupled recept	0.00353549373048801	7
GO:0060179	male mating behavior	0.0036449378369946	9
GO:0032984	protein-containing complex disassembly	0.00383827345780887	10
GO:0009187	cyclic nucleotide metabolic process	0.00413721975409851	6
GO:0007602	phototransduction	0.00473956290065129	8
GO:0007019	microtubule depolymerization	0.00473956290065129	5
GO:0046883	regulation of hormone secretion	0.00473956290065129	5
GO:0017157	regulation of exocytosis	0.00478322156990265	6
GO:0010035	response to inorganic substance	0.00478322156990265	10
GO:0060627	regulation of vesicle-mediated transport	0.00478322156990265	12
GO:0051124	synaptic assembly at neuromuscular junction	0.00478322156990265	13
GO:0006898	receptor-mediated endocytosis	0.00564975595135205	8
GO:0009914	hormone transport	0.00564975595135205	5
GO:0046879	hormone secretion	0.00564975595135205	5
GO:0003002	regionalization	0.00630540320317093	28
GO:0043270	positive regulation of ion transport	0.00633850384911752	6
GO:0050770	regulation of axonogenesis	0.00633850384911752	7
GO:0008049	male courtship behavior	0.00764718190969136	8
GO:0007163	establishment or maintenance of cell polarity	0.00772047819107093	15
GO:0009628	response to abiotic stimulus	0.00772271289742522	25
GO:0006897	endocytosis	0.00791111141827415	14
GO:0044057	regulation of system process	0.00910534778194718	8
GO:0050769	positive regulation of neurogenesis	0.00910534778194718	8
GO:1904064	positive regulation of cation transmembrane transport	0.00979843098212165	5
GO:0045467	R7 cell development	0.0104559765573879	4
GO:0046058	cAMP metabolic process	0.0104559765573879	4
GO:0030431	sleep	0.0106945003833365	9
GO:0007476	imaginal disc-derived wing morphogenesis	0.0121329146678282	18
GO:0051261	protein depolymerization	0.0122114161554864	6
GO:0050807	regulation of synapse organization	0.0122114161554864	13
GO:0031114	regulation of microtubule depolymerization	0.0131339686661085	4
GO:0008306	associative learning	0.0133326669954545	7
GO:0048488	synaptic vesicle endocytosis	0.0135048077438649	6
GO:0140238	presynaptic endocytosis	0.0135048077438649	6
GO:0007265	Ras protein signal transduction	0.0135048077438649	12
GO:0010876	lipid localization	0.0135048077438649	12
GO:0051962	positive regulation of nervous system development	0.0145149142043433	10
GO:0034767	positive regulation of ion transmembrane transport	0.015250202016244	5
GO:0035212	cell competition in a multicellular organism	0.0158789261580626	4
GO:0042063	gliogenesis	0.0171865634639882	9
GO:0051094	positive regulation of developmental process	0.0171865634639882	16
GO:0035239	tube morphogenesis	0.0171865634639882	27
GO:0016325	oocyte microtubule cytoskeleton organization	0.0171865634639882	5
GO:0034764	positive regulation of transmembrane transport	0.0171865634639882	5
GO:0016049	cell growth	0.0171865634639882	12
GO:0007423	sensory organ development	0.017611187896528	26
GO:0048588	developmental cell growth	0.0181303387939011	8
GO:0007472	wing disc morphogenesis	0.0181303387939011	18
GO:0051960	regulation of nervous system development	0.0181303387939011	15
GO:0007600	sensory perception	0.0181303387939011	22
GO:0002791	regulation of peptide secretion	0.0181303387939011	4
GO:0045167	asymmetric protein localization involved in cell fate de	0.0181303387939011	4
GO:0072375	medium-term memory	0.0181303387939011	4
GO:0090087	regulation of peptide transport	0.0181303387939011	4
GO:0046530	photoreceptor cell differentiation	0.018570951914894	15

GO:1902531	regulation of intracellular signal transduction	0.0193330229467295	21
GO:0007156	homophilic cell adhesion via plasma membrane adhes	0.0195384014161772	6
GO:0010647	positive regulation of cell communication	0.0196657746501876	25
GO:0023056	positive regulation of signaling	0.0196657746501876	25
GO:0090287	regulation of cellular response to growth factor stimulu	0.0208405173702189	7
GO:0002790	peptide secretion	0.0215135826627979	4
GO:0008038	neuron recognition	0.0216118777315351	10
GO:0070887	cellular response to chemical stimulus	0.0220702105595192	26
GO:0007218	neuropeptide signaling pathway	0.0224201751641943	7
GO:0045597	positive regulation of cell differentiation	0.0226763865064952	10
GO:0036465	synaptic vesicle recycling	0.0233954780210234	6
GO:0048599	oocyte development	0.0234963170309438	11
GO:0042044	fluid transport	0.023576652705762	5
GO:0061024	membrane organization	0.0244960151213903	17
GO:0002118	aggressive behavior	0.0247146166431744	4
GO:0007309	oocyte axis specification	0.0247146166431744	10
GO:0016331	morphogenesis of embryonic epithelium	0.0247146166431744	10
GO:0048749	compound eye development	0.0247146166431744	21
GO:0019233	sensory perception of pain	0.0249263416839733	3
GO:0071875	adrenergic receptor signaling pathway	0.0249263416839733	3
GO:0071880	adenylate cyclase-activating adrenergic receptor signa	0.0249263416839733	3
GO:0045466	R7 cell differentiation	0.0251446353752511	7
GO:0048814	regulation of dendrite morphogenesis	0.0256796741408949	5
GO:0035114	imaginal disc-derived appendage morphogenesis	0.0263516151789577	19
GO:0008037	cell recognition	0.0267719529343542	10
GO:1904396	regulation of neuromuscular junction development	0.0267719529343542	10
GO:0035107	appendage morphogenesis	0.0268147088993248	19
GO:0001745	compound eye morphogenesis	0.0268147088993248	18
GO:0031644	regulation of nervous system process	0.0277423660001323	4
GO:0035023	regulation of Rho protein signal transduction	0.0277423660001323	4
GO:0007308	oocyte construction	0.0277423660001323	10
GO:0009952	anterior/posterior pattern specification	0.0278606422933036	13
GO:0009886	post-embryonic animal morphogenesis	0.0290639686406835	24
GO:0010720	positive regulation of cell development	0.0298218593272652	8
GO:0045595	regulation of cell differentiation	0.0305795725261756	17
GO:0001508	action potential	0.0305795725261756	3
GO:0015749	monosaccharide transmembrane transport	0.0305795725261756	3
GO:0048790	maintenance of presynaptic active zone structure	0.0305795725261756	3
GO:0051180	vitamin transport	0.0305795725261756	3
GO:0009584	detection of visible light	0.0306825468744252	5
GO:0009798	axis specification	0.0306995038237613	13
GO:0048737	imaginal disc-derived appendage development	0.0307108811128509	19
GO:2000026	regulation of multicellular organismal development	0.0309650434480106	17
GO:0009620	response to fungus	0.0319334660359537	7
GO:0048736	appendage development	0.0323964180662224	19
GO:0009416	response to light stimulus	0.0326007285415285	11
GO:0001751	compound eye photoreceptor cell differentiation	0.0327180362632879	13
GO:0060562	epithelial tube morphogenesis	0.0339595832614868	24
GO:0045926	negative regulation of growth	0.0351401201077452	9
GO:0048569	post-embryonic animal organ development	0.0351401201077452	24
GO:0015833	peptide transport	0.0351401201077452	4
GO:0048592	eye morphogenesis	0.0351401201077452	18
GO:0090596	sensory organ morphogenesis	0.0351401201077452	18
GO:0035120	post-embryonic appendage morphogenesis	0.0358588866803604	18
GO:0007635	chemosensory behavior	0.0358588866803604	8
GO:0030951	establishment or maintenance of microtubule cytoske	0.0358588866803604	5

GO:0006171	cAMP biosynthetic process	0.0358588866803604	3
GO:0007026	negative regulation of microtubule depolymerization	0.0358588866803604	3
GO:0007414	axonal defasciculation	0.0358588866803604	3
GO:0034219	carbohydrate transmembrane transport	0.0358588866803604	3
GO:0044719	regulation of imaginal disc-derived wing size	0.0358588866803604	3
GO:0045332	phospholipid translocation	0.0358588866803604	3
GO:0065009	regulation of molecular function	0.0358862042918136	22
GO:0009953	dorsal/ventral pattern formation	0.0367218374422518	11
GO:0001654	eye development	0.0367218374422518	21
GO:0048880	sensory system development	0.0367218374422518	21
GO:0150063	visual system development	0.0367218374422518	21
GO:0048598	embryonic morphogenesis	0.0367218374422518	15
GO:0001754	eye photoreceptor cell differentiation	0.0370930614906129	13
GO:0002052	positive regulation of neuroblast proliferation	0.0380406646357153	4
GO:0043954	cellular component maintenance	0.0380406646357153	4
GO:0050767	regulation of neurogenesis	0.0385863174384134	10
GO:0009967	positive regulation of signal transduction	0.0386089545850974	22
GO:0010038	response to metal ion	0.0389059740515754	6
GO:0007155	cell adhesion	0.0408943846407463	14
GO:0045807	positive regulation of endocytosis	0.0419942641165596	5
GO:0042551	neuron maturation	0.0420572924573037	6
GO:0007615	anesthesia-resistant memory	0.0420974491672822	3
GO:0034204	lipid translocation	0.0420974491672822	3
GO:0099558	maintenance of synapse structure	0.0420974491672822	3
GO:0052652	cyclic purine nucleotide metabolic process	0.0420974491672822	4
GO:0072583	clathrin-dependent endocytosis	0.0420974491672822	4
GO:2000179	positive regulation of neural precursor cell proliferation	0.0420974491672822	4
GO:0098742	cell-cell adhesion via plasma-membrane adhesion mo	0.0429725815380095	7
GO:0009266	response to temperature stimulus	0.0429725815380095	10
GO:0030534	adult behavior	0.043260845748038	11
GO:0007224	smoothened signaling pathway	0.0439488307060621	8
GO:0050832	defense response to fungus	0.0439488307060621	6
GO:0008582	regulation of synaptic assembly at neuromuscular junc	0.0451433300978168	9
GO:0009190	cyclic nucleotide biosynthetic process	0.0468930192118648	4
GO:0032411	positive regulation of transporter activity	0.0468930192118648	4
GO:0032414	positive regulation of ion transmembrane transporter a	0.0468930192118648	4
GO:0045570	regulation of imaginal disc growth	0.0484843973062099	5
GO:0010817	regulation of hormone levels	0.0484843973062099	8
GO:0071692	protein localization to extracellular region	0.0484843973062099	8
GO:0031111	negative regulation of microtubule polymerization or d	0.048768825560735	3
GO:0042542	response to hydrogen peroxide	0.048768825560735	3
GO:0043271	negative regulation of ion transport	0.048768825560735	3
GO:0097035	regulation of membrane lipid distribution	0.048768825560735	3
GO:0051606	detection of stimulus	0.048768825560735	15
GO:0007043	cell-cell junction assembly	0.0493813398925534	6
GO:0030100	regulation of endocytosis	0.0493813398925534	6

REFERENCES

Adam, R.C., Yang, H., Rockowitz, S., Larsen, S.B., Nikolova, M., Oristian, D.S., Polak, L., Kadaja, M., Asare, A., Zheng, D., et al. (2015). Pioneer factors govern super-enhancer dynamics in stem cell plasticity and lineage choice. Nature 521, 366–370. https://doi.org/10.1038/nature14289.

Amcheslavsky, A., Nie, Y., Li, Q., He, F., Tsuda, L., Markstein, M., and Ip, Y.T. (2014). Gene expression profiling identifies the zinc-finger protein Charlatan as a regulator of intestinal stem cells in Drosophila. Development 141, 2621–2632. https://doi.org/10.1242/dev.106237.

Andriatsilavo, M., Stefanutti, M., Siudeja, K., Perdigoto, C.N., Boumard, B., Gervais, L., Gillet-Markowska, A., Al Zouabi, L., Schweisguth, F., and Bardin, A.J. (2018). Spen limits intestinal stem cell self-renewal. PLoS Genet. 14, e1007773. https://doi.org/10.1371/journal.pgen.1007773.

Argelaguet, R., Clark, S.J., Mohammed, H., Stapel, L.C., Krueger, C., Kapourani, C.-A., Imaz-Rosshandler, I., Lohoff, T., Xiang, Y., Hanna, C.W., et al. (2019). Multi-omics profiling of mouse gastrulation at single-cell resolution. Nature 1–5. https://doi.org/10.1038/s41586-019-1825-8.

Aughey, G.N., Estacio Gomez, A., Thomson, J., Yin, H., and Southall, T.D. (2018). CATaDa reveals global remodelling of chromatin accessibility during stem cell differentiation in vivo. ELife 7, e32341. https://doi.org/10.7554/eLife.32341.

Avgustinova, A., and Benitah, S.A. (2016). Epigenetic control of adult stem cell function. Nature Reviews Molecular Cell Biology 17, 643–658. https://doi.org/10.1038/nrm.2016.76.

Balakireva, M., Stocker, R.F., Gendre, N., and Ferveur, J.-F. (1998). Voila, a New Drosophila Courtship Variant that Affects the Nervous System: Behavioral, Neural, and Genetic Characterization. J. Neurosci. 18, 4335–4343. https://doi.org/10.1523/JNEUROSCI.18-11-04335.1998.

Boumard, B., and Bardin, A.J. (2021). An amuse-bouche of stem cell regulation: Underlying principles and mechanisms from adult Drosophila intestinal stem cells. Current Opinion in Cell Biology 73, 58–68. https://doi.org/10.1016/j.ceb.2021.05.007.

Buenrostro, J.D., Wu, B., Chang, H.Y., and Greenleaf, W.J. (2015). ATAC-seq: A Method for Assaying Chromatin Accessibility Genome-Wide. Current Protocols in Molecular Biology 109, 21.29.1-21.29.9. https://doi.org/10.1002/0471142727.mb2129s109.

Buszczak, M., Paterno, S., and Spradling, A.C. (2009). Drosophila Stem Cells Share a Common Requirement for the Histone H2B Ubiquitin Protease Scrawny. Science 323, 248–251. https://doi.org/10.1126/science.1165678.

Cryderman, D.E., Grade, S.K., Li, Y., Fanti, L., Pimpinelli, S., and Wallrath, L.L. (2005). Role of Drosophila HP1 in euchromatic gene expression. Developmental Dynamics 232, 767–774. https://doi.org/10.1002/dvdy.20310.

De Lucia, F., Ni, J.-Q., Vaillant, C., and Sun, F.-L. (2005). HP1 modulates the transcription of cell-cycle regulators in Drosophila melanogaster. Nucleic Acids Research 33, 2852–2858. https://doi.org/10.1093/nar/gki584.

Delandre, C., and Marshall, O.J. (2019). United colours of chromatin? Developmental genome organisation in flies. Biochemical Society Transactions BST20180605. https://doi.org/10.1042/BST20180605.

Dutta, D., Xiang, J., and Edgar, B.A. (2013). RNA Expression Profiling from FACS-Isolated Cells of the Drosophila Intestine. Current Protocols in Stem Cell Biology 27. https://doi.org/10.1002/9780470151808.sc02f02s27.

Dutta, D., Dobson, A.J., Houtz, P.L., Gläßer, C., Revah, J., Korzelius, J., Patel, P.H., Edgar, B.A., and Buchon, N. (2015). Regional Cell-Specific Transcriptome Mapping Reveals Regulatory Complexity in the Adult Drosophila Midgut. Cell Reports 12, 346–358. https://doi.org/10.1016/j.celrep.2015.06.009.

Erez, N., Israitel, L., Bitman-Lotan, E., Wong, W.H., Raz, G., Cornelio-Parra, D.V., Danial, S., Flint Brodsly, N., Belova, E., Maksimenko, O., et al. (2021). A Non-stop identity complex (NIC) supervises enterocyte identity and protects from premature aging. ELife 10, e62312. https://doi.org/10.7554/eLife.62312.

Ernst, J., and Kellis, M. (2010). Discovery and characterization of chromatin states for systematic annotation of the human genome. Nature Biotechnology 28, 817–825. https://doi.org/10.1038/nbt.1662.

Filion, G.J., van Bemmel, J.G., Braunschweig, U., Talhout, W., Kind, J., Ward, L.D., Brugman, W., de Castro, I.J., Kerkhoven, R.M., Bussemaker, H.J., et al. (2010). Systematic Protein Location Mapping Reveals Five Principal Chromatin Types in Drosophila Cells. Cell 143, 212–224. https://doi.org/10.1016/j.cell.2010.09.009.

Flavahan, W.A., Gaskell, E., and Bernstein, B.E. (2017). Epigenetic plasticity and the hallmarks of cancer. Science 357. https://doi.org/10.1126/science.aal2380.

Flint Brodsly, N., Bitman-Lotan, E., Boico, O., Shafat, A., Monastirioti, M., Gessler, M., Delidakis, C., Rincon-Arano, H., and Orian, A. (2019). The transcription factor Hey and nuclear lamins specify and maintain cell identity. ELife 8, e44745. https://doi.org/10.7554/eLife.44745.

Flora, P., Li, M.-Y., Galbo, P.M., Astorkia, M., Zheng, D., and Ezhkova, E. (2021). Polycomb repressive complex 2 in adult hair follicle stem cells is dispensable for hair regeneration. PLoS Genet 17, e1009948. https://doi.org/10.1371/journal.pgen.1009948.

Gaspar-Maia, A., Alajem, A., Meshorer, E., and Ramalho-Santos, M. (2011). Open chromatin in pluripotency and reprogramming. Nature Reviews Molecular Cell Biology 12, 36–47. https://doi.org/10.1038/nrm3036.

Gervais, L., and Bardin, A.J. (2017). Tissue homeostasis and aging: new insight from the fly intestine. Current Opinion in Cell Biology 48, 97–105. https://doi.org/10.1016/j.ceb.2017.06.005.

Gervais, L., Beek, M. van den, Josserand, M., Sallé, J., Stefanutti, M., Perdigoto, C.N., Skorski, P., Mazouni, K., Marshall, O.J., Brand, A.H., et al. (2019). Stem Cell Proliferation Is Kept in Check by the Chromatin Regulators Kismet/CHD7/CHD8 and Trr/MLL3/4. Developmental Cell 49, 556-573.e6. https://doi.org/10.1016/j.devcel.2019.04.033.

Gorkin, D.U., Barozzi, I., Zhao, Y., Zhang, Y., Huang, H., Lee, A.Y., Li, B., Chiou, J., Wildberg, A., Ding, B., et al. (2020). An atlas of dynamic chromatin landscapes in mouse fetal development. Nature 583, 744–751. https://doi.org/10.1038/s41586-020-2093-3.

Guo, X., Yin, C., Yang, F., Zhang, Y., Huang, H., Wang, J., Deng, B., Cai, T., Rao, Y., and Xi, R. (2019). The Cellular Diversity and Transcription Factor Code of Drosophila Enteroendocrine Cells. Cell Reports 29, 4172-4185.e5. https://doi.org/10.1016/j.celrep.2019.11.048.

Ho, L., and Crabtree, G.R. (2010). Chromatin remodelling during development. Nature 463, 474–484. https://doi.org/10.1038/nature08911.

Ho, J.W.K., Jung, Y.L., Liu, T., Alver, B.H., Lee, S., Ikegami, K., Sohn, K.-A., Minoda, A., Tolstorukov, M.Y., Appert, A., et al. (2014). Comparative analysis of metazoan chromatin organization. Nature 512, 449–452. https://doi.org/10.1038/nature13415.

Hu, J., Gu, L., Ye, Y., Zheng, M., Xu, Z., Lin, J., Du, Y., Tian, M., Luo, L., Wang, B., et al. (2018). Dynamic placement of the linker histone H1 associated with nucleosome arrangement and gene transcription in early Drosophila embryonic development. Cell Death Dis 9, 765. https://doi.org/10.1038/s41419-018-0819-z.

Hu, Y., Comjean, A., Perkins, L.A., Perrimon, N., and Mohr, S.E. (2015). GLAD: an Online Database of Gene List Annotation for Drosophila . J. Genomics 3, 75–81. https://doi.org/10.7150/jgen.12863.

Jadhav, U., Nalapareddy, K., Saxena, M., O'Neill, N.K., Pinello, L., Yuan, G.-C., Orkin, S.H., and Shivdasani, R.A. (2016). Acquired Tissue-Specific Promoter Bivalency Is a Basis for PRC2 Necessity in Adult Cells. Cell 165, 1389–1400. https://doi.org/10.1016/j.cell.2016.04.031.

Jadhav, U., Saxena, M., O'Neill, N.K., Saadatpour, A., Yuan, G.-C., Herbert, Z., Murata, K., and Shivdasani, R.A. (2017). Dynamic Reorganization of Chromatin Accessibility Signatures during Dedifferentiation of Secretory Precursors into Lgr5+ Intestinal Stem Cells. Cell Stem Cell 21, 65-77.e5. https://doi.org/10.1016/j.stem.2017.05.001.

Jiang, H., Patel, P.H., Kohlmaier, A., Grenley, M.O., McEwen, D.G., and Edgar, B.A. (2009). Cytokine/Jak/Stat Signaling Mediates Regeneration and Homeostasis in the Drosophila Midgut. Cell 137, 1343–1355. https://doi.org/10.1016/j.cell.2009.05.014.

Jiang, H., Tian, A., and Jiang, J. (2016). Intestinal stem cell response to injury: lessons from Drosophila. Cellular and Molecular Life Sciences 73, 3337–3349. https://doi.org/10.1007/s00018-016-2235-9.

Jin, Y., Xu, J., Yin, M.-X., Lu, Y., Hu, L., Li, P., Zhang, P., Yuan, Z., Ho, M.S., Ji, H., et al. (2013). Brahma is essential for Drosophila intestinal stem cell proliferation and regulated by Hippo signaling. ELife 2. https://doi.org/10.7554/eLife.00999.

Kazakevych, J., Sayols, S., Messner, B., Krienke, C., and Soshnikova, N. (2017). Dynamic changes in chromatin states during specification and differentiation of adult intestinal stem cells. Nucleic Acids Research 45, 5770–5784. https://doi.org/10.1093/nar/gkx167.

Kharchenko, P.V., Alekseyenko, A.A., Schwartz, Y.B., Minoda, A., Riddle, N.C., Ernst, J., Sabo, P.J., Larschan, E., Gorchakov, A.A., Gu, T., et al. (2011). Comprehensive analysis of the chromatin landscape in Drosophila melanogaster. Nature 471, 480–485. https://doi.org/10.1038/nature09725.

Kim, T.-H., Li, F., Ferreiro-Neira, I., Ho, L.-L., Luyten, A., Nalapareddy, K., Long, H., Verzi, M., and Shivdasani, R.A. (2014). Broadly permissive intestinal chromatin underlies lateral inhibition and cell plasticity. Nature 506, 511–515. https://doi.org/10.1038/nature12903.

Kolasinska-Zwierz, P., Down, T., Latorre, I., Liu, T., Liu, X.S., and Ahringer, J. (2009). Differential chromatin marking of introns and expressed exons by H3K36me3. Nature Genetics 41, 376–381. https://doi.org/10.1038/ng.322.

Lee, D.H., Li, Y., Shin, D.-H., Yi, S.A., Bang, S.-Y., Park, E.K., Han, J.-W., and Kwon, S.H. (2013). DNA microarray profiling of genes differentially regulated by three heterochromatin protein 1 (HP1) homologs in Drosophila. Biochemical and Biophysical Research Communications 434, 820–828. https://doi.org/10.1016/j.bbrc.2013.04.020.

Lemaitre, B., and Miguel-Aliaga, I. (2013). The Digestive Tract of Drosophila melanogaster. Annual Review of Genetics 47, 377–404. https://doi.org/10.1146/annurev-genet-111212-133343.

Li, Z., Guo, X., Huang, H., Wang, C., Yang, F., Zhang, Y., Wang, J., Han, L., Jin, Z., Cai, T., et al. (2020). A Switch in Tissue Stem Cell Identity Causes Neuroendocrine Tumors in Drosophila Gut. Cell Reports 30, 1724-1734.e4. https://doi.org/10.1016/j.celrep.2020.01.041.

Lien, W.-H., Guo, X., Polak, L., Lawton, L.N., Young, R.A., Zheng, D., and Fuchs, E. (2011). Genome-wide Maps of Histone Modifications Unwind In Vivo Chromatin States of the Hair Follicle Lineage. Cell Stem Cell 9, 219–232. https://doi.org/10.1016/j.stem.2011.07.015.

Lin, C.-H., Li, B., Swanson, S., Zhang, Y., Florens, L., Washburn, M.P., Abmayr, S.M., and Workman, J.L. (2008). Heterochromatin Protein 1a Stimulates Histone H3 Lysine 36 Demethylation by the Drosophila KDM4A Demethylase. Molecular Cell 32, 696–706. https://doi.org/10.1016/j.molcel.2008.11.008.

Lu, X., Wontakal, S.N., Emelyanov, A.V., Morcillo, P., Konev, A.Y., Fyodorov, D.V., and Skoultchi, A.I. (2009). Linker histone H1 is essential for Drosophila development, the establishment of pericentric heterochromatin, and a normal polytene chromosome structure. Genes Dev. 23, 452–465. https://doi.org/10.1101/gad.1749309.

Lu, X., Wontakal, S.N., Kavi, H., Kim, B.J., Guzzardo, P.M., Emelyanov, A.V., Xu, N., Hannon, G.J., Zavadil, J., Fyodorov, D.V., et al. (2013). Drosophila H1 regulates the genetic activity of heterochromatin by recruitment of Su(var)3-9. Science 340, 78–81. https://doi.org/10.1126/science.1234654.

Ma, Y., Chen, Z., Jin, Y., and Liu, W. (2013). Identification of a histone acetyltransferase as a novel regulator of Drosophila intestinal stem cells. FEBS Letters 587, 1489–1495. https://doi.org/10.1016/j.febslet.2013.03.013.

Marshall, O.J., and Brand, A.H. (2015). damidseq_pipeline: an automated pipeline for processing DamID sequencing datasets: Fig. 1. Bioinformatics 31, 3371–3373. https://doi.org/10.1093/bioinformatics/btv386.

Marshall, O.J., and Brand, A.H. (2017). Chromatin state changes during neural development revealed by in vivo cell-type specific profiling. Nature Communications 8. https://doi.org/10.1038/s41467-017-02385-4.

Marshall, O.J., Southall, T.D., Cheetham, S.W., and Brand, A.H. (2016). Cell-type-specific profiling of protein–DNA interactions without cell isolation using targeted DamID with next-

generation sequencing. Nature Protocols 11, 1586–1598. https://doi.org/10.1038/nprot.2016.084.

Martin, E.W., Krietsch, J., Reggiardo, R.E., Sousae, R., Kim, D.H., and Forsberg, E.C. (2021). Chromatin accessibility maps provide evidence of multilineage gene priming in hematopoietic stem cells. Epigenetics Chromatin 14, 2. https://doi.org/10.1186/s13072-020-00377-1.

Meshorer, E., and Misteli, T. (2006). Chromatin in pluripotent embryonic stem cells and differentiation. Nature Reviews Molecular Cell Biology 7, 540–546. https://doi.org/10.1038/nrm1938.

Micchelli, C.A., and Perrimon, N. (2006). Evidence that stem cells reside in the adult Drosophila midgut epithelium. Nature 439, 475–479. https://doi.org/10.1038/nature04371.

Mikkelsen, T.S., Ku, M., Jaffe, D.B., Issac, B., Lieberman, E., Giannoukos, G., Alvarez, P., Brockman, W., Kim, T.-K., Koche, R.P., et al. (2007). Genome-wide maps of chromatin state in pluripotent and lineage-committed cells. Nature 448, 553–560. https://doi.org/10.1038/nature06008.

Nègre, N., Brown, C.D., Ma, L., Bristow, C.A., Miller, S.W., Wagner, U., Kheradpour, P., Eaton, M.L., Loriaux, P., Sealfon, R., et al. (2011). A cis -regulatory map of the Drosophila genome. Nature 471, 527–531. https://doi.org/10.1038/nature09990.

Ohlstein, B., and Spradling, A. (2006). The adult Drosophila posterior midgut is maintained by pluripotent stem cells. Nature 439, 470–474. https://doi.org/10.1038/nature04333.

Park, A.R., Liu, N., Neuenkirchen, N., Guo, Q., and Lin, H. (2019). The Role of Maternal HP1a in Early Drosophila Embryogenesis via Regulation of Maternal Transcript Production. Genetics 211, 201–217. https://doi.org/10.1534/genetics.118.301704.

Piacentini, L., Fanti, L., Negri, R., Vescovo, V.D., Fatica, A., Altieri, F., and Pimpinelli, S. (2009). Heterochromatin Protein 1 (HP1a) Positively Regulates Euchromatic Gene Expression through RNA Transcript Association and Interaction with hnRNPs in Drosophila. PLOS Genetics 5, e1000670. https://doi.org/10.1371/journal.pgen.1000670.

Raab, J.R., Tulasi, D.Y., Wager, K.E., Morowitz, J.M., Magness, S.T., and Gracz, A.D. (2019). Quantitative classification of chromatin dynamics reveals regulators of intestinal stem cell differentiation. Development dev.181966. https://doi.org/10.1242/dev.181966.

Schoelz, J.M., and Riddle, N.C. (2022). Functions of HP1 proteins in transcriptional regulation. Epigenetics & Chromatin 15, 1–15. https://doi.org/10.1186/s13072-022-00453-8.

Southall, T.D., Gold, K.S., Egger, B., Davidson, C.M., Caygill, E.E., Marshall, O.J., and Brand, A.H. (2013). Cell-Type-Specific Profiling of Gene Expression and Chromatin Binding without Cell Isolation: Assaying RNA Pol II Occupancy in Neural Stem Cells. Developmental Cell 26, 101–112. https://doi.org/10.1016/j.devcel.2013.05.020.

Sun, J., Wei, H.-M., Xu, J., Chang, J.-F., Yang, Z., Ren, X., Lv, W.-W., Liu, L.-P., Pan, L.-X., Wang, X., et al. (2015). Histone H1-mediated epigenetic regulation controls germline stem cell self-renewal by modulating H4K16 acetylation. Nature Communications 6. https://doi.org/10.1038/ncomms9856.

Sun, J., Wang, X., Xu, R.-G., Mao, D., Shen, D., Wang, X., Qiu, Y., Han, Y., Lu, X., Li, Y., et al. (2021). HP1c regulates development and gut homeostasis by suppressing Notch signaling through Su(H). EMBO Reports 16. .

Tauc, H.M., Tasdogan, A., Meyer, P., and Pandur, P. (2017). Nipped-A regulates intestinal stem cell proliferation in Drosophila. Development 144, 612–623. https://doi.org/10.1242/dev.142703.

Tauc, H.M., Rodriguez-Fernandez, I.A., Hackney, J.A., Pawlak, M., Ronnen Oron, T., Korzelius, J., Moussa, H.F., Chaudhuri, S., Modrusan, Z., Edgar, B.A., et al. (2021). Age-related changes in polycomb gene regulation disrupt lineage fidelity in intestinal stem cells. ELife 10, e62250. https://doi.org/10.7554/eLife.62250.

Veenstra, J.A., Agricola, H.-J., and Sellami, A. (2008). Regulatory peptides in fruit fly midgut. Cell Tissue Res 334, 499–516. https://doi.org/10.1007/s00441-008-0708-3.

van der Velde, A., Fan, K., Tsuji, J., Moore, J.E., Purcaro, M.J., Pratt, H.E., and Weng, Z. (2021). Annotation of chromatin states in 66 complete mouse epigenomes during development. Commun Biol 4, 1–15. https://doi.org/10.1038/s42003-021-01756-4.

Wang, C., Guo, X., and Xi, R. (2014). EGFR and Notch signaling respectively regulate proliferative activity and multiple cell lineage differentiation of Drosophila gastric stem cells. Cell Res 24, 610–627. https://doi.org/10.1038/cr.2014.27.

Willcockson, M.A., Healton, S.E., Weiss, C.N., Bartholdy, B.A., Botbol, Y., Mishra, L.N., Sidhwani, D.S., Wilson, T.J., Pinto, H.B., Maron, M.I., et al. (2020). H1 histones control the epigenetic landscape by local chromatin compaction. Nature https://doi.org/10.1038/s41586-020-3032-z.

Wu, J., Huang, B., Chen, H., Yin, Q., Liu, Y., Xiang, Y., Zhang, B., Liu, B., Wang, Q., Xia, W., et al. (2016). The landscape of accessible chromatin in mammalian preimplantation embryos. Nature 534, 652–657. https://doi.org/10.1038/nature18606.

Zeng, X., Chauhan, C., and Hou, S.X. (2010). Characterization of midgut stem cell- and enteroblast-specific Gal4 lines in drosophila. Genesis 48, 607–611. https://doi.org/10.1002/dvg.20661.

Zeng, X., Lin, X., and Hou, S.X. (2013). The Osa-containing SWI/SNF chromatin-remodeling complex regulates stem cell commitment in the adult Drosophila intestine. Development 140, 3532–3540. https://doi.org/10.1242/dev.096891.

Chapter 2: Stem Cell Proliferation Is Kept in Check by the Chromatin Regulators Kismet/CHD7/CHD8 and Trr/MLL3/4

In this Chapter, I will present my contribution to a paper published by the lab in 2019. In this article, Louis Gervais investigated the role of two conserved chromatin remodeling factors, Kismet and Trithorax-related (Trr), in the regulation of ISC self-renewal. I joined the project at my arrival in the lab and generated data that completed the characterization of Kismet and Trr in ISCs. The full article is in Annex 1, and the figures I contributed to are in the next pages.

Gervais L, van den Beek M., **Josserand M**, Sallé J, Stefanutti M, Perdigoto CN, Skorski P, Mazouni K, Marshall OJ, Brand AH, Schweisguth F, Bardin AJ. (2019) Stem Cell Proliferation Is Kept in Check by the Chromatin Regulators Kismet/CHD7/CHD8 and Trr/MLL3/4. *Developmental Cell.*

kismet, the fly ortholog of mammalian *CHD7/8*, was initially identified as an ISC regulator candidate in an EMS screen (Perdigoto, 2010), where *kismet* mutant clones induced accumulation of ISCs. *kismet* limits ISC proliferation in a stem-cell-autonomous manner through regulation of EGFR signaling, without affecting terminal differentiation. To further understand how Kismet regulates self-renewal, the genome-wide binding of Kismet was profiled in ISCs using Targeted DamID. Given that Kismet is a chromatin remodeling protein with important functions in development and adult tissues (see details in Introduction, part II), we aimed to better understand the nature of the chromatin environment of Kismet binding sites. Therefore, we profiled the binding sites of other chromatin-associated proteins, RNA Pol II, Polycomb, Brahma, HP1 and H1 in ISCs, which gave a first overview of the chromatin landscape in ISCs (**Fig. 4B, S5H**).

First, the whole-genome binding profiles of RNA Pol II, Brahma, Polycomb, HP1 and H1 in ISCs were consistent with the known properties of these proteins. Using a dimension reduction method called UMAP, we represented the distribution of all GATC sites based on the binding sites of each protein (**Fig. 4C**). This way, we showed that Kismet co-localized with active regions of the genome defined by RNA Pol II and Brahma binding, while it was depleted in regions enriched in Polycomb, H1 and HP1, which are representative of more repressive chromatin states. We then compared the genes that were significantly bound by each protein,

which confirmed that Kismet-bound genes significantly overlapped with RNA Pol II and Brahma-bound genes, as well as expressed genes in ISCs (**Fig. 4F-I**). In contrast, there was little overlap with Polycomb, HP1 and H1-bound genes (**Fig. 4D-E).** Then, we showed that Kismet was enriched at the TSS of ISC active genes, including many known ISC-enriched genes (**Fig. 4J, Fig. S5B**). Furthermore, Kismet was enriched at developmental enhancers but not at housekeeping enhancers as defined in embryonic S2 cells, in contrast with RNA Pol II that was enriched at both developmental and housekeeping enhancers (**Fig. 4K**).

Next, other TrxG genes were tested for a function in ISC, reasoning that they could act with Kismet. Knockdown of the histone methyltransferase encoding gene *trr* (*MLL3/4* in mammals) led to a phenotype similar to that of *kismet* mutant in ISCs. Given this function of *trr* in regulating ISC self-renewal, we examined Trr binding sites as previously done for Kismet. Trr was also found to overlap with RNA Pol II and Brahma binding profiles and to be enriched at active genes (**Fig. 6C-D**). Moreover, we found that 73% of Kismet-bound genes were also bound by Trr (**Fig. 6F**). RNA-seq performed on FACS-sorted ISCs in *kismet* or *trr* knockdown contexts further revealed that they co-regulated several hundreds of genes (**Fig. 6H-I**). Among these was found *Cbl*, also bound by both Kismet and Trr by DamID (**Fig. 6L**). Additional genetic experiments showed that *Cbl* was necessary to maintain basal levels of ISC proliferation by modulating EGFR signaling (**Fig. 6M-P**). Therefore, *Cbl* is likely one of the downstream targets of Kismet and Trr that limits ISC self-renewal.

In summary, this study identified two novel regulators of stem cell proliferation in the *Drosophila* intestine, Kismet and Trr. Genome-wide profiling of Kismet and Trr and RNA-seq data show that Kismet and Trr co-localize at transcriptionally active chromatin and suggest that they co-act to limit stem cell proliferation through regulation of Cbl, leading to downregulation of EGFR signaling.

More specifically, my contribution to the paper was as follows:

- I performed DamID experiments to generate the binding profiles of Brahma, HP1 and H1 in ISCs (3 replicates for each).
- The bio-informatic analyses of the different binding profiles presented in Figure 4 and Figure S5 are the results of a joint work between Louis Gervais, Marius van den Beek (former postdoc of the lab, bio-informatician) and myself. In particular, Marius and I worked together on generating the workflow for peak calling and peak assignment to

genes. I then performed the analyses showing protein enrichments at specific groups of genes or enhancers.

- I carried out the DamID experiments for Trr (3 replicates) and performed part of the subsequent bio-informatic analyses presented in Figure 6.

When I generated these data and did the subsequent analyses, we were building my PhD project, which aimed to define and characterize chromatin states in ISCs and their progeny in order to gain insight into chromatin changes occurring during differentiation in the adult midgut. Therefore, the experiments and analyses I performed during my first year in the lab were used to complete the findings about Kismet but were also the part of the data used for modeling chromatin states in the intestinal lineage, as part of my main PhD work.

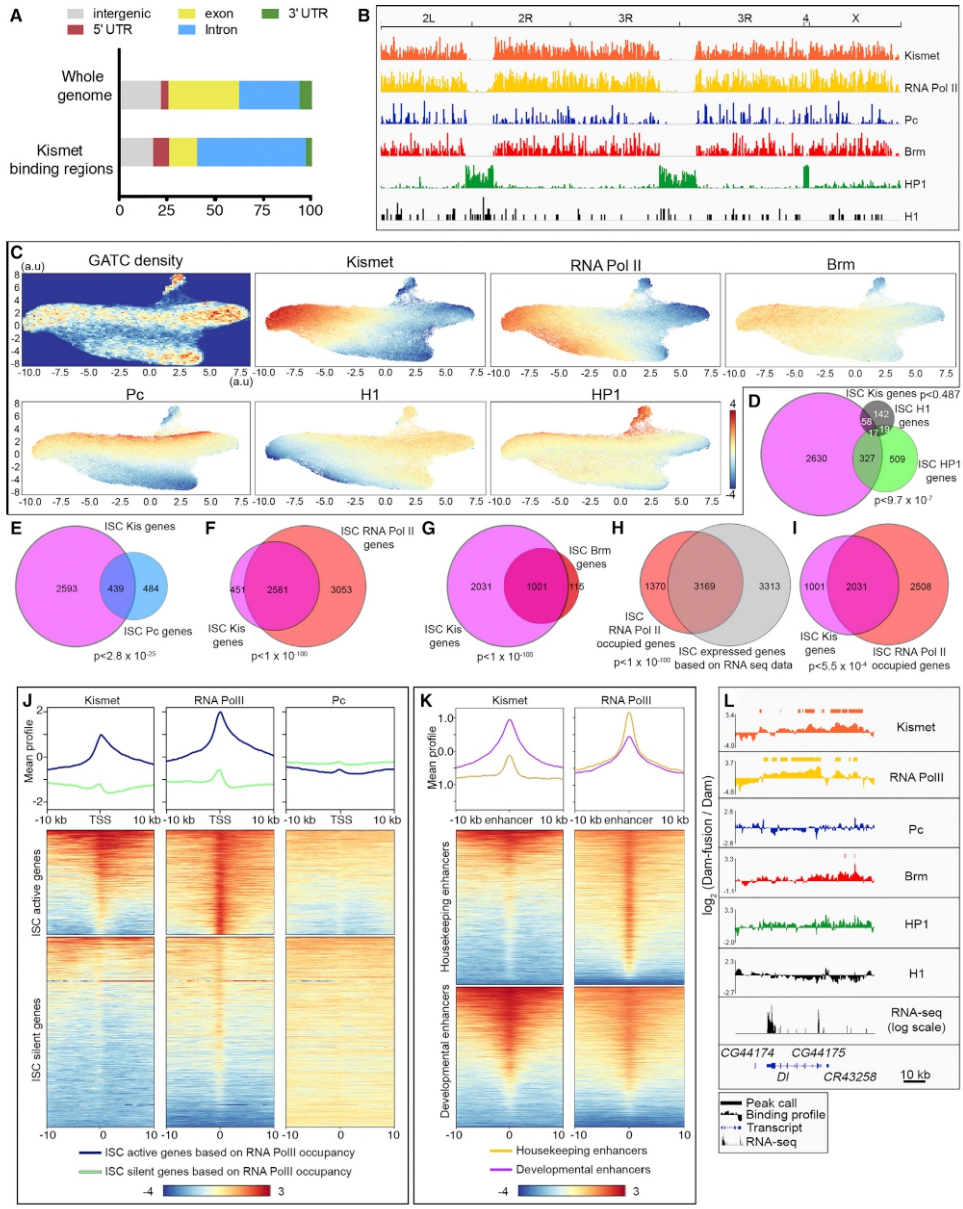

Figure 4. Genome-wide Mapping of Kismet Relative to RNA Pol II, Brm, Pc, HP1, and H1

(A) Kismet DamID-seq showed an enrichment of methylated GATCs in the introns and 5′UTRs of genes. Unassembled regions of the genome were not considered.

(legend continued on next page)

(B) Genome-wide overview of the DamID binding peak density in ISCs of Kismet, RNA Pol II, Polycomb (Pc), Brahma (Brm), HP1, and H1.

(C) UMAP clustering of GATC sites based on 7 DamID fusion proteins (see STAR Methods) in the ISC. Density of GATC sites throughout the genome used for clustering followed by the plots representing the binding of each protein over GATC sites.

(D–I) Venn diagrams of genes with peaks of the DamID-seq data in ISCs: Kismet versus HP1 or H1 (D) versus Pc (E) versus RNA Pol II (F) and versus Brm (G). Genes with a significant mean RNA Pol II occupancy determined by DamID versus transcriptionally active genes based on RNA-seq from Dutta et al., 2015 (H) and versus genes with peaks of Kismet (I).

(J) Mean position and metaplot of Kismet, RNA Pol II, and Pc in ISCs relative to the TSS for genes classified by their activity based on RNA Pol II occupancy. Kismet was significantly enriched over the TSS of active genes.

(K) Mean position and metaplot of Kismet and RNA Pol II in ISC relative to previously defined "developmental" or "housekeeping" enhancers in S2 cells from Zabidi et al., 2015. Kismet was found enriched over developmental enhancers.

(L) Wild-type RNA-seq, Dam-Kis, Dam-RNA Pol II, Dam-Pc, Dam-Brm, Dam-HP1, and Dam-H1 ISC binding profiles and peaks alignments over the genomic region surrounding the ISC-specific gene *Delta*.

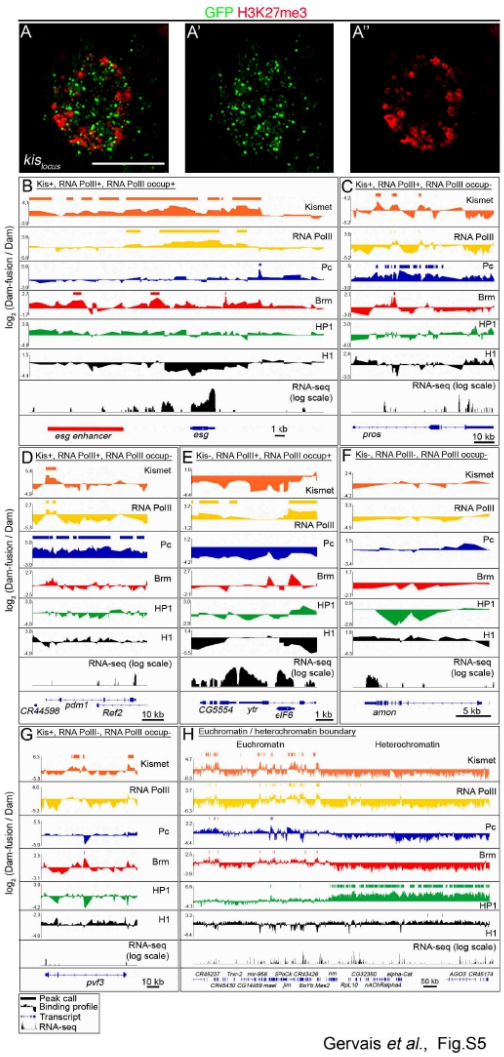

Gervais *et al.*, Fig.S5

Figure S5. Kismet distribution on lineage specific genes, related to Figure 4.

(A-A") Super-resolution image of Kismet distribution (Kismet-FLAP tagged kis_{locus} marked by GFP, GREEN) in the nuclei of enterocytes. Kismet was found to be enriched in regions generally lacking the H3K27me3 repressive mark (RED). Scale bar = 5µm. **(B-H)** Wild-type RNAseq, as well as Dam-Kis, Dam-RNA Pol II, Dam-Pc, Dam-Brm, Dam-HP1, Dam-H1 ISC binding profiles and peaks alignments over: (B) the genomic region of the gene *esg,* expressed in the ISCs (having significant RNA Pol II occupancy); (C, D) the genomic region of genes not expressed in the ISCs with low level of Dam-RNA Pol II recruitment (RNA Pol II mean occupancy not significant) though bound by Kismet such as *pros* (C) and *pdm1* (D); (E) the genomic region of genes *ytr* and *eIF6* not bound by Kismet but expressed in ISCs; (F, G) the genomic region of genes not expressed in ISCs *amon* (EE specific), and *pyf3* (EE enriched) (G); (H) the chromosome 3L pericentromeric region at the euchromatin / heterochromatin boundary.

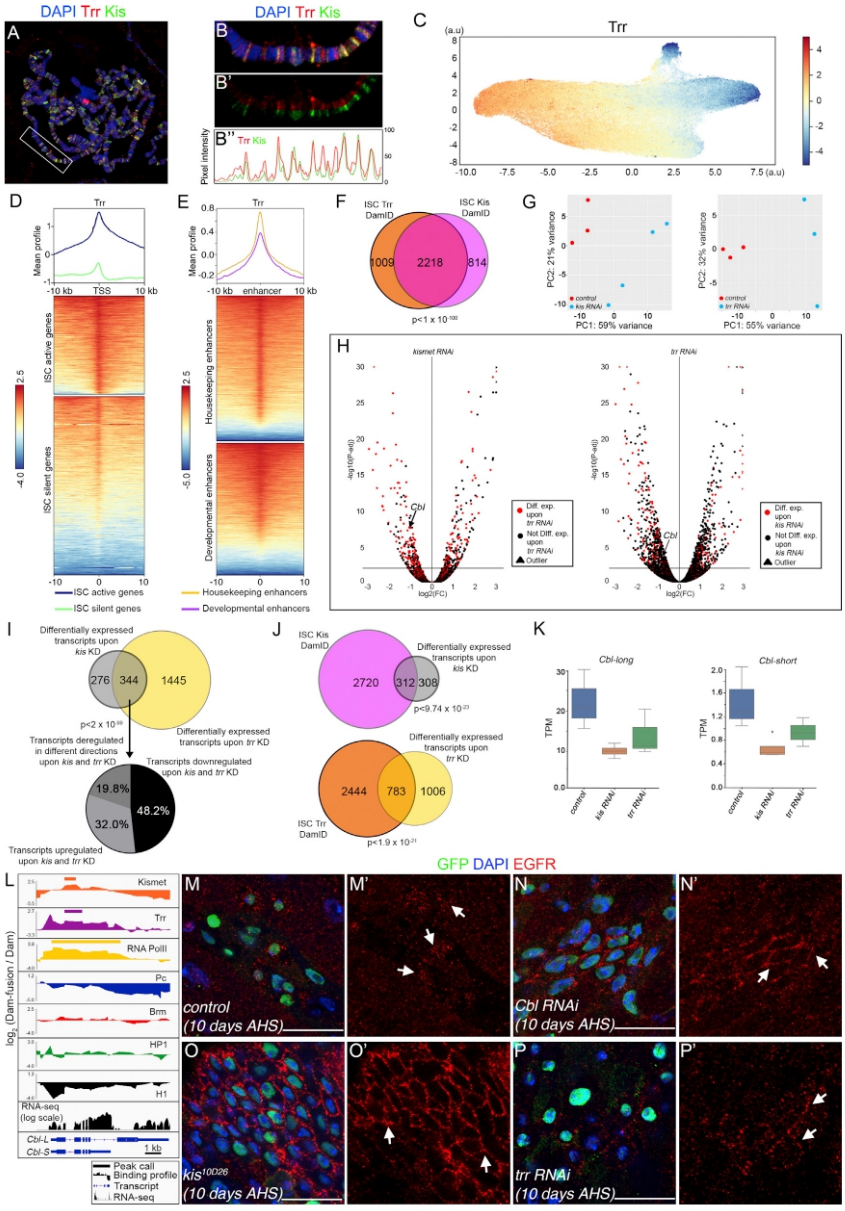

Figure 6. Genome-wide Mapping of Trr DNA Binding Sites and Genes Regulated by Kismet and Trr

(A) Kismet and Trr localization on polytene chromosomes of the salivary gland.

(B–B″) Magnification of the chromosome highlighted in (A). Fluorescent intensity in (B″).

(legend continued on next page)

(C) Trr binding in the ISC clustered using UMAP based on 7 DamID fusion proteins (STAR Methods and Figure 4C).

(D) Mean position and metaplot of Trr in ISCs plotted relative to the TSS for genes according to their activity based on RNA Pol II occupancy shows its enrichment over the TSS of active genes.

(E) Mean position and metaplot of Trr in ISC over previously defined "developmental" or "housekeeping" enhancers in S2 cells from Zabidi et al., 2015.

(F) Overlap between genes with peaks of Kismet versus Trr.

(G) Principal-component analysis of RNA-seq.

(H) Differentially expressed genes; red points highlight common genes.

(I) Upper: overlap between genes with RNAs deregulated upon *kis* and *trr* knockdown in the ISCs. Lower: proportion of RNAs altered in *kis* and *trr* knockdown.

(J) Upper: genes with peaks of Kismet and deregulated after *kis* knockdown in the ISCs. Lower: genes with peaks of Trr and deregulated after *trr* KD in the ISCs.

(K) RNA-seq data showing downregulation of the 2 *Cbl* isoforms upon either *kis* RNAi and *trr* RNAi in the ISC.

(L) Alignement at the *Cbl* locus of wild-type RNA-seq, Kismet, Trr, RNA Pol II, Pc, Brm, HP1, H1 binding profiles and peaks as determined by DamID-seq in ISCs.

(M–P′) clone of wild-type (M and M′), *Cbl* RNAi (N and N′), *kis*^{10D26} (O and O′) and *trr RNAi* (P and P′), 10 days AHS. Arrows show EGFR-positive cells. Scale bars, 20 μm.

Chapter 3: Exploring the role of candidate genes in the intestinal lineage

In Chapter 1, we identified the main chromatin state transitions followed by genes with essential roles in the regulation of ISC activity and lineage specification. Therefore, we hypothesized that genes following the same chromatin state transitions could have similar roles. In particular, we wanted to test whether the chromatin state of a gene can be predictive of its expression pattern or its function. In this chapter, I will detail how I chose candidate genes and the genetic experiments I performed to explore their role in the intestinal lineage. I focused on (1) candidates for a role in regulating ISC activity and (2) candidates for a role in EE or EC cell fate specification.

For each gene, I examined its expression pattern in the midgut based on antibodies or reporters, depending on the availability of reagents. Then, I performed loss of function and overexpression experiments to address gene function, using available RNAi, mutant and UAS lines. These are preliminary experiments that should be considered as a screen for further investigation rather than a precise characterization of each gene's function.

I. Testing candidate genes for a role in the regulation of ISC activity

I.A. Choice of candidate genes

In our analyses of chromatin state transitions at genes, we observed that transcription factor-encoding genes with essential roles in ISC regulation, such as *esg*, were subjected to a transition from an active chromatin state in ISCs (Yellow or Red) to the Polycomb-enriched BlueM or BlueR states upon differentiation. Therefore, I looked at all the genes undergoing this type of transition and applied additional criteria to select candidates (**Fig. 1**). In particular, I looked for genes encoding transcription factors, and transcribed in ISCs (rpkm>1) based on published RNA-seq data (Dutta et al., 2015). I also considered known data from the literature and reagents availability, which led to reduce the number of candidates to three genes: *senseless* (*sens*), *senseless-2* (*sens-2*) and *48 related 2* (*Fer2*). We predicted that these genes may be important regulators of ISC proliferation or differentiation.

Sens is a zinc-finger transcription factor involved in the development of the peripheral nervous system (Jafar-Nejad et al., 2003, 2006; Nolo et al., 2000). It physically interacts with bHLH proneural proteins as a co-activator of the expression of proneural genes (Acar, 2006).

It also has a role in eye photoreceptor differentiation through regulation of EGFR signaling (Frankfort and Mardon, 2004; Frankfort et al., 2004; Xie et al., 2007). Given that proneural proteins such as Daughterless and Scute are also involved in the regulation of ISC differentiation through the interplay with Notch signaling (Bardin et al., 2010), we chose *sens* as a candidate despite a low transcription level in ISCs (rpkm = 0,48).

The function of *sens-2*, a homolog of *sens*, is unknown but we reasoned that as a homolog of *sens*, it was worth testing its function as well. Also, *sens-2* was reported as expressed in particular EE subtypes (Guo et al., 2019), but rpkm values suggest that it is expressed in other midgut cell types too (**Fig. 1**).

Fer2 encodes a conserved bHLH transcription factor involved in various nervous system processes. It was first identified for its role in circadian rhythm (Nagoshi et al., 2010). It was also shown to be required for the development and the survival of dopaminergic neurons in the adult brain through protection against oxidative stress, a function conserved in mammals (Dib et al., 2014; Miozzo et al., 2022). Given that several transcription factors with important functions in the nervous system also play roles in the intestinal lineage, *Fer2* appeared as a good candidate.

Gene	State ISC	State EB	State EC	State EE	rpkm ISC	rpkm EB	rpkm EC	rpkm EE
sens	Yellow	BlueR	BlueR	BlueM	0,48	0,02	0,02	0,48
sens-2	Red	Yellow	BlueR	BlueR	2,03	1,09	1,97	2,60
Fer2	Red	BlueR	BlueR	Green	2,93	1,72	3,31	1,42
bib	Red	Green	Black	Green	1,74	1,14	1,43	0,25

Figure 1. List of candidate genes for a role in ISCs.
Chromatin state is indicated for each cell type. Rpkm values are from (Dutta et al., 2015).

In addition, I selected one candidate undergoing another chromatin state transition of interest: active state in ISCs to Black in ECs and in the Black/BlueR/Green state in EEs, a pattern observed for components of the Notch pathway (**Fig. 3F of Chapter 1**). By applying the same criteria as mentioned above, the gene *big brain* (*bib*) was chosen as a fourth candidate (**Fig. 1**). *Bib* was first identified as a neurogenic gene necessary for development of the nervous system, but no genetic interaction with other neurogenic genes or Notch has been shown (Rao et al., 1992). It encodes a transmembrane protein that acts as a cation channel but may also have a role in cell adhesion (Rao et al., 1990; Tatsumi et al., 2009). Although the cellular function of *bib* in neurogenesis remains unclear, it was suggested that it could increase Notch signaling by potentiating Notch-Delta binding (Doherty et al., 1997). It has also been shown

that *bib* is required for copper accumulation, likely through recycling of copper transporters (Wang et al., 2014b). Finally, a genome-wide genetic screen for regulators of ISCs identified *bib* as a potential negative regulator of ISC to EC differentiation, similarly to negative regulators of the Notch pathway (Zeng et al., 2015).

I.B. Expression pattern of *sens*, *sens-2*, *Fer2* and *bib*

To examine the expression of *sens*, I used an anti-sens antibody and performed immunostainings on *esgGal4 Su(H)GAL80ts* fly midguts, in which GFP is specifically expressed in ISCs. Overall, Sens could not be detected in the intestine, suggesting that protein levels were very low or absent.

For *senseless-2*, I crossed a *sens-2-GAL4* reporter line with a *UAS-2XGFP* line. GFP was detected in large patches of ECs in the R5 region only (**Fig. 2A**), and rarely in isolated ECs in the rest of the midgut (**Fig. 2B**). *Delta*$^{+}$ ISCs and *pros*$^{+}$ EEs were GFP^{-}, suggesting that *sens-2* is expressed only in a sub-population of ECs. Since this reporter line has not been validated, this result should be considered with caution.

The expression of *Fer2* was explored using a *Fer2-GAL4* line crossed with *UAS-2XGFP* and two fly strains carrying Fer2-GFP tagged constructs. No GFP could be detected in any of the reporter lines. At this time, Gwenn Le Meur, an engineer in the lab, was developing and optimizing RNA Fluorescence *In Situ* Hybridization (FISH) techniques to detect mRNA in the midgut. We used RNAscope®, a highly sensitive technique, to examine *Fer2* mRNA localization in midgut cells. However, no mRNA was detected, indicating that *Fer2* is not transcribed in the midgut. This goes against the published rpkm values, suggesting that *Fer2* might be transcribed very transiently or in specific spatial and temporal windows.

Bib expression pattern was investigated using (i) an anti-bib antibody and (ii) a *bib-GAL4* reporter strain crossed with *UAS-2XGFP*. Bib antibody staining was either absent or very weak depending on the regions (**Fig. 2C-D**). There was a nuclear staining in some ECs, which is inconsistent with the expected subcellular localization of a membrane protein (**Fig. 1D**). It is likely that the signal was mostly non-specific staining. Consistent with this, no GFP signal was detected in the *bib-GAL4;UAS-2XGFP* midguts. Therefore, it is unclear whether *bib* is expressed in midgut cells, as the low rpkm values could explain that we were not able to detect it. It could also be transiently expressed.

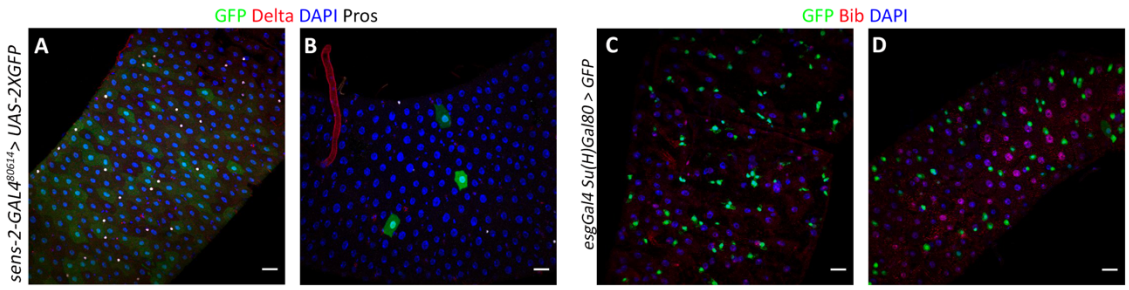

Figure 2. Sens-2 and Bib are detected heterogeneously along the midgut.
A-B. Midguts immunostained for GFP, Delta, Pros and DAPI. Representative images of the R5 posterior region (**A**) and of a middle midgut region (**B**). **C-D**. Midguts immunostained for GFP, Bib and DAPI. Two different regions of the same midgut are shown. Scale bars: 20 µm.

I.C. Testing *sens*, *sens-2*, *Fer2* and *bib* for a role in ISCs

Although I was not able to detect the expression of the four candidate genes in the midgut, I did not exclude a potential role for these genes, possibly through transient or very low expression levels. For each gene, I performed (i) knockdown and overexpression specifically in ISCs/EBs using *esgGal4*^{ts} flies, (ii) knockdown or overexpression in GFP-labeled mitotic clones using the Mosaic Analysis with a Repressible Cell Marker (MARCM) technique. This allowed me to assess ISC proliferation in these different genetic contexts.

senseless

Knockdown of *sens* using RNAi resulted in an increase in the number of PH3$^+$ cells in two replicates out of three, suggesting that *sens* may limit ISC proliferation (**Fig. 3A**). In parallel, I used the mutant line *sens*^{E2} *FRT80B* to generate mutant clones (**Fig. 3B-C**). At 7 days or 10 days after heatshock, there was a mild but significant decrease in the number of GFP$^+$ cells and Delta$^+$ cells, in two out of three replicates (**Fig. 3D-E**). This suggests that ISC division may be reduced, which is in opposition to the results of increased ISC division upon RNAi knockdown in ISCs/EBs. In order to discriminate these contradictory results, *sens-RNAi* was expressed in "flipout" clones, which results in expressing GFP and the RNAi in the cells that derive from ISCs/EBs using the *esgGAL4* driver. Thus, it targets all *esg*$^+$ cells and marks their progeny. As there was much variability in clone size between guts within both control and *sens-RNAi* conditions, I classified the guts into 3 categories depending on their clone composition: (1) small clones, isolated GFP$^+$ cells and a few large clones, (2) only very large clones spanning over the whole gut, (3) mix of isolated GFP$^+$ cells and large clones. In two replicates, there was

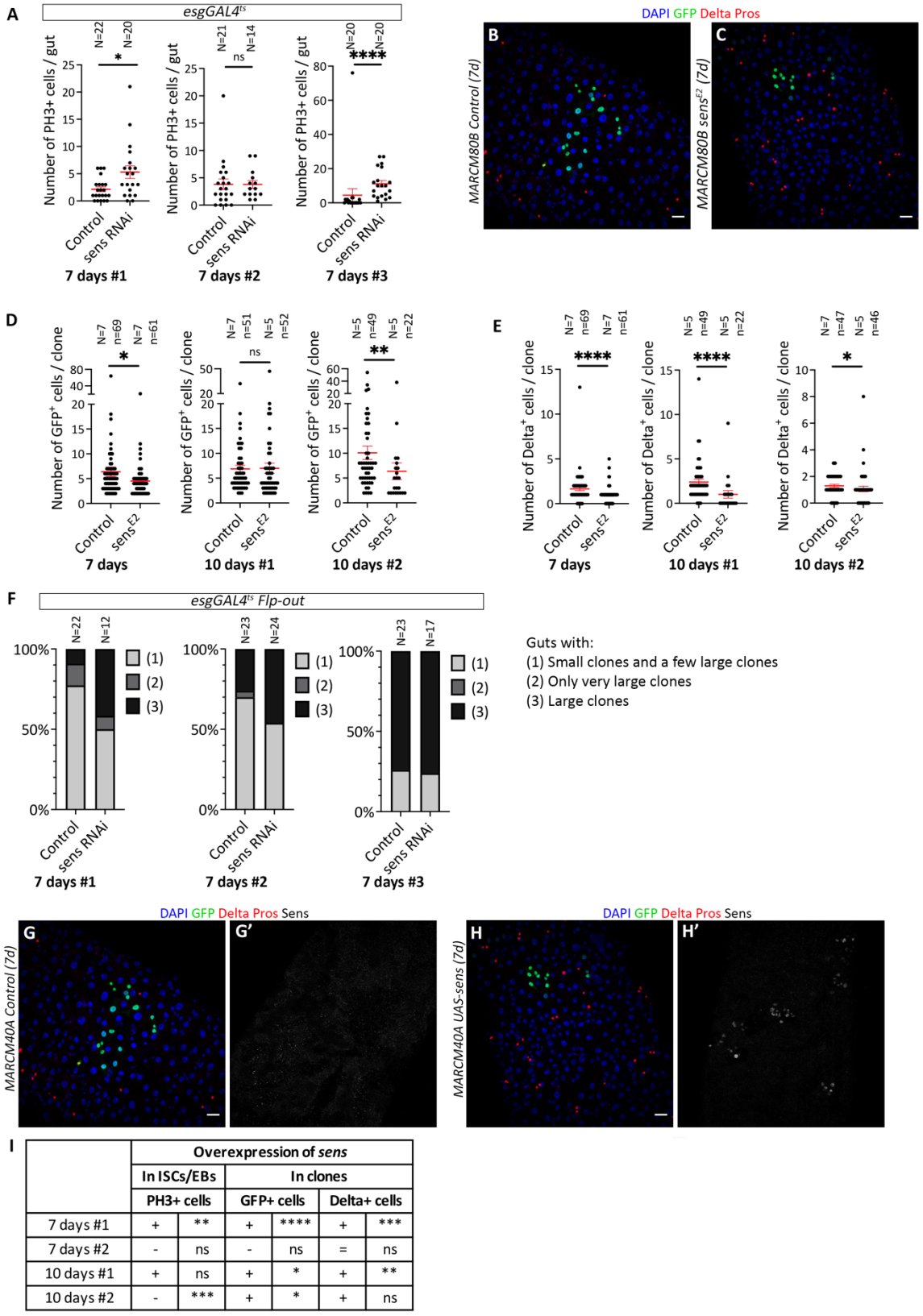

I

	Overexpression of *sens*					
	In ISCs/EBs		In clones			
	PH3+ cells		GFP+ cells		Delta+ cells	
7 days #1	+	**	+	****	+	***
7 days #2	-	ns	-	ns	=	ns
10 days #1	+	ns	+	*	+	**
10 days #2	-	***	+	*	+	ns

Figure 3. Loss of function and overexpression of *senseless* in the midgut cause inconsistent and mild phenotypes.

A. Quantification of PH3$^+$ cells per gut in 3 replicates. **B**. Control clones (**B**) and *sens* mutant clones (**C**) in midguts immunostained for GFP, Delta (membrane), Pros (nuclear) 7 days after heatshock. **D-E.** Quantifications of the

numbers of GFP$^+$ cells per clones (**D**) and Delta$^+$ cells per clone (**E**), 7 days or 10 days after heatshock. N=number of guts, n=number of clones. **F**. Distribution of guts with control clones and *sens RNAi*-expressing clones in the 3 different categories. **G-H**. Control clones (**G**) and *UAS-sens* clones (**H**) in midguts immunostained for GFP, Delta, Pros and Sens 7 days after heatshock. **I**. Table summarizing the phenotypes observed upon *sens* overexpression. + for increase, - for decrease.
Significance was assessed with a two-tailed Mann-Whitney test. Mean values in red, error bars are SEM. ns for non-significant, * for p<0.05, ** for p<0.01, *** for p<0.001, **** for p<0.0001. Scale bars: 20 µm.

a higher proportion of guts with large clones (category 3) in *sens-RNAi* condition than in the control (**Fig. 3F**). However, this effect was not seen in the third replicate. Therefore, these experiments did not allow the identification of a clear effect of *sens* loss of function. Overexpressing *sens* in ISCs/EBs or in mitotic clones led to minor changes in proliferation or clone size, but these were very variable between replicates (data summarized in **Fig. 3I**). Overall, these results showed inconsistent and mild phenotypes, which made difficult any interpretation regarding the function of *sens* in the intestinal lineage.

senseless-2

Sens-2 knockdown was achieved using two RNAi lines. Proliferation was not affected when *sens-2* RNAi was expressed in ISCs/EBs (**Fig. 4A**). For analysis of MARCM clones, I defined three categories of clones (small = 1-6 cells, medium = 6-20 cells, large = >20 cells) and counted the number of clones in each category. The distribution of clones in the different classes was very similar between the control and the two *sens-2 RNAi* lines (**Fig. 4B**). As for *sens*, overexpression of *sens-2* led to mostly not significant and inconsistent results between replicates in terms of proliferation or clone composition (**Fig. 4C**). Therefore, we could not identify any function for *sens-2* in regulating ISC proliferation in homeostasis, but there might be mild effects or differentiation defects that would be detected only with a more precise quantification.

Importantly, the quantification of PH3$^+$ cells in *sens* and *sens-2* experiments showed a high variability between control guts. The intestine is very responsive to environmental signals, notably through ISC proliferation. This variability has already been observed in the lab and makes difficult the interpretation of some experiments, we thus reasoned that the nature of the food used to feed the flies was probably responsible for many external stimuli that trigger a proliferation response. Therefore, for the next experiments, flies were fed with a

"poor" food medium, which reduces the quantity of nutrients ingested and thus the sensitivity of guts to external stress.

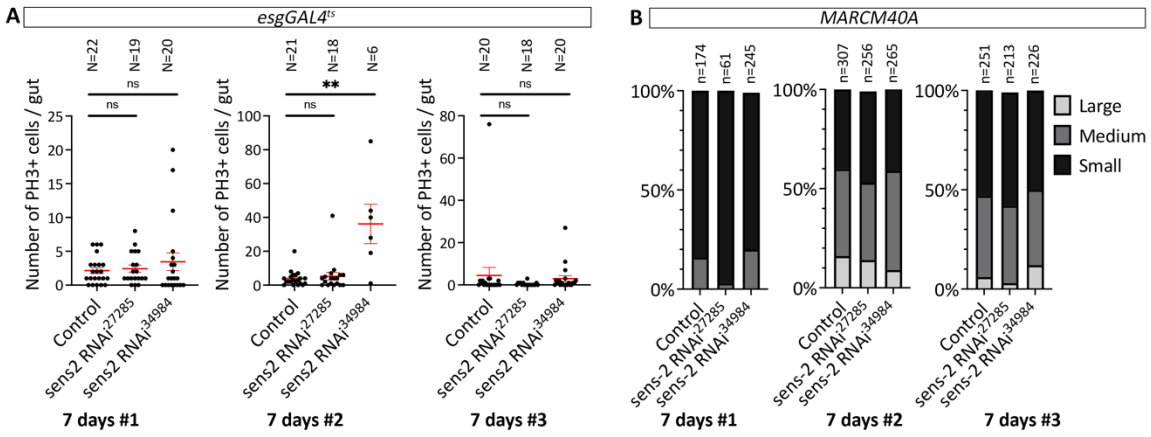

C

	Overexpression of *sens-2*					
	In ISCs/EBs		In clones			
	PH3+ cells		GFP+ cells		Delta+ cells	
7 days #1	+	**	+	****	+	****
7 days #2	=	ns	-	*	-	ns
10 days #1	=	ns	=	ns	+	ns
10 days #2	-	****	+	ns	=	ns

Figure 4. Knockdown and overexpression of *senseless-2* in the midgut cause inconsistent phenotypes.
A. Quantification of PH3⁺ cells per gut in 3 replicates. **B**. Distribution of control clones and *sens-2 RNAi*-expressing clones (2 fly strains) in 3 categories of clone size. n=number of clones. **I**. Table summarizing the phenotypes observed upon *sens-2* overexpression. + for increase, - for decrease.
Significance was assessed with a two-tailed Mann-Whitney test. Mean values in red, error bars are SEM. ns for non-significant, * for p<0.05, ** for p<0.01, *** for p<0.001, **** for p<0.0001.

Fer2

Fer2 function in ISC proliferation was investigated using four different RNAi lines. One of them (*Fer2-RNAi*^{28697}) resulted in a significant increase in PH3⁺ cell numbers but only in one replicate (**Fig. 5A**). *Fer2-RNAi#4* also showed a mild increase in proliferation, but the other RNAi strains had no effect. Expression of *Fer2-RNAi*^{28697} in induced mitotic clones showed a mild increase in the proportion of medium and large clones (**Fig. 5B**). These results indicate that *Fer2* knockdown may induce a slight increase in ISC proliferation.

Fer2 overexpression caused a significant decrease in the number of dividing cells, which was observed with two different UAS-Fer2 fly strains, but this result was not seen in all replicates (**Fig. 5C**). However, midguts exhibiting PH3⁺ cell numbers comparable to control guts displayed a specific pattern where all the dividing cells were spatially limited to one region of the midgut and not all along the midgut as in the control condition. In addition, there was

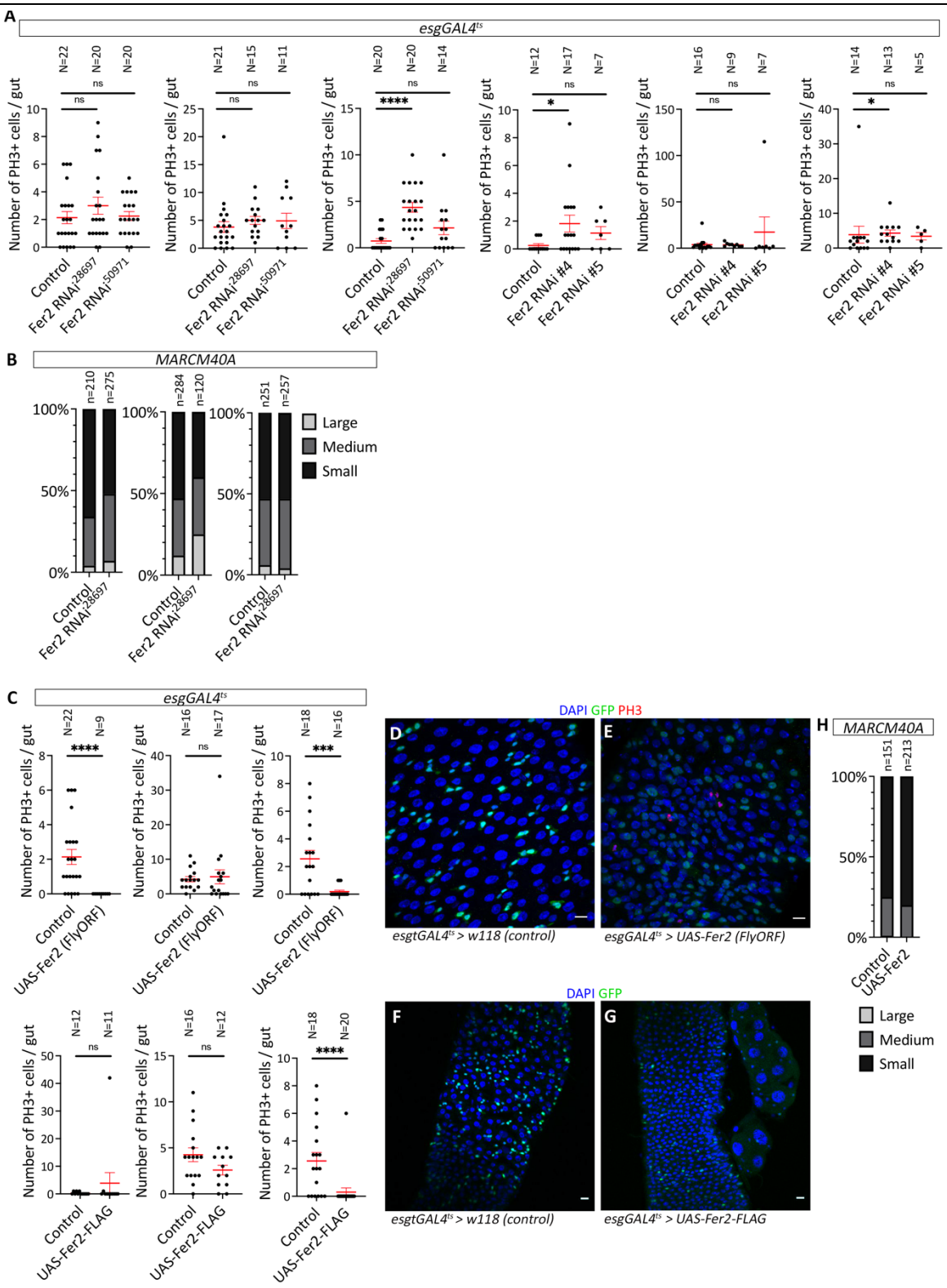

Figure 5. *Fer2* overexpression in ISCs/EBs suggests a role in regulating ISC proliferation.
A. Quantification of PH3$^+$ cells per gut in 3 replicates for each fly strain. **B**. Distribution of control clones and *Fer2 RNAi*-expressing clones in 3 categories of clone size. **C**. Quantification of PH3$^+$ cells per gut in 3 replicates for each fly strain. **D**-**G**. Control midguts (**D**, **F**) and midguts with ISB/EB-specific expression of *UAS-Fer2* (**E**, **G**) immunostained for GFP, Delta and PH3 7 days after RNAi induction. **E**. Region with an increase in the number of GFP$^+$ cells and PH3$^+$ cells. **G**. Representative region of the rest of the midgut showing a reduction in the number of GFP$^+$ cells. **H**. Distribution of guts with control clones and *UAS-Fer2*-expressing clones in the 3 different categories. Significance was assessed with a two-tailed Mann-Whitney test. Mean values in red, error bars are SEM. ns for non-significant, * for p<0.05, *** for p<0.001, **** for p<0.0001. Scale bars, 20 µm.

an aggregation of GFP$^+$ cells in this region, indicating a local increase in proliferation (**Fig. 5D-E**). However, the rest of the midgut showed a global reduction of GFP$^+$ cells in both *UAS-Fer2* strains, consistent with the absence of PH3$^+$ dividing cells (**Fig. 5F-G**). Therefore, these results suggest that *Fer2* overexpression caused a global reduction of proliferation, likely leading to the loss of ISCs/EBs progenitors, except in one region where proliferation was increased. These observations indicate that *Fer2* overexpression in ISCs/EBs has region-specific effects. Overexpression of *Fer2* in MARCM clones did not lead to major differences in clone size compared to control clones (**Fig. 5H**), and the observed clones were not limited to the proliferative region observed in *esgGal4ts>UAS-Fer2* midguts. However, this was done in only one replicate and should be confirmed.

Overall, this characterization of *Fer2* in the midgut showed that it is not expressed in homeostasis, but it cannot be excluded by *Fer2* is upregulated in other contexts. Our overexpression experiments suggest that it could, for example, have a role in limiting proliferation in the context of recovery after an environmental stress.

bib

bib RNAi expressed in ISCs/EBs using the *esgGal4ts* driver resulted in a decrease in the number of PH3$^+$ cells (**Fig. 6A**). This was accompanied by a global reduction of GFP$^+$ cells throughout the gut (not shown), but some regions still had GFP$^+$ cell numbers compared to the ones in the control. In the midguts where *bib RNAi* was induced in mitotic clones, large clones were absent, and there was an increase in the proportion of small clones compared to the clone size distribution of control clones (**Fig. 6B**). Together, these results suggest that *bib* may be required to maintain ISC proliferation.

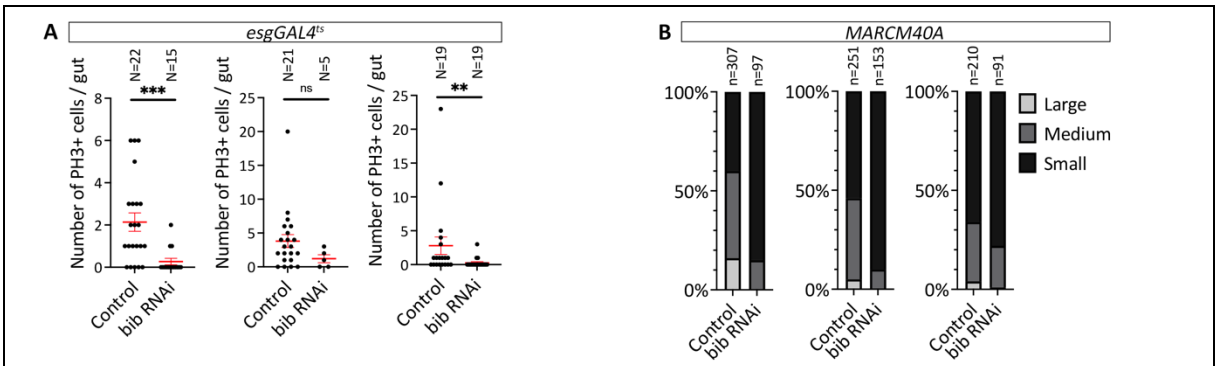

Figure 6. Knockdown of *bib* in the midgut suggests a role in maintaining ISC proliferation.
A. Quantification of PH3$^+$ cells per gut in 3 replicates. **B**. Distribution of control clones and *bib RNAi*-expressing clones in 3 categories of clone size. n=number of clones. Significance was assessed with a two-tailed Mann-Whitney test. Mean values in red, error bars are SEM. ns for non-significant, ** for p<0.01, *** for p<0.001.

II. Testing candidate genes for a role in cell fate specification

II.A. Choice of candidate genes

In this second part, I focused on another type of chromatin state transition: from BlueR in ISCs to Yellow or Red in ECs/EEs. Indeed, the major cell fate regulators *nub* and *pros*, as well as *mirror* and *Pox neuro*, follow this transition, suggesting that genes undergoing the same transition could have a role in cell fate specification. Among the genes following this particular transition, I focused on genes expressed in ECs or EEs but not expressed in ISCs (rpkm<1). As many EC-expressed genes were found in the BlueM state, I included it in "active states" in ECs. In order to choose candidates that would be specific to either EC or EE, I excluded the genes that were expressed or in active states in the other cell type, respectively. Additional data from the literature led to the selection of three candidates: *POU domain protein 2* (*pdm2*) for a role in EC cells, *Fire exit* (*Fie*) and *beta amyloid protein precursor-like* (*Appl*) for a role in EE cells (**Fig. 7**).

Gene	State ISC	State EB	State EC	State EE	rpkm ISC	rpkm EB	rpkm EC	rpkm EE
pdm2	BlueR	BlueR	BlueM	BlueR	0,19	0,00	1,37	0,54
Fie	BlueR	Green	Black	Red	0,44	0,16	0,34	11,55
Appl	BlueR	BlueR	Black	Red	0,06	0,03	0,30	5,20

Figure 7. List of candidate genes for a role in cell fate regulation.
Chromatin state is indicated for each cell type. Rpkm values are from (Dutta et al., 2015).

pdm2 is a homolog of *nub/pdm1*, which was our strongest argument for a role in EC specification. Both *nub* and *pdm2* have crucial and redundant functions in segmentation and early neurogenesis (Bhat and Schedl; Bhat et al., 1995; Grosskortenhaus et al., 2006; Tran and Doe, 2008). In particular, *pdm2* is required the specification of ganglion mother cells identity and their subsequent neuronal progeny. While *nub* was shown to be sufficient to trigger ISC to EC differentiation in the adult midgut (Korzelius et al., 2014), a role for *pdm2* in adult tissues remains unknown.

Fie encodes a transmembrane protein expressed in a portion of glia cells during development (With et al., 2003). Although no function was found for *Fie*, the rpkm values in the midgut suggest that it is expressed in EEs at levels comparable to those of *prospero* and it is marked by the same chromatin states in each cell type.

Appl is part of the family of APP genes associated with Alzheimer's disease in humans (Luo et al., 1990). It has been extensively studied for its functions in various neuronal

processes including nervous system development, neuronal wiring, axonal growth, neuron death, neuroglial interactions, memory and circadian rhythm (Kessissoglou et al., 2020; Li et al., 2004; Luna et al., 2017; Mora et al., 2013; Preat and Goguel, 2016; Soldano et al., 2013). *Appl* encodes a glycoprotein that can be cleaved and secreted. As for *Fie*, *Appl* was found in our study with a chromatin state and rpkm pattern that suggested a potential function in EEs (**Fig. 7**).

II.B. Expression pattern of *pdm2*, *Fie* and *Appl*

To determine *pdm2* expression pattern, midguts with ISC-specific GFP expression (*esgGAL4Su(H)GAL80ts* driver) were stained with an anti-Pdm2 antibody. Pdm2 staining was detected at low levels in the nuclei of some ECs but not in GFP$^+$ cells or small diploid cells, suggesting that it is specifically expressed in a subset of ECs (**Fig. 8A**). As pdm2 is marked by the Blue Mixed state in ECs, it is possible that this state reflects in that case heterogeneity between ECs that express and ECs that do not express *pdm2*.

The *Fie* expression profile was examined using a *Fie-GAL4* reporter line crossed with *UAS-2XGFP*. Overall, no GFP was detected in the midgut, suggesting that *Fie* is not expressed or at low levels.

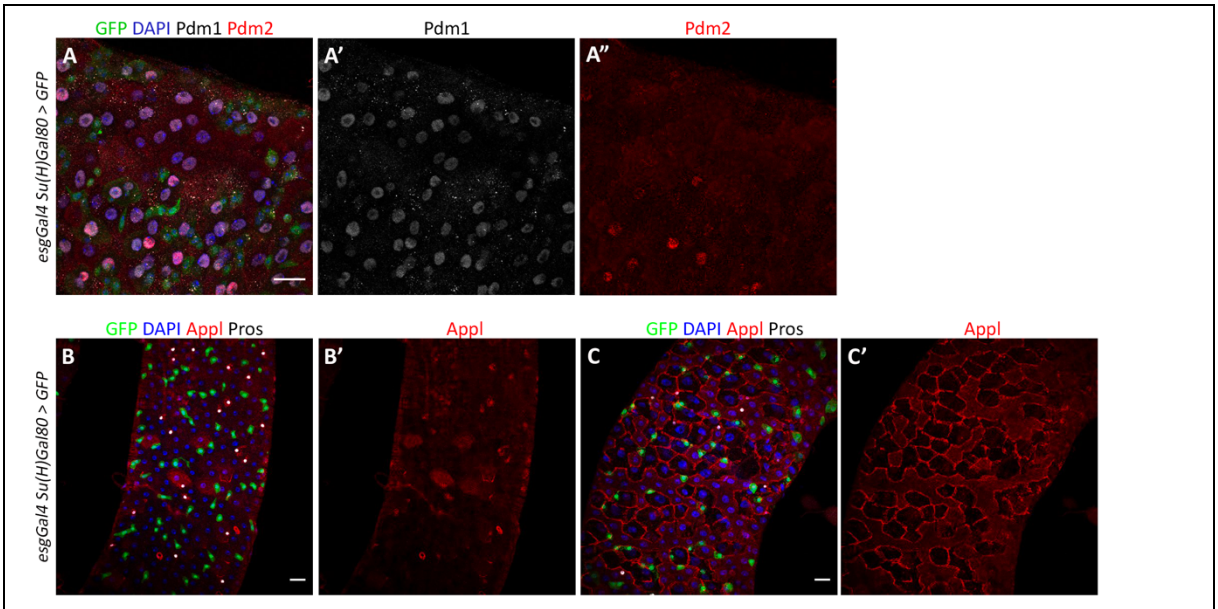

Figure 8. Expression patterns of *pdm2* and *Appl* in the midgut.
A. Midguts immunostained for GFP, Pdm1, Pdm2 and DAPI. **B-C**. Two different regions of midguts immunostained for GFP, Appl, Pros and DAPI. Scale bars: 20 µm.

Appl was detected in the gut with an anti-Appl antibody. Staining was observed heterogeneously along the midgut (**Fig. 8B-C**). In some regions, there was a weak cytoplasmic staining, sometimes in Pros$^+$ cells (**Fig. 8B**). However, in the rest of the gut Appl was mostly enriched at membranes of ECs and did not seem specific to Pros$^+$ cells (**Fig. 8C**). Membrane staining at ECs could also reflect the cleaved and secreted form of Appl.

II.C. Testing *pdm2*, *Fie* and *Appl* for a role in EC or EE cell fates

pdm2

In order to determine whether *pdm2* has a role in maintaining EC identity, I first performed *pdm2* knockdown specifically in ECs using the *MyoGAL4^{ts}* driver. Overall, the number, distribution and morphology of ECs based on GFP expression and nuclear size did not seem affected in the midgut (not shown). *pdm2* RNAi induction in MARCM clones resulted in similar distribution of clone size compared to control clones, based on the classification explained above (**Fig. 9A**). The presence of ECs, based on nuclear size, in *pdm2* RNAi-expressing clones, suggested that EC formation was not strikingly affected. Therefore, these preliminary results suggest that *pdm2* does not have a major role in EC specification, which might be due to redundancy with *pdm1*/*nub*.

Fie

Fie knockdown in EEs using the *prosGAL4^{ts}* driver did not lead to any obvious change in the number or distribution of EEs in midgut (not shown). However, there was a higher proportion of small clones among the clones expressing *Fie RNAi*, compared to the clone size distribution in control clones (**Fig. 9B**). Further quantification of clone cell type composition would be needed to address whether this effect is due to a decrease or ISC proliferation or a defect of differentiation.

Appl

To test *Appl* function, *Appl* mutant clones were generated (*Appl^d* allele). A precise characterization of clone size and composition has not been done yet, but a quick comparison between control and mutant clones showed that the size of the clones did not seem to differ, and EE cells were still produced in *Appl* mutant clones. This suggests that *Appl* is not essential for EE differentiation but requires further analysis to be confirmed.

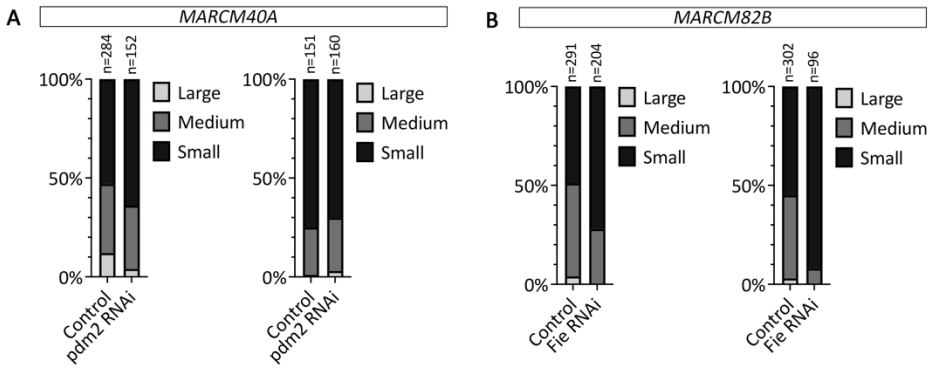

Figure 9. Knockdown of *pdm2* and *Fie* in mitotic clones.
A-B. Distribution of control clones and *pdm2 RNAi*-expressing clones (**A**) *or Fie RNAi*-expressing clones (**B**) in 3 categories of clone size. n=number of clones.

III. CONCLUSION

In this part, I explored the expression pattern and function of candidate genes in the intestinal lineage. For most of these genes, knockdown and overexpression experiments did not lead to strong phenotypes, or these were inconsistent between replicates or fly strains. Therefore, I did not investigate further the function of these genes. Nevertheless, some mild phenotypes for *Fer2*, *bib*, and *Fie* were observed, opening the path for potential further studies. In particular, *bib* seems required to maintain basal levels of ISC proliferation. Another hypothesis is that *bib* knockdown causes ISCs to prematurely differentiate into ECs, as it was previously suggested in a screen (Zeng et al., 2015). A more accurate characterization of cell type composition in *bib RNAi*-expressing clones would give more insight into this possibility.

Regarding our initial hypothesis, it seems that the chromatin state of *sens* and *sens-2* was not predictive of their function in the lineage. On the other hand, our approach allowed us to identify *Fer2* and *bib* as potential regulators of ISC proliferation. The effect of *Pdm2*, *Fie* and *Appl* loss of function need to be further characterized to conclude. Nevertheless, this is only a limited number of candidates and there are other candidate genes that could be tested.

MATERIALS AND METHODS

Fly stocks

The following fly stocks were used in this work: *esgGAL4 UAS-GFP;Su(H)GBE-GAL80 tubGAL80^{ts}* (Wang et al., 2014), *esgGAL4;tubGAL80^{ts} UAS-GFP* (*esgGAL4^{ts}*) (Jiang et al., 2009), *MyoIAGAL4;tubGAL80^{ts} UAS-GFP* (Jiang et al., 2009), *GAL4prosVoila tubGAL80^{ts}* (Balakireva et

al., 1998), *w*^{118} (gift from M. McVey), *w*^{118}*;UAS-2XGFP*, *esgGal4 UAS-GFP tubGAL80ts;UAS-flpact-FRT-CD2-FRT-Gal4* (*esgGAL4*^{ts} *Flp-out*) (from B. Edgar).

For RNAi and overexpression experiments, the following lines were used: *sens-2 RNAi* (BL34984), *sens-2 RNAi* (BL27285), *Fer2 RNAi* (BL28697), *Fer2 RNAi* (BL50971), *pdm2 RNAi* (BL29543), *bib RNAi* (BL57493) from the Bloomington Drosophila Stock Center (BDSC); *sens RNAi* (VDRC 106028), *bib RNAi* (VDRC 8893), *Fie RNAi* (VDRC 102047), from the Vienna Drosophila RNAi Center (VDRC); *UAS-Fer2* and *UAS-pdm2* from FlyORF; *UAS-flp/CyO;Sens*^{E2} *FRT80B/TM6*, *UAS-sens*, *UAS-sens-2* (gifts from H. Belen); *UAS-Fer2-FLAG*, *UAS-Fer2miRNA 4*, *UAS-Fer2miRNA 5* (gifts from E. Nagoshi).

To test the expression pattern of candidate genes, the following lines were used: *Appl-GAL4* (BL32040), *sens-2-GAL4* (BL80614), *sens-2-GAL4* (BL73765), *Fer2-GAL4* (BL26483), *bib-GAL4* (BL23729), *Fer2-GFP* (BL6455), *Fer2-GFP* (BL53114) from the Bloomington Drosophila Stock Center (BDSC); *Fie-GAL4* (gift from V. Auld), *Fer2-GAL4*, *Fer2-GFP* (gifts from E. Nagoshi).

Induction of transgenes in ISCs/EBs and in mitotic clones

For quantification of PH3^{+} cells, 3-day old female flies with the RNAi and overexpression transgenes mentioned above were kept at 18°C for 2 days and shifted to 29°C for 7 days (or 10 days when indicated) to induce transgene expression.

Mitotic clones expressing RNAi or overexpression constructs, and mutant clones were generated with the Mosaic Analysis with Repressible Cell Marker (MARCM) technique. The following stocks were used: *MARCM40A*, *FRT40A*, *MARCM80B*, *FRT80B*, *MARCM82B*, *FRT82B*, *MARCM19A*, *FRT19A*. 3-day old adult female flies were maintained at 25°C, heat-shocked at 36.5°C for 35 min to induce clones and dissected 7 or 10 days after heat-shock.

Immunostainings

Flies were dissected in PBS 1X to isolate whole guts associated with Malpighian tubules. Guts were fixated in 4% PFA for 2 hours, rinsed in PBT (PBS 1X, 0,1% Triton-X 100) and then cut at the anterior and posterior sides in order to keep midguts only. Midguts were incubated in 50% glycerol/PBS 1X for 30 min to make waste exit, rinsed in PBT and incubated with primary antibodies overnight at 4°C. Then, midguts were rinsed with PBT and incubated with secondary antibodies for 3 hours at room temperature. Next, they were washed in PBT and

incubated with DAPI (1:1000,) for 5 min and equilibrated in 50% glycerol/PBS 1X before being mounted on slides.

The following primary antibodies were used: mouse anti-Delta (1:2000, DSHB C594.9B), rabbit anti-PH3 (1:2000, Millipore), chicken anti-GFP (1:1000, Invitrogen), mouse anti-Prospero (1:2000, DHSB), rabbit anti-Pdm1 (1:1000, gift from Huang), rat anti-Pdm2 (1:100, Abcam), guinea pig anti-Sens (1:1000, gift from H. Belen), rabbit anti-Appl (1:1000, clone B63.3, gift from B. De Strooper), rabbit anti-bib (1:500, gift from Y.N. Jan).

Imaging and quantifications

Imaging was conducted using a Zeiss LSM900 confocal microscope and the ZEN software at the Curie Institute imaging facility (PICT). Images were acquired with a 40X oil objective. For stack images, z-step was set at 1 to 1.5 µm. Quantifications of $PH3^+$ cells were done with a Leica epifluorescence microscope. Image analysis was performed using Fiji software followed by image assembly using Adobe Photoshop. Statistical analyses were performed in Prism using the two-tailed Mann-Whitney test. Significant values were reported as ns for non-significant, * for $p<0.05$, ** for $p<0.01$, *** for $p<0.001$ and ****$p<0.0001$.

REFERENCES

Acar, M. (2006). Senseless physically interacts with proneural proteins and functions as a transcriptional co-activator. Development 133, 1979–1989. https://doi.org/10.1242/dev.02372.

Balakireva, M., Stocker, R.F., Gendre, N., and Ferveur, J.-F. (1998). Voila, a New Drosophila Courtship Variant that Affects the Nervous System: Behavioral, Neural, and Genetic Characterization. J. Neurosci. 18, 4335–4343. https://doi.org/10.1523/JNEUROSCI.18-11-04335.1998.

Bardin, A.J., Perdigoto, C.N., Southall, T.D., Brand, A.H., and Schweisguth, F. (2010). Transcriptional control of stem cell maintenance in the Drosophila intestine. Development 137, 705–714. https://doi.org/10.1242/dev.039404.

Bhat, K.M., and Schedl, P. The Drosophila miti-mere gene, a member of the POU family, is required for the specification of the RP2/sibling lineage during neurogenesis. 19. .

Bhat, K.M., Poole, S.J., and Schedl, P. (1995). The miti-mere and pdm1 genes collaborate during specification of the RP2/sib lineage in Drosophila neurogenesis. Mol Cell Biol 15, 4052–4063. https://doi.org/10.1128/MCB.15.8.4052.

Dib, P.B., Gnägi, B., Daly, F., Sabado, V., Tas, D., Glauser, D.A., Meister, P., and Nagoshi, E. (2014). A Conserved Role for p48 Homologs in Protecting Dopaminergic Neurons from Oxidative Stress. PLOS Genetics 10, e1004718.

https://doi.org/10.1371/journal.pgen.1004718.

Doherty, D., Jan, L.Y., and Jan, Y.N. (1997). The Drosophila neurogenic gene big brain, which encodes a membrane- associated protein, acts cell autonomously and can act synergistically with Notch and Delta. 13. .

Dutta, D., Dobson, A.J., Houtz, P.L., Gläßer, C., Revah, J., Korzelius, J., Patel, P.H., Edgar, B.A., and Buchon, N. (2015). Regional Cell-Specific Transcriptome Mapping Reveals Regulatory Complexity in the Adult Drosophila Midgut. Cell Reports 12, 346–358. https://doi.org/10.1016/j.celrep.2015.06.009.

Frankfort, B.J., and Mardon, G. (2004). Senseless represses nuclear transduction of Egfr pathway activation. Development 131, 563–570. https://doi.org/10.1242/dev.00941.

Frankfort, B.J., Pepple, K.L., Mamlouk, M., Rose, M.F., and Mardon, G. (2004). Senseless is required for pupal retinal development in Drosophila. Genesis 38, 182–194. https://doi.org/10.1002/gene.20018.

Grosskortenhaus, R., Robinson, K.J., and Doe, C.Q. (2006). Pdm and Castor specify late-born motor neuron identity in the NB7-1 lineage. Genes Dev. 20, 2618–2627. https://doi.org/10.1101/gad.1445306.

Guo, X., Yin, C., Yang, F., Zhang, Y., Huang, H., Wang, J., Deng, B., Cai, T., Rao, Y., and Xi, R. (2019). The Cellular Diversity and Transcription Factor Code of Drosophila Enteroendocrine Cells. Cell Reports 29, 4172-4185.e5. https://doi.org/10.1016/j.celrep.2019.11.048.

Jafar-Nejad, H., Acar, M., Nolo, R., Lacin, H., Pan, H., Parkhurst, S.M., and Bellen, H.J. (2003). Senseless acts as a binary switch during sensory organ precursor selection. Genes Dev 17, 2966–2978. https://doi.org/10.1101/gad.1122403.

Jafar-Nejad, H., Tien, A.-C., Acar, M., and Bellen, H.J. (2006). Senseless and Daughterless confer neuronal identity to epithelial cells in the Drosophila wing margin. Development 133, 1683–1692. https://doi.org/10.1242/dev.02338.

Kessissoglou, I.A., Langui, D., Hasan, A., Maral, M., Dutta, S.B., Hiesinger, P.R., and Hassan, B.A. (2020). The Drosophila amyloid precursor protein homologue mediates neuronal survival and neuroglial interactions. PLOS Biology 18, e3000703. https://doi.org/10.1371/journal.pbio.3000703.

Korzelius, J., Naumann, S.K., Loza-Coll, M.A., Chan, J.S., Dutta, D., Oberheim, J., Gläßer, C., Southall, T.D., Brand, A.H., Jones, D.L., et al. (2014). Escargot maintains stemness and suppresses differentiation in Drosophila intestinal stem cells. The EMBO Journal 33, 2967–2982. https://doi.org/10.15252/embj.201489072.

Li, Y., Liu, T., Peng, Y., Yuan, C., and Guo, A. (2004). Specific functions ofDrosophila amyloid precursor-like protein in the development of nervous system and nonneural tissues. J. Neurobiol. 61, 343–358. https://doi.org/10.1002/neu.20048.

Luna, A.J.F., Perier, M., and Seugnet, L. (2017). Amyloid Precursor Protein in Drosophila Glia Regulates Sleep and Genes Involved in Glutamate Recycling. J. Neurosci. 37, 4289–4300. https://doi.org/10.1523/JNEUROSCI.2826-16.2017.

Luo, L., Martin-Morris, L., and White, K. (1990). Identification, secretion, and neural expression of APPL, a Drosophila protein similar to human amyloid protein precursor. J. Neurosci. 10, 3849–3861. https://doi.org/10.1523/JNEUROSCI.10-12-03849.1990.

Miozzo, F., Valencia-Alarcón, E.P., Stickley, L., Majcin Dorcikova, M., Petrelli, F., Tas, D.,

Loncle, N., Nikonenko, I., Bou Dib, P., and Nagoshi, E. (2022). Maintenance of mitochondrial integrity in midbrain dopaminergic neurons governed by a conserved developmental transcription factor. Nat Commun 13, 1426. https://doi.org/10.1038/s41467-022-29075-0.

Mora, N., Almudi, I., Alsina, B., Corominas, M., and Serras, F. (2013). β amyloid protein precursor-like (Appl) is a Ras1/MAPK-regulated gene required for axonal targeting in Drosophila photoreceptor neurons. Journal of Cell Science 126, 53–59. https://doi.org/10.1242/jcs.114785.

Nagoshi, E., Sugino, K., Kula, E., Okazaki, E., Tachibana, T., Nelson, S., and Rosbash, M. (2010). Dissecting differential gene expression within the circadian neuronal circuit of Drosophila. Nat Neurosci 13. https://doi.org/10.1038/nn.2451.

Nolo, R., Abbott, L.A., and Bellen, H.J. (2000). Senseless, a Zn finger transcription factor, is necessary and sufficient for sensory organ development in Drosophila. Cell 102, 349–362. https://doi.org/10.1016/s0092-8674(00)00040-4.

Preat, T., and Goguel, V. (2016). Role of Drosophila Amyloid Precursor Protein in Memory Formation. Frontiers in Molecular Neuroscience 9. .

Rao, Y., Jan, L.Y., and Jan, Y.N. (1990). Similarity of the product of the Drosophila neurogenic gene big brain to transmembrane channel proteins. Nature 345, 163–167. https://doi.org/10.1038/345163a0.

Rao, Y., Bodmer, R., Jan, L.Y., and Jan, Y.N. (1992). The big brain gene of Drosophila functions to control the number of neuronal precursors in the peripheral nervous system. Development 116, 31–40. https://doi.org/10.1242/dev.116.1.31.

Soldano, A., Okray, Z., Janovska, P., Tmejová, K., Reynaud, E., Claeys, A., Yan, J., Atak, Z.K., De Strooper, B., Dura, J.-M., et al. (2013). The Drosophila Homologue of the Amyloid Precursor Protein Is a Conserved Modulator of Wnt PCP Signaling. PLoS Biol 11. https://doi.org/10.1371/journal.pbio.1001562.

Tatsumi, K., Tsuji, S., Miwa, H., Morisaku, T., Nuriya, M., Orihara, M., Kaneko, K., Okano, H., and Yasui, M. (2009). Drosophila big brain does not act as a water channel, but mediates cell adhesion. FEBS Letters 583, 2077–2082. https://doi.org/10.1016/j.febslet.2009.05.035.

Tran, K.D., and Doe, C.Q. (2008). Pdm and Castor close successive temporal identity windows in the NB3-1 lineage. Development 135, 3491–3499. https://doi.org/10.1242/dev.024349.

Wang, J., Binks, T., Warr, C.G., and Burke, R. (2014). Vacuolar-type H+-ATPase subunits and the neurogenic protein big brain are required for optimal copper and zinc uptake†. Metallomics 6, 2100–2108. https://doi.org/10.1039/c4mt00196f.

With, S., Rice, T., Salinas, C., and Auld, V. (2003). Fire exit is a potential four transmembrane protein expressed in developingDrosophila glia. Genesis 35, 143–152. https://doi.org/10.1002/gene.10177.

Xie, B., Charlton-Perkins, M., McDonald, E., Gebelein, B., and Cook, T. (2007). Senseless functions as a molecular switch for color photoreceptor differentiation in Drosophila. Development 134, 4243–4253. https://doi.org/10.1242/dev.012781.

Zeng, X., Han, L., Singh, S.R., Liu, H., Neumüller, R.A., Yan, D., Hu, Y., Liu, Y., Liu, W., Lin, X., et al. (2015). Genome-wide RNAi Screen Identifies Networks Involved in Intestinal Stem Cell Regulation in Drosophila. Cell Reports 10, 1226–1238. https://doi.org/10.1016/j.celrep.2015.01.051.

DISCUSSION

General conclusion

During my PhD, I explored chromatin states in the *Drosophila* lineage in order to characterize the chromatin state changes associated with stem cell differentiation in the context of adult tissue homeostasis. This study revealed the existence of seven chromatin states that define the chromatin organization in intestinal stem cells and their progeny. Examining chromatin state transitions occurring during differentiation highlighted the major chromatin state changes followed by functionally relevant groups of genes such as stem cell-associated genes, cell fate regulators and physiology-related genes. We also uncovered lineage-specific chromatin state transitions that might be important for cell fate decisions towards the EC or EE lineage. Furthermore, we explored the effect of genetic perturbation of HP1 and H1 on chromatin accessibility, transcription and tissue homeostasis. While HP1 is required to preserve heterochromatin, our results suggest that it also regulates the expression of genes with cellular metabolic functions independently of chromatin accessibility. Furthermore, HP1 is necessary to maintain ISC proliferation. Finally, we found a role for Histone H1 in regulating the EE transcriptional program in ISCs, suggesting that it could prime the ISCs towards the EE fate. In parallel, I also tested the role of candidate genes in the intestinal lineage, based on the chromatin state transitions followed by these genes. In addition, at the beginning of my thesis I contributed to the characterization of Kismet and Trr at the whole-genome scale.

In this part, I will discuss the significance of these results in light of the past and current literature, and the limitations of some of our findings. I will also discuss the new questions that were raised following this work and provide some perspectives for future research in the field.

I. Cell-type specific chromatin state modeling: strengths, limits and new insight into chromatin state variations in the lineage

Novelty of the approach

In this study, chromatin states are defined as the “specific combination of chromatin marks”. Defining these combinations was achieved through HMM-based chromatin state modeling, which has proven to provide powerful models that reveal more accurate and relevant chromatin features in a given genome (Ernst and Kellis, 2010; Filion et al., 2010).

However, a limited number of *in vivo* chromatin studies have used this approach and rather focused on profiling common individual histone modifications or chromatin-modifying proteins. Recent collaborative efforts in the frame of the ENCODE project gave more insights into chromatin remodeling during development by using chromatin state modeling methods, but similar approaches in adult tissues are still missing. This can be due to technical limitations imposed by *in vivo* adult model systems: genome-wide profiling using ChIP-seq requires large amounts of starting material, which is difficult to obtain for specific populations of cells. Here, we circumvented these limits by using Targeted DamID (Southall et al., 2013), which does not require cell sorting and allows the cell-type specific genome-wide mapping of a protein of interest *in vivo*. By profiling RNA Pol II, Brahma, Polycomb, HP1 and Histone H1 along the genome and applying HMM to the data, we provide for the first time cell-type specific chromatin state maps of a homeostatic adult tissue, the *Drosophila* intestine. In contrast to most of previous chromatin state models, we focused on chromatin states at genes to gain insights into the chromatin state changes associated with groups of genes that reflect stem cell or differentiated cell identity, or are important regulators of cell type specification. Other chromatin state studies instead focused more on chromatin changes at enhancers and promoters (detailed in part II.B.3 of the introduction). Both approaches are likely complementary to gain full understanding of the relevance of chromatin state transitions during adult stem cell differentiation. We believe that our DamID data and chromatin state maps could further be processed and exploited in a way that allows such characterization of regulatory elements, notably by using chromatin accessibility profiles obtained by CATaDa (Aughey et al., 2018).

Seven chromatin states define the chromatin organization in the *Drosophila* intestinal lineage

The seven states that emerged from the modeling displayed characteristics that were similar to those of the previously identified chromatin states in *Drosophila* cultured cells and developing brain (Filion et al., 2010; Marshall et al., 2016). This confirmed that the combinations of the 5 proteins profiled reflect well the distinct chromatin types first identified by Filion et al. In addition to the Yellow, Red, Blue, Green and Black states, we found two other states, Yellow Weak and Blue Mixed. The Yellow Weak state, almost exclusively found at gene bodies, might reflect a permissive state at genes with low or transient transcription. The Blue

Mixed state, characterized by high levels of Polycomb, RNA Pol II and Brahma binding, could reflect heterogeneity between cells that have slight differences in their transcriptome within each cell type. For instance, several region-specific transcription factor-encoding genes known to be expressed in a region-specific manner in the fly gut (*labial*, *sob*, *exex*) are found in the BlueM state in ISCs. However, many other regional genes are also found in other states. Another hypothesis is the previously described "balanced state" (Gaertner et al., 2012), where the RNA Pol II is paused at the gene promoters while Polycomb maintains a chromatin environment that prevents transcription elongation. This phenomenon was reported in the context of *Drosophila* development, where it is thought to maintain developmental genes in a state which is permissive for future expression during differentiation, in a similar way as the bivalent domains in mammals (Gaertner et al., 2012; Lagha et al., 2013). We did not identify a clear correlation with specific categories of genes between the BlueM and BlueR states, as both were generally enriched in developmental terms like segmentation, pattern specification, morphogenesis. Overall, the gene ontology categories enriched in each state were similar to the ones of the five chromatin types described by Filion *et al*. in embryonic cells, indicating that these broad categories of genes are subjected to the same type of chromatin regulation in the adult. Nevertheless, our cell type-specific approach allowed us to identify chromatin state changes at genes with more specific functions in the intestine, as detailed later in this Discussion.

Complexity of the HP1-enriched Green state

Our chromatin state model also highlighted some intricacies for the Green state, that was found in two groups with slight differences. As they were both strongly enriched in HP1 and defined as the same type of state by the HMM algorithm, we decided to keep them as one unique Green state. The first group of Green sub-states (left of the heatmaps, Fig. 2A) was strongly enriched in HP1 with some H1 binding, and found at pericentromeric regions, thus corresponding to constitutive heterochromatin. The second group of Green sub-states (found close to Yellow in the heatmaps) displayed enrichment of HP1 along with low RNA Pol II in ISCs, EBs and ECs. In EEs, this second Green group was instead associated with an enrichment of HP1, H1 and Polycomb, suggesting that part of the Green state in EEs is specific to the chromatin organization of this cell type. In all four cell types, the second Green group was more widely distributed over the genome (not shown) than the first Green group. This profile

is consistent with the presence of HP1 binding in euchromatic regions at active genes in flies and mammals (Vakoc et al., 2005; de Wit et al., 2007). It has also been proposed that HP1 may co-occupy a subset of genes at their TSS with RNA Pol II (Yin et al., 2011). In our data, the combination of HP1 and low RNA Pol II binding appears in part of the Green state, suggesting that it is not always a repressive state. Therefore, this example shows that the reductionist approach of chromatin state modeling is useful to facilitate analyses, but it might lead to loss of information in some cases. It seems that the challenge is to find the right balance between trust in the outcome of a robust modelling algorithm and the biological interpretations we make in light of our knowledge.

Chromatin states and transcriptional states

In our characterization of chromatin states, we studied the correlation between chromatin states and transcript levels. On average, transcriptional states correlated well with our categorization of active, intermediate and repressive chromatin states. However, there were also many genes marked by a chromatin state that did not reflect their transcript level based on the RNA-seq dataset that we used. Several hypotheses can explain this discrepancy. First, the Yellow and Red states do not always display RNA Pol II binding. They likely reflect an open and permissive chromatin, where the recruitment of specific transcription factors may be more determinant for the transcription of particular genes and explain low transcript levels in these active states. This recruitment may also depend on the chromatin state of distal elements such as enhancers. In addition, the Red state is quite heterogeneous in terms of binding of RNA Pol II, Brahma, HP1 and Polycomb. This could reflect heterogeneity between different cells, or a chromatin organization that relies on complex interplay between various factors to fine-tune transcription. On a technical aspect, one limitation is the assignment of one single chromatin state per gene, which can bring a bias for the genes that are marked by different chromatin states along their entire length. The presence of other genes within the introns of long genes might also introduce a bias.

These limits imply that the transitions between active and repressive chromatin states may not reflect transcription changes thoroughly. Therefore, it is important to consider these correlations with cautious regarding further interpretations.

Lineage-specific chromatin organization and dynamics

Our analysis of chromatin state changes occurring upon differentiation at genes revealed EE and EC-specific transitions. In particular, a large proportion of genes marked by the Red active state in ISCs undergo transitions to repressive states in ECs, while they remain in Red in EEs. This lineage-specific chromatin changes are notably observed at genes enriched in ISCs, or with important functions in the regulation of ISC differentiation, suggesting distinct modes of regulation of these "stem cell genes" during differentiation. Interestingly, these lineage-specific chromatin state transitions were also observed at the genome-wide scale. In particular, reduction of the Red state coverage in ECs and reduction of the Black state coverage in EEs occurred at intergenic regions too. This might implicate differences in the chromatin state of distal regulatory elements and in the subsequent long-range interactions. These observations also suggest differences in the chromatin organization of some portions of the genome between EEs and ECs. One hypothesis to explore is the link between the polyploidy of ECs and their chromatin organization, which might explain differences with EEs.

By comparing our data with chromatin state transitions observed in the developing brain, we suggest that similar chromatin changes occur during neuronal and EE differentiation. In the mouse intestine, chromatin studies have focused on chromatin changes at regulatory elements, identifying secretory lineage-specific enhancers (Jadhav et al., 2017; Raab et al., 2019). It would be interesting to determine if such changes at enhancers occur in the *Drosophila* EE cells.

Intermediate chromatin state transitions during EC differentiation

By generating chromatin state maps in EBs, we gained more insight into the chromatin state changes occurring during EC differentiation Our data revealed several intermediate transitions in the EC precursors (the EBs), and in particular a large set of genes that are found transitioning from an active state in ISCs to a Polycomb-enriched Blue state or HP1-enriched Green state in EBs first, and then to a Black state in ECs. The fact that key regulators of ISC differentiation undergo this type of chromatin state transition may indicate a functional role in the regulation of these genes. As the Black state is condensed and devoid of common chromatin marks, it is possible that its establishment is preceded by a step of chromatin compaction achieved by chromatin-associated factors found in the Green and Blue states, such as HP1 and PcG proteins. Consistent with this idea, it was recently suggested through Hi-

C and ATAC-seq experiments that H1 proteins could maintain a compacted state at regions that are initially marked by PRC2 during lineage specification in the mammalian hematopoietic system (Yusufova et al., 2021). Chromatin accessibility profiling by CATaDa in ISCs, EBs and ECs suggest, however, that most of chromatin accessibility changes occur during EB to EC differentiation (Aughey et al., 2018). The Blue and Green states in EBs might also promote a chromatin environment that prevents the binding of transcription activators at stem cell genes, in order to efficiently silence the stem cell program and facilitate the acquisition of the EC identity.

It will be interesting to determine if such intermediate chromatin changes also occur in EEPs during EE differentiation. During neuronal differentiation, the major chromatin state transitions previously mentioned occur neuron maturation rather than during the production of ganglion mother cells and immature neurons (Marshall and Brand, 2017). If we hypothesize that chromatin remodeling is similar between neuronal and EE differentiation, it is possible that major chromatin state differences appear between EEPs and EEs. Identifying a good EEP marker will be crucial to profile chromatin states in these precursors and address these questions.

II. Towards a better understanding of the functional relevance of repressive states

Revisiting Polycomb-mediated repression

Our data highlighted the Polycomb-enriched Blue Mixed and Blue Repressive states as markers of transcription factors with major roles in the regulation of the intestinal lineage. Whether BlueM and BlueR represent two distinct states with different consequences for the regulation of these genes is unclear, thus I will consider them together in the following statements. Here, ISC/EB transcription factors become marked by the Blue state in differentiated enterocytes. Similar observations have been reported in some adult tissues such as in the mammalian intestine, where a subset of “ISC signature genes” gain H3K27me3 in differentiated cells (Jadhav et al., 2016; Kazakevych et al., 2017). In the mouse hair follicle, several hair follicle stem cell-specific genes, including transcription factors, acquire H3K27me3 in their progeny (Lien et al., 2011). We also noticed that in EEs, the decreased transcription of some of ISC/EB transcription factors upon differentiation seems to correlate more with the

Red and Green states. Importantly, these states in EEs are more heterogeneous than in ECs and often include Polycomb binding. This could support the idea that the distinct combinations of chromatin binding proteins represent different modes of chromatin regulation depending on the lineage though and it does not exclude a potential role for Polycomb in this regulation. Therefore, more studies comparing Polycomb-marked chromatin between adult stem cells and their progeny will be needed to address whether stem cell-specific transcription factor silencing in differentiated cells is generally associated with a Polycomb-enriched chromatin state.

Given that the BlueR state marked the main cell fate regulators of EC and EE specification in ISCs, we expected that loss of Polycomb binding could derepress these genes and lead to premature differentiation. This was not observed in (Tauc et al., 2021), where Polycomb knockdown instead altered the production of EEs. During my PhD, I tested our initial hypothesis of Pc-mediated differentiation defects by inducing *E(z)* mutant clones or *E(z)-RNAi* expressing clones, reasoning that the loss of H3K27me3 could perturb the repression of cell fate genes and alter lineage decisions. Unlike the data presented by Tauc et al., I did not observe any reproducible effect on EE numbers in clones (data not shown). However, my experiments were performed at an earlier time point after clone induction compared to what was done by Tauc et al., and the method of quantifying cell types was different. The discrepancy between these results can also be explained by the only partial loss H3K27me3 in my experiments, which was not assessed in Tauc et al., where the authors show the decrease in H3K27me2 instead. Globally, it might be difficult to assess the functional relevance of Polycomb-enriched chromatin states since gene repression can rely on the redundancy with other factors found in canonical and non-canonical Polycomb complexes, and there is growing evidence of context-specific Polycomb mechanisms (Kim and Kingston, 2022). Moreover, the consequences of PcG protein depletion in adult stem cells are likely difficult to assess due to the tissue turnover rates, since it can take several rounds of division to dilute H3K27me3, as shown in the mammalian intestine (Jadhav et al., 2020). This hurdle could be overcome by inducing PcG depletion for longer times, but it also may lead to indirect effects. Another possibility could be to overexpress H3K27 demethylases to remove H3K27me3.

Therefore, these recent studies point towards complex and context-dependent roles of PcG proteins in adult tissues, compared to their well-characterized roles in development. Our

data suggest that Polycomb-marked chromatin is a marker of important regulators of the ISC lineage, but its direct function remains questionable.

New insight into the functional relevance of the Black state

The Black state, as initially described in *Drosophila* cultured cells (Filion et al., 2010), has also been found in other chromatin state models in *Drosophila*, human cell lines, mouse and worm under various names ("null", "background", "quiescent", "low signal") (Ernst and Kellis, 2010; Ho et al., 2014; Kharchenko et al., 2011; Kundaje et al., 2015; Marshall and Brand, 2017; van der Velde et al., 2021). Although it covers between 30 and 70% of genomes, it is very poorly characterized, likely because it is devoid of histone modifications. Nevertheless, it covers a high number of silent genes in all organisms studied. A recent study mapping chromatin states across tissues during mouse development gave some more insight into "quiescent states", that are likely the equivalent of the Black state since they are low levels of histone marks (van der Velde et al., 2021). While, in general, the genomic regions found in quiescent states are highly similar among different tissues and timepoints, some tissue-specific genes are marked by this state in other tissues where they need to be repressed, suggesting a previously uncharacterized mode of silencing of this type of genes. In this study, we found the Black state to be involved in several chromatin state transitions followed by functional categories of genes that show variations in expression within the intestinal lineage.

First of all, a set of ISC-enriched genes and genes that regulate early cell fate decisions undergo a transition from active states in ISCs to the Black state in ECs. This suggests that, except for transcription factors, stem cell genes repressed in ECs are found in the Black state rather than in the Pc-enriched or HP1-enriched state, which contrasts with previous findings in developmental contexts (Hawkins et al., 2010; Marshall and Brand, 2017; Zhu et al., 2013). This observation is less prevalent in EEs, since the same stem cell genes remain in active states upon EE differentiation.

Secondly, we found that EC and EE physiology-related genes undergo a "Black to active" transition upon their activation during differentiation. How this chromatin state change occurs remains unclear. Pioneer factors, given their ability to target and open condensed chromatin, could be involved. They have roles in cell fate specification and reprogramming, by priming genes for rapid induction through recruitment of chromatin remodeling enzymes and other transcription factors (Iwafuchi-Doi and Zaret, 2016). A classic example is the pioneer factor

FoxA, that was notably shown to maintain accessible nucleosomes at tissue-specific enhancers in the adult mouse liver (Iwafuchi-Doi et al., 2016). Interestingly, we observed that chromatin accessibility at the TSS of genes undergoing the Black to active transition was higher than at genes that are always marked by the Black state. This observation would be consistent with the hypothesis that particular transcription factors – yet to be identified – underlie this "more accessible" state to prime these genes for future activation. Nevertheless, the specific functions of pioneer factors have been recently challenged (Hansen et al., 2022). The authors of this study found that FoxA and a non-pioneer transcription factor, HNF4A, can equally bind nucleosomes and activate genes, arguing against a sequential recruitment of the pioneer and non-pioneer factors. This finding suggests that other transcription factors could have the ability to target inaccessible sites and facilitate transcription at these sites. To explore these hypotheses, we performed motif analysis on the genes following the "Black to active" transition and selected candidate transcription factors that could specifically regulate physiology-related genes.

In summary, our data revealed new insight into the functional relevance of the Black state in the intestinal lineage. Future work will be needed to better understand the regulation of the genes marked by the Black state during tissue homeostasis. Given that this "low signal" state has been found in other organisms, a better characterization of the genes marked by this state would be interesting to determine if our findings can be extended to other tissues.

Perturb chromatin states: technical limits

During my PhD, I wanted to add a functional dimension to the description of chromatin states in the lineage. In particular, I aimed to alter chromatin states by knocking-down chromatin-associated factors that are important for the establishment or the maintenance of these states: E(z) (results mentioned above in the text), HP1 and H1. Although these proteins are enriched in the Blue, Green and Black states respectively, it is expected that their loss could perturb other states in which they also display some binding. It is technically not possible to define chromatin states by Targeted DamID profiling of chromatin proteins in a knockdown context. Indeed, cell type-specific expression of the Dam-fusion constructs rely on the UAS-GAL4 system, which is also commonly used to express RNAi against a given gene. Expressing both transgenes at the same time would not give an accurate result of the effect of the knockdown condition on chromatin. Indeed, methylation by the Dam is stable and would

occur before the RNAi machinery efficiently degrade RNAs. Also, the Dam-fusion is expressed for only 24 hours, which might not be enough to detect the effects of the knockdown on chromatin-binding profiles. Therefore, we instead chose to assess the effects of HP1 and H1 knockdown in ISCs/EBs at three levels: chromatin accessibility, transcriptome and tissue homeostasis.

Effects of HP1 knockdown in ISCs/EBs are context-dependent

By comparing the effects of HP1 knockdown on chromatin accessibility and transcription with our chromatin state data, we identified context-dependent roles for HP1 in ISCs/EBs. First, chromatin accessibility marked by ATAC-seq peaks was increased almost exclusively at pericentromeric regions marked by the Green state, demonstrating that HP1 role in compaction is limited to these heterochromatic domains, at least compaction measured by ATAC-seq. Second, transcription changes were not limited to genes located in pericentromeric regions, suggesting that HP1 function in transcription regulation may be independent of chromatin accessibility. Consistent with this notion, previous studies showed HP1 positive effects on transcription at euchromatic genes (Cryderman et al., 2005; De Lucia et al., 2005; Lee et al., 2013; Park et al., 2019). HP1 appears to facilitate transcription elongation by stimulating H3K36 demethylation (Lin et al., 2008) and interacting with heterogeneous nuclear ribonucleoproteins (hnRNPs), involved in RNA processing (Piacentini et al., 2009). In our RNA-seq data, 56% of downregulated genes upon HP1 knockdown fall in the Yellow state in ISCs and EBs. As the Yellow state frequently comprises HP1 binding and is enriched at gene bodies, this finding favors the hypothesis of a direct role of HP1 in promoting the transcription of these genes. We further showed that HP1 knockdown induces the downregulation of genes involved in translation-related processes, which could explain the decrease of ISC proliferation. We will test whether we observe a global decrease in the translation process in ISCs/EBs upon HP1 knockdown.

In summary, by comparing RNA-seq and ATAC-seq analyses upon HP1 knockdown with our chromatin state maps, we demonstrated that HP1 has various roles in ISCs/EBs, which are not limited to the regions marked by the Green state. In particular, our data reveals that many housekeeping genes found in the Yellow state require HP1 for their proper expression. We suggest that defect in translation could be one of the mechanisms underlying ISC proliferation decrease. Nevertheless, deregulation of genes involved in metabolic functions could also

reflect a cellular stress response to perturbation in the structure of pericentric chromatin. Further experiments looking more carefully at each potential mechanism will be needed to better understand the role HP1 in ISC regulation.

Uncovering a role for Histone H1 in EE fate priming

In this work, H1 knockdown in ISCs/EBs had little effect on chromatin accessibility as assessed by the analysis of differentially accessible ATAC-seq peaks. This result was a bit surprising since H1 depletion in other *in vivo* contexts led to a global alteration of chromatin structure (Fan et al., 2005; Torres et al., 2016; Willcockson et al., 2020; Yusufova et al., 2021). This could be explained by the fact that the depletion of H1 is only partial in our experiment, since ISCs/EBs expressing H1 RNAi still display low levels of H1 staining. This is possibly due to the slow rate of ISC division. Moreover, our analysis was limited to the detection of differentially accessible peaks. Assessing global accessibility changes might reveal differences on a wider scale. Nevertheless, the more accessible regions upon H1 knockdown were mostly marked by the Black, Green and Blue repressive states in ISCs and EBs, consistent with a role of H1 in maintaining chromatin compaction. Consistent with this, the most upregulated genes upon H1 knockdown were found in the Black and Green state, but were not located close to the differentially accessible regions found by ATAC-seq. Moreover, the vast majority of deregulated genes were marked by active or intermediate chromatin states. This suggests that transcription changes are likely due to indirect effects of H1 depletion. Another hypothesis is that H1 has roles in transcription regulation which are independent of chromatin accessibility, or which cannot be detected by ATAC-seq. The use of bioinformatics tools measuring nucleosome occupancy or nucleosome repeat length could be useful to determine if these parameters are affected (Yan et al., 2020).

Surprisingly, H1 knockdown in ISCs/EBs leads to the downregulation of a large part of the EE transcriptional program. Indeed, we observed a decrease in EE numbers in the midgut upon H1 depletion. We propose a role for H1 in EE fate priming in ISCs, that would facilitate the activation of EE-identity genes upon differentiation. The population of cells where this priming would occur is unclear, since H1 RNAi was expressed in ISCs and EBs in our experiments using the *esgGAL4* driver. It is also possible that EE precursors (EEPs) retain some *esg* expression and that the phenotype observed is due to the inability of EEPs to differentiate

into EEs. Single-cell RNA-seq could address this hypothesis. Then, to better understand the mechanisms through which H1 regulates EE-identity genes, we could perform motif analysis on deregulated genes and differentially accessible regions in H1 knockdown to identify potential transcriptional activators or repressors that would mediate H1 effects on transcription.

Using chromatin states to identify new stem cell regulators

We hypothesized that the chromatin state of a gene could be predictive of its expression pattern or function. This hypothesis was based on the fact that functional categories of genes underwent particular chromatin state transitions upon differentiation. Here, the chromatin state of the seven candidate genes did not seem predictive of their expression pattern, except for Pdm2 that was detected in a subset of ECs. Other levels of gene expression regulation can explain discrepancy between chromatin state, rpkm values and protein levels. Nevertheless, our experiments suggest that *bib* and *Fer2* could have a role in the regulation of ISC proliferation. Moreover, the effects of the depletion of *pdm2*, *Fie* and *Appl* have not been fully characterized here and we cannot exclude that there were mild phenotypes that we did not detect in our preliminary experiments. Testing additional candidates would be necessary to conclude regarding the predictive power of chromatin states in this study. The choice of candidates could be adjusted, for instance by focusing on the chromatin state at the promoter instead of considering the prevalent state covering the gene.

III. Final conclusion and future perspectives

This PhD work provided a description of combinatorial chromatin states in the stem cells and differentiated cells of an adult homeostatic tissue, the *Drosophila* midgut. It gave new insight into the modes of regulation of genes that are critical for stem cell activity and differentiation in the lineage, as well as physiology-related genes specific of midgut terminally differentiated cells. Therefore, I believe that this work will provide a large resource for investigating further aspects of chromatin regulation in this adult homeostatic tissue as well as in other contexts such as environmental stress. For instance, the transcriptional changes in response to infection have been particularly well characterized in the midgut (Buchon et al., 2009; Jiang et al., 2016), but how proliferative signals are integrated at the level of the chromatin organization remains unknown. Diet changes also alter stem cell behavior (O'Brien

et al., 2011). Future projects in our lab include the study of chromatin organization in response to diet changes, which will also help to identify potential new regulators of the midgut response to environmental cues.

The cell-type specific DamID profiles of the 5 proteins, the chromatin state maps and the ATAC-seq data in ISCs/EBs represent a large amount of data, and this work did not explore all the possibilities of biological interpretations provided by this data. We focused on chromatin states and transitions of interest regarding our initial questions, but there is likely more to discover there. In addition, the chromatin state maps generated in this project could be used to compare with other datasets, such as the binding sites of known transcription factors. One can imagine that future research in the field will also include the description of chromatin at the 3D level. New *in vivo* techniques such as DamC, a modified version of DamID to detect chromosomal interactions (Redolfi et al., 2019), or single-cell Hi-C, could allow the characterization of chromatin folding in the intestinal lineage. Genome-wide profiling of histone marks should also be facilitated by the improvement of profiling techniques that require less amount of starting material, such as CUT&RUN or CUT&Tag (Kaya-Okur et al., 2019; Skene and Henikoff, 2017). These could, for instance, allow chromatin marks profiling in knockdown contexts. Therefore, integrating different types of genome-wide chromatin maps would improve our understanding of chromatin states in the midgut.

On a broader level and long-term view, I believe that my PhD work demonstrates the interest of better characterizing chromatin states in specific adult lineages. Cell-type specific chromatin state modeling combined with functional studies of chromatin-associated proteins in mammalian adult tissues might considerably improve our understanding of the regulatory networks that control cell differentiation, cell identity and plasticity and how these processes are deregulated in disease. It may also help to better identify the epigenetic barriers to reprogramming and the chromatin changes occurring during oncogenic transformation.

BIBLIOGRAPHY

Adam, R.C., and Fuchs, E. (2016). The Yin and Yang of Chromatin Dynamics In Stem Cell Fate Selection. Trends in Genetics 32, 89–100. https://doi.org/10.1016/j.tig.2015.11.002.

Adam, R.C., Yang, H., Rockowitz, S., Larsen, S.B., Nikolova, M., Oristian, D.S., Polak, L., Kadaja, M., Asare, A., Zheng, D., et al. (2015). Pioneer factors govern super-enhancer dynamics in stem cell plasticity and lineage choice. Nature 521, 366–370. https://doi.org/10.1038/nature14289.

Adam, R.C., Yang, H., Ge, Y., Infarinato, N.R., Gur-Cohen, S., Miao, Y., Wang, P., Zhao, Y., Lu, C.P., Kim, J.E., et al. (2020). NFI transcription factors provide chromatin access to maintain stem cell identity while preventing unintended lineage fate choices. Nature Cell Biology https://doi.org/10.1038/s41556-020-0513-0.

Ahmed, K., Dehghani, H., Rugg-Gunn, P., Fussner, E., Rossant, J., and Bazett-Jones, D.P. (2010). Global Chromatin Architecture Reflects Pluripotency and Lineage Commitment in the Early Mouse Embryo. PLoS ONE 5, e10531. https://doi.org/10.1371/journal.pone.0010531.

Akmammedov, A., Geigges, M., and Paro, R. (2019). Bivalency in Drosophila embryos is associated with strong inducibility of Polycomb target genes. Fly 13, 42–50. https://doi.org/10.1080/19336934.2019.1619438.

Allfrey, V.G., Faulkner, R., and Mirsky, A.E. (1964). ACETYLATION AND METHYLATION OF HISTONES AND THEIR POSSIBLE ROLE IN THE REGULATION OF RNA SYNTHESIS*. Proc Natl Acad Sci U S A 51, 786–794. .

Amcheslavsky, A., Song, W., Li, Q., Nie, Y., Bragatto, I., Ferrandon, D., Perrimon, N., and Ip, Y.T. (2014a). Enteroendocrine Cells Support Intestinal Stem-Cell-Mediated Homeostasis in Drosophila. Cell Reports 9, 32–39. https://doi.org/10.1016/j.celrep.2014.08.052.

Amcheslavsky, A., Nie, Y., Li, Q., He, F., Tsuda, L., Markstein, M., and Ip, Y.T. (2014b). Gene expression profiling identifies the zinc-finger protein Charlatan as a regulator of intestinal stem cells in Drosophila. Development 141, 2621–2632. https://doi.org/10.1242/dev.106237.

Andriatsilavo, M., Stefanutti, M., Siudeja, K., Perdigoto, C.N., Boumard, B., Gervais, L., Gillet-Markowska, A., Al Zouabi, L., Schweisguth, F., and Bardin, A.J. (2018). Spen limits intestinal stem cell self-renewal. PLoS Genet. 14, e1007773. https://doi.org/10.1371/journal.pgen.1007773.

Antonello, Z.A., Reiff, T., Ballesta-Illan, E., and Dominguez, M. (2015). Robust intestinal homeostasis relies on cellular plasticity in enteroblasts mediated by miR-8-Escargot switch. EMBO J. 34, 2025–2041. https://doi.org/10.15252/embj.201591517.

Argelaguet, R., Clark, S.J., Mohammed, H., Stapel, L.C., Krueger, C., Kapourani, C.-A., Imaz-Rosshandler, I., Lohoff, T., Xiang, Y., Hanna, C.W., et al. (2019). Multi-omics profiling of mouse gastrulation at single-cell resolution. Nature 1–5. https://doi.org/10.1038/s41586-019-1825-8.

Aughey, G.N., Estacio Gomez, A., Thomson, J., Yin, H., and Southall, T.D. (2018). CATaDa reveals global remodelling of chromatin accessibility during stem cell differentiation in vivo. ELife 7, e32341. https://doi.org/10.7554/eLife.32341.

Aughey, G.N., Cheetham, S.W., and Southall, T.D. (2019). DamID as a versatile tool for understanding gene regulation. Development 146, dev173666. https://doi.org/10.1242/dev.173666.

Avgustinova, A., and Benitah, S.A. (2016). Epigenetic control of adult stem cell function. Nature Reviews Molecular Cell Biology 17, 643–658. https://doi.org/10.1038/nrm.2016.76.

Azuara, V., Perry, P., Sauer, S., Spivakov, M., Jørgensen, H.F., John, R.M., Gouti, M., Casanova, M., Warnes, G., Merkenschlager, M., et al. (2006). Chromatin signatures of pluripotent cell lines. Nature Cell Biology 8, 532–538. https://doi.org/10.1038/ncb1403.

Bajpai, R., Chen, D.A., Rada-Iglesias, A., Zhang, J., Xiong, Y., Helms, J., Chang, C.-P., Zhao, Y., Swigut, T., and Wysocka, J. (2010). CHD7 cooperates with PBAF to control multipotent neural crest formation. Nature 463, 958–962. https://doi.org/10.1038/nature08733.

Bannister, A.J., and Kouzarides, T. (2011). Regulation of chromatin by histone modifications. Cell Research 21, 381–395. https://doi.org/10.1038/cr.2011.22.

Bannister, A.J., Zegerman, P., Partridge, J.F., Miska, E.A., Thomas, J.O., Allshire, R.C., and Kouzarides, T. (2001). Selective recognition of methylated lysine 9 on histone H3 by the HP1 chromo domain. Nature 410, 120–124. https://doi.org/10.1038/35065138.

Bardin, A.J., Perdigoto, C.N., Southall, T.D., Brand, A.H., and Schweisguth, F. (2010). Transcriptional control of stem cell maintenance in the Drosophila intestine. Development 137, 705–714. https://doi.org/10.1242/dev.039404.

Barisic, D., Stadler, M.B., Iurlaro, M., and Schübeler, D. (2019). Mammalian ISWI and SWI/SNF selectively mediate binding of distinct transcription factors. Nature 569, 136–140. https://doi.org/10.1038/s41586-019-1115-5.

Barker, N., van Es, J.H., Kuipers, J., Kujala, P., van den Born, M., Cozijnsen, M., Haegebarth, A., Korving, J., Begthel, H., Peters, P.J., et al. (2007). Identification of stem cells in small intestine and colon by marker gene Lgr5. Nature 449, 1003–1007. https://doi.org/10.1038/nature06196.

Barski, A., Cuddapah, S., Cui, K., Roh, T.-Y., Schones, D.E., Wang, Z., Wei, G., Chepelev, I., and Zhao, K. (2007). High-Resolution Profiling of Histone Methylations in the Human Genome. Cell 129, 823–837. https://doi.org/10.1016/j.cell.2007.05.009.

Bednar, J., Horowitz, R.A., Grigoryev, S.A., Carruthers, L.M., Hansen, J.C., Koster, A.J., and Woodcock, C.L. (1998). Nucleosomes, linker DNA, and linker histone form a unique structural motif that directs the higher-order folding and compaction of chromatin. Proceedings of the National Academy of Sciences 95, 14173–14178. https://doi.org/10.1073/pnas.95.24.14173.

Bernstein, B.E., Mikkelsen, T.S., Xie, X., Kamal, M., Huebert, D.J., Cuff, J., Fry, B., Meissner, A., Wernig, M., Plath, K., et al. (2006). A Bivalent Chromatin Structure Marks Key Developmental Genes in Embryonic Stem Cells. Cell 125, 315–326. https://doi.org/10.1016/j.cell.2006.02.041.

Bhattacharya, D., Talwar, S., Mazumder, A., and Shivashankar, G.V. (2009). Spatio-Temporal Plasticity in Chromatin Organization in Mouse Cell Differentiation and during Drosophila Embryogenesis. Biophysical Journal 96, 3832–3839. https://doi.org/10.1016/j.bpj.2008.11.075.

Biteau, B., and Jasper, H. (2011). EGF signaling regulates the proliferation of intestinal stem cells in Drosophila. Development 138, 1045–1055. https://doi.org/10.1242/dev.056671.

Biteau, B., and Jasper, H. (2014). Slit/Robo signaling regulates cell fate decisions in the intestinal stem cell lineage of Drosophila. Cell Rep 7, 1867–1875. https://doi.org/10.1016/j.celrep.2014.05.024.

Bolzer, A., Kreth, G., Solovei, I., Koehler, D., Saracoglu, K., Fauth, C., Müller, S., Eils, R., Cremer, C., Speicher, M.R., et al. (2005). Three-Dimensional Maps of All Chromosomes in Human Male Fibroblast Nuclei and Prometaphase Rosettes. PLoS Biol 3, e157. https://doi.org/10.1371/journal.pbio.0030157.

Boumard, B., and Bardin, A.J. (2021). An amuse-bouche of stem cell regulation: Underlying principles and mechanisms from adult Drosophila intestinal stem cells. Current Opinion in Cell Biology 73, 58–68. https://doi.org/10.1016/j.ceb.2021.05.007.

Boveri, T. (1909). Die Blastomerenkerne von Ascaris megalocephala und die Theorie der Chromosomenindividualität (Engelmann).

Boyer, L.A., Plath, K., Zeitlinger, J., Brambrink, T., Medeiros, L.A., Lee, T.I., Levine, S.S., Wernig, M., Tajonar, A., Ray, M.K., et al. (2006). Polycomb complexes repress developmental regulators in murine embryonic stem cells. Nature 441, 349–353. https://doi.org/10.1038/nature04733.

Buchon, N., Broderick, N.A., Poidevin, M., Pradervand, S., and Lemaitre, B. (2009). Drosophila Intestinal Response to Bacterial Infection: Activation of Host Defense and Stem Cell Proliferation. Cell Host & Microbe 5, 200–211. https://doi.org/10.1016/j.chom.2009.01.003.

Buchon, N., Broderick, N.A., Kuraishi, T., and Lemaitre, B. (2010). DrosophilaEGFR pathway coordinates stem cell proliferation and gut remodeling following infection. BMC Biology 8. https://doi.org/10.1186/1741-7007-8-152.

Buchon, N., Osman, D., David, F.P.A., Yu Fang, H., Boquete, J.-P., Deplancke, B., and Lemaitre, B. (2013). Morphological and Molecular Characterization of Adult Midgut Compartmentalization in Drosophila. Cell Reports 3, 1725–1738. https://doi.org/10.1016/j.celrep.2013.04.001.

Buddika, K., Huang, Y.-T., Ariyapala, I.S., Butrum-Griffith, A., Norrell, S.A., O'Connor, A.M., Patel, V.K., Rector, S.A., Slovan, M., Sokolowski, M., et al. (2021). Coordinated repression of pro-differentiation genes via P-bodies and transcription maintains Drosophila intestinal stem cell identity. Current Biology 0. https://doi.org/10.1016/j.cub.2021.11.032.

Buszczak, M., Paterno, S., and Spradling, A.C. (2009). Drosophila Stem Cells Share a Common Requirement for the Histone H2B Ubiquitin Protease Scrawny. Science 323, 248–251. https://doi.org/10.1126/science.1165678.

Cai, H., and Levine, M. (1995). Modulation of enhancer-promoter interactions by insulators in the Drosophila embryo. Nature 376, 533–536. https://doi.org/10.1038/376533a0.

Calo, E., and Wysocka, J. (2013). Modification of Enhancer Chromatin: What, How, and Why? Molecular Cell 49, 825–837. https://doi.org/10.1016/j.molcel.2013.01.038.

Cardozo Gizzi, A.M., Cattoni, D.I., Fiche, J.-B., Espinola, S.M., Gurgo, J., Messina, O., Houbron, C., Ogiyama, Y., Papadopoulos, G.L., Cavalli, G., et al. (2019). Microscopy-Based

Chromosome Conformation Capture Enables Simultaneous Visualization of Genome Organization and Transcription in Intact Organisms. Molecular Cell 74, 212-222.e5. https://doi.org/10.1016/j.molcel.2019.01.011.

Cenik, B.K., and Shilatifard, A. (2021). COMPASS and SWI/SNF complexes in development and disease. Nat Rev Genet 22, 38–58. https://doi.org/10.1038/s41576-020-0278-0.

Chen, H., Levo, M., Barinov, L., Fujioka, M., Jaynes, J.B., and Gregor, T. (2018a). Dynamic interplay between enhancer–promoter topology and gene activity. Nat Genet 50, 1296–1303. https://doi.org/10.1038/s41588-018-0175-z.

Chen, J., Xu, N., Huang, H., Cai, T., and Xi, R. (2016). A feedback amplification loop between stem cells and their progeny promotes tissue regeneration and tumorigenesis. ELife 5. https://doi.org/10.7554/eLife.14330.

Chen, J., Xu, N., Wang, C., Huang, P., Huang, H., Jin, Z., Yu, Z., Cai, T., Jiao, R., and Xi, R. (2018b). Transient Scute activation via a self-stimulatory loop directs enteroendocrine cell pair specification from self-renewing intestinal stem cells. Nature Cell Biology 20, 152–161. https://doi.org/10.1038/s41556-017-0020-0.

Chetverina, D., Erokhin, M., and Schedl, P. (2021). GAGA factor: a multifunctional pioneering chromatin protein. Cellular and Molecular Life Sciences https://doi.org/10.1007/s00018-021-03776-z.

Chiarella, A.M., Lu, D., and Hathaway, N.A. (2020). Epigenetic Control of a Local Chromatin Landscape. International Journal of Molecular Sciences 21, 943. https://doi.org/10.3390/ijms21030943.

Cirillo, L.A., Lin, F.R., Cuesta, I., Friedman, D., Jarnik, M., and Zaret, K.S. (2002). Opening of Compacted Chromatin by Early Developmental Transcription Factors HNF3 (FoxA) and GATA-4. Molecular Cell 9, 279–289. https://doi.org/10.1016/S1097-2765(02)00459-8.

Clapier, C.R., Iwasa, J., Cairns, B.R., and Peterson, C.L. (2017). Mechanisms of action and regulation of ATP-dependent chromatin-remodelling complexes. Nat Rev Mol Cell Biol 18, 407–422. https://doi.org/10.1038/nrm.2017.26.

Constantinescu, D., Gray, H.L., Sammak, P.J., Schatten, G.P., and Csoka, A.B. (2006). Lamin A/C Expression Is a Marker of Mouse and Human Embryonic Stem Cell Differentiation. Stem Cells 24, 177–185. https://doi.org/10.1634/stemcells.2004-0159.

Creyghton, M.P., Cheng, A.W., Welstead, G.G., Kooistra, T., Carey, B.W., Steine, E.J., Hanna, J., Lodato, M.A., Frampton, G.M., Sharp, P.A., et al. (2010). Histone H3K27ac separates active from poised enhancers and predicts developmental state. Proceedings of the National Academy of Sciences 107, 21931–21936. https://doi.org/10.1073/pnas.1016071107.

Croft, J.A., Bridger, J.M., Boyle, S., Perry, P., Teague, P., and Bickmore, W.A. (1999). Differences in the Localization and Morphology of Chromosomes in the Human Nucleus. Journal of Cell Biology 145, 1119–1131. https://doi.org/10.1083/jcb.145.6.1119.

Cryderman, D.E., Grade, S.K., Li, Y., Fanti, L., Pimpinelli, S., and Wallrath, L.L. (2005). Role of Drosophila HP1 in euchromatic gene expression. Developmental Dynamics 232, 767–774. https://doi.org/10.1002/dvdy.20310.

De Lucia, F., Ni, J.-Q., Vaillant, C., and Sun, F.-L. (2005). HP1 modulates the transcription of cell-cycle regulators in Drosophila melanogaster. Nucleic Acids Research 33, 2852–2858. https://doi.org/10.1093/nar/gki584.

Deng, T., Zhu, Z.I., Zhang, S., Leng, F., Cherukuri, S., Hansen, L., Mariño-Ramírez, L., Meshorer, E., Landsman, D., and Bustin, M. (2013). HMGN1 Modulates Nucleosome Occupancy and DNase I Hypersensitivity at the CpG Island Promoters of Embryonic Stem Cells. Molecular and Cellular Biology 33, 3377–3389. https://doi.org/10.1128/MCB.00435-13.

Deuring, R., Fanti, L., Armstrong, J.A., Sarte, M., Papoulas, O., Prestel, M., Daubresse, G., Verardo, M., Moseley, S.L., Berloco, M., et al. (2000). The ISWI Chromatin-Remodeling Protein Is Required for Gene Expression and the Maintenance of Higher Order Chromatin Structure In Vivo. Molecular Cell 5, 355–365. https://doi.org/10.1016/S1097-2765(00)80430-X.

Dixon, J.R., Selvaraj, S., Yue, F., Kim, A., Li, Y., Shen, Y., Hu, M., Liu, J.S., and Ren, B. (2012). Topological domains in mammalian genomes identified by analysis of chromatin interactions. Nature 485, 376–380. https://doi.org/10.1038/nature11082.

Dorigo, B., Schalch, T., Kulangara, A., Duda, S., Schroeder, R.R., and Richmond, T.J. (2004). Nucleosome Arrays Reveal the Two-Start Organization of the Chromatin Fiber. Science 306, 1571–1573. https://doi.org/10.1126/science.1103124.

Dorsett, D. (2019). The Many Roles of Cohesin in Drosophila Gene Transcription. Trends in Genetics 35, 542–551. https://doi.org/10.1016/j.tig.2019.04.002.

Dutta, D., Dobson, A.J., Houtz, P.L., Gläßer, C., Revah, J., Korzelius, J., Patel, P.H., Edgar, B.A., and Buchon, N. (2015). Regional Cell-Specific Transcriptome Mapping Reveals Regulatory Complexity in the Adult Drosophila Midgut. Cell Reports 12, 346–358. https://doi.org/10.1016/j.celrep.2015.06.009.

Efroni, S., Duttagupta, R., Cheng, J., Dehghani, H., Hoeppner, D.J., Dash, C., Bazett-Jones, D.P., Le Grice, S., McKay, R.D.G., Buetow, K.H., et al. (2008). Global Transcription in Pluripotent Embryonic Stem Cells. Cell Stem Cell 2, 437–447. https://doi.org/10.1016/j.stem.2008.03.021.

Eissenberg, J.C., and Elgin, S.C.R. (2014). HP1a: a structural chromosomal protein regulating transcription. Trends in Genetics 30, 103–110. https://doi.org/10.1016/j.tig.2014.01.002.

Eltsov, M., MacLellan, K.M., Maeshima, K., Frangakis, A.S., and Dubochet, J. (2008). Analysis of cryo-electron microscopy images does not support the existence of 30-nm chromatin fibers in mitotic chromosomes in situ. Proceedings of the National Academy of Sciences 105, 19732–19737. https://doi.org/10.1073/pnas.0810057105.

ENCODE Project Consortium (2004). The ENCODE (ENCyclopedia Of DNA Elements) Project. Science 306, 636–640. https://doi.org/10.1126/science.1105136.

Erez, N., Israitel, L., Bitman-Lotan, E., Wong, W.H., Raz, G., Cornelio-Parra, D.V., Danial, S., Flint Brodsly, N., Belova, E., Maksimenko, O., et al. (2021). A Non-stop identity complex (NIC) supervises enterocyte identity and protects from premature aging. ELife 10, e62312. https://doi.org/10.7554/eLife.62312.

Ernst, J., and Kellis, M. (2010). Discovery and characterization of chromatin states for systematic annotation of the human genome. Nature Biotechnology 28, 817–825. https://doi.org/10.1038/nbt.1662.

Ezhkova, E., Lien, W.-H., Stokes, N., Pasolli, H.A., Silva, J.M., and Fuchs, E. (2011). EZH1 and EZH2 cogovern histone H3K27 trimethylation and are essential for hair follicle homeostasis and wound repair. Genes Dev. 25, 485–498. https://doi.org/10.1101/gad.2019811.

Fan, Y., Nikitina, T., Zhao, J., Fleury, T.J., Bhattacharyya, R., Bouhassira, E.E., Stein, A., Woodcock, C.L., and Skoultchi, A.I. (2005). Histone H1 Depletion in Mammals Alters Global Chromatin Structure but Causes Specific Changes in Gene Regulation. Cell 123, 1199–1212. https://doi.org/10.1016/j.cell.2005.10.028.

Feng, W., Khan, M.A., Bellvis, P., Zhu, Z., Bernhardt, O., Herold-Mende, C., and Liu, H.-K. (2013). The Chromatin Remodeler CHD7 Regulates Adult Neurogenesis via Activation of SoxC Transcription Factors. Cell Stem Cell 13, 62–72. https://doi.org/10.1016/j.stem.2013.05.002.

Feng, W., Kawauchi, D., Körkel-Qu, H., Deng, H., Serger, E., Sieber, L., Lieberman, J.A., Jimeno-González, S., Lambo, S., Hanna, B.S., et al. (2017). Chd7 is indispensable for mammalian brain development through activation of a neuronal differentiation programme. Nat Commun 8, 14758. https://doi.org/10.1038/ncomms14758.

Filion, G.J., van Bemmel, J.G., Braunschweig, U., Talhout, W., Kind, J., Ward, L.D., Brugman, W., de Castro, I.J., Kerkhoven, R.M., Bussemaker, H.J., et al. (2010). Systematic Protein Location Mapping Reveals Five Principal Chromatin Types in Drosophila Cells. Cell 143, 212–224. https://doi.org/10.1016/j.cell.2010.09.009.

Finch, J.T., and Klug, A. (1976). Solenoidal model for superstructure in chromatin. Proc. Natl. Acad. Sci. U.S.A. 73, 1897–1901. https://doi.org/10.1073/pnas.73.6.1897.

Flavahan, W.A., Gaskell, E., and Bernstein, B.E. (2017). Epigenetic plasticity and the hallmarks of cancer. Science 357. https://doi.org/10.1126/science.aal2380.

Flemming, W. (1882). Zellsubstanz, Kern und Zelltheilung (Leipzig: F.C.W. Vogel).

Flint Brodsly, N., Bitman-Lotan, E., Boico, O., Shafat, A., Monastirioti, M., Gessler, M., Delidakis, C., Rincon-Arano, H., and Orian, A. (2019). The transcription factor Hey and nuclear lamins specify and maintain cell identity. ELife 8, e44745. https://doi.org/10.7554/eLife.44745.

Foo, S.M., Sun, Y., Lim, B., Ziukaite, R., O'Brien, K., Nien, C.-Y., Kirov, N., Shvartsman, S.Y., and Rushlow, C.A. (2014). Zelda Potentiates Morphogen Activity by Increasing Chromatin Accessibility. Current Biology 24, 1341–1346. https://doi.org/10.1016/j.cub.2014.04.032.

Fre, S., Bardin, A., Robine, S., and Louvard, D. (2011). Notch signaling in intestinal homeostasis across species: the cases of Drosophila, Zebrafish and the mouse. Experimental Cell Research 317, 2740–2747. https://doi.org/10.1016/j.yexcr.2011.06.012.

Fudenberg, G., Imakaev, M., Lu, C., Goloborodko, A., Abdennur, N., and Mirny, L.A. (2016). Formation of Chromosomal Domains by Loop Extrusion. Cell Reports 15, 2038–2049. https://doi.org/10.1016/j.celrep.2016.04.085.

Fyodorov, D.V., Zhou, B.-R., Skoultchi, A.I., and Bai, Y. (2017). Emerging roles of linker histones in regulating chromatin structure and function. Nature Reviews Molecular Cell Biology 19, 192–206. https://doi.org/10.1038/nrm.2017.94.

Gaertner, B., Johnston, J., Chen, K., Wallaschek, N., Paulson, A., Garruss, A.S., Gaudenz, K., De Kumar, B., Krumlauf, R., and Zeitlinger, J. (2012). Poised RNA Polymerase II Changes over Developmental Time and Prepares Genes for Future Expression. Cell Reports 2, 1670–1683. https://doi.org/10.1016/j.celrep.2012.11.024.

Gardner, K.E., Allis, C.D., and Strahl, B.D. (2011). OPERating ON Chromatin, a Colorful Language where Context Matters. Journal of Molecular Biology 409, 36–46. https://doi.org/10.1016/j.jmb.2011.01.040.

Gaspar-Maia, A., Alajem, A., Polesso, F., Sridharan, R., Mason, M.J., Heidersbach, A., Ramalho-Santos, J., McManus, M.T., Plath, K., Meshorer, E., et al. (2009). Chd1 regulates open chromatin and pluripotency of embryonic stem cells. Nature 460, 863–868. https://doi.org/10.1038/nature08212.

Gaspar-Maia, A., Alajem, A., Meshorer, E., and Ramalho-Santos, M. (2011). Open chromatin in pluripotency and reprogramming. Nature Reviews Molecular Cell Biology 12, 36–47. https://doi.org/10.1038/nrm3036.

Ge, Y., and Fuchs, E. (2018). Stretching the limits: from homeostasis to stem cell plasticity in wound healing and cancer. Nat. Rev. Genet. 19, 311–325. https://doi.org/10.1038/nrg.2018.9.

Gervais, L., and Bardin, A.J. (2017). Tissue homeostasis and aging: new insight from the fly intestine. Current Opinion in Cell Biology 48, 97–105. https://doi.org/10.1016/j.ceb.2017.06.005.

Gervais, L., Beek, M. van den, Josserand, M., Sallé, J., Stefanutti, M., Perdigoto, C.N., Skorski, P., Mazouni, K., Marshall, O.J., Brand, A.H., et al. (2019). Stem Cell Proliferation Is Kept in Check by the Chromatin Regulators Kismet/CHD7/CHD8 and Trr/MLL3/4. Developmental Cell 49, 556-573.e6. https://doi.org/10.1016/j.devcel.2019.04.033.

Ghavi-Helm, Y., Jankowski, A., Meiers, S., Viales, R.R., Korbel, J.O., and Furlong, E.E.M. (2019). Highly rearranged chromosomes reveal uncoupling between genome topology and gene expression. Nat Genet 51, 1272–1282. https://doi.org/10.1038/s41588-019-0462-3.

Gorkin, D.U., Barozzi, I., Zhao, Y., Zhang, Y., Huang, H., Lee, A.Y., Li, B., Chiou, J., Wildberg, A., Ding, B., et al. (2020). An atlas of dynamic chromatin landscapes in mouse fetal development. Nature 583, 744–751. https://doi.org/10.1038/s41586-020-2093-3.

Grosselin, K., Durand, A., Marsolier, J., Poitou, A., Marangoni, E., Nemati, F., Dahmani, A., Lameiras, S., Reyal, F., Frenoy, O., et al. (2019). High-throughput single-cell ChIP-seq identifies heterogeneity of chromatin states in breast cancer. Nat Genet 51, 1060–1066. https://doi.org/10.1038/s41588-019-0424-9.

Grossniklaus, U., and Paro, R. (2014). Transcriptional Silencing by Polycomb-Group Proteins. Cold Spring Harb Perspect Biol 6. https://doi.org/10.1101/cshperspect.a019331.

Grosswendt, S., Kretzmer, H., Smith, Z.D., Kumar, A.S., Hetzel, S., Wittler, L., Klages, S., Timmermann, B., Mukherji, S., and Meissner, A. (2020). Epigenetic regulator function through mouse gastrulation. Nature 1–7. https://doi.org/10.1038/s41586-020-2552-x.

Guo, Z., and Ohlstein, B. (2015). Bidirectional Notch signaling regulates Drosophila intestinal stem cell multipotency. Science 350, aab0988. https://doi.org/10.1126/science.aab0988.

Guo, X., Yin, C., Yang, F., Zhang, Y., Huang, H., Wang, J., Deng, B., Cai, T., Rao, Y., and Xi, R. (2019). The Cellular Diversity and Transcription Factor Code of Drosophila Enteroendocrine Cells. Cell Reports 29, 4172-4185.e5. https://doi.org/10.1016/j.celrep.2019.11.048.

Hamada, M., Ono, Y., Fujimaki, R., and Asai, K. (2015). Learning chromatin states with factorized information criteria. Bioinformatics 31, 2426–2433. https://doi.org/10.1093/bioinformatics/btv163.

Hansen, J.L., Loell, K.J., and Cohen, B.A. (2022). A test of the pioneer factor hypothesis using ectopic liver gene activation. ELife 11, e73358. https://doi.org/10.7554/eLife.73358.

Hao, X., Wang, S., Lu, Y., Yu, W., Li, P., Jiang, D., Guo, T., Li, M., Li, J., Xu, J., et al. (2020). Lola regulates Drosophila adult midgut homeostasis via non-canonical Hippo signaling. Elife 9. https://doi.org/10.7554/eLife.47542.

Hawkins, R.D., Hon, G.C., Lee, L.K., Ngo, Q., Lister, R., Pelizzola, M., Edsall, L.E., Kuan, S., Luu, Y., Klugman, S., et al. (2010). Distinct Epigenomic Landscapes of Pluripotent and Lineage-Committed Human Cells. Cell Stem Cell 6, 479–491. https://doi.org/10.1016/j.stem.2010.03.018.

He, L., Si, G., Huang, J., Samuel, A.D.T., and Perrimon, N. (2018). Mechanical regulation of stem-cell differentiation by the stretch-activated Piezo channel. Nature 555, 103–106. https://doi.org/10.1038/nature25744.

Heintzman, N.D., Hon, G.C., Hawkins, R.D., Kheradpour, P., Stark, A., Harp, L.F., Ye, Z., Lee, L.K., Stuart, R.K., Ching, C.W., et al. (2009). Histone modifications at human enhancers reflect global cell-type-specific gene expression. Nature 459, 108–112. https://doi.org/10.1038/nature07829.

Heitz, E. (1928). Das Heterochromatin der Moose (Bornträger).

Hnisz, D., Abraham, B.J., Lee, T.I., Lau, A., Saint-André, V., Sigova, A.A., Hoke, H.A., and Young, R.A. (2013). Super-Enhancers in the Control of Cell Identity and Disease. Cell 155, 934–947. https://doi.org/10.1016/j.cell.2013.09.053.

Hnisz, D., Shrinivas, K., Young, R.A., Chakraborty, A.K., and Sharp, P.A. (2017). A Phase Separation Model for Transcriptional Control. Cell 169, 13–23. https://doi.org/10.1016/j.cell.2017.02.007.

Ho, L., and Crabtree, G.R. (2010). Chromatin remodelling during development. Nature 463, 474–484. https://doi.org/10.1038/nature08911.

Ho, J.W.K., Jung, Y.L., Liu, T., Alver, B.H., Lee, S., Ikegami, K., Sohn, K.-A., Minoda, A., Tolstorukov, M.Y., Appert, A., et al. (2014). Comparative analysis of metazoan chromatin organization. Nature 512, 449–452. https://doi.org/10.1038/nature13415.

Ho, L., Ronan, J.L., Wu, J., Staahl, B.T., Chen, L., Kuo, A., Lessard, J., Nesvizhskii, A.I., Ranish, J., and Crabtree, G.R. (2009). An embryonic stem cell chromatin remodeling complex, esBAF, is essential for embryonic stem cell self-renewal and pluripotency. Proceedings of the National Academy of Sciences 106, 5181–5186. https://doi.org/10.1073/pnas.0812889106.

Hung, R.-J., Hu, Y., Kirchner, R., Liu, Y., Xu, C., Comjean, A., Tattikota, S.G., Li, F., Song, W., Sui, S.H., et al. (2020). A cell atlas of the adult Drosophila midgut. PNAS https://doi.org/10.1073/pnas.1916820117.

Hurd, E.A., Capers, P.L., Blauwkamp, M.N., Adams, M.E., Raphael, Y., Poucher, H.K., and Martin, D.M. (2007). Loss of Chd7 function in gene-trapped reporter mice is embryonic lethal and associated with severe defects in multiple developing tissues. Mamm Genome 18, 94–104. https://doi.org/10.1007/s00335-006-0107-6.

Isono, K., Fujimura, Y., Shinga, J., Yamaki, M., O-Wang, J., Takihara, Y., Murahashi, Y., Takada, Y., Mizutani-Koseki, Y., and Koseki, H. (2005). Mammalian Polyhomeotic Homologues Phc2 and Phc1 Act in Synergy To Mediate Polycomb Repression of Hox Genes. Molecular and Cellular Biology 25, 6694–6706. https://doi.org/10.1128/MCB.25.15.6694-6706.2005.

Iwafuchi-Doi, M. (2019). The mechanistic basis for chromatin regulation by pioneer transcription factors. WIREs Systems Biology and Medicine 11, e1427. https://doi.org/10.1002/wsbm.1427.

Iwafuchi-Doi, M., and Zaret, K.S. (2016). Cell fate control by pioneer transcription factors. Development 143, 1833–1837. https://doi.org/10.1242/dev.133900.

Iwafuchi-Doi, M., Donahue, G., Kakumanu, A., Watts, J.A., Mahony, S., Pugh, B.F., Lee, D., Kaestner, K.H., and Zaret, K.S. (2016). The Pioneer Transcription Factor FoxA Maintains an Accessible Nucleosome Configuration at Enhancers for Tissue-Specific Gene Activation. Molecular Cell 62, 79–91. https://doi.org/10.1016/j.molcel.2016.03.001.

Iwasaki, Y.W., Murano, K., Ishizu, H., Shibuya, A., Iyoda, Y., Siomi, M.C., Siomi, H., and Saito, K. (2016). Piwi Modulates Chromatin Accessibility by Regulating Multiple Factors Including Histone H1 to Repress Transposons. Molecular Cell 63, 408–419. https://doi.org/10.1016/j.molcel.2016.06.008.

Jacobs, J., Atkins, M., Davie, K., Imrichova, H., Romanelli, L., Christiaens, V., Hulselmans, G., Potier, D., Wouters, J., Taskiran, I.I., et al. (2018). The transcription factor Grainy head primes epithelial enhancers for spatiotemporal activation by displacing nucleosomes. Nat Genet 50, 1011–1020. https://doi.org/10.1038/s41588-018-0140-x.

Jacobs, J.J.L., Kieboom, K., Marino, S., DePinho, R.A., and van Lohuizen, M. (1999). The oncogene and Polycomb-group gene bmi-1 regulates cell proliferation and senescence through the ink4a locus. Nature 397, 164–168. https://doi.org/10.1038/16476.

Jadhav, U., Nalapareddy, K., Saxena, M., O'Neill, N.K., Pinello, L., Yuan, G.-C., Orkin, S.H., and Shivdasani, R.A. (2016). Acquired Tissue-Specific Promoter Bivalency Is a Basis for PRC2 Necessity in Adult Cells. Cell 165, 1389–1400. https://doi.org/10.1016/j.cell.2016.04.031.

Jadhav, U., Saxena, M., O'Neill, N.K., Saadatpour, A., Yuan, G.-C., Herbert, Z., Murata, K., and Shivdasani, R.A. (2017). Dynamic Reorganization of Chromatin Accessibility Signatures during Dedifferentiation of Secretory Precursors into Lgr5+ Intestinal Stem Cells. Cell Stem Cell 21, 65-77.e5. https://doi.org/10.1016/j.stem.2017.05.001.

Jadhav, U., Manieri, E., Nalapareddy, K., Madha, S., Chakrabarti, S., Wucherpfennig, K., Barefoot, M., and Shivdasani, R.A. (2020). Replicational Dilution of H3K27me3 in Mammalian Cells and the Role of Poised Promoters. Molecular Cell https://doi.org/10.1016/j.molcel.2020.01.017.

Jerkovic´, I., and Cavalli, G. (2021). Understanding 3D genome organization by multidisciplinary methods. Nat Rev Mol Cell Biol 22, 511–528. https://doi.org/10.1038/s41580-021-00362-w.

Jiang, H., Patel, P.H., Kohlmaier, A., Grenley, M.O., McEwen, D.G., and Edgar, B.A. (2009). Cytokine/Jak/Stat Signaling Mediates Regeneration and Homeostasis in the Drosophila Midgut. Cell 137, 1343–1355. https://doi.org/10.1016/j.cell.2009.05.014.

Jiang, H., Tian, A., and Jiang, J. (2016). Intestinal stem cell response to injury: lessons from Drosophila. Cellular and Molecular Life Sciences 73, 3337–3349. https://doi.org/10.1007/s00018-016-2235-9.

Jin, Y., Xu, J., Yin, M.-X., Lu, Y., Hu, L., Li, P., Zhang, P., Yuan, Z., Ho, M.S., Ji, H., et al. (2013). Brahma is essential for Drosophila intestinal stem cell proliferation and regulated by Hippo signaling. ELife 2. https://doi.org/10.7554/eLife.00999.

Jin, Z., Chen, J., Huang, H., Wang, J., Lv, J., Yu, M., Guo, X., Zhang, Y., Cai, T., and Xi, R. (2020). The Drosophila Ortholog of Mammalian Transcription Factor Sox9 Regulates Intestinal Homeostasis and Regeneration at an Appropriate Level. Cell Reports 31, 107683. https://doi.org/10.1016/j.celrep.2020.107683.

Jude, C.D., Climer, L., Xu, D., Artinger, E., Fisher, J.K., and Ernst, P. (2007). Unique and Independent Roles for MLL in Adult Hematopoietic Stem Cells and Progenitors. Cell Stem Cell 1, 324–337. https://doi.org/10.1016/j.stem.2007.05.019.

Kadoch, C., Hargreaves, D.C., Hodges, C., Elias, L., Ho, L., Ranish, J., and Crabtree, G.R. (2013). Proteomic and bioinformatic analysis of mammalian SWI/SNF complexes identifies extensive roles in human malignancy. Nat Genet 45, 592–601. https://doi.org/10.1038/ng.2628.

Kaji, K., Caballero, I.M., MacLeod, R., Nichols, J., Wilson, V.A., and Hendrich, B. (2006). The NuRD component Mbd3 is required for pluripotency of embryonic stem cells. Nat Cell Biol 8, 285–292. https://doi.org/10.1038/ncb1372.

Kassis, J.A., Kennison, J.A., and Tamkun, J.W. (2017). Polycomb and Trithorax Group Genes in Drosophila. Genetics 206, 1699–1725. https://doi.org/10.1534/genetics.115.185116.

Kaya-Okur, H.S., Wu, S.J., Codomo, C.A., Pledger, E.S., Bryson, T.D., Henikoff, J.G., Ahmad, K., and Henikoff, S. (2019). CUT&Tag for efficient epigenomic profiling of small samples and single cells. Nat Commun 10, 1930. https://doi.org/10.1038/s41467-019-09982-5.

Kazakevych, J., Sayols, S., Messner, B., Krienke, C., and Soshnikova, N. (2017). Dynamic changes in chromatin states during specification and differentiation of adult intestinal stem cells. Nucleic Acids Research 45, 5770–5784. https://doi.org/10.1093/nar/gkx167.

Kharchenko, P.V., Alekseyenko, A.A., Schwartz, Y.B., Minoda, A., Riddle, N.C., Ernst, J., Sabo, P.J., Larschan, E., Gorchakov, A.A., Gu, T., et al. (2011). Comprehensive analysis of the chromatin landscape in Drosophila melanogaster. Nature 471, 480–485. https://doi.org/10.1038/nature09725.

Kim, J.J., and Kingston, R.E. (2022). Context-specific Polycomb mechanisms in development. Nat Rev Genet 1–16. https://doi.org/10.1038/s41576-022-00499-0.

Kim, K.H., and Roberts, C.W.M. (2016). Targeting EZH2 in cancer. Nat Med 22, 128–134. https://doi.org/10.1038/nm.4036.

Kim, J.-M., Kim, K., Punj, V., Liang, G., Ulmer, T.S., Lu, W., and An, W. (2015). Linker histone H1.2 establishes chromatin compaction and gene silencing through recognition of H3K27me3. Sci Rep 5, 16714. https://doi.org/10.1038/srep16714.

Kim, T.-H., Li, F., Ferreiro-Neira, I., Ho, L.-L., Luyten, A., Nalapareddy, K., Long, H., Verzi, M., and Shivdasani, R.A. (2014). Broadly permissive intestinal chromatin underlies lateral inhibition and cell plasticity. Nature 506, 511–515. https://doi.org/10.1038/nature12903.

King, H.W., and Klose, R.J. (2017). The pioneer factor OCT4 requires the chromatin remodeller BRG1 to support gene regulatory element function in mouse embryonic stem cells. ELife 6, e22631. https://doi.org/10.7554/eLife.22631.

Kingston, R.E., and Tamkun, J.W. (2014). Transcriptional Regulation by Trithorax-Group Proteins. Cold Spring Harbor Perspectives in Biology 6, a019349–a019349. https://doi.org/10.1101/cshperspect.a019349.

Klein, D.C., and Hainer, S.J. (2019). Genomic methods in profiling DNA accessibility and factor localization. Chromosome Res https://doi.org/10.1007/s10577-019-09619-9.

Klemm, S.L., Shipony, Z., and Greenleaf, W.J. (2019). Chromatin accessibility and the regulatory epigenome. Nat Rev Genet 20, 207–220. https://doi.org/10.1038/s41576-018-0089-8.

Kornberg, R.D. (1977). Structure of Chromatin. 26. .

Kornberg, R.D., and Lorch, Y. (2020). Primary Role of the Nucleosome. Molecular Cell 79, 371–375. https://doi.org/10.1016/j.molcel.2020.07.020.

Korzelius, J., Naumann, S.K., Loza-Coll, M.A., Chan, J.S., Dutta, D., Oberheim, J., Gläßer, C., Southall, T.D., Brand, A.H., Jones, D.L., et al. (2014). Escargot maintains stemness and suppresses differentiation in Drosophila intestinal stem cells. The EMBO Journal 33, 2967–2982. https://doi.org/10.15252/embj.201489072.

Korzelius, J., Azami, S., Ronnen-Oron, T., Koch, P., Baldauf, M., Meier, E., Rodriguez-Fernandez, I.A., Groth, M., Sousa-Victor, P., and Jasper, H. (2019). The WT1-like transcription factor Klumpfuss maintains lineage commitment of enterocyte progenitors in the Drosophila intestine. Nat Commun 10. https://doi.org/10.1038/s41467-019-12003-0.

Kouzarides, T. (2007). Chromatin Modifications and Their Function. Cell 128, 693–705. https://doi.org/10.1016/j.cell.2007.02.005.

Krejčí, J., Uhlířová, R., Galiová, G., Kozubek, S., Šmigová, J., and Bártová, E. (2009). Genome-wide reduction in H3K9 acetylation during human embryonic stem cell differentiation. Journal of Cellular Physiology 219, 677–687. https://doi.org/10.1002/jcp.21714.

Kubik, S., O'Duibhir, E., de Jonge, W.J., Mattarocci, S., Albert, B., Falcone, J.-L., Bruzzone, M.J., Holstege, F.C.P., and Shore, D. (2018). Sequence-Directed Action of RSC Remodeler and General Regulatory Factors Modulates +1 Nucleosome Position to Facilitate Transcription. Molecular Cell 71, 89-102.e5. https://doi.org/10.1016/j.molcel.2018.05.030.

Kundaje, A., Meuleman, W., Ernst, J., Bilenky, M., Yen, A., Heravi-Moussavi, A., Kheradpour, P., Zhang, Z., Wang, J., Ziller, M.J., et al. (2015). Integrative analysis of 111 reference human epigenomes. Nature 518, 317–330. https://doi.org/10.1038/nature14248.

Kurisaki, A., Hamazaki, T.S., Okabayashi, K., Iida, T., Nishine, T., Chonan, R., Kido, H., Tsunasawa, S., Nishimura, O., Asashima, M., et al. (2005). Chromatin-related proteins in pluripotent mouse embryonic stem cells are downregulated after removal of leukemia inhibitory factor. Biochemical and Biophysical Research Communications 335, 667–675. https://doi.org/10.1016/j.bbrc.2005.07.128.

Lachner, M., O'Carroll, D., Rea, S., Mechtler, K., and Jenuwein, T. (2001). Methylation of histone H3 lysine 9 creates a binding site for HP1 proteins. Nature 410, 116–120. https://doi.org/10.1038/35065132.

Lagha, M., Bothma, J.P., Esposito, E., Ng, S., Stefanik, L., Tsui, C., Johnston, J., Chen, K., Gilmour, D.S., Zeitlinger, J., et al. (2013). Paused Pol II Coordinates Tissue Morphogenesis in the Drosophila Embryo. Cell 153, 976–987. https://doi.org/10.1016/j.cell.2013.04.045.

Lammerding, J., Fong, L.G., Ji, J.Y., Reue, K., Stewart, C.L., Young, S.G., and Lee, R.T. (2006). Lamins A and C but Not Lamin B1 Regulate Nuclear Mechanics*. Journal of Biological Chemistry 281, 25768–25780. https://doi.org/10.1074/jbc.M513511200.

Landry, J., Sharov, A.A., Piao, Y., Sharova, L.V., Xiao, H., Southon, E., Matta, J., Tessarollo, L., Zhang, Y.E., Ko, M.S.H., et al. (2008). Essential Role of Chromatin Remodeling Protein Bptf in Early Mouse Embryos and Embryonic Stem Cells. PLOS Genetics 4, e1000241. https://doi.org/10.1371/journal.pgen.1000241.

Lee, C.-K., Shibata, Y., Rao, B., Strahl, B.D., and Lieb, J.D. (2004). Evidence for nucleosome depletion at active regulatory regions genome-wide. Nat Genet 36, 900–905. https://doi.org/10.1038/ng1400.

Lee, D.H., Li, Y., Shin, D.-H., Yi, S.A., Bang, S.-Y., Park, E.K., Han, J.-W., and Kwon, S.H. (2013). DNA microarray profiling of genes differentially regulated by three heterochromatin protein 1 (HP1) homologs in Drosophila. Biochemical and Biophysical Research Communications 434, 820–828. https://doi.org/10.1016/j.bbrc.2013.04.020.

Lee, T.I., Jenner, R.G., Boyer, L.A., Guenther, M.G., Levine, S.S., Kumar, R.M., Chevalier, B., Johnstone, S.E., Cole, M.F., Isono, K., et al. (2006). Control of Developmental Regulators by Polycomb in Human Embryonic Stem Cells. Cell 125, 301–313. https://doi.org/10.1016/j.cell.2006.02.043.

Lessard, J., Wu, J.I., Ranish, J.A., Wan, M., Winslow, M.M., Staahl, B.T., Wu, H., Aebersold, R., Graef, I.A., and Crabtree, G.R. (2007). An Essential Switch in Subunit Composition of a Chromatin Remodeling Complex during Neural Development. Neuron 55, 201–215. https://doi.org/10.1016/j.neuron.2007.06.019.

Li, Y., Pang, Z., Huang, H., Wang, C., Cai, T., and Xi, R. (2017). Transcription Factor Antagonism Controls Enteroendocrine Cell Specification from Intestinal Stem Cells. Scientific Reports 7. https://doi.org/10.1038/s41598-017-01138-z.

Lichter, P., Cremer, T., Borden, J., Manuelidis, L., and Ward, D.C. (1988). Delineation of individual human chromosomes in metaphase and interphase cells by in situ suppression hybridization using recombinant DNA libraries. Hum Genet 80, 224–234. https://doi.org/10.1007/BF01790090.

Lieberman-Aiden, E., van Berkum, N.L., Williams, L., Imakaev, M., Ragoczy, T., Telling, A., Amit, I., Lajoie, B.R., Sabo, P.J., Dorschner, M.O., et al. (2009). Comprehensive Mapping of Long-Range Interactions Reveals Folding Principles of the Human Genome. Science 326, 289–293. https://doi.org/10.1126/science.1181369.

Lien, W.-H., Guo, X., Polak, L., Lawton, L.N., Young, R.A., Zheng, D., and Fuchs, E. (2011). Genome-wide Maps of Histone Modifications Unwind In Vivo Chromatin States of the Hair Follicle Lineage. Cell Stem Cell 9, 219–232. https://doi.org/10.1016/j.stem.2011.07.015.

Lin, C.-H., Li, B., Swanson, S., Zhang, Y., Florens, L., Washburn, M.P., Abmayr, S.M., and Workman, J.L. (2008). Heterochromatin Protein 1a Stimulates Histone H3 Lysine 36 Demethylation by the Drosophila KDM4A Demethylase. Molecular Cell 32, 696–706. https://doi.org/10.1016/j.molcel.2008.11.008.

Loh, Y.-H., Zhang, W., Chen, X., George, J., and Ng, H.-H. (2007). Jmjd1a and Jmjd2c histone H3 Lys 9 demethylases regulate self-renewal in embryonic stem cells. Genes Dev. 21, 2545–2557. https://doi.org/10.1101/gad.1588207.

Lu, X., Wontakal, S.N., Kavi, H., Kim, B.J., Guzzardo, P.M., Emelyanov, A.V., Xu, N., Hannon, G.J., Zavadil, J., Fyodorov, D.V., et al. (2013). Drosophila H1 regulates the genetic activity of heterochromatin by recruitment of Su(var)3-9. Science 340, 78–81. https://doi.org/10.1126/science.1234654.

Luger, K. (1997). Crystal structure of the nucleosome core particle at 2.8 A˚ resolution. 389, 10. .

Lugt, N.M. van der, Domen, J., Linders, K., Roon, M. van, Robanus-Maandag, E., Riele, H. te, Valk, M. van der, Deschamps, J., Sofroniew, M., and Lohuizen, M. van (1994). Posterior transformation, neurological abnormalities, and severe hematopoietic defects in mice with a targeted deletion of the bmi-1 proto-oncogene. Genes Dev. 8, 757–769. https://doi.org/10.1101/gad.8.7.757.

Lupiáñez, D.G., Kraft, K., Heinrich, V., Krawitz, P., Brancati, F., Klopocki, E., Horn, D., Kayserili, H., Opitz, J.M., Laxova, R., et al. (2015). Disruptions of Topological Chromatin Domains Cause Pathogenic Rewiring of Gene-Enhancer Interactions. Cell 161, 1012–1025. https://doi.org/10.1016/j.cell.2015.04.004.

Lyko, F., Ramsahoye, B.H., and Jaenisch, R. (2000). DNA methylation in Drosophila melanogaster. Nature 408, 538–540. https://doi.org/10.1038/35046205.

Ma, Y., Chen, Z., Jin, Y., and Liu, W. (2013). Identification of a histone acetyltransferase as a novel regulator of Drosophila intestinal stem cells. FEBS Letters 587, 1489–1495. https://doi.org/10.1016/j.febslet.2013.03.013.

Manuelidis, L. (1985). Individual interphase chromosome domains revealed by in situ hybridization. Hum Genet 71, 288–293. https://doi.org/10.1007/BF00388453.

Marianes, A., and Spradling, A.C. (2013). Physiological and stem cell compartmentalization within the Drosophila midgut. ELife 2. https://doi.org/10.7554/eLife.00886.

Marie, C., Clavairoly, A., Frah, M., Hmidan, H., Yan, J., Zhao, C., Van Steenwinckel, J., Daveau, R., Zalc, B., Hassan, B., et al. (2018). Oligodendrocyte precursor survival and differentiation requires chromatin remodeling by Chd7 and Chd8. Proceedings of the National Academy of Sciences 115, E8246–E8255. https://doi.org/10.1073/pnas.1802620115.

Marshall, O.J., and Brand, A.H. (2017). Chromatin state changes during neural development revealed by in vivo cell-type specific profiling. Nature Communications 8. https://doi.org/10.1038/s41467-017-02385-4.

Marshall, O.J., Southall, T.D., Cheetham, S.W., and Brand, A.H. (2016). Cell-type-specific profiling of protein–DNA interactions without cell isolation using targeted DamID with next-generation sequencing. Nature Protocols 11, 1586–1598. https://doi.org/10.1038/nprot.2016.084.

Martire, S., and Banaszynski, L.A. (2020). The roles of histone variants in fine-tuning chromatin organization and function. Nat Rev Mol Cell Biol 21, 522–541. https://doi.org/10.1038/s41580-020-0262-8.

McMahon, K.A., Hiew, S.Y.-L., Hadjur, S., Veiga-Fernandes, H., Menzel, U., Price, A.J., Kioussis, D., Williams, O., and Brady, H.J.M. (2007). Mll Has a Critical Role in Fetal and Adult Hematopoietic Stem Cell Self-Renewal. Cell Stem Cell 1, 338–345. https://doi.org/10.1016/j.stem.2007.07.002.

Melcer, S., Hezroni, H., Rand, E., Nissim-Rafinia, M., Skoultchi, A., Stewart, C.L., Bustin, M., and Meshorer, E. (2012). Histone modifications and lamin A regulate chromatin protein dynamics in early embryonic stem cell differentiation. Nat Commun 3, 910. https://doi.org/10.1038/ncomms1915.

Meng, F.W., and Biteau, B. (2015). A Sox Transcription Factor Is a Critical Regulator of Adult Stem Cell Proliferation in the Drosophila Intestine. Cell Reports 13, 906–914. https://doi.org/10.1016/j.celrep.2015.09.061.

Meng, F.W., Rojas Villa, S.E., and Biteau, B. (2020). Sox100B Regulates Progenitor-Specific Gene Expression and Cell Differentiation in the Adult Drosophila Intestine. Stem Cell Reports https://doi.org/10.1016/j.stemcr.2020.01.003.

Meshorer, E., and Misteli, T. (2006). Chromatin in pluripotent embryonic stem cells and differentiation. Nature Reviews Molecular Cell Biology 7, 540–546. https://doi.org/10.1038/nrm1938.

Meshorer, E., Yellajoshula, D., George, E., Scambler, P.J., Brown, D.T., and Misteli, T. (2006). Hyperdynamic Plasticity of Chromatin Proteins in Pluripotent Embryonic Stem Cells. Developmental Cell 10, 105–116. https://doi.org/10.1016/j.devcel.2005.10.017.

Micchelli, C.A., and Perrimon, N. (2006). Evidence that stem cells reside in the adult Drosophila midgut epithelium. Nature 439, 475–479. https://doi.org/10.1038/nature04371.

Miguel-Aliaga, I., Jasper, H., and Lemaitre, B. (2018). Anatomy and Physiology of the Digestive Tract of Drosophila melanogaster. Genetics 210, 357–396. https://doi.org/10.1534/genetics.118.300224.

Mikkelsen, T.S., Ku, M., Jaffe, D.B., Issac, B., Lieberman, E., Giannoukos, G., Alvarez, P., Brockman, W., Kim, T.-K., Koche, R.P., et al. (2007). Genome-wide maps of chromatin state in pluripotent and lineage-committed cells. Nature 448, 553–560. https://doi.org/10.1038/nature06008.

Moore, J.E., Purcaro, M.J., Pratt, H.E., Epstein, C.B., Shoresh, N., Adrian, J., Kawli, T., Davis, C.A., Dobin, A., Kaul, R., et al. (2020). Expanded encyclopaedias of DNA elements in the human and mouse genomes. Nature 583, 699–710. https://doi.org/10.1038/s41586-020-2493-4.

Morgan, M.A.J., and Shilatifard, A. (2020). Reevaluating the roles of histone-modifying enzymes and their associated chromatin modifications in transcriptional regulation. Nature Genetics 52, 1271–1281. https://doi.org/10.1038/s41588-020-00736-4.

Morin, R.D., Johnson, N.A., Severson, T.M., Mungall, A.J., An, J., Goya, R., Paul, J.E., Boyle, M., Woolcock, B.W., Kuchenbauer, F., et al. (2010). Somatic mutations altering EZH2

(Tyr641) in follicular and diffuse large B-cell lymphomas of germinal-center origin. Nat Genet 42, 181–185. https://doi.org/10.1038/ng.518.

Morozumi, Y., Boussouar, F., Tan, M., Chaikuad, A., Jamshidikia, M., Colak, G., He, H., Nie, L., Petosa, C., de Dieuleveult, M., et al. (2016). Atad2 is a generalist facilitator of chromatin dynamics in embryonic stem cells. Journal of Molecular Cell Biology 8, 349–362. https://doi.org/10.1093/jmcb/mjv060.

Mujtaba, S., Zeng, L., and Zhou, M.-M. (2007). Structure and acetyl-lysine recognition of the bromodomain. Oncogene 26, 5521–5527. https://doi.org/10.1038/sj.onc.1210618.

Mundorf, J., Donohoe, C.D., McClure, C.D., Southall, T.D., and Uhlirova, M. (2019). Ets21c Governs Tissue Renewal, Stress Tolerance, and Aging in the Drosophila Intestine. Cell Reports 27, 3019-3033.e5. https://doi.org/10.1016/j.celrep.2019.05.025.

Nalabothula, N., McVicker, G., Maiorano, J., Martin, R., Pritchard, J.K., and Fondufe-Mittendorf, Y.N. (2014). The chromatin architectural proteins HMGD1 and H1 bind reciprocally and have opposite effects on chromatin structure and gene regulation. BMC Genomics 15, 1–14. https://doi.org/10.1186/1471-2164-15-92.

Nègre, N., Brown, C.D., Ma, L., Bristow, C.A., Miller, S.W., Wagner, U., Kheradpour, P., Eaton, M.L., Loriaux, P., Sealfon, R., et al. (2011). A cis -regulatory map of the Drosophila genome. Nature 471, 527–531. https://doi.org/10.1038/nature09990.

Nora, E.P., Goloborodko, A., Valton, A.-L., Gibcus, J.H., Uebersohn, A., Abdennur, N., Dekker, J., Mirny, L.A., and Bruneau, B.G. (2017). Targeted Degradation of CTCF Decouples Local Insulation of Chromosome Domains from Genomic Compartmentalization. Cell 169, 930-944.e22. https://doi.org/10.1016/j.cell.2017.05.004.

O'Brien, L.E., Soliman, S.S., Li, X., and Bilder, D. (2011). Altered Modes of Stem Cell Division Drive Adaptive Intestinal Growth. Cell 147, 603–614. https://doi.org/10.1016/j.cell.2011.08.048.

Ohlstein, B., and Spradling, A. (2006). The adult Drosophila posterior midgut is maintained by pluripotent stem cells. Nature 439, 470–474. https://doi.org/10.1038/nature04333.

Okumura, T., Takeda, K., Kuchiki, M., Akaishi, M., Taniguchi, K., and Adachi-Yamada, T. (2016). GATAe regulates intestinal stem cell maintenance and differentiation in Drosophila adult midgut. Developmental Biology 410, 24–35. https://doi.org/10.1016/j.ydbio.2015.12.017.

Olins, A.L., and Olins, D.E. (1974). Spheroid Chromatin Units (v Bodies). Science, New Series 183, 330–332. .

Orphanides, G., LeRoy, G., Chang, C.-H., Luse, D.S., and Reinberg, D. (1998). FACT, a Factor that Facilitates Transcript Elongation through Nucleosomes. Cell 92, 105–116. https://doi.org/10.1016/S0092-8674(00)80903-4.

Ou, H.D., Phan, S., Deerinck, T.J., Thor, A., Ellisman, M.H., and O'Shea, C.C. (2017). ChromEMT: Visualizing 3D chromatin structure and compaction in interphase and mitotic cells. Science 357, eaag0025. https://doi.org/10.1126/science.aag0025.

Park, A.R., Liu, N., Neuenkirchen, N., Guo, Q., and Lin, H. (2019). The Role of Maternal HP1a in Early Drosophila Embryogenesis via Regulation of Maternal Transcript Production. Genetics 211, 201–217. https://doi.org/10.1534/genetics.118.301704.

Park, I., Qian, D., Kiel, M., Becker, M.W., Pihalja, M., Weissman, I.L., Morrison, S.J., and Clarke, M.F. (2003). Bmi-1 is required for maintenance of adult self-renewing haematopoietic stem cells. Nature 423, 302–305. https://doi.org/10.1038/nature01587.

Park, S.-H., Park, S.H., Kook, M.-C., Kim, E.-Y., Park, S., and Lim, J.H. (2004). Ultrastructure of Human Embryonic Stem Cells and Spontaneous and Retinoic Acid-Induced Differentiating Cells. Ultrastructural Pathology 28, 229–238. https://doi.org/10.1080/01913120490515595.

Pengelly, A.R., Kalb, R., Finkl, K., and Müller, J. (2015). Transcriptional repression by PRC1 in the absence of H2A monoubiquitylation. Genes Dev. 29, 1487–1492. https://doi.org/10.1101/gad.265439.115.

Piacentini, L., Fanti, L., Negri, R., Vescovo, V.D., Fatica, A., Altieri, F., and Pimpinelli, S. (2009). Heterochromatin Protein 1 (HP1a) Positively Regulates Euchromatic Gene Expression through RNA Transcript Association and Interaction with hnRNPs in Drosophila. PLOS Genetics 5, e1000670. https://doi.org/10.1371/journal.pgen.1000670.

Pickersgill, H., Kalverda, B., de Wit, E., Talhout, W., Fornerod, M., and van Steensel, B. (2006). Characterization of the Drosophila melanogaster genome at the nuclear lamina. Nat Genet 38, 1005–1014. https://doi.org/10.1038/ng1852.

Pietersen, A.M., Evers, B., Prasad, A.A., Tanger, E., Cornelissen-Steijger, P., Jonkers, J., and Lohuizen, M. van (2008). Bmi1 Regulates Stem Cells and Proliferation and Differentiation of Committed Cells in Mammary Epithelium. Current Biology 18, 1094–1099. https://doi.org/10.1016/j.cub.2008.06.070.

Piunti, A., and Shilatifard, A. (2021). The roles of Polycomb repressive complexes in mammalian development and cancer. Nat Rev Mol Cell Biol https://doi.org/10.1038/s41580-021-00341-1.

Raab, J.R., Tulasi, D.Y., Wager, K.E., Morowitz, J.M., Magness, S.T., and Gracz, A.D. (2019). Quantitative classification of chromatin dynamics reveals regulators of intestinal stem cell differentiation. Development dev.181966. https://doi.org/10.1242/dev.181966.

Rada-Iglesias, A., Bajpai, R., Swigut, T., Brugmann, S.A., Flynn, R.A., and Wysocka, J. (2011). A unique chromatin signature uncovers early developmental enhancers in humans. Nature 470, 279–283. https://doi.org/10.1038/nature09692.

Ramachandran, A., Omar, M., Cheslock, P., and Schnitzler, G.R. (2003). Linker Histone H1 Modulates Nucleosome Remodeling by Human SWI/SNF*. Journal of Biological Chemistry 278, 48590–48601. https://doi.org/10.1074/jbc.M309033200.

Rao, S.S.P., Huntley, M.H., Durand, N.C., Stamenova, E.K., Bochkov, I.D., Robinson, J.T., Sanborn, A.L., Machol, I., Omer, A.D., Lander, E.S., et al. (2014). A 3D Map of the Human Genome at Kilobase Resolution Reveals Principles of Chromatin Looping. Cell 159, 1665–1680. https://doi.org/10.1016/j.cell.2014.11.021.

Rao, S.S.P., Huang, S.-C., Hilaire, B.G.S., Engreitz, J.M., Perez, E.M., Kieffer-Kwon, K.-R., Sanborn, A.L., Johnstone, S.E., Bascom, G.D., Bochkov, I.D., et al. (2017). Cohesin Loss Eliminates All Loop Domains. Cell 171, 305-320.e24. https://doi.org/10.1016/j.cell.2017.09.026.

Ratel, D., Ravanat, J.-L., Berger, F., and Wion, D. (2006). N6-methyladenine: the other methylated base of DNA. Bioessays 28, 309–315. https://doi.org/10.1002/bies.20342.

Rea, S., Eisenhaber, F., O'Carroll, D., Strahl, B.D., Sun, Z.-W., Schmid, M., Opravil, S., Mechtler, K., Ponting, C.P., Allis, C.D., et al. (2000). Regulation of chromatin structure by site-specific histone H3 methyltransferases. Nature 406, 593–599. https://doi.org/10.1038/35020506.

Reddy, K.L., Zullo, J.M., Bertolino, E., and Singh, H. (2008). Transcriptional repression mediated by repositioning of genes to the nuclear lamina. Nature 452, 243–247. https://doi.org/10.1038/nature06727.

Redolfi, J., Zhan, Y., Valdes-Quezada, C., Kryzhanovska, M., Guerreiro, I., Iesmantavicius, V., Pollex, T., Grand, R.S., Mulugeta, E., Kind, J., et al. (2019). DamC reveals principles of chromatin folding in vivo without crosslinking and ligation. Nature Structural & Molecular Biology 26, 471. https://doi.org/10.1038/s41594-019-0231-0.

Ren, F., Shi, Q., Chen, Y., Jiang, A., Ip, Y.T., Jiang, H., and Jiang, J. (2013). Drosophila Myc integrates multiple signaling pathways to regulate intestinal stem cell proliferation during midgut regeneration. Cell Research 23, 1133–1146. https://doi.org/10.1038/cr.2013.101.

Ricci, M.A., Manzo, C., García-Parajo, M.F., Lakadamyali, M., and Cosma, M.P. (2015). Chromatin Fibers Are Formed by Heterogeneous Groups of Nucleosomes In Vivo. Cell 160, 1145–1158. https://doi.org/10.1016/j.cell.2015.01.054.

Robinson, P.J., and Rhodes, D. (2006). Structure of the '30nm' chromatin fibre: A key role for the linker histone. Current Opinion in Structural Biology 16, 336–343. https://doi.org/10.1016/j.sbi.2006.05.007.

Robson, L.G., Foggia, V.D., Radunovic, A., Bird, K., Zhang, X., and Marino, S. (2011). Bmi1 Is Expressed in Postnatal Myogenic Satellite Cells, Controls Their Maintenance and Plays an Essential Role in Repeated Muscle Regeneration. PLOS ONE 6, e27116. https://doi.org/10.1371/journal.pone.0027116.

Sallé, J., Gervais, L., Boumard, B., Stefanutti, M., Siudeja, K., and Bardin, A.J. (2017). Intrinsic regulation of enteroendocrine fate by Numb. EMBO J 36, 1928–1945. https://doi.org/10.15252/embj.201695622.

Saxena, M., and Shivdasani, R.A. (2020). Epigenetic Signatures and Plasticity of Intestinal and Other Stem Cells. 23. .

Schardin, M., Cremer, T., Hager, H.D., and Lang, M. (1985). Specific staining of human chromosomes in Chinese hamster x man hybrid cell lines demonstrates interphase chromosome territories. Hum Genet 71, 281–287. https://doi.org/10.1007/BF00388452.

Schlesinger, S., and Meshorer, E. (2019). Open Chromatin, Epigenetic Plasticity, and Nuclear Organization in Pluripotency. Developmental Cell 48, 135–150. https://doi.org/10.1016/j.devcel.2019.01.003.

Schnetz, M.P., Bartels, C.F., Shastri, K., Balasubramanian, D., Zentner, G.E., Balaji, R., Zhang, X., Song, L., Wang, Z., LaFramboise, T., et al. (2009). Genomic distribution of CHD7 on chromatin tracks H3K4 methylation patterns. Genome Res. 19, 590–601. https://doi.org/10.1101/gr.086983.108.

Schnetz, M.P., Handoko, L., Akhtar-Zaidi, B., Bartels, C.F., Pereira, C.F., Fisher, A.G., Adams, D.J., Flicek, P., Crawford, G.E., LaFramboise, T., et al. (2010). CHD7 Targets Active Gene

Enhancer Elements to Modulate ES Cell-Specific Gene Expression. PLOS Genetics 6, e1001023. https://doi.org/10.1371/journal.pgen.1001023.

Schwabish, M.A., and Struhl, K. (2007). The Swi/Snf Complex Is Important for Histone Eviction during Transcriptional Activation and RNA Polymerase II Elongation In Vivo. Molecular and Cellular Biology 27, 6987–6995. https://doi.org/10.1128/MCB.00717-07.

Scopelliti, A., Cordero, J.B., Diao, F., Strathdee, K., White, B.H., Sansom, O.J., and Vidal, M. (2014). Local control of intestinal stem cell homeostasis by enteroendocrine cells in the adult Drosophila midgut. Curr. Biol. 24, 1199–1211. https://doi.org/10.1016/j.cub.2014.04.007.

Serebreni, L., and Stark, A. (2021). Insights into gene regulation: From regulatory genomic elements to DNA-protein and protein-protein interactions. Current Opinion in Cell Biology 70, 58–66. https://doi.org/10.1016/j.ceb.2020.11.009.

Sexton, T., Yaffe, E., Kenigsberg, E., Bantignies, F., Leblanc, B., Hoichman, M., Parrinello, H., Tanay, A., and Cavalli, G. (2012). Three-Dimensional Folding and Functional Organization Principles of the Drosophila Genome. Cell 148, 458–472. https://doi.org/10.1016/j.cell.2012.01.010.

Shah, R.N., Grzybowski, A.T., Elias, J., Chen, Z., Hattori, T., Lechner, C.C., Lewis, P.W., Koide, S., Fierz, B., and Ruthenburg, A.J. (2021). Re-evaluating the role of nucleosomal bivalency in early development (Molecular Biology).

Shevelyov, Y.Y., Lavrov, S.A., Mikhaylova, L.M., Nurminsky, I.D., Kulathinal, R.J., Egorova, K.S., Rozovsky, Y.M., and Nurminsky, D.I. (2009). The B-type lamin is required for somatic repression of testis-specific gene clusters. Proceedings of the National Academy of Sciences 106, 3282–3287. https://doi.org/10.1073/pnas.0811933106.

Shi, Y., Lan, F., Matson, C., Mulligan, P., Whetstine, J.R., Cole, P.A., Casero, R.A., and Shi, Y. (2004). Histone Demethylation Mediated by the Nuclear Amine Oxidase Homolog LSD1. Cell 119, 941–953. https://doi.org/10.1016/j.cell.2004.12.012.

Simic, R., Lindstrom, D.L., Tran, H.G., Roinick, K.L., Costa, P.J., Johnson, A.D., Hartzog, G.A., and Arndt, K.M. (2003). Chromatin remodeling protein Chd1 interacts with transcription elongation factors and localizes to transcribed genes. EMBO J 22, 1846–1856. https://doi.org/10.1093/emboj/cdg179.

Singhal, N., Graumann, J., Wu, G., Araúzo-Bravo, M.J., Han, D.W., Greber, B., Gentile, L., Mann, M., and Schöler, H.R. (2010). Chromatin-Remodeling Components of the BAF Complex Facilitate Reprogramming. Cell 141, 943–955. https://doi.org/10.1016/j.cell.2010.04.037.

Skene, P.J., and Henikoff, S. (2017). An efficient targeted nuclease strategy for high-resolution mapping of DNA binding sites. Elife 6, e21856. https://doi.org/10.7554/eLife.21856.

Srinivasan, S., Dorighi, K.M., and Tamkun, J.W. (2008). Drosophila Kismet Regulates Histone H3 Lysine 27 Methylation and Early Elongation by RNA Polymerase II. PLOS Genetics 4, e1000217. https://doi.org/10.1371/journal.pgen.1000217.

Staahl, B.T., Tang, J., Wu, W., Sun, A., Gitler, A.D., Yoo, A.S., and Crabtree, G.R. (2013). Kinetic Analysis of npBAF to nBAF Switching Reveals Exchange of SS18 with CREST and

Integration with Neural Developmental Pathways. J. Neurosci. 33, 10348–10361. https://doi.org/10.1523/JNEUROSCI.1258-13.2013.

Steensel, B. van, and Henikoff, S. (2000). Identification of in vivo DNA targets of chromatin proteins using tethered Dam methyltransferase. Nat Biotechnol 18, 424–428. https://doi.org/10.1038/74487.

Stopka, T., and Skoultchi, A.I. (2003). The ISWI ATPase Snf2h is required for early mouse development. Proceedings of the National Academy of Sciences 100, 14097–14102. https://doi.org/10.1073/pnas.2336105100.

Strahl, B.D., and Allis, C.D. (2000). The language of covalent histone modi®cations. 403, 5. .

Strickfaden, H. (2021). Reflections on the organization and the physical state of chromatin in eukaryotic cells. Genome 64, 311–325. https://doi.org/10.1139/gen-2020-0132.

Strom, A.R., Emelyanov, A.V., Mir, M., Fyodorov, D.V., Darzacq, X., and Karpen, G.H. (2017). Phase separation drives heterochromatin domain formation. Nature 547, 241–245. https://doi.org/10.1038/nature22989.

Sze, C.C., Cao, K., Collings, C.K., Marshall, S.A., Rendleman, E.J., Ozark, P.A., Chen, F.X., Morgan, M.A., Wang, L., and Shilatifard, A. (2017). Histone H3K4 methylation-dependent and -independent functions of Set1A/COMPASS in embryonic stem cell self-renewal and differentiation. Genes Dev. 31, 1732–1737. https://doi.org/10.1101/gad.303768.117.

Tauc, H.M., Tasdogan, A., Meyer, P., and Pandur, P. (2017). Nipped-A regulates intestinal stem cell proliferation in Drosophila. Development 144, 612–623. https://doi.org/10.1242/dev.142703.

Tauc, H.M., Rodriguez-Fernandez, I.A., Hackney, J.A., Pawlak, M., Ronnen Oron, T., Korzelius, J., Moussa, H.F., Chaudhuri, S., Modrusan, Z., Edgar, B.A., et al. (2021). Age-related changes in polycomb gene regulation disrupt lineage fidelity in intestinal stem cells. ELife 10, e62250. https://doi.org/10.7554/eLife.62250.

Taverna, S.D., Li, H., Ruthenburg, A.J., Allis, C.D., and Patel, D.J. (2007). How chromatin-binding modules interpret histone modifications: lessons from professional pocket pickers. Nat Struct Mol Biol 14, 1025–1040. https://doi.org/10.1038/nsmb1338.

The modENCODE Consortium, Roy, S., Ernst, J., Kharchenko, P.V., Kheradpour, P., Negre, N., Eaton, M.L., Landolin, J.M., Bristow, C.A., Ma, L., et al. (2010). Identification of Functional Elements and Regulatory Circuits by Drosophila modENCODE. Science 330, 1787–1797. https://doi.org/10.1126/science.1198374.

Thurman, R.E., Rynes, E., Humbert, R., Vierstra, J., Maurano, M.T., Haugen, E., Sheffield, N.C., Stergachis, A.B., Wang, H., Vernot, B., et al. (2012). The accessible chromatin landscape of the human genome. Nature 489, 75–82. https://doi.org/10.1038/nature11232.

Torres, C.M., Biran, A., Burney, M.J., Patel, H., Henser-Brownhill, T., Cohen, A.-H.S., Li, Y., Ben-Hamo, R., Nye, E., Spencer-Dene, B., et al. (2016). The linker histone H1.0 generates epigenetic and functional intratumor heterogeneity. Science 353, aaf1644. https://doi.org/10.1126/science.aaf1644.

Tsukada, Y., Fang, J., Erdjument-Bromage, H., Warren, M.E., Borchers, C.H., Tempst, P., and Zhang, Y. (2006). Histone demethylation by a family of JmjC domain-containing proteins. Nature 439, 811–816. https://doi.org/10.1038/nature04433.

Turner, B.M. (2007). Defining an epigenetic code. Nat Cell Biol 9, 2–6. https://doi.org/10.1038/ncb0107-2.

Vakoc, C.R., Mandat, S.A., Olenchock, B.A., and Blobel, G.A. (2005). Histone H3 Lysine 9 Methylation and HP1γ Are Associated with Transcription Elongation through Mammalian Chromatin. Molecular Cell 19, 381–391. https://doi.org/10.1016/j.molcel.2005.06.011.

van der Velde, A., Fan, K., Tsuji, J., Moore, J.E., Purcaro, M.J., Pratt, H.E., and Weng, Z. (2021). Annotation of chromatin states in 66 complete mouse epigenomes during development. Commun Biol 4, 1–15. https://doi.org/10.1038/s42003-021-01756-4.

Villa, S.E.R., Meng, F.W., and Biteau, B. (2019). Zfh2 controls progenitor cell activation and differentiation in the adult Drosophila intestinal absorptive lineage. PLOS Genetics 15, e1008553. https://doi.org/10.1371/journal.pgen.1008553.

Villaseñor, R., and Baubec, T. (2021). Regulatory mechanisms governing chromatin organization and function. Current Opinion in Cell Biology 70, 10–17. https://doi.org/10.1016/j.ceb.2020.10.015.

Vissers, L.E.L.M., van Ravenswaaij, C.M.A., Admiraal, R., Hurst, J.A., de Vries, B.B.A., Janssen, I.M., van der Vliet, W.A., Huys, E.H.L.P.G., de Jong, P.J., Hamel, B.C.J., et al. (2004). Mutations in a new member of the chromodomain gene family cause CHARGE syndrome. Nat Genet 36, 955–957. https://doi.org/10.1038/ng1407.

Voigt, P., LeRoy, G., Drury, W.J., Zee, B.M., Son, J., Beck, D.B., Young, N.L., Garcia, B.A., and Reinberg, D. (2012). Asymmetrically Modified Nucleosomes. Cell 151, 181–193. https://doi.org/10.1016/j.cell.2012.09.002.

Voncken, J.W., Roelen, B.A.J., Roefs, M., de Vries, S., Verhoeven, E., Marino, S., Deschamps, J., and van Lohuizen, M. (2003). Rnf2 (Ring1b) deficiency causes gastrulation arrest and cell cycle inhibition. Proceedings of the National Academy of Sciences 100, 2468–2473. https://doi.org/10.1073/pnas.0434312100.

Vos, S.M. (2021). Understanding transcription across scales: From base pairs to chromosomes. Molecular Cell 81, 1601–1616. https://doi.org/10.1016/j.molcel.2021.03.002.

Waddington, C. H. (1957). The strategy of the genes : a discussion of some aspects of theoretical biology / by C.H. Waddington.

Wen, B., Wu, H., Shinkai, Y., Irizarry, R.A., and Feinberg, A.P. (2009). Large histone H3 lysine 9 dimethylated chromatin blocks distinguish differentiated from embryonic stem cells. Nat Genet 41, 246–250. https://doi.org/10.1038/ng.297.

Wiblin, A.E., Cui, W., Clark, A.J., and Bickmore, W.A. (2005). Distinctive nuclear organisation of centromeres and regions involved in pluripotency in human embryonic stem cells. Journal of Cell Science 118, 3861–3868. https://doi.org/10.1242/jcs.02500.

Willcockson, M.A., Healton, S.E., Weiss, C.N., Bartholdy, B.A., Botbol, Y., Mishra, L.N., Sidhwani, D.S., Wilson, T.J., Pinto, H.B., Maron, M.I., et al. (2020). H1 histones control the epigenetic landscape by local chromatin compaction. Nature https://doi.org/10.1038/s41586-020-3032-z.

de Wit, E., Greil, F., and van Steensel, B. (2007). High-Resolution Mapping Reveals Links of HP1 with Active and Inactive Chromatin Components. PLoS Genetics 3, e38. https://doi.org/10.1371/journal.pgen.0030038.

Wolffe, A.P., and Hayes, J.J. (1999). Chromatin disruption and modification. Nucleic Acids Res 27, 711–720. .

Wu, J., Huang, B., Chen, H., Yin, Q., Liu, Y., Xiang, Y., Zhang, B., Liu, B., Wang, Q., Xia, W., et al. (2016). The landscape of accessible chromatin in mammalian preimplantation embryos. Nature 534, 652–657. https://doi.org/10.1038/nature18606.

Xu, C., Franklin, B., Tang, H.-W., Regimbald-Dumas, Y., Hu, Y., Ramos, J., Bosch, J.A., Villalta, C., He, X., and Perrimon, N. (2020). An in vivo RNAi screen uncovers the role of AdoR signaling and adenosine deaminase in controlling intestinal stem cell activity. PNAS 117, 464–471. https://doi.org/10.1073/pnas.1900103117.

Yan, F., Powell, D.R., Curtis, D.J., and Wong, N.C. (2020). From reads to insight: a hitchhiker's guide to ATAC-seq data analysis. Genome Biology 21, 22. https://doi.org/10.1186/s13059-020-1929-3.

Yin, C., and Xi, R. (2018). A Phyllopod-Mediated Feedback Loop Promotes Intestinal Stem Cell Enteroendocrine Commitment in Drosophila. Stem Cell Reports 10, 43–57. https://doi.org/10.1016/j.stemcr.2017.11.014.

Yin, H., Sweeney, S., Raha, D., Snyder, M., and Lin, H. (2011). A High-Resolution Whole-Genome Map of Key Chromatin Modifications in the Adult Drosophila melanogaster. PLoS Genetics 7, e1002380. https://doi.org/10.1371/journal.pgen.1002380.

Yu, B.D., Hess, J.L., Horning, S.E., Brown, G.A., and Korsmeyer, S.J. (1995). Altered Hox expression and segmental identity in Mll-mutant mice. Nature 378, 505–508. https://doi.org/10.1038/378505a0.

Yusufova, N., Kloetgen, A., Teater, M., Osunsade, A., Camarillo, J.M., Chin, C.R., Doane, A.S., Venters, B.J., Portillo-Ledesma, S., Conway, J., et al. (2021). Histone H1 loss drives lymphoma by disrupting 3D chromatin architecture. Nature 589, 299–305. https://doi.org/10.1038/s41586-020-3017-y.

Zalc, A., Sinha, R., Gulati, G.S., Wesche, D.J., Daszczuk, P., Swigut, T., Weissman, I.L., and Wysocka, J. (2021). Reactivation of the pluripotency program precedes formation of the cranial neural crest. Science 371, eabb4776. https://doi.org/10.1126/science.abb4776.

Zaret, K.S., and Carroll, J.S. (2011). Pioneer transcription factors: establishing competence for gene expression. Genes Dev. 25, 2227–2241. https://doi.org/10.1101/gad.176826.111.

Zeng, X., and Hou, S.X. (2015). Enteroendocrine cells are generated from stem cells through a distinct progenitor in the adult Drosophila posterior midgut. Development 142, 644–653. https://doi.org/10.1242/dev.113357.

Zeng, X., Lin, X., and Hou, S.X. (2013). The Osa-containing SWI/SNF chromatin-remodeling complex regulates stem cell commitment in the adult Drosophila intestine. Development 140, 3532–3540. https://doi.org/10.1242/dev.096891.

Zhai, Z., Kondo, S., Ha, N., Boquete, J.-P., Brunner, M., Ueda, R., and Lemaitre, B. (2015). Accumulation of differentiating intestinal stem cell progenies drives tumorigenesis. Nature Communications 6. https://doi.org/10.1038/ncomms10219.

Zhai, Z., Boquete, J.-P., and Lemaitre, B. (2017). A genetic framework controlling the differentiation of intestinal stem cells during regeneration in Drosophila. PLOS Genetics 13, e1006854. https://doi.org/10.1371/journal.pgen.1006854.

Zhu, J., Adli, M., Zou, J.Y., Verstappen, G., Coyne, M., Zhang, X., Durham, T., Miri, M., Deshpande, V., De Jager, P.L., et al. (2013). Genome-wide Chromatin State Transitions Associated with Developmental and Environmental Cues. Cell 152, 642–654. https://doi.org/10.1016/j.cell.2012.12.033.

(2012). Human mitotic chromosomes consist predominantly of irregularly folded nucleosome fibres without a 30-nm chromatin structure. The EMBO Journal 31, 1644–1653. https://doi.org/10.1038/emboj.2012.35.

ANNEX

Article

Developmental Cell

Stem Cell Proliferation Is Kept in Check by the Chromatin Regulators Kismet/CHD7/CHD8 and Trr/MLL3/4

Graphical Abstract

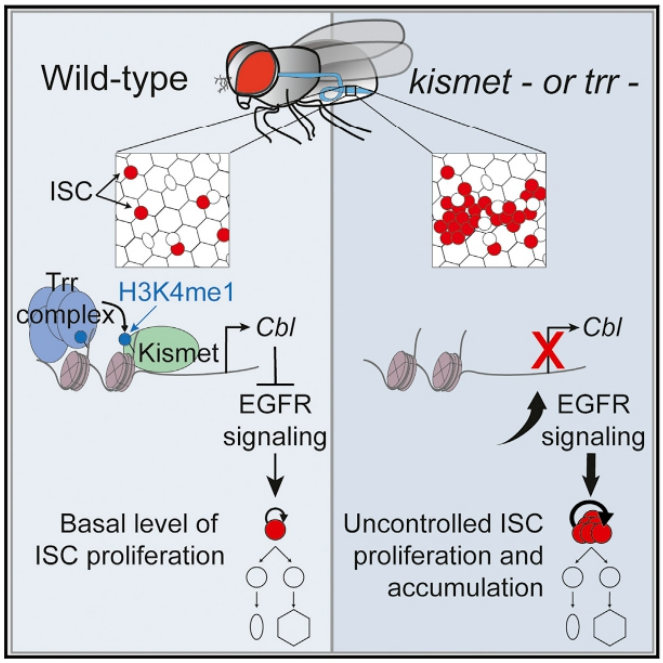

Highlights

- Chromatin modifiers Kismet and Trr limit intestinal stem cell proliferation
- Kismet and Trr colocalize at transcriptionally active regions and co-regulate genes
- EGFR negative regulator *Cbl* is a target gene of Kismet and Trr
- Kismet and Trr limit EGFR signaling in ISCs, preventing tumor-like ISC accumulation

Authors

Louis Gervais, Marius van den Beek, Manon Josserand, ..., Andrea H. Brand, François Schweisguth, Allison J. Bardin

Correspondence

louis.gervais@curie.fr (L.G.), allison.bardin@curie.fr (A.J.B.)

In Brief

Stem cell proliferation control is essential to maintaining tissue homeostasis. Gervais et al. compare *Drosophila* intestinal stem cell (ISC) whole-genome profiling of chromatin modifier Kismet/CHD7/CHD8 binding to DamID reporters of different chromatin states and demonstrate that Kismet and Trr/MLL3/4 are regulators of ISC self-renewal by limiting EGFR signaling.

Gervais et al., 2019, Developmental Cell *49*, 556–573
May 20, 2019
https://doi.org/10.1016/j.devcel.2019.04.033

CellPress

Developmental Cell
Article

Stem Cell Proliferation Is Kept in Check by the Chromatin Regulators Kismet/CHD7/CHD8 and Trr/MLL3/4

Louis Gervais,[1,2,*] Marius van den Beek,[1,2,7] Manon Josserand,[1,2,7] Jérémy Sallé,[1,2,8] Marine Stefanutti,[1,2] Carolina N. Perdigoto,[1,2] Patricia Skorski,[1,2] Khallil Mazouni,[5,6] Owen J. Marshall,[3,4] Andrea H. Brand,[3] François Schweisguth,[5,6] and Allison J. Bardin[1,2,9,*]

[1]Institut Curie, PSL Research University, CNRS UMR 3215, INSERM U934, Stem Cells and Tissue Homeostasis Group, Paris, France
[2]Sorbonne Universités, UPMC Univ Paris 6, Paris, France
[3]The Gurdon Institute and Department of Physiology, Development and Neuroscience, University of Cambridge, Cambridge CB2 1QN, UK
[4]Menzies Institute for Medical Research, University of Tasmania, 17 Liverpool Street Hobart, Tasmania, 7000, Australia
[5]Institut Pasteur, Department of Developmental and Stem Cell Biology, Paris 75015, France
[6]CNRS, URA2578, Rue du Dr Roux, Paris 75015, France
[7]These authors contributed equally
[8]Present address: CNRS UMR 7592, Institut Jacques Monod, 15 Rue Hélène Brion, Paris CEDEX 13 75205, France
[9]Lead Contact
*Correspondence: louis.gervais@curie.fr (L.G.), allison.bardin@curie.fr (A.J.B.)
https://doi.org/10.1016/j.devcel.2019.04.033

SUMMARY

Chromatin remodeling accompanies differentiation, however, its role in self-renewal is less well understood. We report that in *Drosophila*, the chromatin remodeler Kismet/CHD7/CHD8 limits intestinal stem cell (ISC) number and proliferation without affecting differentiation. Stem-cell-specific whole-genome profiling of Kismet revealed its enrichment at transcriptionally active regions bound by RNA polymerase II and Brahma, its recruitment to the transcription start site of activated genes and developmental enhancers and its depletion from regions bound by Polycomb, Histone H1, and heterochromatin Protein 1. We demonstrate that the Trithorax-related/MLL3/4 chromatin modifier regulates ISC proliferation, colocalizes extensively with Kismet throughout the ISC genome, and co-regulates genes in ISCs, including *Cbl*, a negative regulator of Epidermal Growth Factor Receptor (EGFR). Loss of *kismet* or *trr* leads to elevated levels of EGFR protein and signaling, thereby promoting ISC self-renewal. We propose that Kismet with Trr establishes a chromatin state that limits EGFR proliferative signaling, preventing tumor-like stem cell overgrowths.

INTRODUCTION

Regulation of stem cell proliferation rates is critical in adult tissues, which need to maintain basal renewal and undergo damage-induced regenerative responses. Consequently, the dysregulation of stem cell proliferation can have pathological effects. Ample evidence now supports a functional link between the deregulated proliferation of stem cells and cancer initiation, as well as metastatic progression (de Sousa e Melo et al., 2017; Flavahan et al., 2017). Interestingly, the loss of epigenetic control is a major contributor to stem cell misregulation including proliferation deregulation during aging (Brunet and Rando, 2017; Challen et al., 2014; Ko et al., 2011). Therefore, in addition to roles of epigenetic regulation during differentiation of stem-cell-derived lineages, chromatin modulation also has important, though not yet well understood, roles in the control of stem cell proliferation.

A useful model to investigate adult stem cell regulation is the *Drosophila* midgut, which is maintained by around 1,000 multipotent intestinal stem cells (ISCs). Most ISC divisions lead to asymmetric daughter cell fates, resulting in a self-renewed ISC and a sister enteroblast (EB) cell (Figure 1A). A majority of EBs receive high levels of Notch signaling and differentiate into enterocyte cells (ECs). Rare stem cell divisions produce an enteroendocrine precursor cell (EEP) with low or no Notch signaling, which is thought to divide once to make two enteroendocrine cells (EEs) (Chen et al., 2018; Ohlstein and Spradling, 2007; Sallé et al., 2017). In response to epithelial damage, several signaling pathways become activated and coordinate ISC proliferation and differentiation (see for review, Jiang et al., 2016). Of primary importance are signals that the ISCs receive to activate the Jak/Stat and Epidermal Growth Factor Receptor (EGFR) pathways (Biteau and Jasper, 2011; Buchon et al., 2010, 2009; Jiang et al., 2011, 2009; Wang et al., 2014; Xu et al., 2011). Moreover, other pathways such as Insulin, Hippo, Jun Kinase, BMP, Wnt, and Hedgehog also control ISC proliferation (Biteau et al., 2008; Cordero et al., 2012; Li et al., 2013, 2014; Lin et al., 2008; O'Brien et al., 2011; Ren et al., 2010; Shaw et al., 2010; Staley and Irvine, 2010; Tian and Jiang, 2014; Tian et al., 2015, 2017). Evidence suggests that there are also mechanisms to limit ISC responsiveness, tuning down cell division when sufficient renewal has occurred (Guo et al., 2013; Hochmuth et al., 2011), though this process is not well understood.

Here, we report on the identification of a regulator that is essential to limit ISC proliferation: *kismet*, similar to the

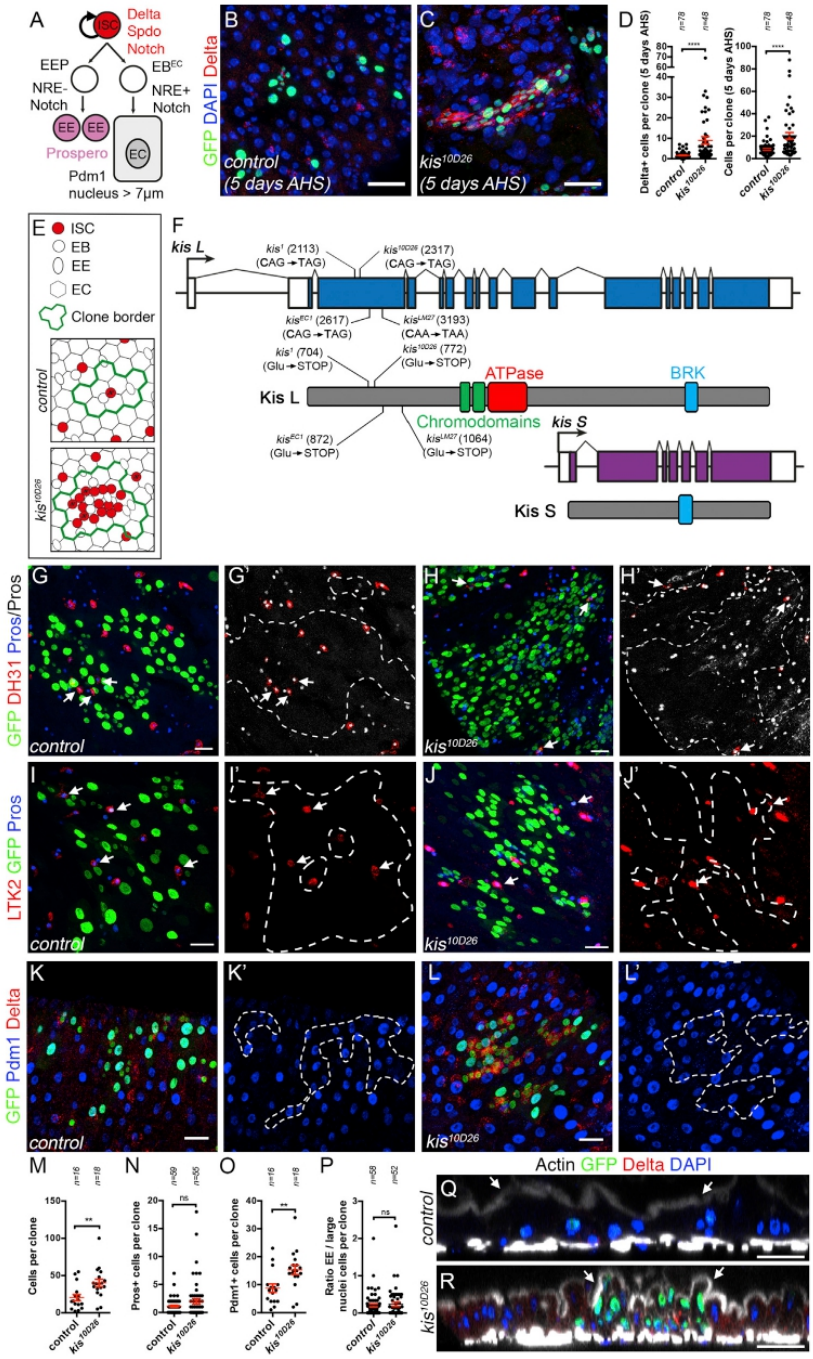

Figure 1. Loss of *kismet* Provokes ISC Accumulation without Affecting Terminal Differentiation

(A) The ISCs divide to self-renew and to produce a precursor cell, the EB, that subsequently terminally differentiates into an EC or is thought to divide once as an EEP to produce two EE cells.

(legend continued on next page)

chromodomain-containing chromatin remodeling factors CHD7 and CHD8. Mammalian CHD7 is associated with transcriptionally active genes at enhancers, super-enhancers, and promoters where it can both activate and repress transcription (Hnisz et al., 2013; Schnetz et al., 2009, 2010). *kismet* was originally identified as a "trithorax group" gene because of its ability to dominantly suppress *Polycomb* mutant phenotypes (Kennison and Tamkun, 1988). Studies using the polytene chromosomes of the salivary gland have shown that Kismet is associated with transcriptionally active chromatin, where it recruits the histone methyl transferases Trithorax and Ash1. Ash1 recruitment, in turn, is thought to promote H3K36me2, leading to the inhibition of Histone H3K27me3 (Dorighi and Tamkun, 2013). In addition, as *kismet* mutants show a reduction in elongating RNA polymerase II (RNA Pol II), Kismet was proposed to promote transcription elongation (Srinivasan et al., 2008). Whether Kismet acts in other tissues via similar molecular effectors is not currently known.

CHD7/CHD8 and Kismet have essential functions during development and in adult tissues. In humans, inactivation of CHD7 causes a spectrum of congenital defects called CHARGE syndrome, (Coloboma, Heart defects, Atsresia choanae, Retarded growth and development, Genital abnormalities and Ear anomalies) (Bajpai et al., 2010; Vissers et al., 2004). Moreover, *CHD7* is essential for neural development and adult neural stem cell maintenance and is deregulated in cancers (Feng et al., 2013, 2017; Jones et al., 2015; Pleasance et al., 2010; Robinson et al., 2012). *CHD8* mutations are associated with neurodevelopmental defects in autism spectrum disorders (Neale et al., 2012; O'Roak et al., 2012; Talkowski et al., 2012). In *Drosophila*, *kismet* mutants have defects in developmental patterning with homeotic transformations as well as alteration of circadian rhythm and memory (Daubresse et al., 1999; Dubruille et al., 2009; Melicharek et al., 2010; Terriente-Félix et al., 2010, 2011). However, to date, functions of *kismet* in stem cells have not been described.

Here, we demonstrate that Kismet is an important regulator of ISCs, essential to limit basal levels of ISC proliferation. DNA adenine methyltransferase identification sequencing (DamID-seq) of Kismet compared with DamID reporters of different chromatin states, including activated (Brahma and RNA Pol II) and repressed states (Polycomb, Histone H1, Heterochromatin Protein 1 [HP1]), demonstrated that Kismet preferentially localized to transcriptionally active regions of the genome and to developmental enhancers. In addition, our data suggest that Kismet acts in ISCs with the H3K4 monomethyltransferase, Trithorax-related complex (Trr; mammalian MLL3/4). We find that Trr and Kismet co-localize in the genome and co-regulate the transcription of many genes, including *Cbl*, a negative regulator of EGFR signaling. Our data therefore demonstrate that the chromatin regulators Kismet/CHD7/CHD8 and Trr complex/MLL3/4 function together to limit basal levels of ISC proliferation and identify *Cbl* as a key downstream target gene allowing control of EGFR signaling.

RESULTS

Identification of *kismet* as an Essential Gene Controlling Stem Cell Homeostasis

We screened for EMS-induced mutations affecting ISC activity and intestinal homeostasis (C.P., F.S., and A.B., unpublished data) and found one line (10D26) that showed an increase in the size of mutant clones generated in the midgut of adult flies (Figures 1B and 1C) and had a higher proportion of cells expressing Delta, an ISC marker (8.9 Delta+ cells; 44% of clone) when compared to the control (1.6 Delta+ cells, 20% of clone; Figure 1D). In addition, these cells expressed the ISC marker Sanpodo (Perdigoto et al., 2011) (Figures S1A and S1B). Therefore, 10D26 mutant clones induce aberrant accumulation of stem cells (Figure 1E).

Deficiency mapping followed by failure to complement three known alleles of the *kismet* gene ($kismet^{1}$, $kismet^{EC1}$, and $kismet^{LM27}$) indicated that 10D26 harbored a lethal mutation in *kismet*. *kismet* encodes a conserved chromatin remodeling factor, similar to *CHD7* and *CHD8* in mammals. *kismet* encodes a long (Kismet-L) and short (Kismet-S) isoform, with only Kismet-L containing two chromodomains and an SNF2-like ATPase/helicase domain, required for nucleosome remodeling activity (Bouazoune and Kingston, 2012) (Figure 1F). All four alleles correspond to nonsense mutations early in *kismet-L* coding sequence (Figure 1F). Clones for $kismet^{EC1}$, $kismet^{LM27}$, and $kismet^{1}$ reproduced $kismet^{10D26}$ phenotypes (Figures S1C, S1D, S1O, S1Q, S1S, S1U, and S1V). No phenotype was observed outside of clones, arguing against dominant-negative action of truncated proteins (Figures 1C, S1D, S1O, S1Q, and S1S). $kismet^{10D26}$ phenotypes were rescued by a transgenic BAC construct (kis_{locus}) encompassing the genomic locus containing *kismet* fused to a FLAP tag-encoding sequence (STAR Methods; Figures S1C–S1F). In addition, the expression of *kismet-L* cDNA, rescued clone size and increased stem cell number phenotypes of $kismet^{10D26}$, $kismet^{EC1}$, $kismet^{LM27}$, and $kismet^{1}$ alleles (Figures S1G, S1H, and S1M–S1V). In contrast, *kismet-S* cDNA expression did not rescue $kismet^{10D26}$ phenotypes (Figures S1I, S1J, S1M, and S1N). Therefore, we conclude that *kismet-L* is required for normal midgut homeostasis. We will henceforth refer to *kismet-L* as "*kismet*." Interestingly, the overexpression of an ATPase-dead version ($Kismet^{K2060R}$)

(B and C) Wild-type (B) and kis^{10D26} mutant (C) MARCM clones, 5 days after heat shock (AHS).
(D) Quantification of (B) and (C).
(E) Scheme of wild-type and *kismet* mutant clones.
(F) Scheme of *kismet* gene and Kismet protein (Long and short isoforms: Kis L and Kis S): chromodomains (green), ATPase domain (red), BRK domain (blue). All *kis* alleles resulted in nonsense mutations: nucleotide changes and corresponding putative resulting truncated proteins are shown.
(G–L) Wild-type and kis^{10D26} MARCM clones at 9 days AHS. Arrows in (G)–(H′) and (I)–(J′) show EE cells marked by DH31 or LTK2, respectively.
(M–P) Quantification of the total cells per clone (M), number of EE cells per clone (Prospero+) (N), number of ECs (Pdm1+ cells per clone) (O), and the ratio of EE (Prospero+ cells / EC (polyploid nucleus >7 μm) per clone (P).
(Q and R) Vertical sections through the midgut epithelium of control (Q) and kis^{10D26} mutant (R) MARCM clones, 9 days AHS. Arrows show apical membrane.
In (D) and (M)–(P), A two-tailed Mann-Whitney statistical test was used; mean values in red; error bars, SEM; ns = non-significant, $^{**}p < 0.01$, $^{****}p < 0.0001$. Scale bars, 20 μm.

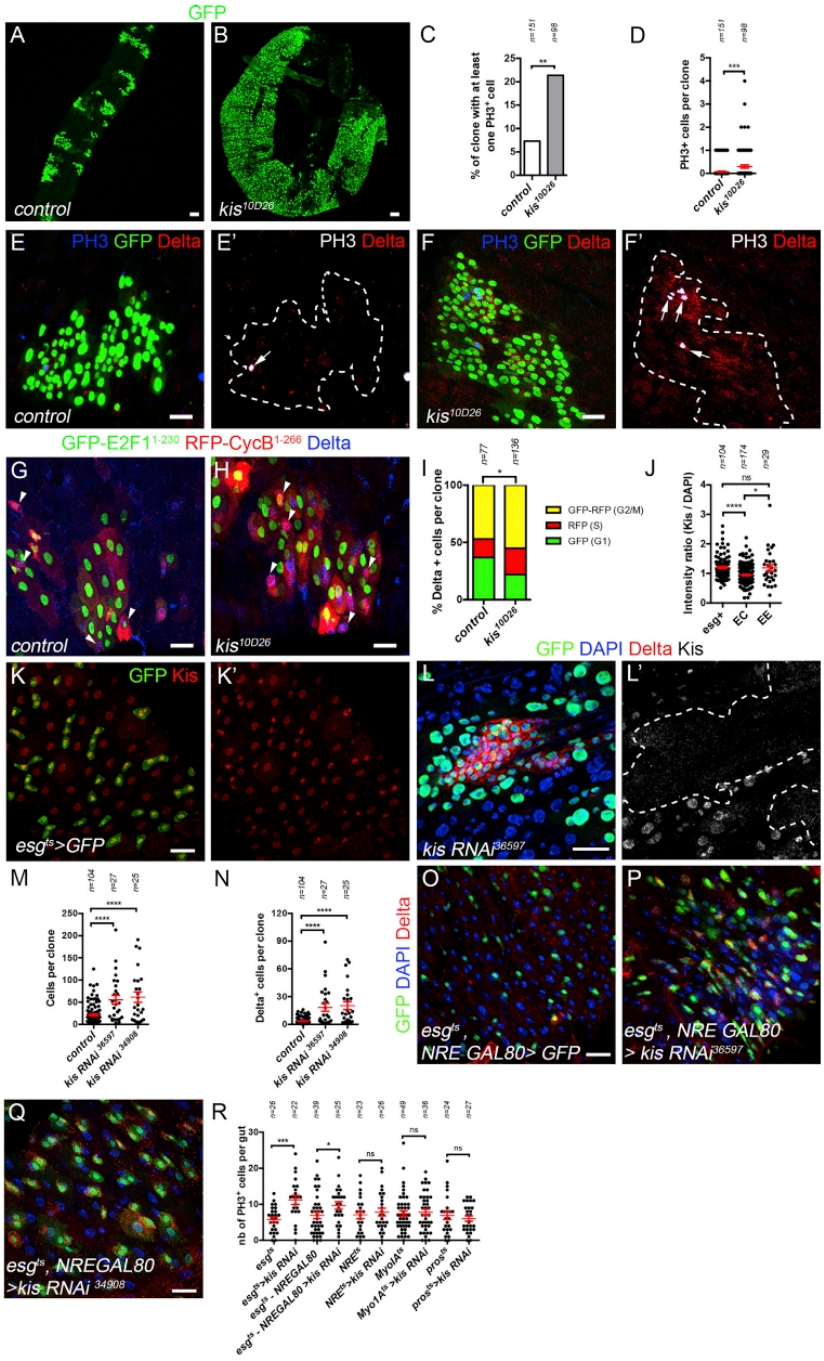

Figure 2. Loss of *kismet* Activity Promotes ISC Proliferation

(A and B) Wild-type (A) and *kis*^{10D26} (B), MARCM clones at 30 days AHS.

(C and D) Quantification of the percent of clones with at least one PH3+ cell (C) and the average number of PH3+ cell per clone (D) from (E)–(F′).

(legend continued on next page)

also showed a partial rescue of the mutant phenotype (Figures S1K–S1N). These data suggest that additional functional domains of Kismet are important for stem cell regulation, possibly by bridging interactions with other factors.

We then asked whether terminal differentiation was affected by the loss of *kismet*. *kismet* mutant clones, like wild-type clones, were able to produce terminally differentiated EC (Pdm1) and EE cells (Pros), though they made more per clone, consistent with larger clone sizes (Figures 1G–1P). Additional markers for differentiated EEs (peptide hormones DH31 and LTK2) and ECs (apical brush border) were detected in *kismet* mutants (Figures 1G–1J′, 1Q, and 1R). Thus, we conclude that loss of *kismet* function in ISCs results in increased stem cell numbers, without major defects in terminal differentiation.

Kismet Activity Limits Proliferation and Self-Renewal of the ISC

We then hypothesized that an increase in ISC numbers could be due to altered proliferation. Consistent with this, at 30 days after heat shock (AHS), *kismet* mutant tissue took over most of the midgut (Figures 2A and 2B), suggesting that mutant clones have a growth advantage over both heterozygous and wild-type cells.

Since ISCs are the primary dividing cell type in the midgut, we then assessed ISC proliferation using phospho-Histone H3 (PH3) as a marker for mitotic cells. 7.6% of the control clones had at least one and never more than one mitotic cell per clone (Figures 2C–2E′). In contrast, 21.4% of *kismet* mutant clones had at least one mitotic cell, and clones with more than one dividing cell were detected (Figures 2C, 2D, 2F, and 2F′). We assessed cell cycle parameters using the Fly-FUCCI system (Zielke et al., 2014) and found that *kismet* mutants had an increased proportion of ISCs in S phase and G2/early M at the expense of the G1 fraction (Figures 2G–2I). Together, these data further support the idea that *kismet* mutant ISCs have deregulated proliferation.

Kismet Controls Cell Division in a Stem-Cell-Autonomous Manner

To determine in which cell *kismet* activity is required, we first assessed its expression profile in the intestine. An antibody recognizing the C-terminal part shared by the short and long forms of Kismet showed enrichment in cells positive for Escargot (esg), a marker of ISCs and EBs, and in EE cells compared to ECs (Figures 2J–2K′). To test cell-type-specific requirements of *kismet*, we verified that expressing *kismet RNAi* constructs mimicked *kismet* mutant phenotypes and led to the loss of Kismet protein (Figures 2L–2N and S2A–S2E′). ISC-specific or ISC and EB simultaneous knockdown of *kismet* led to an accumulation of ISCs and increased proliferation (Figures 2O–2R, S2F, and S2G). However, *kismet* knockdown in EEs, ECs, or in EB cells only did not show ISC phenotypes (Figures 2R and S2H–S2M). We conclude that *kismet* activity is required in ISCs to limit their proliferation to a basal level and to prevent abnormal expansion of their pool.

Kismet Mutant Cells Activate Notch Signaling and Can Differentiate upon Forced Notch Activation

We next explored a potential impact of *kismet* on the Notch signaling pathway, which limits stem cell numbers by controlling daughter-cell-fate decisions (Bardin et al., 2010; Micchelli and Perrimon, 2006; Ohlstein and Spradling, 2006). We reasoned that as a regulator of transcription, Kismet might be necessary for expression of *Notch*. This was not the case, and Notch-expressing cells were in fact more abundant because of the accumulation of ISCs (Figures S3A and S3B). Furthermore, a reporter for the Notch pathway (NRE-lacZ; Notch Responsive Element), which is restricted to the EC-committed EB cells in wild-type tissue, was still expressed in *kismet* mutant clones, though absent from the extra Delta+ cells (Figures S3C–S3F).

We further examined whether *kismet* mutants might block Notch target gene activation. To test this, we induced *kismet* mutant clones and allowed 10 days of growth to accumulate extra ISCs (Figure S3G). We then induced expression of an active form of Notch in the mutant cells (N^{Act}) by shifting to 29°C to inactivate a temperature-sensitive GAL80 ($GAL80^{ts}$). At 18°C, control guts showed isolated Delta+ ISCs, whereas those with induced *kismet* mutant clones showed clusters of Delta+ ISCs (Figures S3H and S3I). However, expression of N^{Act} in *kismet* mutant clones that had accumulated ISCs caused differentiation of ISCs into ECs (Figures S3J, S3K, and S3L). Therefore, we conclude that *kismet* inactivation leads to the accumulation of extra-ISCs that maintain their potential to differentiate and activate Notch, though alteration in the kinetics of Notch signaling activation could not be excluded.

Kismet Is Required to Maintain a Basal Level of Activation of EGFR Signaling

As EGFR signaling is one of the primary signaling pathways controlling ISC proliferation (Biteau and Jasper, 2011; Buchon et al., 2010; Jiang et al., 2011), we then investigated whether *kismet*

(E–F′) Wild-type (E and E′), and kis^{10D26} (F and F′), 9 days AHS MARCM clones (arrows show PH3+ cells).
(G and H) Wild-type (G) and kis^{10D26} (H), MARCM clones 9 days AHS expressing UAS-GFP-$E2f^{1-230}$, UAS-mRFP-$CycB^{1-266}$ FUCCI system allowing cell cycle stage determination (G1, nuclear GFP+; S: RFP+; and G2/M, GFP+ and RFP+; arrowheads show Delta+ ISCs).
(I) Quantification of the percent ISCs (from G and H).
(J) Mean Kismet fluorescence intensity normalized by mean DAPI staining in ISCs (esg+), EEs (diploid esg−), and ECs (polyploid cells) from (K) and (K′).
(K and K′) Kismet showed ubiquitous nuclear expression with a stronger accumulation in esg+ progenitor cells (ISCs and EBs) marked by GFP and EE cells (diploid GFP−).
(L and L′) *kismet* RNAi-expressing clones, 9 days AHS, had depleted Kismet protein and reproduced kis^{10D26} phenotypes.
(M and N) Quantification of the number of cells per clone (M) and ISCs (Delta+) per clone (N) in wild-type and *kis RNAis* expressing clones.
(O–Q) ISC-specific expression of GFP alone (O) or with *kis RNAi* BL36597 (P) or with *kis RNAi* BL34908 (Q) for 10 days at 29°C using esg^{ts}- *NRE-GAL80* driver.
(R) Quantification of the number of PH3+ cells per posterior midgut expressing *kis* RNAi in the ISCs and EBs (esg^{ts} driver), in ISCs only (esg^{ts}- *NRE-GAL80* driver), in EBs only (NRE^{ts}), in ECs only ($Myo1A^{ts}$) for 10 days, or in EE cells ($pros^{ts}$) for 10 days.
A Fisher's exact test was used in (C). A two-tailed Mann-Whitney test was used in (D), (J), (M), (N), and (R). A χ^2 test was used for (I). Mean values in red; error bars, SEM; ns = non-significant, *p < 0.05, **p < 0.01, ***p < 0.001, ****p < 0.0001. Scale bars, 20 μm.

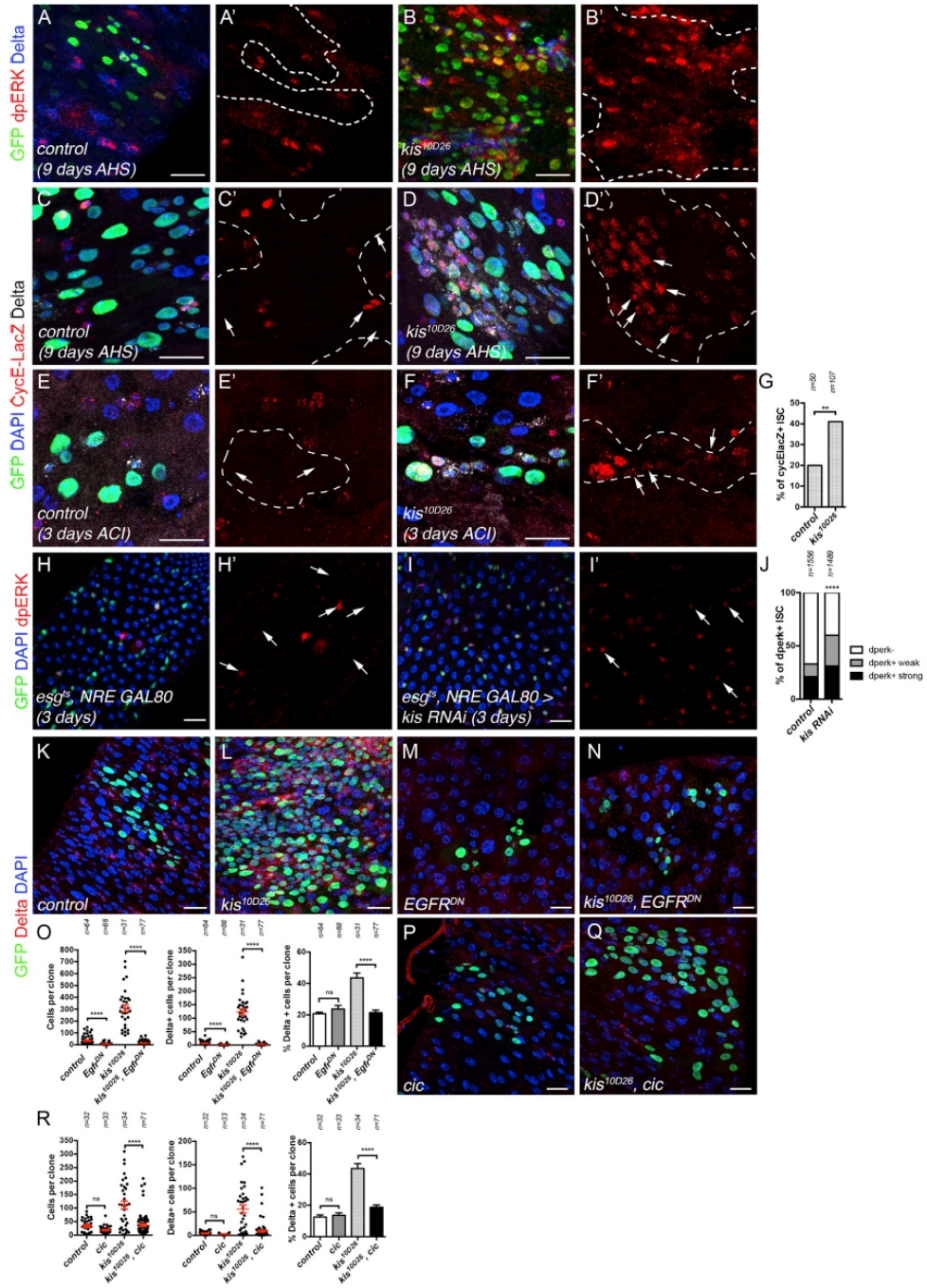

Figure 3. Kismet Controls Proliferation by Regulating EGFR Pathway Activity

(A–D′) Wild-type (A, A′, C, and C′) and *kis*^{10D26} (B, B′, D, and D′), 9 days AHS MARCM clones. EGFR signaling, detected by dpERK (A–B′) and EGFR target CycE-LacZ (C–D′), was increased in *kis*^{10D26} clones.

(legend continued on next page)

mutant stem cells may have increased EGFR signaling. In wild-type clones at 10 days AHS, a marker for activation of the EGFR pathway, dpERK, was weak in ISCs and mostly absent in other clonal cells (Figures 3A and 3A′). In *kismet* mutant clones, dpERK was strongly induced in ISCs and other cells of the clone (Figures 3B and 3B′). In addition, a reporter of *cyclin E*, acting downstream of EGFR signaling to regulate proliferation, was more highly induced in *kismet* mutant clones compared to wild-type at 9 days AHS and as early as 3 days AHS (Figures 3C–3G). Consistent with the rapid activation of EGFR signaling in *kismet* mutants, an increased proportion of ISCs with dpERK signaling was detected as early as 3 days after *kismet* RNAi induction in ISCs (Figures 3H–3J). Furthermore, the abnormal self-renewal of ISCs induced by the loss of *kismet* was abolished upon blocking EGFR signaling using a dominant negative form of EGFR ($EGFR^{DN}$) or expression of *capicua* (*cic*), a downstream repressor of EGFR target genes (Figures 3K–3R). Not only was *kismet* mutant clone size reduced when EGFR signaling was downregulated, but there was also a reduction in the percent of ISCs per clone, returning to wild type (Figures 3O and 3R). This suggests that ectopic activation of EGFR signaling in *kismet* mutant clones drives extra cell division and promotes the accumulation of stem cells.

Previous work has shown that additional stress signaling pathways can further stimulate ISC proliferation due to feedback on EGFR signaling (Patel et al., 2015). In addition to EGFR signaling, Jun kinase signaling (assayed by puc-LacZ) and Jak/Stat signaling (assayed by 10XSTAT GFP) were also activated in ISCs of 9 days *kismet* mutant clones (Figures S4A–S4D′). The genetic inactivation of Yki, Stat, Insulin, and Jun kinase also reduced ISC proportion in *kismet* mutants (Figure S4E). In order to determine whether these pathways may also act early with EGFR signaling in *kismet* mutant stem cells to drive ISC proliferation, we examined a 3-day time point after clone induction. We did not detect early activation of the Jak/Stat ligands, Upd-LacZ, or the Jun Kinase reporter puc-LacZ in ISCs or Upd3-LacZ in ECs (Figures S4F–S4N). This argues against early activation of Jak/Stat and Jun Kinase pathways being initiating defects in *kismet* mutant responsible for ISC proliferation. Therefore, our data suggest that an initial enhancement of EGFR signaling occurs, followed by activation of additional pathways during the following 10 days of clone growth and further driving mutant clone growth. We conclude that Kismet is required to limit EGFR signaling in ISCs.

Kismet Localizes to Chromatin Enriched in RNA Pol II and Brahma and Depleted for HP1, Histone H1, and Polycomb

To further understand how Kismet regulates ISC self-renewal, we identified Kismet-bound regions of the ISC genome using a targeted DamID-seq strategy (STAR Methods) (Marshall et al., 2016). A Dam-Kismet (Dam-Kis) fusion protein construct was expressed in ISCs using *esg^{ts}*, *NRE-GAL80* for 1 day and significantly methylated GATC sites as compared to Dam-alone control expression were determined. Kismet distribution revealed enrichment in introns and 5′ UTRs (Figure 4A). We identified 3,032 genes containing Kismet peaks, defined by two consecutive significant GATC sites ($p < 0.01$) (Table S1).

To gain further insight into the type of chromatin bound by Kismet, we took advantage of DamID lines mapping different active and inactive chromatin states. Active regions are rich in RNA Pol II and Brahma, whereas inactive states are enriched in Polycomb (a reader of Histone H3K27me3), Histone H1, or HP1 (a reader of histone H3K9me3) (Marshall and Brand, 2017). Global patterns of Histone H1, HP1, and Polycomb binding were consistent with localization to repressed regions of the genome, whereas Brahma and RNA Pol II along with Kismet were enriched in active genic regions (Figures 4B and 4L). Histone H1 and HP1 were largely excluded from genic regions with HP1 strongly enriched at centromere-proximal regions of the genome and the 4th chromosome, which is largely heterochromatic in flies (Figures S5H and 4B). These data are fully consistent with data from the nervous system (Marshall and Brand, 2017). We then examined global distribution of Kismet relative to RNA Pol II, Brahma, Polycomb, Histone H1, and HP1 using uniform manifold approximation and projection for dimension reduction (UMAP; Figure 4C [McInnes et al., 2018]). This approach allows the visualization and separation in a two-dimensional space, similar to a t-SNE (t-distributed stochastic neighbor embedding) plot, of GATC sites based on methylation levels by each of these factors (Figure 4C, GATC density map). Globally, Kismet had little overlap on UMAP with Histone H1 and HP1 (Figure 4C) or with genes containing peaks of Histone H1 and HP1 (2.5% and 11.3%, respectively; Figure 4D; Table S2). A majority of Kismet-rich GATC sites did not have strong Polycomb enrichment (Figure 4C; Table S2) and 14.5% of genes with Kismet peaks also had peaks of Polycomb (Figure 4E). Consistent with this, super-resolution imaging in polyploid EC cells, which allow better spatial resolution than ISCs, showed that Kismet and Histone H3K27me3 poorly colocalized (Figures S5A–S5A″). Therefore, we conclude that Kismet does not substantially localize to repressed chromatin domains.

Our data suggested, however, that Kismet more strongly overlapped with activated chromatin states, visualized on UMAP by Kismet enrichment with RNA Pol II and also to some extent with Brahma, a SWI/SNF chromatin remodeling factor associated with histone H3K27ac (Figure 4C). 85.1% of genes with peaks for Kismet also had peaks for RNA Pol II and 33.0% had a peak for Brahma (Figures 4F and 4G; Table S2). Together,

(E–F′) Wild-type (E and E′), and *kis^{10D26}* (F and F′), 3 days AHS MARCM clones expressing CycE-LacZ.
(G) Proportion of ISCs expressing CycE-lacZ from (E) and (F′).
(H and I) ISC-specific expression of GFP (H) or *kis RNAi* (BL34908) (I), 3 days at 29°C.
(J) Quantification of proportion of ISCs showing strong, weak, or no dpERK from (H)–(I′).
(K–N) 12-day AHS clones: wild-type (K), *kis^{10D26}* mutant (L), expressing *UAS-EGFR^{DN}* (M), and *kis^{10D26}* mutant expressing *UAS-EGFR^{DN}* (N).
(O) Clone size, number of Delta+ cells/clone, and % of Delta+ cells/clone from (K)–(N).
(P and Q) 10-day AHS clones: wild-type expressing *cic* (P) and *kis^{10D26}* mutant expressing *cic* (Q).
(R) Clone size, number of Delta+ cells/clone, and % of Delta+ cells/clone from (P) and (Q).
Results compared using a chi-square test in (G) and (J) and a two-tailed Mann-Whitney test in (O) and (R). Mean values in red; error bars, SEM; ns = non-significant, $^{**}p < 0.01$, $^{****}p > 0.0001$. Arrows highlight ISCs. Scale bars, 20 μm.

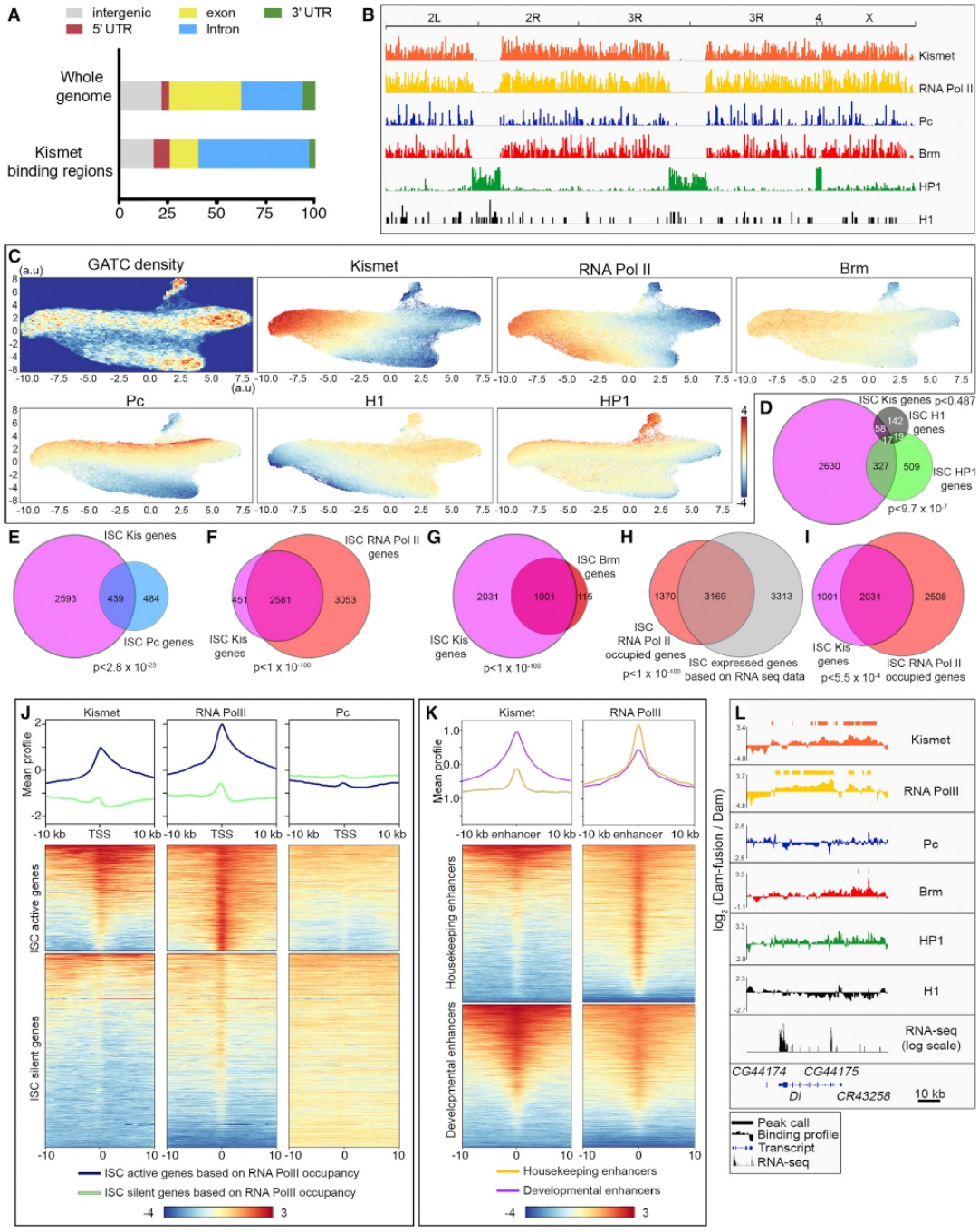

Figure 4. Genome-wide Mapping of Kismet Relative to RNA Pol II, Brm, Pc, HP1, and H1

(A) Kismet DamID-seq showed an enrichment of methylated GATCs in the introns and 5′UTRs of genes. Unassembled regions of the genome were not considered.

(legend continued on next page)

these data suggest that Kismet localizes to transcriptionally active regions of the genome while being depleted in repressed chromatin.

Kismet Localizes to Transcriptionally Active Genomic Regions and Developmental Enhancers

We then assessed how Kismet localized relative to active genes and enhancers. We established a list of expressed or "active" ISC genes based on Dam-RNA Pol II gene occupancy, a good proxy for gene expression (Marshall and Brand, 2015; Southall et al., 2013) (STAR Methods). 4,539 genes had significant occupancy suggesting that they are expressed, including many known ISC-enriched genes (*esg, sox21a, Delta,* and *spdo*; Table S3). Accordingly, these genes strongly overlap with published RNA sequencing (RNA-seq) data for ISC express genes (Dutta et al., 2015) (Figure 4H). We found that 67.0% of the genes with Kismet peaks were also occupied by RNA Pol II (Figure 4I). Genes enriched for Kismet and RNA Pol II or enriched for one but not the other were also detected (examples in Figures S5B–S5H). Separately analyzing ISC genes that were active (Dam-RNA Pol II occupied) or silent (Dam-RNA Pol II not occupied) revealed that Kismet, like its mammalian homologs CHD7/CHD8, was preferentially enriched around the transcription start sites (TSSs) of active genes (Figure 4J) (Schnetz et al., 2009, 2010).

Interestingly, while Kismet showed a strong enrichment for active genes (Figure 4J), it was also associated with a subset of silent genes in ISCs that are expressed in differentiated EE (Pros) and EC cells (Pdm1): 163 of 569 EE+ EC specifically enriched genes had Kismet peaks (from published RNA-seq (Dutta et al., 2015; see STAR Methods; examples in Figures S5C and S5D). Thus, while we detected no obvious roles in terminal differentiation, Kismet appeared to mark a subset of genes in ISCs that will be expressed during differentiation.

We then investigated the binding profiles of Kismet and RNA Pol II at previously published enhancers defined in S2 cells as being either "developmental" or "housekeeping" (Zabidi et al., 2015). Interestingly, Kismet showed enrichment over developmental enhancers, whereas RNA Pol II was enriched over both types of enhancers (Figure 4K). Thus, we conclude that Kismet is broadly distributed on many active genes in ISCs and is enriched at developmental enhancers.

Knockdown of the Components of the Trr COMPASS-like Complex Mimic *kismet* Mutant Phenotypes

Kismet has previously been shown to restrict Histone H3K27me3 marks in the salivary gland (Dorighi and Tamkun, 2013; Srinivasan et al., 2008, 2005). Therefore, we examined whether *kismet* inactivation in the gut had a similar effect on limiting Histone H3K27me3 but found no detectable global increase in H3K27me3 in *kismet* mutants (Figures S6A and S6B′). Previous studies have shown that Kismet acts in the salivary gland cells via recruitment of the histone methyltransferases Ash1 and Trx (Dorighi and Tamkun, 2013). Arguing against this possibility, we found that neither *ash1* nor *trx* clonal loss led to deregulation of ISC proliferation (Figures S6C–S6E, S6H, and S6I). Similarly, Brahma has been shown to co-localize with Kismet and share similar functions in transcription elongation (Armstrong et al., 2002; Srinivasan et al., 2005). However, consistent with previously published data in the intestine, *brahma*-RNAi-expressing clones were smaller and had fewer ISCs per clone than controls (Figures S6F, S6H, and S6I) (Jin et al., 2013). Therefore, our data suggest that Kismet mediates its action on ISC proliferation through direct or indirect interaction with additional chromatin regulators.

We reasoned that additional Trithorax group genes might function with Kismet and sought to identify these factors. To this end, we tested the effect of the histone methyl transferases-encoding genes (Mohan et al., 2011): dSet1 (Set1A/Set1B in mammals), and Trr (MLL3/4 in mammals). The clonal expression of a previously validated RNAi construct against *set1* (Herz et al., 2012) had no obvious effects on ISCs or clone size (Figure S6G). However, knockdown of genes encoding Trr-complex proteins (Trr, Lost polyhomeotic domains of Trr [Lpt], and the histone demethylase Utx) revealed phenotypes similar to *kismet* (Figures 5A–5F). They had an increased number of cells per clone and Delta+ cells per clone (Figures 5A, 5B, 5E, and 5F). Clones of the trr^{B} mutant allele showed less severe but significant accumulation of extra-Delta+ diploid ISCs (Figures S6J–S6L′). Furthermore, the knockdown of *lpt* and *Utx* also exhibited *kismet*-mutant-like phenotypes (Figures 5C–5F). Analysis of Trr, Lpt, and Utx showed ubiquitous expression in the cell types of the midgut (Figures 5G–5J′). Utx, however, was enriched in the ISC and EB (esg+) progenitor cells and EEs similar to Kismet localization (Figures 5G–5H), and Lpt was enriched in EEs (Figures 5I and 5I′). The phenotypic similarity between *kismet* alleles and knockdown of *trr*-complex genes suggests they may collaborate to regulate ISC function. This idea is further supported by our findings that Kismet is enriched at developmental enhancers and that the Trr/MLL3/4 complexes have well-described functions in activating enhancers (Dorighi et al., 2017; Herz et al., 2012; Hu et al., 2013; Lee et al., 2013). Thus, we hypothesize that Kismet regulates ISC proliferation in conjunction with the Trr complex.

(B) Genome-wide overview of the DamID binding peak density in ISCs of Kismet, RNA Pol II, Polycomb (Pc), Brahma (Brm), HP1, and H1.
(C) UMAP clustering of GATC sites based on 7 DamID fusion proteins (see STAR Methods) in the ISC. Density of GATC sites throughout the genome used for clustering followed by the plots representing the binding of each protein over GATC sites.
(D–I) Venn diagrams of genes with peaks of the DamID-seq data in ISCs: Kismet versus HP1 or H1 (D) versus Pc (E) versus RNA Pol II (F) and versus Brm (G). Genes with a significant mean RNA Pol II occupancy determined by DamID versus transcriptionally active genes based on RNA-seq from Dutta et al., 2015 (H) and versus genes with peaks of Kismet (I).
(J) Mean position and metaplot of Kismet, RNA Pol II, and Pc in ISCs relative to the TSS for genes classified by their activity based on RNA Pol II occupancy. Kismet was significantly enriched over the TSS of active genes.
(K) Mean position and metaplot of Kismet and RNA Pol II in ISC relative to previously defined "developmental" or "housekeeping" enhancers in S2 cells from Zabidi et al., 2015. Kismet was found enriched over developmental enhancers.
(L) Wild-type RNA-seq, Dam-Kis, Dam-RNA Pol II, Dam-Pc, Dam-Brm, Dam-HP1, and Dam-H1 ISC binding profiles and peaks alignments over the genomic region surrounding the ISC-specific gene *Delta*.

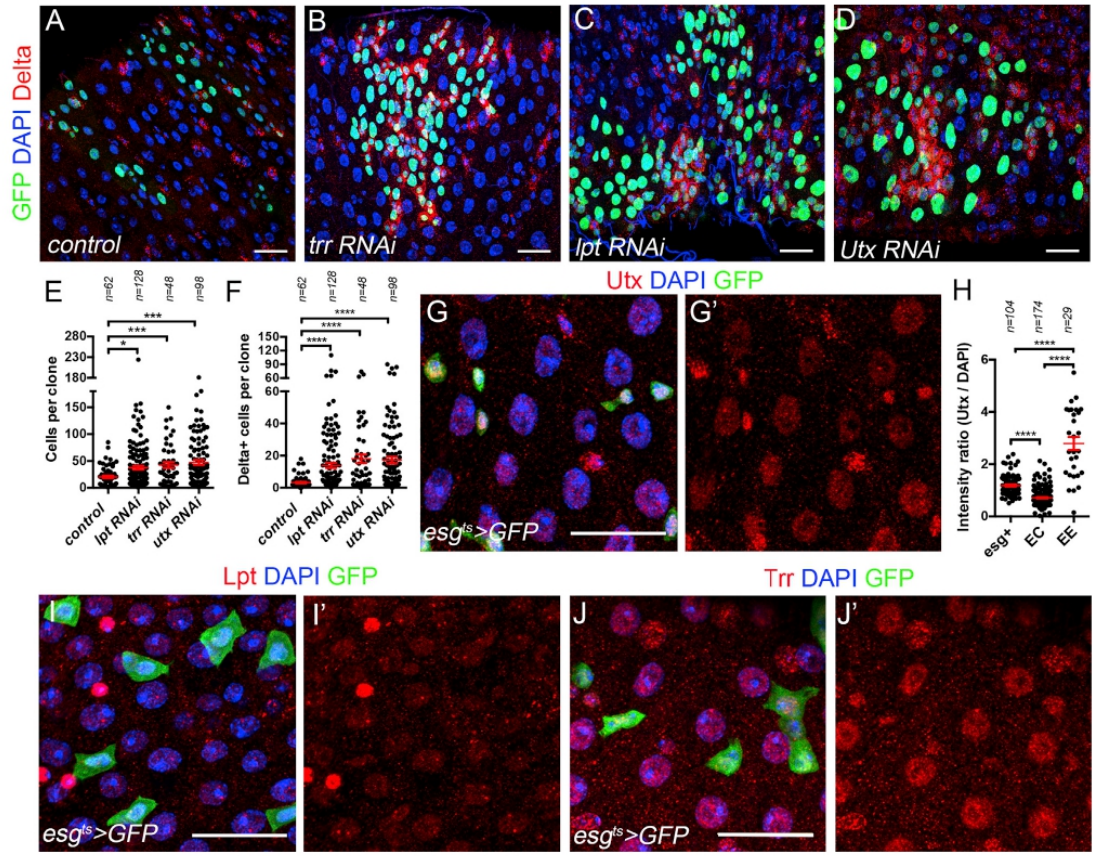

Figure 5. Loss of Trr COMPASS-like Complex Activity Induces Abnormal ISC Accumulation

(A–D) Wild-type (A), *trr RNAi* (B), *lpt RNAi* (C), or *Utx RNAi* (D) at 9 days AHS clones.

(E and F) Average number of cells (E) and ISCs (F) per clone from (A)–(D).

(G and G′) Utx was ubiquitously expressed but enriched in esg>GFP+ cells and in EE (esg>GFP− diploid cells).

(H) Mean Utx staining fluorescence intensity normalized by the mean DAPI staining in ISCs, EEs, and ECs (polyploid cells) from (G) and (G′).

(I and I′) Lpt was ubiquitously expressed but enriched in EE cells (diploid; esg>GFP−).

(J and J′) Trr was uniformly expressed in all midgut cell types.

In (E), (F), and (H), a two-tailed Mann-Whitney statistical test was used. Mean values in red; error bars, SEM; n = non-significant, *p < 0.05, ***p < 0.001, ****p < 0.0001. Scale bars, 20 μm.

Genome-wide Co-occupancy of Kismet and Trr and Co-regulation of Genes

A prediction of collaboration between Kismet and Trr complex is that they may co-bind and co-regulate genes. We found that the distribution of Kismet on polytene chromosomes largely overlapped with Trr (Figures 6A–6B″) and in ISCs using targeted DamID-seq of Trr (Figure 6C). Like Kismet, Trr was enriched over the TSS of active genes as compared to inactive genes (based on RNA Pol II occupancy; Figure 6D). Interestingly, while Kismet had preferential enrichment for developmental enhancers (Figure 4K), Trr was equally enriched at both developmental and housekeeping enhancers (Figure 6E). Examining peaks in genes, 73.2% of Kismet-bound genes were co-bound by Trr (Figure 6F; Table S4). We conclude that Kismet and Trr share genome-wide localization and binding to the genes, supporting our hypothesis that they act in concert.

We then wanted to assess whether similar genes might be deregulated upon *kismet* or *trr* knockdown. To this end, we used fluorescence-activated cell sorting (FACS) to sort adult ISCs (*esg^ts^>GFP*; *NRE-GAL80*) of controls (white RNAi) or those expressing RNAi against *kismet* or *trr* and performed RNA-seq (Figures 6G–6I; Table S5). Interestingly, 50.3% of genes having altered RNA upon *kismet* knockdown and 43.8% of genes having altered RNA levels upon *trr* knockdown showed Kismet and Trr binding by DamID-seq, respectively (Figure 6J). This suggests that these genes are directly regulated by Kismet and Trr. However, the deregulated genes represented only 10.3% and 24.3% of the total Kismet and Trr-bound genes, respectively.

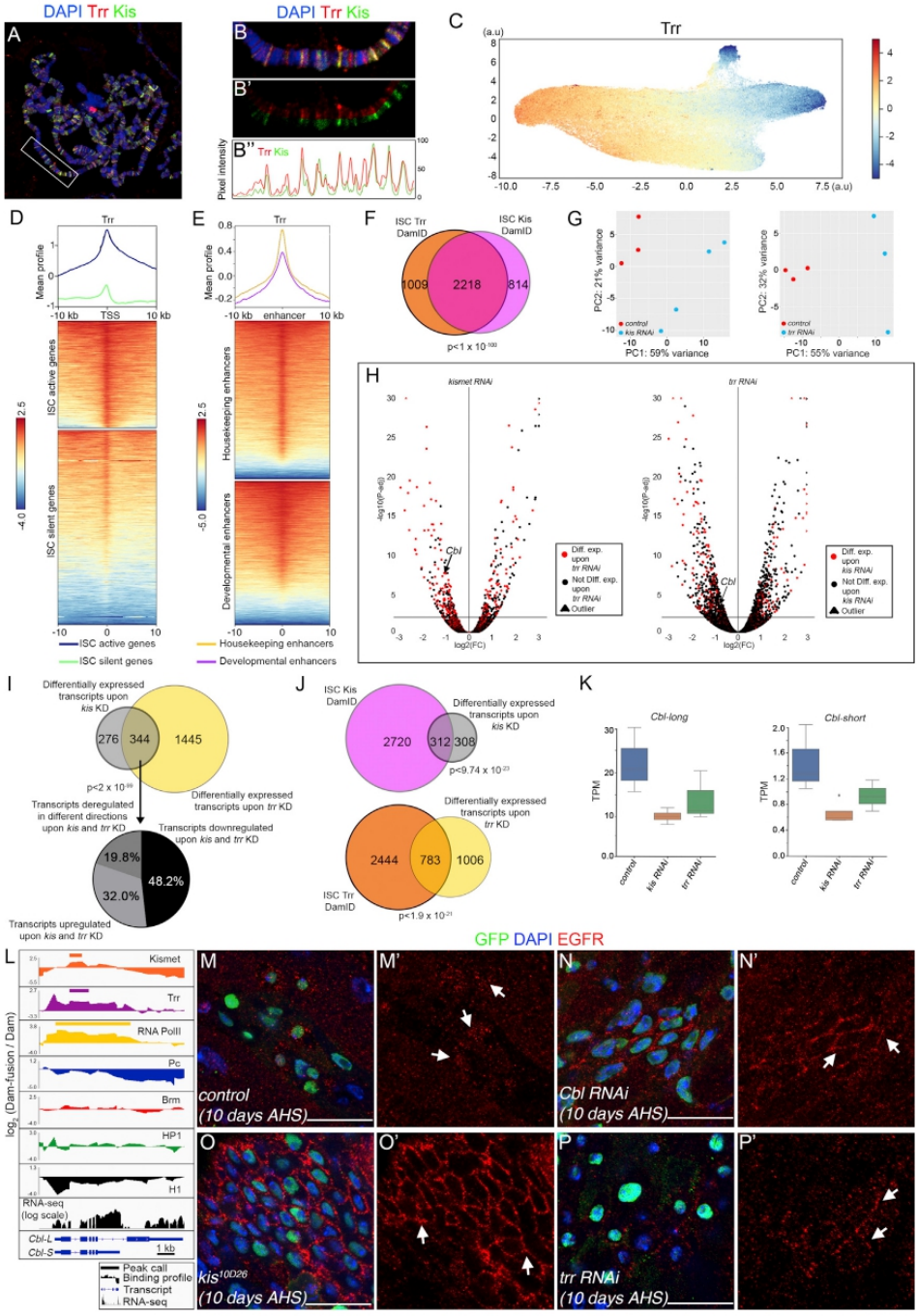

Figure 6. Genome-wide Mapping of Trr DNA Binding Sites and Genes Regulated by Kismet and Trr

(A) Kismet and Trr localization on polytene chromosomes of the salivary gland.

(B–B″) Magnification of the chromosome highlighted in (A). Fluorescent intensity in (B″).

(legend continued on next page)

Therefore, the genetic perturbation of relatively general chromatin binding factors can affect a limited subset of genes. This likely underlies the specific phenotypes of general chromatin factors noted both here in ISCs and in other contexts, such as during human development (Bajpai et al., 2010; Schulz et al., 2014b; Vissers et al., 2004).

Importantly, we found that 55.5% of the RNAs altered upon knockdown of *kismet* were also altered in *trr* knockdown (Figure 6I). This represented 19.2% of the *trr*-altered transcripts. Among these genes deregulated upon both *kismet* and *trr* knockdowns, 80.2% are in the same direction, with a decrease in transcript level (Figure 6I).

Overall, these data strongly support our hypothesis that Kismet and Trr co-bind throughout the genome and co-regulate gene expression.

Kismet and Trr Promote Expression of the E3 Ligase Cbl to Maintain Low Levels of the EGF Receptor

Our previous data indicated that *kismet* mutant ISCs have increased EGFR signaling (Figures 3A–3G). Similarly, upon *trr* knockdown, we found deregulation of dpERK (Figures S7A–S7B′). The similarities in loss-of-function phenotypes of *kismet* and *trr*, the colocalization in the genome, the co-regulation of many genes, and deregulation of EGFR signaling led us to propose that Kismet and the Trr complex act together to limit ISC self-renewal through EGFR regulation.

Assessing our DamID-seq and RNA-seq data for regulators of EGFR signaling, we identified *Cbl*, encoding an E3 ligase known to promote degradation of EGFR (Duan et al., 2003; Hime et al., 1997; Levkowitz et al., 1999; Meisner et al., 1997; Pai et al., 2000; Soubeyran et al., 2002). *Cbl* was bound by both Kismet and Trr and, long and short isoforms of *Cbl* were downregulated upon inactivation of *kismet* and *trr* (Figures 6H, 6K, and 6L). Of note, none of the core components of the Hippo pathway are deregulated upon *kismet* knockdown, arguing against this pathway being involved in initiation of *kismet* mutant phenotypes. If Kismet and Trr control the levels of EGFR via Cbl, then *kismet* and *trr* knockdown contexts would lead to increased EGFR protein. Clones expressing RNAi against *Cbl*, *kismet*, or mutant for *kismet*, had a strong increase in EGFR levels, both in clones at 10 days AHS and upon 3-day induction in ISCs (Figures 6M–6O′, S6O–S6R′, and S6T). Knockdown of *trr* also showed increased EGFR levels in 10 days clones (Figures 6P and 6P′), although upon 3-day knockdown in ISC, this was less pronounced than that of *kismet* knockdown (Figures S6Q, S6S, and S6T), consistent with *Cbl* transcripts being less reduced upon *trr* knockdown than upon *kismet* knockdown (Figure 6K). Furthermore, the expression of *Cbl-L* isoform (but not *Cbl-S*) in *kismet* RNAi-expressing clones rescued clone size and accumulation of Delta+ cells supporting that *Cbl* acts downstream of Kismet to regulate ISC self-renewal (Figures 7A–7H). In agreement with previous work (Jiang et al., 2011), the knockdown of *Cbl* led to larger clones with increased numbers of Dl+ ISCs and excessive proliferation (Figures 7I–7O). In addition, *trr* mutant phenotypes could be suppressed by conditions that lowered EGFR signaling (expression of EGFR-DN or *cic*; Figures 7P–7W).

Finally, if *kismet* and *trr* act on similar target genes, we would predict that their combined phenotype would be like *kismet* mutants, which is indeed what was found (Figures S7C–S7G). Together, our data suggest that one of the downstream targets of Kismet and Trr required to maintain a basal level of ISC proliferation is the E3 ligase encoding gene *Cbl*, which modulates EGFR protein levels and signaling activation.

DISCUSSION

Through an unbiased genetic screen, we have identified the chromatin remodeling factor Kismet/CHD7/CHD8, as a regulator of stem cell proliferation in the fly intestine. By establishing the first genome-wide binding map of Kismet in *Drosophila*, our data revealed a large overlap with transcriptionally active regions. Interestingly, our genome-wide mapping and RNA-seq data suggest that Kismet mediates its role on ISCs through collaboration with the Trr complex and that the negative regulator of EGFR, *Cbl*, is one critical downstream direct target of *kismet* and *trr*, leading to the deregulation of EGFR signaling. Altogether, our data uncover an important level of chromatin regulation required to dampen the ISC proliferative response in routine homeostasis.

In response to homeostatic cell turnover and induced damage, many signaling pathways regulate ISC proliferation rates, though how chromatin regulation impinges on this was not understood. Our data show that Kismet and Trr play essential roles in preventing excess ISC proliferation through limiting EGFR signaling, which may be required after stress for the return to basal levels of proliferation. In addition to EGFR signaling, we find that inhibition of additional pathways can suppress *kismet* phenotypes, reminiscent to "niche appropriation" described for *Notch* mutant tissue: after initial deregulation of stem cell proliferation and local tissue perturbation due to *Notch* inactivation, multiple signaling pathways become activated, including Jnk and Jak/Stat

(C) Trr binding in the ISC clustered using UMAP based on 7 DamID fusion proteins (STAR Methods and Figure 4C).
(D) Mean position and metaplot of Trr in ISCs plotted relative to the TSS for genes according to their activity based on RNA Pol II occupancy shows its enrichment over the TSS of active genes.
(E) Mean position and metaplot of Trr in ISC over previously defined "developmental" or "housekeeping" enhancers in S2 cells from Zabidi et al., 2015.
(F) Overlap between genes with peaks of Kismet versus Trr.
(G) Principal-component analysis of RNA-seq.
(H) Differentially expressed genes; red points highlight common genes.
(I) Upper: overlap between genes with RNAs deregulated upon *kis* and *trr* knockdown in the ISCs. Lower: proportion of RNAs altered in *kis* and *trr* knockdown.
(J) Upper: genes with peaks of Kismet and deregulated after *kis* knockdown in the ISCs. Lower: genes with peaks of Trr and deregulated after *trr* KD in the ISCs.
(K) RNA-seq data showing downregulation of the 2 *Cbl* isoforms upon either *kis* RNAi and *trr* RNAi in the ISC.
(L) Alignement at the *Cbl* locus of wild-type RNA-seq, Kismet, Trr, RNA Pol II, Pc, Brm, HP1, H1 binding profiles and peaks as determined by DamID-seq in ISCs.
(M–P′) clone of wild-type (M and M′), *Cbl* RNAi (N and N′), kis^{10D26} (O and O′) and *trr RNAi* (P and P′), 10 days AHS. Arrows show EGFR-positive cells. Scale bars, 20 μm.

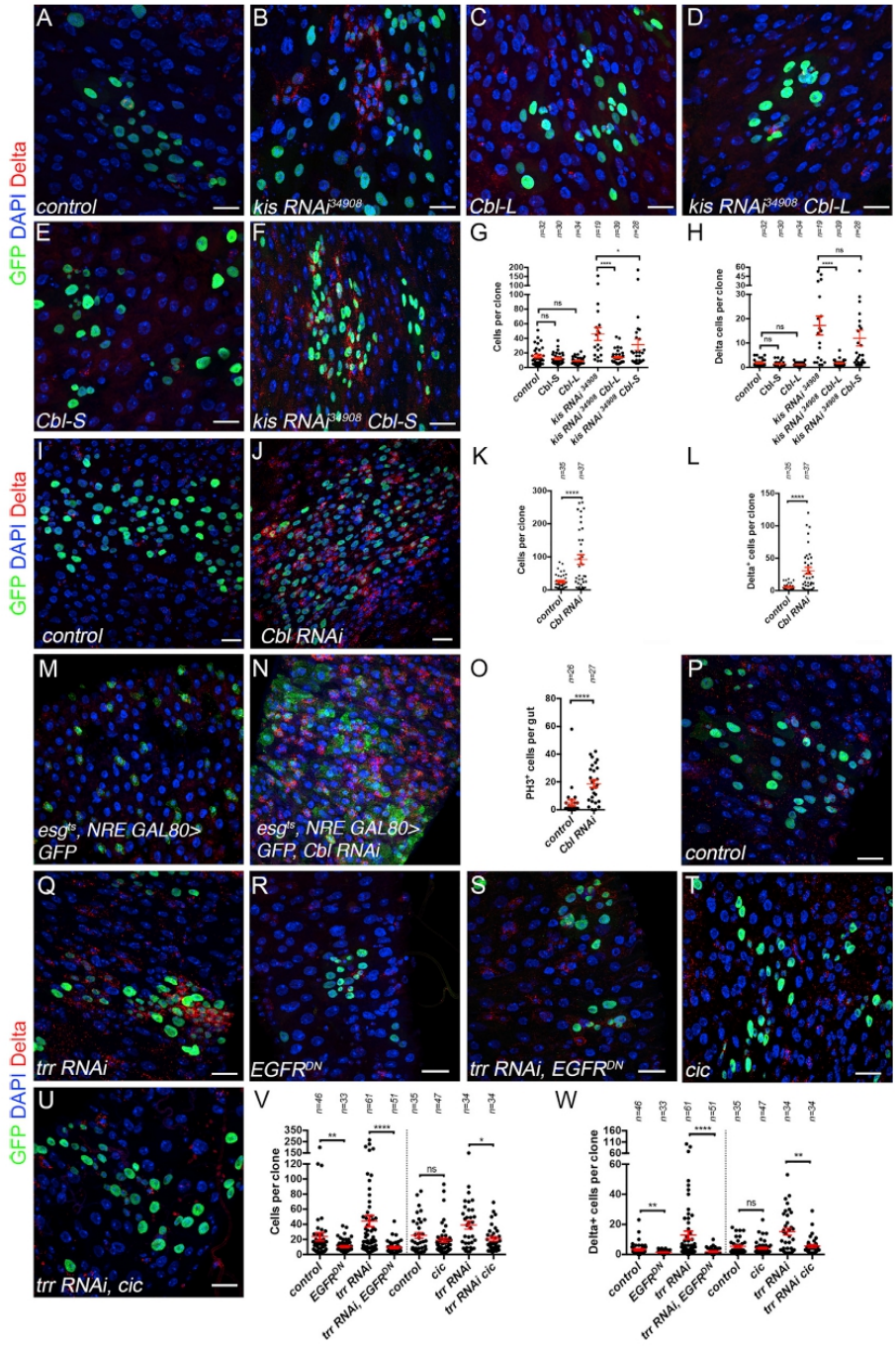

Figure 7. Trr and Kismet Regulates EGFR Activity through the Control of *Cbl* Expression

(A–F) Clone of wild-type (A), *kis RNAi*^{34908} (B), *UAS-Cbl-L* (C), both *kis RNAi*^{34908} and *UAS-Cbl-L* (D), *UAS-Cbl-S* (E), and both *kis RNAi*^{34908} and *UAS-Cbl-S* (F) at 9 days AHS.

(legend continued on next page)

signaling, which function together to further drive ISC proliferation (Patel et al., 2015). Thus, our findings suggest that niche appropriation is a general property of rapidly proliferating tissues that create stress signals in the gut, further fueling cell division.

Interestingly, our findings suggested that Kismet is enriched at genes that are expressed not only in ISCs but also at a subset of genes that is OFF in the stem cell but will be later turned ON during the differentiation process. Of note, we did not detect obvious defects in terminal cell fate differentiation in *kismet* mutant clones using well-characterized markers of EE and EC cells. Further analysis of *kismet* mutant EE and EC cells will determine whether there are more subtle defects in differentiation or not. This raises the possibility that Kismet may be a good marker of pre-patterning of lineage-specific genes.

Our data suggest that Kismet cooperates with the Trr complex to regulate many genes. CHARGE syndrome, due to a heterozygous mutation of *CHD7* in humans, has extensive phenotypic overlap with Kabuki syndrome, caused by mutation of *MLL4* (also known as *KMT2D* and *MLL2*) and *UTX* (also known as *KDM6A*) (Butcher et al., 2017; Miyake et al., 2013; Ng et al., 2010; Schulz et al., 2014a). These data raise the question of a similar collaboration between these enzymes in human development. The Trr/MLL3/4 complexes establish the H3K4me1 mark, enriched at primed and active enhancers and, to some extent, promoters. Could Kismet/CHD7 remodeling activity promote H3K4me1? Our data argue against this since H3K4me1 was reduced in the gut upon knockdown of *trr* and *lpt* (Figures S7L–S7N′), but not altered in *kismet* mutant clones (Figures S7O and S7O′). In addition, no obvious defects were detected in histone H3K27ac in *kismet* mutant clones (Figures S6M–S6N′) or protein levels of Trr in *kismet* mutants or of Kismet in *trr* mutants were found (Figures S7H–S7K′). It is possible, however, that Kismet/CHD7 might promote the methyltransferase-independent activity of Trr/MLL3/4 that has been shown to regulate enhancer efficiency (Dorighi et al., 2017; Rickels et al., 2017). Further evidence suggesting a molecular link between Kismet/CHD7/CHD8 and the Trr/MLL3/4 complex comes from co-immunoprecipitation (coIP) between Kismet and CBP, a binding partner of the Trr complex component Utx and between CHD7/CHD8 and the MLL3/4 complex components WDR, ASH2L, and RbBP5 (Schulz et al., 2014a; Thompson et al., 2008; Tie et al., 2012). Thus, we speculate that Kismet and the Trr complex may both be necessary for regulation of a subset of genes, such as *Cbl*.

In addition to similar phenotypes of *CHD7* and *MLL4* mutations on human development, both *CHD7* and *MLL3/4* complex components are mutated in cancers. CHD7 is found as a highly expressed fusion protein in small cell lung cancers (Pleasance et al., 2010). A subset of colorectal carcinomas and gastric cancers were found to have frequent mutations in both *CHD7* and its closely related gene, *CHD8* (Kim et al., 2011; Sawada et al., 2013; Tahara et al., 2014). Mutations in *CHD7* and in the MLL3/4 complex are frequently found in medulloblastoma, and MLL3/4 is also found inactivated in many additional cancers (Ford and Dingwall, 2015; Robinson et al., 2012). How deregulating *CHD7* and *MLL3/4* may impact cancer progression is not entirely clear, though recent studies linking enhancer and super-enhancer deregulation to cancer formation suggest that the deregulation of enhancers upon mutation of Kismet/CHD7 and the Trr/MLL3/4 complex could drive aberrant proliferation (Herz et al., 2014; Hnisz et al., 2013). While much of what we know about chromatin regulation in stem cells comes from studies of cultured embryonic stem cells, our work provides insight into *in vivo* roles of chromatin remodeling factors in control of adult stem cell self-renewal and proliferation programs. Our findings that Kismet and the Trr complex loss lead to dramatic alteration of ISC proliferation indicate that the *Drosophila* intestine will be a useful model to probe the relationship between chromatin regulation and stem cell proliferation control.

STAR★METHODS

Detailed methods are provided in the online version of this paper and include the following:

- KEY RESOURCES TABLE
- CONTACT FOR REAGENT AND RESOURCE SHARING
- EXPERIMENTAL MODEL AND SUBJECT DETAILS
- METHOD DETAILS
  - Generation of Transgenic Flies
  - Clonal Analysis and Gal4 Expression
  - Immunofluorescence and Imaging
  - DamID-Seq Analysis
  - RNAseq Analysis
- QUANTIFICATION AND STATISTICAL ANALYSIS
- DATA AND SOFTWARE AVAILABILITY

SUPPLEMENTAL INFORMATION

Supplemental Information can be found online at https://doi.org/10.1016/j.devcel.2019.04.033.

ACKNOWLEDGMENTS

We would like to thank the members of the Bardin team and P.-A. Defossez for comments on the manuscript. We thank O. Ayrault and A. Forget for help with biochemical experiments; C. Carré for help with polytene experiments; and S. Maffioletti, A. Osnato, and T. Gonçalves for their technical help on some experiments. We thank A. Shilatifard, B.A. Edgar, D.R. Marenda, S. Bray, M. Haenlin, J. Skeath, J. Veenstra, and the Bloomington and Vienna stock centers for

(G and H) Average number of cells and ISC per clone from (A)–(F).
(I and J) Clones of wild-type (I) and *Cbl* RNAi (J) 10 days AHS.
(K and L) Average number of cells and ISC per clone from (I) and (J).
(M and N) ISC-specific expression of GFP (M) and *Cbl RNAi* (N) driven by esg^{ts}- *NRE-GAL80* for 10 days at 29°C. *Cbl* knockdown results in an accumulation of GFP, Delta+ cells.
(O) Quantification of number of PH3+ cells per gut from (M) and (N).
(P–U) Clone of wild-type (P), *trr RNAi* (Q), *UAS-*$EGFR^{DN}$ (R), both *trr RNAi* and *UAS-*$EGFR^{DN}$ (S), *UAS-cic* (T), and both *trr RNAi* and *UAS-cic* (U) at 10 days AHS.
(V and W) Clone size (V) and number of Delta+ per clone (W) from (P)–(U). Results were compared using a two-tailed Mann-Whitney statistical test. Mean values in red; error bars, SEM; n = non-significant, *p < 0.05, **p < 0.01, ****p < 0.0001. Scale bars, 20 μm.

antibodies and fly lines. The Bardin laboratory is supported by project grants to A.B.: 2017 prize from Fondation Schlumberger, Worldwide Cancer Research, ATIP-AVENIR, La Ligue Contre le Cancer, and Fondation ARC, the Charge Syndrome Foundation, and labelisation of the Fondation pour la Recherche Medicale as well as funding from the program "Investissements d'Avenir" launched by the French Government and implemented by ANR; references: ANR SoMuSeq-STEM (A.B.), Labex DEEP (ANR-11-LBX-0044) and IDEX PSL (ANR-10-IDEX-0001-02 P.S.L.). We would like to acknowledge the Cell and Tissue Imaging Facility/UMR3215 (PICT-IBiSA) of the Institut Curie, member of the French National Research Infrastructure France-BioImaging, ANR-10- INBS-04, and T. Piolot for help on the OMX microscope. We thank the NGS platform of the Institut Curie, which is supported by grants ANR-10-EQPX-03 and ANR10-INBS-09-08 and Canceropôle IdF. F.S. is supported by Labex REVIVE (ANR-10-LABX-0073). Work in the Brand lab was funded by the Royal Society Darwin Trust Research Professorship, Wellcome Trust Senior Investigator award 103792, Biological Sciences Research Council project grant BB/L00786X/1 (to A.H.B.), and European Molecular Biology Organization long-term fellowship ALTF 423-2011 (to O.J.M.). A.H.B. acknowledges core funding to the Gurdon Institute from the Wellcome Trust (092096) and the Royal Society, United Kingdom (C6946/A14492).

AUTHOR CONTRIBUTIONS

L.G. performed a majority of the experiments. M.v.d.B. developed peak calling methodology, analyzed RNA-seq data, and performed UMAP plots. M.J., L.G., and J.S. performed DamID-seq and helped with bioinformatic analysis. O.J.M. and A.H.B. contributed to targeted DamID-seq experiments. C.N.P., A.J.B., and F.S. designed the genetic screen, which was performed by C.N.P. and A.J.B. M.S., P.S., and K.M. built plasmids. The "polii.gene.call" script was designed by O.J.M. and used by L.G. L.G. and A.J.B. conceived and supervised the study, analyzed the data, and wrote the manuscript with contributions from the other authors.

DECLARATION OF INTERESTS

The authors declare no competing interests.

Received: January 10, 2018
Revised: March 15, 2019
Accepted: April 18, 2019
Published: May 20, 2019

REFERENCES

Adachi-Yamada, T., Nakamura, M., Irie, K., Tomoyasu, Y., Sano, Y., Mori, E., Goto, S., Ueno, N., Nishida, Y., and Matsumoto, K. (1999). p38 mitogen-activated protein kinase can be involved in transforming growth factor beta superfamily signal transduction in Drosophila wing morphogenesis. Mol. Cell. Biol. *19*, 2322–2329.

Afgan, E., Baker, D., van den Beek, M., Blankenberg, D., Bouvier, D., Čech, M., Chilton, J., Clements, D., Coraor, N., Eberhard, C., et al. (2016). The Galaxy platform for accessible, reproducible and collaborative biomedical analyses: 2016 update. Nucleic Acids Res. *44*, W3–W10.

Armstrong, J.A., Papoulas, O., Daubresse, G., Sperling, A.S., Lis, J.T., Scott, M.P., and Tamkun, J.W. (2002). The Drosophila BRM complex facilitates global transcription by RNA polymerase II. EMBO J. *21*, 5245–5254.

Bajpai, R., Chen, D.A., Rada-Iglesias, A., Zhang, J., Xiong, Y., Helms, J., Chang, C.P., Zhao, Y., Swigut, T., and Wysocka, J. (2010). CHD7 cooperates with PBAF to control multipotent neural crest formation. Nature *463*, 958–962.

Balakireva, M., Stocker, R.F., Gendre, N., and Ferveur, J.F. (1998). Voila, a new Drosophila courtship variant that affects the nervous system: behavioral, neural, and genetic characterization. J. Neurosci. *18*, 4335–4343.

Bardin, A.J., Perdigoto, C.N., Southall, T.D., Brand, A.H., and Schweisguth, F. (2010). Transcriptional control of stem cell maintenance in the Drosophila intestine. Development *137*, 705–714.

Biteau, B., Hochmuth, C.E., and Jasper, H. (2008). JNK activity in somatic stem cells causes loss of tissue homeostasis in the aging Drosophila Gut. Cell Stem Cell *3*, 442–455.

Biteau, B., and Jasper, H. (2011). EGF signaling regulates the proliferation of intestinal stem cells in Drosophila. Development *138*, 1045–1055.

Bouazoune, K., and Kingston, R.E. (2012). Chromatin remodeling by the CHD7 protein is impaired by mutations that cause human developmental disorders. Proc. Natl. Acad. Sci. USA *109*, 19238–19243.

Brennan, K., Tateson, R., Lieber, T., Couso, J.P., Zecchini, V., and Arias, A.M. (1999). The abruptex mutations of notch disrupt the establishment of proneural clusters in Drosophila. Dev. Biol. *216*, 230–242.

Brunet, A., and Rando, T.A. (2017). Interaction between epigenetic and metabolism in aging stem cells. Curr. Opin. Cell Biol. *45*, 1–7.

Buchon, N., Broderick, N.A., Kuraishi, T., and Lemaitre, B. (2010). Drosophila EGFR pathway coordinates stem cell proliferation and gut remodeling following infection. BMC Biol. *8*, 152.

Buchon, N., Broderick, N.A., Poidevin, M., Pradervand, S., and Lemaitre, B. (2009). Drosophila intestinal response to bacterial infection: activation of host defense and stem cell proliferation. Cell Host Microbe *5*, 200–211.

Buff, E., Carmena, A., Gisselbrecht, S., Jiménez, F., and Michelson, A.M. (1998). Signalling by the Drosophila epidermal growth factor receptor is required for the specification and diversification of embryonic muscle progenitors. Development *125*, 2075–2086.

Butcher, D.T., Cytrynbaum, C., Turinsky, A.L., Siu, M.T., Inbar-Feigenberg, M., Mendoza-Londono, R., Chitayat, D., Walker, S., Machado, J., Caluseriu, O., et al. (2017). CHARGE and Kabuki syndromes: gene-specific DNA methylation signatures identify epigenetic mechanisms linking these clinically overlapping conditions. Am. J. Hum. Genet. *100*, 773–788.

Challen, G.A., Sun, D., Mayle, A., Jeong, M., Luo, M., Rodriguez, B., Mallaney, C., Celik, H., Yang, L., Xia, Z., et al. (2014). Dnmt3a and Dnmt3b have overlapping and distinct functions in hematopoietic stem cells. Cell Stem Cell *15*, 350–364.

Chen, J., Xu, N., Wang, C., Huang, P., Huang, H., Jin, Z., Yu, Z., Cai, T., Jiao, R., and Xi, R. (2018). Transient Scute activation via a self-stimulatory loop directs enteroendocrine cell pair specification from self-renewing intestinal stem cells. Nat. Cell Biol. *20*, 152–161.

Choksi, S.P., Southall, T.D., Bossing, T., Edoff, K., de Wit, E., Fischer, B.E., van Steensel, B., Micklem, G., and Brand, A.H. (2006). Prospero acts as a binary switch between self-renewal and differentiation in Drosophila neural stem cells. Dev. Cell *11*, 775–789.

Cordero, J.B., Stefanatos, R.K., Scopelliti, A., Vidal, M., and Sansom, O.J. (2012). Inducible progenitor-derived Wingless regulates adult midgut regeneration in Drosophila. EMBO J. *31*, 3901–3917.

Daubresse, G., Deuring, R., Moore, L., Papoulas, O., Zakrajsek, I., Waldrip, W.R., Scott, M.P., Kennison, J.A., and Tamkun, J.W. (1999). The Drosophila kismet gene is related to chromatin-remodeling factors and is required for both segmentation and segment identity. Development *126*, 1175–1187.

de Sousa e Melo, F., Kurtova, A.V., Harnoss, J.M., Kljavin, N., Hoeck, J.D., Hung, J., Anderson, J.E., Storm, E.E., Modrusan, Z., Koeppen, H., et al. (2017). A distinct role for Lgr5+ stem cells in primary and metastatic colon cancer. Nature *543*, 676–680.

Dietzl, G., Chen, D., Schnorrer, F., Su, K.C., Barinova, Y., Fellner, M., Gasser, B., Kinsey, K., Oppel, S., Scheiblauer, S., et al. (2007). A genome-wide transgenic RNAi library for conditional gene inactivation in Drosophila. Nature *448*, 151–156.

Dorighi, K.M., Swigut, T., Henriques, T., Bhanu, N.V., Scruggs, B.S., Nady, N., Still, C.D., II, Garcia, B.A., Adelman, K., and Wysocka, J. (2017). Mll3 and Mll4 facilitate enhancer RNA synthesis and transcription from promoters independently of H3K4 monomethylation. Mol. Cell *66*, 568–576.e4.

Dorighi, K.M., and Tamkun, J.W. (2013). The trithorax group proteins Kismet and ASH1 promote H3K36 dimethylation to counteract Polycomb group repression in Drosophila. Development *140*, 4182–4192.

Duan, L., Miura, Y., Dimri, M., Majumder, B., Dodge, I.L., Reddi, A.L., Ghosh, A., Fernandes, N., Zhou, P., Mullane-Robinson, K., et al. (2003). Cbl-mediated

ubiquitinylation is required for lysosomal Sorting of epidermal growth factor receptor but is dispensable for endocytosis. J. Biol. Chem. *278*, 28950–28960.

Dubruille, R., Murad, A., Rosbash, M., and Emery, P. (2009). A constant light-genetic screen identifies KISMET as a regulator of circadian photoresponses. PLoS Genet. *5*, e1000787.

Dutta, D., Dobson, A.J., Houtz, P.L., Gläßer, C., Revah, J., Korzelius, J., Patel, P.H., Edgar, B.A., and Buchon, N. (2015). Regional cell-specific transcriptome mapping reveals regulatory complexity in the adult Drosophila Midgut. Cell Rep. *12*, 346–358.

Dutta, D., Xiang, J., and Edgar, B.A. (2013). RNA expression profiling from FACS-isolated cells of the Drosophila intestine. Curr. Protoc. Stem Cell Biol. *27*. Unit 2F.2.

Ekas, L.A., Baeg, G.H., Flaherty, M.S., Ayala-Camargo, A., and Bach, E.A. (2006). JAK/STAT signaling promotes regional specification by negatively regulating wingless expression in Drosophila. Development *133*, 4721–4729.

Feng, W., Kawauchi, D., Körkel-Qu, H., Deng, H., Serger, E., Sieber, L., Lieberman, J.A., Jimeno-González, S., Lambo, S., Hanna, B.S., et al. (2017). Chd7 is indispensable for mammalian brain development through activation of a neuronal differentiation programme. Nat. Commun. *8*, 1–14.

Feng, W., Khan, M.A., Bellvis, P., Zhu, Z., Bernhardt, O., Herold-Mende, C., and Liu, H.K. (2013). The chromatin remodeler CHD7 regulates adult neurogenesis via activation of SoxC transcription factors. Cell Stem Cell *13*, 62–72.

Flavahan, W.A., Gaskell, E., and Bernstein, B.E. (2017). Epigenetic plasticity and the hallmarks of cancer. Science *357*, eaal2380.

Ford, D.J., and Dingwall, A.K. (2015). The cancer COMPASS: navigating the functions of MLL complexes in cancer. Cancer Genet. *208*, 178–191.

Furriols, M., and Bray, S. (2001). A model Notch response element detects Suppressor of Hairless–dependent molecular switch. Curr. Biol. *11*, 60–64.

Gindhart, J.G., and Kaufman, T.C. (1995). Identification of Polycomb and trithorax group responsive elements in the regulatory region of the Drosophila homeotic gene Sex combs reduced. Genetics *139*, 797–814.

Gramates, L.S., Marygold, S.J., Santos, G.D., Urbano, J.M., Antonazzo, G., Matthews, B.B., Rey, A.J., Tabone, C.J., Crosby, M.A., Emmert, D.B., et al. (2017). FlyBase at 25: looking to the future. Nucleic Acids Res. *45*, D663–D671.

Guo, Z., Driver, I., and Ohlstein, B. (2013). Injury-induced BMP signaling negatively regulates Drosophila midgut homeostasis. J. Cell Biol. *201*, 945–961.

Haelterman, N.A., Jiang, L., Li, Y., Bayat, V., Sandoval, H., Ugur, B., Tan, K.L., Zhang, K., Bei, D., Xiong, B., et al. (2014). Large-scale identification of chemically induced mutations in Drosophila melanogaster. Genome Res. *24*, 1707–1718.

Herz, H.M., Hu, D., and Shilatifard, A. (2014). Enhancer malfunction in cancer. Mol. Cell *53*, 859–866.

Herz, H.M., Mohan, M., Garruss, A.S., Liang, K., Takahashi, Y.H., Mickey, K., Voets, O., Verrijzer, C.P., and Shilatifard, A. (2012). Enhancer-associated H3K4 monomethylation by trithorax-related, the Drosophila homolog of mammalian Mll3/Mll4. Genes Dev. *26*, 2604–2620.

Hime, G.R., Dhungat, M.P., Ng, A., and Bowtell, D.D. (1997). D-Cbl, the Drosophila homologue of the c-Cbl proto-oncogene, interacts with the Drosophila EGF receptor in vivo, despite lacking C-terminal adaptor binding sites. Oncogene *14*, 2709–2719.

Hnisz, D., Abraham, B.J., Lee, T.I., Lau, A., Saint-André, V., Sigova, A.A., Hoke, H.A., and Young, R.A. (2013). Super-enhancers in the control of cell identity and disease. Cell *155*, 934–947.

Hochmuth, C.E., Biteau, B., Bohmann, D., and Jasper, H. (2011). Redox regulation by keap1 and nrf2 controls intestinal stem cell proliferation in Drosophila. Cell Stem Cell *8*, 188–199.

Hu, D., Gao, X., Morgan, M.A., Herz, H.M., Smith, E.R., and Shilatifard, A. (2013). The MLL3/MLL4 branches of the COMPASS family function as major histone H3K4 monomethylases at enhancers. Mol. Cell. Biol. *33*, 4745–4754.

Jiang, H., Grenley, M.O., Bravo, M.J., Blumhagen, R.Z., and Edgar, B.A. (2011). EGFR/Ras/MAPK signaling mediates adult midgut epithelial homeostasis and regeneration in drosophila. Cell Stem Cell *8*, 84–95.

Jiang, H., Patel, P.H., Kohlmaier, A., Grenley, M.O., McEwen, D.G., and Edgar, B.A. (2009). Cytokine/Jak/stat signaling mediates regeneration and homeostasis in the Drosophila Midgut. Cell *137*, 1343–1355.

Jiang, H., Tian, A., and Jiang, J. (2016). Intestinal stem cell response to injury: lessons from Drosophila. Cell. Mol. Life Sci. *73*, 3337–3349.

Jin, Y., Ha, N., Forés, M., Xiang, J., Gläßer, C., Maldera, J., Jiménez, G., and Edgar, B.A. (2015). EGFR/Ras signaling controls drosophila intestinal stem cell proliferation via capicua-regulated genes. PLoS Genet. *11*, e1005634.

Jin, Y., Xu, J., Yin, M.X., Lu, Y., Hu, L., Li, P., Zhang, P., Yuan, Z., Ho, M.S., Ji, H., et al. (2013). Brahma is essential for Drosophila intestinal stem cell proliferation and regulated by Hippo signaling. Elife *2*, e00999.

Jones, K.M., Sarić, N., Russell, J.P., Andoniadou, C.L., Scambler, P.J., and Basson, M.A. (2015). CHD7 maintains neural stem cell quiescence and prevents premature stem cell depletion in the adult hippocampus. Stem Cells *33*, 196–210.

Kennison, J.A., and Tamkun, J.W. (1988). Dosage-dependent modifiers of polycomb and antennapedia mutations in Drosophila. Proc. Natl. Acad. Sci. USA *85*, 8136–8140.

Kim, M.S., Chung, N.G., Kang, M.R., Yoo, N.J., and Lee, S.H. (2011). Genetic and expressional alterations of CHD genes in gastric and colorectal cancers. Histopathology *58*, 660–668.

Ko, M., Bandukwala, H.S., An, J., Lamperti, E.D., Thompson, E.C., Hastie, R., Tsangaratou, A., Rajewsky, K., Koralov, S.B., and Rao, A. (2011). Ten-Eleven-Translocation 2 (TET2) negatively regulates homeostasis and differentiation of hematopoietic stem cells in mice. Proc. Natl. Acad. Sci. USA *108*, 14566–14571.

Langmead, B., and Salzberg, S.L. (2012). Fast gapped-read alignment with Bowtie. Nat. Methods *9*, 357–359.

Lee, J.E., Wang, C., Xu, S., Cho, Y.W., Wang, L., Feng, X., Baldridge, A., Sartorelli, V., Zhuang, L., Peng, W., et al. (2013). H3K4 mono- and di-methyltransferase MLL4 is required for enhancer activation during cell differentiation. Elife *2*, e01503.

Lee, T., and Luo, L. (1999). Mosaic analysis with a repressible cell marker for studies of gene function in neuronal morphogenesis. Neuron *22*, 451–461.

Levkowitz, G., Waterman, H., Ettenberg, S.A., Katz, M., Tsygankov, A.Y., Alroy, I., Lavi, S., Iwai, K., Reiss, Y., Ciechanover, A., et al. (1999). Ubiquitin ligase activity and tyrosine phosphorylation underlie suppression of growth factor signaling by c-Cbl/Sli-1. Mol. Cell *4*, 1029–1040.

Li, H., Qi, Y., and Jasper, H. (2013). Dpp signaling determines regional stem cell identity in the regenerating adult drosophila gastrointestinal tract. Cell Rep. *4*, 10–18.

Li, Z., Guo, Y., Han, L., Zhang, Y., Shi, L., Huang, X., and Lin, X. (2014). Debra-mediated Cl degradation controls tissue homeostasis in drosophila adult midgut. Stem Cell Reports *2*, 135–144.

Lin, G., Xu, N., and Xi, R. (2008). Paracrine Wingless signalling controls self-renewal of Drosophila intestinal stem cells. Nature *455*, 1119–1123.

Love, M.I., Huber, W., and Anders, S. (2014). Moderated estimation of fold change and dispersion for RNA-seq data with DESeq2. Genome Biol. *15*, 550.

Marshall, O.J., and Brand, A.H. (2015). damidseq_pipeline: an automated pipeline for processing DamID sequencing datasets. Bioinformatics *31*, 3371–3373.

Marshall, O.J., and Brand, A.H. (2017). Chromatin state changes during neural development revealed by in vivo cell-type specific profiling. Nat. Commun. *8*, 2271.

Marshall, O.J., Southall, T.D., Cheetham, S.W., and Brand, A.H. (2016). Cell-type-specific profiling of protein–DNAinteractions without cell isolation using targetedDamID with next-generation sequencing. Nat. Protoc. *11*, 1586–1598.

McInnes, L., Healy, J., and Melville, J. (2018). UMAP: uniform manifold approximation and projection for dimension reduction.

Meisner, H., Daga, A., Buxton, J., Fernández, B., Chawla, A., Banerjee, U., and Czech, M.P. (1997). Interactions of Drosophila Cbl with epidermal growth factor receptors and role of Cbl in R7 photoreceptor cell development. Mol. Cell. Biol. *17*, 2217–2225.

Melicharek, D., Shah, A., DiStefano, G., Gangemi, A.J., Orapallo, A., Vrailas-Mortimer, A.D., and Marenda, D.R. (2008). Identification of novel regulators of atonal expression in the developing Drosophila retina. Genetics *180*, 2095–2110.

Melicharek, D.J., Ramirez, L.C., Singh, S., Thompson, R., and Marenda, D.R. (2010). Kismet/CHD7 regulates axon morphology, memory and locomotion in a Drosophila model of CHARGE syndrome. Hum. Mol. Genet. *19*, 4253–4264.

Micchelli, C.A., and Perrimon, N. (2006). Evidence that stem cells reside in the adult Drosophila midgut epithelium. Nature *439*, 475–479.

Miyake, N., Koshimizu, E., Okamoto, N., Mizuno, S., Ogata, T., Nagai, T., Kosho, T., Ohashi, H., Kato, M., Sasaki, G., et al. (2013). MLL2 and KDM6A mutations in patients with Kabuki syndrome. Am. J. Med. Genet. *161A*, 2234–2243.

Mohan, M., Herz, H.M., Smith, E.R., Zhang, Y., Jackson, J., Washburn, M.P., Florens, L., Eissenberg, J.C., and Shilatifard, A. (2011). The COMPASS family of H3K4 methylases in drosophila. Mol. Cell. Biol. *31*, 4310–4318.

Neale, B.M., Kou, Y., Liu, L., Ma'ayan, A., Samocha, K.E., Sabo, A., Lin, C.F., Stevens, C., Wang, L.S., Makarov, V., et al. (2012). Patterns and rates of exonic de novo mutations in autism spectrum disorders. Nature *485*, 242–245.

Ng, S.B., Bigham, A.W., Buckingham, K.J., Hannibal, M.C., McMillin, M.J., Gildersleeve, H.I., Beck, A.E., Tabor, H.K., Cooper, G.M., Mefford, H.C., et al. (2010). Exome sequencing identifies MLL2 mutations as a cause of Kabuki syndrome. Nat. Genet. *42*, 790–793.

O'Roak, B.J., Vives, L., Girirajan, S., Karakoc, E., Krumm, N., Coe, B.P., Levy, R., Ko, A., Lee, C., Smith, J.D., et al. (2012). Sporadic autism exomes reveal a highly interconnected protein network of de novo mutations. Nature *485*, 246–250.

O'Brien, L.E., Soliman, S.S., Li, X., and Bilder, D. (2011). Altered modes of stem cell division drive adaptive intestinal growth. Cell *147*, 603–614.

Ohlstein, B., and Spradling, A. (2006). The adult Drosophila posterior midgut is maintained by pluripotent stem cells. Nature *439*, 470–474.

Ohlstein, B., and Spradling, A. (2007). Multipotent Drosophila intestinal stem cells specify daughter cell fates by differential notch signaling. Science *315*, 988–992.

Pai, L.M., Barcelo, G., and Schüpbach, T. (2000). D-cbl, a negative regulator of the Egfr pathway, is required for dorsoventral patterning in Drosophila oogenesis. Cell *103*, 51–61.

Patel, P.H., Dutta, D., and Edgar, B.A. (2015). Niche appropriation by Drosophila intestinal stem cell tumours. Nat. Cell Biol. *17*, 1182–1192.

Patro, R., Duggal, G., Love, M.I., Irizarry, R.A., and Kingsford, C. (2017). Salmon provides fast and bias-aware quantification of transcript expression. Nat. Methods *14*, 417–419.

Perdigoto, C.N., Schweisguth, F., and Bardin, A.J. (2011). Distinct levels of Notch activity for commitment and terminal differentiation of stem cells in the adult fly intestine. Development *138*, 4585–4595.

Perkins, L.A., Holderbaum, L., Tao, R., Hu, Y., Sopko, R., McCall, K., Yang-Zhou, D., Flockhart, I., Binari, R., Shim, H.S., et al. (2015). The transgenic RNAi project at Harvard Medical School: resources and validation. Genetics *201*, 843–852.

Pleasance, E.D., Stephens, P.J., O'Meara, S., McBride, D.J., Meynert, A., Jones, D., Lin, M.L., Beare, D., Lau, K.W., Greenman, C., et al. (2010). A small-cell lung cancer genome with complex signatures of tobacco exposure. Nature *463*, 184–190.

Quinlan, A.R., and Hall, I.M. (2010). BEDTools: a flexible suite of utilities for comparing genomic features. Bioinformatics *26*, 841–842.

Ramírez, F., Dündar, F., Diehl, S., Grüning, B.A., and Manke, T. (2014). deepTools: a flexible platform for exploring deep-sequencing data. Nucleic Acids Res. *42*, W187–W191.

Ren, F., Wang, B., Yue, T., Yun, E.Y., Ip, Y.T., and Jiang, J. (2010). Hippo signaling regulates Drosophila intestine stem cell proliferation through multiple pathways. Proc. Natl. Acad. Sci. USA *107*, 21064–21069.

Rickels, R., Herz, H.M., Sze, C.C., Cao, K., Morgan, M.A., Collings, C.K., Gause, M., Takahashi, Y.H., Wang, L., Rendleman, E.J., et al. (2017). Histone H3K4 monomethylation catalyzed by Trr and mammalian COMPASS-like proteins at enhancers is dispensable for development and viability. Nat. Genet. *49*, 1647–1653.

Risso, D., Ngai, J., Speed, T.P., and Dudoit, S. (2014). Normalization of RNA-seq data using factor analysis of control genes or samples. Nat. Biotechnol. *32*, 896–902.

Robinson, G., Parker, M., Kranenburg, T.A., Lu, C., Chen, X., Ding, L., Phoenix, T.N., Hedlund, E., Wei, L., Zhu, X., et al. (2012). Novel mutations target distinct subgroups of medulloblastoma. Nature *488*, 43–48.

Sallé, J., Gervais, L., Boumard, B., Stefanutti, M., Siudeja, K., and Bardin, A.J. (2017). Intrinsic regulation of enteroendocrine fate by Numb. EMBO J *36*, 1928–1945, e201695622–18.

Sawada, G., Ueo, H., Matsumura, T., Uchi, R., Ishibashi, M., Mima, K., Kurashige, J., Takahashi, Y., Akiyoshi, S., Sudo, T., et al. (2013). CHD8 is an independent prognostic indicator that regulates Wnt/β-catenin signaling and the cell cycle in gastric cancer. Oncol. Rep. *30*, 1137–1142.

Schnetz, M.P., Bartels, C.F., Shastri, K., Balasubramanian, D., Zentner, G.E., Balaji, R., Zhang, X., Song, L., Wang, Z., Laframboise, T., et al. (2009). Genomic distribution of CHD7 on chromatin tracks H3K4 methylation patterns. Genome Res. *19*, 590–601.

Schnetz, M.P., Handoko, L., Akhtar-Zaidi, B., Bartels, C.F., Pereira, C.F., Fisher, A.G., Adams, D.J., Flicek, P., Crawford, G.E., Laframboise, T., et al. (2010). CHD7 targets active gene enhancer elements to modulate ES cell-specific gene expression. PLoS Genet. *6*, e1001023.

Schulz, Y., Freese, L., Mänz, J., Zoll, B., Völter, C., Brockmann, K., Bögershausen, N., Becker, J., Wollnik, B., and Pauli, S. (2014a). CHARGE and Kabuki syndromes: a phenotypic and molecular link. Hum. Mol. Genet. *23*, 4396–4405.

Schulz, Y., Wehner, P., Opitz, L., Salinas-Riester, G., Bongers, E.M.H.F., van Ravenswaaij-Arts, C.M.A., Wincent, J., Schoumans, J., Kohlhase, J., Borchers, A., et al. (2014b). CHD7, the gene mutated in CHARGE syndrome, regulates genes involved in neural crest cell guidance. Hum. Genet. *133*, 997–1009.

Shaw, R.L., Kohlmaier, A., Polesello, C., Veelken, C., Edgar, B.A., and Tapon, N. (2010). The Hippo pathway regulates intestinal stem cell proliferation during Drosophila adult midgut regeneration. Development *137*, 4147–4158.

Soubeyran, P., Kowanetz, K., Szymkiewicz, I., Langdon, W.Y., and Dikic, I. (2002). Cbl-CIN85-endophilin complex mediates ligand-induced downregulation of EGF receptors. Nature *416*, 183–187.

Southall, T.D., Gold, K.S., Egger, B., Davidson, C.M., Caygill, E.E., Marshall, O.J., and Brand, A.H. (2013). Cell-type-specific profiling of gene expression and chromatin binding without cell isolation: assaying RNA Pol II occupancy in neural stem cells. Dev. Cell *26*, 101–112.

Srinivasan, S., Armstrong, J.A., Deuring, R., Dahlsveen, I.K., McNeill, H., and Tamkun, J.W. (2005). The Drosophila trithorax group protein Kismet facilitates an early step in transcriptional elongation by RNA polymerase II. Development *132*, 1623–1635.

Srinivasan, S., Dorighi, K.M., and Tamkun, J.W. (2008). Drosophila Kismet regulates histone H3 lysine 27 methylation and early elongation by RNA polymerase II. PLoS Genet. *4*, e1000217.

Staley, B.K., and Irvine, K.D. (2010). Warts and Yorkie mediate intestinal regeneration by influencing stem cell proliferation. Curr. Biol. *20*, 1580–1587.

Tahara, T., Yamamoto, E., Madireddi, P., Suzuki, H., Maruyama, R., Chung, W., Garriga, J., Jelinek, J., Yamano, H.O., Sugai, T., et al. (2014). Colorectal carcinomas With CpG island methylator Phenotype 1 frequently contain mutations in chromatin regulators. Gastroenterology *146*, 530–538.e5.

Talkowski, M.E., Rosenfeld, J.A., Blumenthal, I., Pillalamarri, V., Chiang, C., Heilbut, A., Ernst, C., Hanscom, C., Rossin, E., Lindgren, A.M., et al. (2012). Sequencing chromosomal abnormalities reveals neurodevelopmental loci that confer risk across diagnostic boundaries. Cell *149*, 525–537.

Terriente-Félix, A., López-Varea, A., and de Celis, J.F. (2010). Identification of genes affecting wing patterning through a loss-of-function mutagenesis screen and characterization of med15 function during wing development. Genetics *185*, 671–684.

Terriente-Félix, A., Molnar, C., Gómez-Skarmeta, J.L., and de Celis, J.F. (2011). A conserved function of the chromatin ATPase Kismet in the regulation of hedgehog expression. Dev. Biol. *350*, 382–392.

Thompson, B.A., Tremblay, V., Lin, G., and Bochar, D.A. (2008). CHD8 is an ATP-dependent chromatin remodeling factor that regulates beta-catenin target genes. Mol. Cell. Biol. *28*, 3894–3904.

Tian, A., and Jiang, J. (2014). Intestinal epithelium-derived BMP controls stem cell self-renewal in Drosophila adult midgut. Elife *3*, e01857.

Tian, A., Shi, Q., Jiang, A., Li, S., Wang, B., and Jiang, J. (2015). Injury-stimulated Hedgehog signaling promotes regenerative proliferation of Drosophila intestinal stem cells. J. Cell Biol. *208*, 807–819.

Tian, A., Wang, B., and Jiang, J. (2017). Injury-stimulated and self-restrained BMP signaling dynamically regulates stem cell pool size during Drosophila midgut regeneration. Proc. Natl. Acad. Sci. USA *114*, E2699–E2708.

Tie, F., Banerjee, R., Conrad, P.A., Scacheri, P.C., and Harte, P.J. (2012). Histone demethylase UTX and chromatin remodeler BRM bind directly to CBP and modulate acetylation of histone H3 lysine 27. Mol. Cell. Biol. *32*, 2323–2334.

van Steensel, B., and Henikoff, S. (2000). Identification of in vivo DNA targets of chromatin proteins using tethered dam methyltransferase. Nat. Biotechnol. *18*, 424–428.

Vissers, L.E.L.M., van Ravenswaaij, C.M.A., Admiraal, R., Hurst, J.A., de Vries, B.B.A., Janssen, I.M., van der Vliet, W.A., Huys, E.H.L.P.G., de Jong, P.J., Hamel, B.C.J., et al. (2004). Mutations in a new member of the chromodomain gene family cause CHARGE syndrome. Nat. Genet. *36*, 955–957.

Wang, C., Guo, X., and Xi, R. (2014). EGFR and Notch signaling respectively regulate proliferative activity and multiple cell lineage differentiation of Drosophila gastric stem cells. Cell Res. *24*, 610–627.

Xu, N., Wang, S.Q., Tan, D., Gao, Y., Lin, G., and Xi, R. (2011). EGFR, Wingless and JAK/STAT signaling cooperatively maintain Drosophila intestinal stem cells. Dev. Biol. *354*, 31–43.

Zabidi, M.A., Arnold, C.D., Schernhuber, K., Pagani, M., Rath, M., Frank, O., and Stark, A. (2015). Enhancer-core-promotor specificity separates developmental and housekeeping gene regulation. Nature *518*, 556–559.

Zeng, X., Chauhan, C., and Hou, S.X. (2010). Characterization of midgut stem cell- and enteroblast-specific Gal4 lines in drosophila. Genesis *48*, 607–611.

Zielke, N., Korzelius, J., van Straaten, M., Bender, K., Schuhknecht, G.F.P., Dutta, D., Xiang, J., and Edgar, B.A. (2014). Fly-FUCCI: a versatile tool for studying cell proliferation in complex tissues. Cell Rep. *7*, 588–598.

Zink, D., and Paro, R. (1995). Drosophila Polycomb-group regulated chromatin inhibits the accessibility of a trans-activator to its target DNA. EMBO J. *14*, 5660–5671.

STAR★METHODS

KEY RESOURCES TABLE

REAGENT or RESOURCE	SOURCE	IDENTIFIER
Antibodies		
Mouse anti-Delta ECD (1:2000)	DSHB	Cat# c594.9b; RRID: AB_528194
Mouse anti-Notch ECD (1:100)	DSHB	Cat# c458.2h; RRID: AB_528408
Mouse anti-Prospero (MR1A; 1:1000)	DSHB	RRID: AB_528440
Chicken anti-GFP (1:2000)	Abcam	Cat# ab13970; RRID: AB_300798
Goat anti-ßGAL (1:500)	Biogenesis	Cat# 466–1409
Rabbit anti-Pdm1 (1:1000)	Gift from X. Yang, Zhejiang University, China	RRID: AB_2570215
Rabbit anti-PH3 (1:1000) Millipore	Millipore	Cat# 06-570; RRID: AB_310177
Goat anti-Kismet DK20 (1:500)	Santa Cruz	sc-15848; RRID: AB_672122
Rabbit anti-Utx, (1:500)	Gift from A. Shilatifard, Northwestern University Feinberg School of Medicine	RRID: AB_2567973
Rabbit anti-Trr (1:500)	Gift from A. Shilatifard, Northwestern University Feinberg School of Medicine	RRID: AB_2568870
Rabbit anti-Lpt (1:500)	Gift from A. Shilatifard, Northwestern University Feinberg School of Medicine	RRID: AB_2568872
Rabbit anti-H3K4me1 (1:500)	Gift from A. Shilatifard, Northwestern University Feinberg School of Medicine	N/A
Rabbit anti-dpERK (1:200)	Cell Signaling Technology	Cat# 4377; RRID: AB_331775
Rabbit anti-H3K27me3 (1:500)	Diagenode	Cat# C15410195; RRID: AB_2753161
Rabbit anti-H3K27ac (1:2000)	Abcam	Cat# ab4729; RRID: AB_2118291
Mouse anti-EGFR (1:100)	Sigma	Cat# E2906; RRID: AB_609900
Rabbit anti-DH31 (1:500),	Gift from J.A. Veenstra, Université de Bordeaux	RRID: AB_2569126
Rabbit anti-LTK2 (1:1000)	Gift from J.A. Veenstra, Université de Bordeaux	N/A
Chemicals, Peptides, and Recombinant Proteins		
Alexa 647-conjugated phalloidin (1:100)	LifeTechnologies	Cat# A22287: RRID: AB_2620155
Quick ligase	NEB	Cat# M2200S
RNase A	Sigma	Cat# R6513-50MG
T4 DNA ligase	NEB	Cat# B0202S
DpnI	NEB	Cat#R0176L
DpnII	NEB	Cat#R0543L
Sau3AI	NEB	Cat# R0169L
PCR buffer MyTaq HS	Bioline	Cat# BIO-21111
AlwI	NEB	Cat# R0513S
Klenow fragment	NEB	Cat# 210S
T4 polynucleotide kinase	NEB	Cat# M0201S
Elastase	Sigma	Cat# E0258-5MG
Critical Commercial Assays		
Qiaquick PCR Purification kit	Qiagen	Cat# 28104
QIAmp DNA Micro Kit	Qiagen	Cat# 56304
Arcturus PicoPure RNA Isolation Kit	ThermoScientific	Cat# KIT0202

(*Continued on next page*)

Continued

REAGENT or RESOURCE	SOURCE	IDENTIFIER
RNase-Free DNase Set	Qiagen	Cat# 79254
Arcturus™ RiboAmp™ HS PLUS Kit	ThermoScientific	Cat# KIT0525
Deposited Data		
Lists of expressed genes and cell type-specific genes were generated from published RNAseq data in the gut	Dutta et al., 2015	http://flygutseq.buchonlab.com/resources
Experimental Models: Organisms/Strains		
Drosophila: FRT40A kis10D26	This study, Institut Curie Paris.	N/A
Drosophila: UAS-LT3-NDam	Southall et al., 2013	N/A
Drosophila: kis^{1}	Daubresse et al., 1999	Cat# 431, RRID:BDSC_431
Drosophila: UAS-kis-RNAi #36597	BDSC, (Perkins et al., 2015)	Cat# 36597, RRID:BDSC_36597
Drosophila: UAS-kismet RNAi #34908	BDSC, (Perkins et al., 2015)	BDSC Cat# 34908, RRID:BDSC_34908)
Drosophila: UAS-$EGFR^{DN}$	BDSC (Buff et al., 1998)	BDSC Cat# 5364, RRID:BDSC_5364
Drosophila: UAS-lpt-RNAi	BDSC, (Perkins et al., 2015)	BDSC Cat# 25994, RRID:BDSC_25994
Drosophila: UAS-trr-RNAi	BDSC, (Perkins et al., 2015)	BDSC Cat# 29563, RRID:BDSC_29563
Drosophila: UAS-utx-RNAi	BDSC, (Perkins et al., 2015)	BDSC Cat# 34076, RRID:BDSC_34076
Drosophila: FR82B trx^{E2}	BDSC (Gindhart and Kaufman, 1995)	BDSC Cat# 24160, RRID:BDSC_24160
Drosophila: FR19A trr^{B}	BDSC (Haelterman et al., 2014)	BDSC Cat# 57138, RRID:BDSC_57138
Drosophila: UAS-bsk^{DN}	BDSC (Adachi-Yamada et al., 1999)	BDSC Cat# 6409, RRID:BDSC_6409
Drosophila: UAS-yki-RNAi	BDSC, (Perkins et al., 2015)	BDSC Cat# 34067, RRID:BDSC_34067
Drosophila: UAS-InR^{DN}	Gift to BDSC by Exelixis, Inc.	BDSC Cat# 8253, RRID:BDSC_8253
Drosophila: UAS-domeRNAi	BDSC, (Perkins et al., 2015)	BDSC Cat# 34618, RRID:BDSC_34618
Drosophila: UAS-ash1-RNAi # 31050	BDSC, (Perkins et al., 2015)	BDSC Cat# 31050, RRID:BDSC_31050
Drosophila: UAS-ash1-RNAi # 36130	BDSC, (Perkins et al., 2015)	BDSC Cat# 36130, RRID:BDSC_36130
Drosophila: UAS-brm-RNAi	BDSC, (Perkins et al., 2015)	BDSC Cat# 31712, RRID:BDSC_31712
Drosophila: UAS-Cbl-RNAi	BDSC, (Perkins et al., 2015)	BDSC Cat# 27500, RRID:BDSC_27500
Drosophila: UAS-GFP-$E2f^{1-230}$, UAS-mRFP-$CycB^{1-266}$	BDSC (Zielke et al., 2014)	BDSC Cat# 55118, RRID:BDSC_55118
Drosophila: 10XSTAT92E-GFP	BDSC (Ekas et al., 2006)	BDSC Cat# 26198, RRID:BDSC_26198
Drosophila: CycE-lacZ	BDSC Gift by Helena Richardson, Peter MacCallum Cancer Centre to BDSC	BDSC Cat# 30722, RRID:BDSC_30722
Drosophila: UAS-set1-RNAi	VDRC, (Dietzl et al., 2007)	Cat# 40682
Drosophila: UAS-cic-RNAi	VDRC, (Dietzl et al., 2007)	Cat# 103805
Drosophila: FRT40A kis^{LM27}	Gift from D.R. Marenda, Drexel University.	N/A
Drosophila: FRT40A kis^{EC1}	Gift from D.R. Marenda	N/A
Drosophila: NRE-LacZ	Furriols and Bray, 2001	N/A
Drosophila: UAS-$Notch^{cdc10}$	Brennan et al., 1999	N/A
Drosophila: UAS-LT3-NDam-RNAPol II	Southall et al., 2013	N/A
Drosophila: UAS-LT3-Dam-Pc	Marshall and Brand, 2017	N/A
Drosophila: UAS-LT3-Dam-HP1a	Marshall and Brand, 2017	N/A
Drosophila: UAS-LT3-Dam-Brm	Marshall and Brand, 2017	N/A
Drosophila: UAS-LT3-Dam-H1	Marshall and Brand, 2017	N/A
Drosophila: UAS-cic^{HA}	Jin et al., 2015	N/A
Drosophila: pucE69-LacZ	Gift from N.Tapon, Francis Crick Institute, London	N/A
Drosophila: Upd-LacZ	Gift from B.A. Edgar, Huntsman Cancer Institute, Utah	N/A
Drosophila: Upd3.1-LacZ	Gift from B.A. Edgar, Huntsman Cancer Institute, Utah	N/A

(*Continued on next page*)

Continued

REAGENT or RESOURCE	SOURCE	IDENTIFIER
Drosophila: UAS-Cbl-L	Gift from L.M. Pai, Chang Gung University, Taiwan	N/A
Drosophila: UAS-Cbl-S	Gift from L.M. Pai, Chang Gung University, Taiwan	N/A
Drosophila: NRE-GAL4 ; tubGAL80^{ts} UAS-GFP	Zeng et al., 2010	N/A
Drosophila: esg-GAL4, tubGAL80^{ts} UAS-GFP	Jiang et al., 2009	N/A
Drosophila: esg-GAL4 UAS-GFP; Su(H) GBE-GAL80 tubGAL80^{ts}	Wang et al., 2014	N/A
Drosophila: MyoIAGAL4; tubGAL80^{ts} UAS-GFP	Jiang et al., 2009	N/A
Drosophila: pros^{voila}-Gal4, tub-Gal80ts	Balakireva et al., 1998	N/A
Drosophila: w P[hs-FLP] P[pTub-GAL4] P[UAS-nlsGFP]	Bardin et al., 2010	N/A
Drosophila: FRT40A P[pTub-GAL80]	Bardin et al., 2010	N/A
Drosophila: FRT82B P[pTub-GAL80]	Bardin et al., 2010	N/A
Drosophila: w P[hs-FLP]; FRT40A P[pTub-GAL80]; Drosophila: P[UAS-RFP], P[pTub-GAL4]	This paper, Institut Curie, Paris.	N/A
Drosophila: hsflp122 P[pTub-GAL80] FRT19A; P[pAct-GAL4] P[UASGFP]	Lin et al., 2008	N/A
Recombinant DNA		
Drosophila BAC: (P[acman] BAC CH322-128O7)	BACPAC Resources Center	CH322-128O7
Drosophila BAC: (P[acman] BAC CH321-35E09)	BACPAC Resources Center	CH321-35E9
Plasmid: kis$_{locus}$-FLP	This paper, Institut Curie, Paris.	N/A
Plasmid: R6kam-hNGFP	Gift from A. A. Hyman, Max Planck Institute, Dresden.	N/A
Plasmid: UAS- KisS-Flag	This paper, Institut Curie, Paris.	N/A
Plasmid: UAS-KisL-His-Flag	This paper, Institut Curie, Paris.	N/A
Plasmid: UAS-kis-K2060R-His-Flag	This paper, Institut Curie, Paris.	N/A
Plasmid: pUASTattB-LT3-NDam	Southall et al., 2013	N/A
Plasmid: UAS-LT3-Dam-Kis	This paper, Institut Curie, Paris.	N/A
Plasmid: UAS-LT3-Dam-Trr	This paper, Institut Curie, Paris.	N/A
Software and Algorithms		
Prism 7	GraphPad Software	RRID:SCR_002798
FIJI	https://fiji.sc	N/A
Damidseq_pipeline	Marshall and Brand, 2015	https://owenjm.github.io/
bowtie2	Langmead and Salzberg, 2012	http://bowtie-bio.sourceforge.net/bowtie2/index.shtml
bedtools	Quinlan and Hall, 2010	https://bedtools.readthedocs.io/en/latest/index.html
DESeq2	Love et al., 2014	https://bioconductor.org/packages/release/bioc/html/DESeq2.html
deepTools plotHeatmap	Ramírez et al., 2014	https://deeptools.readthedocs.io/en/develop/content/tools/plotHeatmap.html
polii.gene.call	Marshall and Brand, 2015	https://owenjm.github.io/
Galaxy	Afgan et al., 2016	https://usegalaxy.org
IPython		https://ipython.org
Galaxy workflow	IPython notebooks and UMAP code used in this study - Institut Curie Paris	https://github.com/bardin-lab/kismet-analysis

CONTACT FOR REAGENT AND RESOURCE SHARING

Further information and requests for resources and reagents should be directed to and will be fulfilled by the Lead Contact, Allison Bardin (allison.bardin@curie.fr).

EXPERIMENTAL MODEL AND SUBJECT DETAILS

Flies were kept in yeasted tubes at 25°C unless mentioned. The following fly stocks were used in this study: *FRT40A kis*^{10D26} (from C.P., F.S., A.J.B., unpublished genetic screen), *kis*^{1} (#431), *UAS-kis-RNAi* (*#36597*) for Figures 2L–2P, 2R, S2A–S2E′, S2G, S2I, S2K, and S2M and *UAS-kismet RNAi* #34908 for Figures 2M, 2N, 2Q, 3I, 3J, 7B, 7F, S6Q, S6R, and S6T and for *kismet* knockdown RNA-seq condition), *UAS-lpt-RNAi* (#25994), *UAS-trr-RNAi* (#29563), *UAS-utx-RNAi* (#34076), *FR82B trx*^{E2} (#24160), FRT19A *trr*^{B} encoding a putative truncated 512-aa protein *(#57138), UAS-EGFR*^{DN} (#5364), *UAS-bsk*^{DN} (#6409), *UAS-yki-RNAi* (#34067), *UAS-InR*^{DN} (#8253), *UAS-domeRNAi* (#34618), *UAS-ash1-RNAi* (#31050 and #36130), *UAS-brm-RNAi* (#31712), UAS-Cbl-RNAi (#27500), UAS-GFP-E2F$^{1-230}$, UAS-mRFP-CycB$^{1-266}$ (#55118), 10XSTAT92E-GFP (#26198), CycE-lacZ (#30722), (From the Bloomington Drosophila Stock Center, BDSC), *UAS-set1-RNAi* (#40682), *UAS-cic-RNAi* (#103805) (From the Vienna Drosophila RNAi Center, VDRC), *kis*^{LM27} and *kis*^{EC1} (Melicharek et al., 2008), *NRE-LacZ* (Furriols and Bray, 2001), *Nintra*: *UAS-Notch*^{cdc10} is a truncated active version of intracellular Notch, (Brennan et al., 1999), *UAS-LT3-NDam* and *UAS-LT3-NDam-RNAPol II* (Southall et al., 2013) *UAS-LT3-Dam-Pc, UAS-LT3-Dam-HP1a*, *UAS-LT3-Dam-Brm and UAS-LT3-Dam-H1* (Marshall and Brand, 2017), *UAS-cic*^{HA} (Jin et al., 2015), pucE69-LacZ (gift from N.Tapon), Upd-LacZ and Upd3.1-LacZ (gift from B. Edgar), UAS-Cbl-L and UAS-Cbl-S (gift from L.M. Pai). The following Gal4 drivers were used: *NRE-GAL4* ; *tubGAL80*^{ts} *UAS-GFP* (*NRE*^{ts}) (Zeng et al., 2010), *esg-GAL4, tubGAL80*^{ts} *UAS-GFP* (esg^{ts}) (Jiang et al., 2009), *esg-GAL4* UAS-GFP; *Su(H)GBE-GAL80 tubGAL80*^{ts} (*esg*^{ts}*, NREGAL80*) (Wang et al., 2014), *MyoIA-GAL4*; *tubGAL80*^{ts} *UAS-GFP* (*Myo1A*^{ts}) (Jiang et al., 2009). *pros*^{voila}*-Gal4, tub-Gal80ts (pros*^{ts}*)* (Balakireva et al., 1998).

METHOD DETAILS

Generation of Transgenic Flies

kis$_{locus}$ construct containing 524 bp upstream to 12 kb downstream of the *kis* gene was generated starting from *Drosophila* BAC (P[acman] BAC CH321-35E09) that was further altered by recombineering to reduce the genomic size and to add a FLAP cassette N-terminally (amplified from the plasmid R6kam-hNGFP; kindly provided by T. Hyman). The FLAP cassette is composed of green fluorescent protein (GFP), S- and Flag-affinity tags separated by PreScission- and TEV- protease sites. Transgenic flies were generated at Bestgene, Inc. by injection of *attP-9AVK00013*. To generate *UAS-kisL* and *UAS-kisS* transgenic flies, *kis-RA* and *kis-RB* cDNA were respectively amplified from a midgut library and then inserted into the pUASPattB plasmid and tagged with both a 6xHIS N-terminal and a FLAG C-terminal cassette for *kis-RA* and only by a FLAG C-terminal cassette for *kis-RB*. Transgenic flies were generated at Bestgene, Inc. by injection of *attP-3BVK00033* embryos. The mutation of Chd7 K999R, a residue in the highly conserved ATP binding motif of SNF2 superfamily proteins, was shown to prevent its ATPase catalytic activity (Bouazoune and Kingston, 2012). We therefore made the equivalent K2060R mutation in Kismet coding sequence. To generate *UAS-kis-K2060R* transgenic flies, the mutation G>A at 2060th codon was inserted into the pUASP-6His_kis-PA_Flag BAC plasmid by recombineering using the rpsl/neo positive and counterselection system. The final plasmid was tagged with both a 6xHIS N-terminal and a FLAG C-terminal cassettes. Transgenic flies were generated at Bestgene, Inc. by injection of attP-3B-VK00033 embryos. To generate *UAS-Dam-kis* transgenic, *UAST-mCherry-NDam-Myc* sequences amplified from the *pUASTattB-LT3-NDam* plasmid (Southall et al., 2013) were inserted N-terminally to *kis-RA* cDNA *attB* containing vector followed by injection by Bestgene, Inc of *attP2* embryos. To generate *UAS-Dam-trr* transgenic, the *trr* sequence from the ATG to stop codon was obtained starting from *Drosophila* BAC CH322-128O7 that was further altered by recombineering to reduce the genomic size and amplified before insertion C-terminally to *Myc* into *UAST-mCherry-NDam-Myc* plasmid by Gibson Cloning method followed by injection by Bestgene, Inc of P{CaryP}attP2 embryos with the plasmid together with a phiC31 integrase helper plasmid pBS130 as an integrase source.

Clonal Analysis and Gal4 Expression

Clones were generated with the Mosaic Analysis with Repressible Cell Marker (MARCM) technique (Lee and Luo, 1999). The following fly stocks were used for MARCM: hsflp122 P[pTub-GAL80] FRT19A; P[pAct-GAL4] (Lin et al., 2008) to produce GFP marked clones on the X chromosome and P[UASGFP]w P[hs-FLP] P[pTub-GAL4] P[UAS-nlsGFP] associated with either FRT40A P[pTub-GAL80] or FRT82B P[pTub-GAL80] to produce GFP marked clones on the second or the third chromosome respectively, w P[hs-FLP]; FRT40A P[pTub-GAL80]; P[UAS-RFP], P[pTub-GAL4] to produce RFP marked clones on the second chromosome and w P[hs-FLP]; FRT40A P[pTub-GAL80]; P[pTub-GAL4] to produce clones expressing UAS-GFP-E2f$^{1-230}$, UAS-mRFP-CycB$^{1-266}$ FUCCI system. MARCM Clones were induced with a heat shock (35 min at 36.5°C) on 3-day-old adult females and were dissected 5, 9, 10, 12 or 30 days after heat shock.

MARCM^{ts} clones were generated using the following stock: w P[hs-FLP] P[pTub-GAL4] P[UAS-nlsGFP]; FRT40A P[pTub-GAL80]; P[pTub-GAL80^{ts}]. Crosses were maintained at 18°C, before and after 35 minutes heat shock clone induction at 36.5°C in 3-day-old adult females. 10 days AHS, temperature was shifted to 29°C for 3 days before dissection to allow transgenes expression (UAS-GFP and UAS-N^{Act}).

For temporal cell type-specific expression of *kismet RNAi* we used the temperature sensitive inducible UAS-GAL4/GAL80^{ts} system. Crosses and adults were kept at 18°C, the GAL80 permissive temperature. 3-day-old flies were shifted to 29°C for 2, 3 or 10 days to induce RNAi expression.

Immunofluorescence and Imaging

As described previously (Bardin et al., 2010), adult female midguts were dissected in PBS and then fixed at room temperature (RT) for 2 hours in 4% paraformaldehyde. Gut were trimmed and incubated in PBS 50% glycerol for 30 minutes before equilibration in PBS 0.1% Triton X-100 (PBT) to clean the lumen. For anti-Notch^{ECD} staining, guts were fixed for 15 min in 4% formaldehyde/heptane followed methanol treatment and rehydration in PBT as described in (Lin et al., 2008). Fixed samples were then washed in PBT for at least 30 min before addition of primary antibodies (overnight at 4°C or 3-5 hours at RT). After at least 30 min wash, secondary antibodies were incubated 3-5 hours before DAPI staining (1 μg/ml) and mounted in 4% N-propyl-galate, 80% glycerol. Polytene immunostainings were performed on L3 larvae salivary glands chromosomes as described in (Zink and Paro, 1995). Salivary glands were fixed in droplet of 45% acetic acid for 3 min. The coverslip was placed onto a poly-L-lysine coated slide and tapped using the tip of a pencil to spread the chromosomes. The quality of the preparations was checked under phase contrast microscope. Slides were next snap-frozen in liquid nitrogen, and coverslip removed. Slides were immediately put in PBS before replacement by blocking solution (1% BSA, 0.5% Triton X100 in PBS) for 1 hour at RT. 50μl of primary antibody in blocking solution was placed onto the chromosome spreads in a humid chamber (1 hour at 4°C). Slides were washed in PBS 0.5% triton for 15 minutes. Secondary antibodies were incubated for 1 hour before DAPI staining (1ig/ml) and mounted in 4% N-propyl-galate, 80% glycerol.

The following primary antibodies were used: anti-Delta ECD C594.9B (mouse,1:2000, Developmental Studies Hybridoma Bank (DSHB)); anti-GFP (chicken, 1:2000, Abcam), anti-DsRed (rabbit, 1;1000, Clontech), anti-Sanpodo (rabbit, 1:1000; J. Skeath), anti-Notch ECD C458.2H (mouse, 1:100, DSHB), anti-ßGAL (goat, 1:500; Biogenesis), anti-Prospero (mouse, MR1A; 1:1000; DSHB), anti-Pdm1 (rabbit, 1:1000; X. Yang), anti-PH3 (rabbit, 1:1000; Millipore), anti-Kismet DK20 (goat, 1:500; Santa Cruz), anti-Utx, anti-Trr, anti-Lpt and anti-H3K4me1 (Rabbit, 1:500 (Herz et al., 2012)), anti-dpERK (Rabbit, 1:200; Cell Signaling Technology), anti-H3K27me3 (Rabbit, 1:500; Diagenode), anti-H3K27ac (Rabbit, 1:2000; Abcam), anti-EGFR (Mouse, 1:100, Sigma), anti-DH31 (Rabbit, 1:500, J.A Veenstra), anti-LTK2 (Rabbit, 1:1000 J.A Veenstra) and Alexa 647-conjugated phalloidin (1:100, LifeTechnologies). Imaging was performed using Zeiss LSM700 and LSM780 confocal microscopes at the Curie Institute imaging facility with serial optical sections taken at 1 to 1.5-μm intervals (512X512 or 1024X1024) using 20X or 40X oil objectives through the whole-mounted posterior midguts. Representative images are shown in all panels. Super-resolution image was performed with a Structured Imaging Microscope (OMX v3 from Applied Precision-GE Healthcare), equipped with 3 EMCCD, Evolve cameras (Photometrics).

DamID-Seq Analysis

In DamID, the fusion of Dam methyl transferase to a DNA associated protein allows the methylation of surrounding GATC sites of DNA, which can be specifically sequenced (Choksi et al., 2006; van Steensel and Henikoff, 2000). In targeted DamID-Seq, cell type-specific low level expression is achieved, thereby allowing in vivo mapping of chromatin associated factors (Southall et al., 2013).

Using the damidseq_pipeline (Marshall and Brand, 2015) reads in fastq files were aligned to the *Drosophila melanogaster* reference genome version 6 using bowtie2 (Langmead and Salzberg, 2012) and alignments were extended to 300 nucleotides or the first GATC site, whichever occurred first.

For all GATC sites in mappable regions read coverage was counted using bedtools coverage (Quinlan and Hall, 2010). GATC sites with fewer than 5 counts on average were discarded. The remaining GATC sites were split into control counts and DamID fusion counts and tested for statistically significant differences using DESeq2 (Love et al., 2014), which also estimates a variance stabilized $\log_2$ fold enrichment values for each GATC site.

Peaks were called by merging 2 or more consecutive significant GATC sites (adjusted p-value < 0.01, $\log_2$ fold change > 0). Genes were classified as bound by a protein if 2 consecutive GATC sites within the gene body were occupied with an adjusted p-value < 0.01.

Metaplots were produced using deepTools plotHeatmap (Ramírez et al., 2014) using the DESeq2 output that was converted into bigwig files. Developmental and housekeeping S2 cells enhancers are defined in (Zabidi et al., 2015). Lists of expressed genes and cell type-specific genes were generated from published RNAseq data in the gut (Dutta et al., 2015). All genes with rpkm >1 in the ISC were considered as significantly expressed. Lists of genes enriched in each cell type (ISC, EC, EE) were generated by applying the following criteria: (1) the gene rpkm in one specific cell type is at least 2 times higher than the rpkm in each of the other cell types, (2) the gene rpkm in each other cell type is <2. Lists of EE-enriched genes and EC-enriched genes were merged to generate the list of differentiated cell types-enriched genes.

For the calculation of distribution of Kismet bound GATC sites in the genome in Figure 4A the *Drosophila* gene annotation GTF was downloaded from flybase version 6.13 (Gramates et al., 2017). The GTF file was filtered to retain only 3′UTR coding, 5′UTR coding, exon and gene features. The file was then split into a single file per genomic feature and overlapping features were merged using

bedtools. Using bedtools subtract, exonic regions were subtracted from genic regions to obtain intronic regions, and exonic regions were subtracted from overlapping 3′UTR and 5′UTR coding regions. Significantly bound GATC sites were classified as belonging to one of these regions using bedtools intersect.

RNA Pol II occupancy was determined by considering mean ratios (Dam-RNA Pol II/Dam-only) across annotated transcripts using ''polii.gene.call'' script and false discovery rates (FDR) were assigned (Marshall and Brand, 2015; Southall et al., 2013). Genes with an FDR < 0.01 were used as genes active in ISC (Figures 4J and 6D).

All analysis has been done on Galaxy (Afgan et al., 2016).

A 2D UMAP embedding (McInnes et al., 2018) was created from the $\log_2$ values estimated by DESeq2. To evaluate the embedding we plotted the $\log_2$ value for each GATC and each chromatin protein in the UMAP coordinates. We explored effect of varying the n_neighbors, min_dist, n_components and metric parameter and note that varying the parameters results in very similar maps. The parameters used are n_neighbors=30, min_dist=0.0, n_components=2, random_state=42, metric='canberra'.

RNAseq Analysis

For transcriptome profiling of sorted ISC, 3-day-old females with either *UAS-GFP* with *UAS-white-RNAi* (control), or with *UAS-kis RNAi* or with *UAS-trr-RNAi* under the control of esg^{ts} NREGal80 were shifted from 18°C to 29°C for 2 days to induce RNAi expression. For each biological replicate (n=3 for *control, n=4 for kis-RNAi, n=3 for trr-RNAi*) midguts from 100 females were dissected in PBS before FACS sorting isolation of ISC GFP+ cells followed by RNA isolation and amplification as described in (Dutta et al., 2013). Reads were quasi-mapped against the *Drosophila* reference transcriptome fasta (Flybase, release 6.13) using Salmon (Patro et al., 2017). Differential gene expression testing was performed using tximportData, RUVseq (Risso et al., 2014) and DESeq2. Genes with an adjusted p-value < 0.01 were considered differentially expressed. All analysis has been done on Galaxy (Afgan et al., 2016).

QUANTIFICATION AND STATISTICAL ANALYSIS

Image acquisition was followed by data processing with Fiji software and assembled using Adobe Photoshop. Images were processed with a median filter of 1-pixel width before applying Z-stack max projections. All quantification of clonal analysis was limited to the posterior midgut and only clones containing two or more cells (stem cell clones) were scored except for Figure S3J where 1 cell clones were included. Contiguous cells (GFP+ or RFP+) were considered as part of one discrete clone for quantifications. All graphs are scatterplots of raw data to present the full distribution of values observed and all statistical analysis were performed using Prism software. PH3+ cells number per gut was evaluated on the entire midgut (Figure 2D). In Figures 2J and 5H, Kis and Utx staining intensity were quantified within the posterior midgut. The largest nuclear plane for each cell type (esg+ ISC/EB, esg-diploid EE and esg- polyploid Ecs) was determined manually and the average fluorescent intensities of Kismet, Utx and DAPI were calculated with Fiji for these planes. In Figures 5I and 5J, EGFR staining intensity in esg+ cells was quantified per square region within each posterior midgut. The largest plane for each esg+ cell was determined manually in order to measure the cell area and mean fluorescent EGFR intensity with Fiji software and to calculate total EGFR intensity. Statistical analysis were performed using the Graphpad Prism softaware and significance calculated by either two-tailed Mann-Whitney or chi^2 statistical tests with ns for non-significant, * for $p<0.05$, ** for $p<0.01$, *** for $p<0.001$ and ****$p<0.0001$.

DATA AND SOFTWARE AVAILABILITY

Galaxy workflows, IPython notebooks and UMAP code used in the analysis are available at https://github.com/bardin-lab/kismet-analysis. DamID-Seq and RNA-Seq data have been deposited in the Gene Expression Omnibus (GEO). The accession number for DamID-Seq and RNA-Seq data reported in this paper isGSE128941.

Developmental Cell, Volume *49*

Supplemental Information

Stem Cell Proliferation Is Kept in Check by the Chromatin Regulators Kismet/CHD7/CHD8 and Trr/MLL3/4

Louis Gervais, Marius van den Beek, Manon Josserand, Jérémy Sallé, Marine Stefanutti, Carolina N. Perdigoto, Patricia Skorski, Khallil Mazouni, Owen J. Marshall, Andrea H. Brand, François Schweisguth, and Allison J. Bardin

Supplemental Figures and Legends

Figure S1. Characterization of other *kismet* mutant alleles and rescue experiments, related to Figure 1.

(A, B) Wild-type control (A) and kis^{10D26} mutant (B) MARCM clones, 5 days AHS (GFP, GREEN; Sanpodo (Spdo), RED). **(C-E)** A wild-type clone (C), a kis^{10D26} mutant clone (D), and a kis^{10D26} mutant clone with one copy of genomic rescue construct that partially rescued the *kis* mutant phenotype (E; kis_{locus}), at 9 days AHS. **(F)** Quantification of the cells per clone, and the Delta+ cells per clone from (C-E). **(G-L)** Control clones over-expressing *kisL cDNA* (G), *kisS cDNA* (I), or kis^{K2060R} cDNA a *kis* ATPase dead domain form of *kismet* (K) and kis^{10D26} mutant clones over-expressing *kisL* (H), *kisS* (J) or kis^{K2060R} (L) 9 days AHS (GFP, GREEN; DAPI, BLUE, Delta, RED). **(M, N)** Quantification of cells per clone (M), and Delta+ cells per clone (N) from (G-L). **(O-T)** Mutant clones for kis^{EC1} (O), kis^{LM27} (Q), and kis^{1} (S) alone or over-expressing *kisL cDNA* (P), (R) and (T), respectively, 9 days AHS (GFP, GREEN; DAPI, BLUE; Delta, RED). **(U, V)** Quantification of cells per clone (U), and Delta+ cells per clone (V) from (O-T). Results were compared using a two-tailed Mann-Whitney statistical test. Mean values in RED, error bars= SEM. Scale bars=20 μm.

Figure S2. Kismet is not required in EBs and ECs to control ISC accumulation, related to Figure 2.

(A-E') 2 day *kis* RNAi (BL36597) expression in the ISCs/EBs driven by esg^{ts} (A, A'), in ISCs only driven by esg^{ts}- *NREGAL80* (B, B'), in the ECs driven by Myo^{ts} (C,C'), in the EBs driven by NRE^{ts} (D, D'), or in the EEs driven by $pros^{ts}$ (E, E') was sufficient to deplete Kismet protein (GFP, GREEN; DAPI, BLUE; Kismet, WHITE). Arrows point toward cells with depleted Kismet). **(F, G)** esg^{ts} driven expression of GFP only (F) or with a *kis RNAi* (BL36597) (G) in ISCs and EBs for 10 days at 29°C. Knockdown of *kismet* in ISCs and EBs induced an increase in *esg*+ (GFP, GREEN), and Delta+ cells (RED) compared with control (DAPI, BLUE). **(H, I)** Myo^{ts} driven expression of GFP only (H) or along with a *kis* RNAi (BL36597) (I) in ECs for 10d at 29°C. Knockdown of *kismet* in ECs had no impact on Delta+ cell number (RED) when compared to control (GFP, GREEN;

DAPI, BLUE). **(J, K)** *NRE^{ts}* driven expression of GFP alone (J) or with a *kis* RNAi (BL36597) (K) in the EB for 10 days at 29°C. *kismet* EB knockdown had no impact on Delta+ cell number (RED) when compared to control (GFP, GREEN; DAPI, BLUE). **(L, M)** *pros^{ts}* driven expression of GFP alone (L) or with a *kis* RNAi (BL36597) (M) in the EE cells for 10 days at 29°C. *kismet* EE knockdown had no impact on Delta+ cell number (RED) when compared to control (GFP, GREEN; DAPI, BLUE). Scale bars=20 µm.

Figure S3. *kismet* mutant ISCs are able to differentiate in response to Notch signaling activation, related to Figure 3.

(A, B) Notch extra cellular domain (RED) was expressed in most diploid cells in both wild-type control (A), and *kis^{10D26}* mutant (B), clones at 9 days AHS (GFP, GREEN; DAPI, BLUE). **(C-D')** Notch transcriptional reporter activity (NRE-LacZ) was detected in both wild-type control clones (C), and *kis^{10D26}* clones (D), at 9 days AHS (clones outlined in WHITE, GFP, GREEN in C, D; DAPI, BLUE; ßGAL, RED; Delta, GREEN in C', D'). **(E, F)** Quantification of the average number of (NRE+, Delta+) and (NRE-, Delta+) cells per clone (E) and the relative percent of each cell type (F) from (C-D'). **(G)** Experimental set-up: to test the effect of Notch activation on the extra ISCs accumulating in *kis^{10D26}* mutant conditions, wild-type or mutant clones were induced by heat-shock. Flies were maintained for 10 days at 18°C however expression of *UAS-GFP* and *UAS-N^{Act}* (an activated form of Notch) was blocked using GAL80^{ts}, active at 18°C. Flies were either maintained at 18°C or switched to a restrictive temperature of 29°C for 3 days to inactivate GAL80^{ts} thereby allowing GAL4-driven *UAS-GFP* and *UAS-N^{Act}* expression. **(H, I)** Guts 13 days AHS at 18°C containing unmarked wild-type (H), or *kis^{10D26}* mutant clones (I). Note that the *kis^{10D26}* mutant clones could be detected through ISC accumulation marked by Delta (RED; DAPI, BLUE; No GFP and no N^{Act} expression). **(J)** Quantification of total cells per clone, ISCs per clone and ECs per clone after a 3 days switch to 29°C from (J, K). **(K, L)** ISCs were lost upon *UAS-N^{Act}* in wild-type (K), or *kis^{10D26}* mutant clones (L), maintained for 10 days at 18°C AHS before transfer for 3 days at 29°C (GFP, GREEN, DAPI in BLUE and Delta in RED). Most cells in clones had large nuclei,

characteristic of ECs. Results were compared using a two-tailed Mann-Whitney statistical test. Mean values in RED; error bars=SEM. Scale bars=20 μm.

Figure S4. Additional pathways participate to ISC proliferation induced by *kismet* loss, related to Figure 3.

(**A**-**B'**) Wild-type control (A, A'), and kis^{10D26} mutant clones (B, B'), 9 days AHS MARCM clones. As reported in (Biteau et al., 2008) JNK signaling activity, detected by Puc-LacZ (RED in A-B') was detected in wild-type ECs of 15 days old flies but absent in ISCs. While Puc-LacZ was not changed in kis^{10D26} mutant ECs, it was markedly increased in ISCs (clone outlined in WHITE in A', B'; GFP, GREEN; Delta, BLUE; arrowheads point toward ISC). **(C**-**D')** Wild-type control (C, C'), and kis^{10D26} mutant clones (D, D'), 9 days AHS MARCM clones. JAK/STAT signaling, detected by 10X-STATGFP (GREEN in C-D') was markedly increased in kis^{10D26} mutant clones (clone outlined in WHITE in C', D'; RFP, RED; DAPI, BLUE). **(E)** Quantification of the number of cells per clone, the number of Delta+ cells per clone, and the % of Delta+ cells per clone from 12 day old wild-type control, kis^{10D26} mutant clones, expressing a dominant form of JNK pathway component *basket* (bsk^{DN}), an RNAi construct targeting the JAK/STAT receptor coding gene *dome* (*dome*), expressing a dominant negative form of Insulin receptor (InR^{DN}) or an RNAi construct targeting the Hippo pathway component Yki (*yki RNAi* construct). **(F**-**M')** Wild-type control (F, F', I, I', L, L'), and kis^{10D26} mutant clones (G G', J, J', M, M'), 3 days AHS MARCM clones. Ligands of JAK/STAT Upd (expressed in ISC and EC) and Upd3 (expressed in the EC) respectively detected using Upd-LacZ (RED in F-G', arrowheads point toward ISC) and Upd3-LacZ (RED in I-J', arrowheads point toward EC) and JNK activity reporter Puc-lacZ (RED in L-M', arrowheads points toward ISC) were not increased in *kismet* mutants at 3 days AHS (clone outlined in WHITE in F', G', I', M'; GFRP, GREEN; DAPI, BLUE). **(H, K, N)** Quantification of the proportion of ISC expressing Upd-LacZ (H), EC expressing Upd3-lacZ (K) and ISC expressing Puc-LacZ (N) in clones from (F-M'). Results compared with two-tailed Mann-Whitney statistical test in (E) and a Chi2 test in (H, K and N). Mean values in RED, error bars= SEM. Scale bars=20 μm.

Figure S5. Kismet distribution on lineage specific genes, related to Figure 4.

(A-A") Super-resolution image of Kismet distribution (Kismet-FLAP tagged kis_{locus} marked by GFP, GREEN) in the nuclei of enterocytes. Kismet was found to be enriched in regions generally lacking the H3K27me3 repressive mark (RED). Scale bar = 5µm. **(B-H)** Wild-type RNAseq, as well as Dam-Kis, Dam-RNA Pol II, Dam-Pc, Dam-Brm, Dam-HP1, Dam-H1 ISC binding profiles and peaks alignments over: (B) the genomic region of the gene *esg,* expressed in the ISCs (having significant RNA Pol II occupancy); (C, D) the genomic region of genes not expressed in the ISCs with low level of Dam-RNA Pol II recruitment (RNA Pol II mean occupancy not significant) though bound by Kismet such as *pros* (C) and *pdm1* (D); (E) the genomic region of genes *ytr* and *eIF6* not bound by Kismet but expressed in ISCs; (F, G) the genomic region of genes not expressed in ISCs *amon* (EE specific), and *pvf3* (EE enriched) (G); (H) the chromosome 3L pericentromeric region at the euchromatin / heterochromatin boundary.

Figure S6. *trr* but not *ash1*, *trx*, *brm* and *set1* chromatin modifiers regulates ISC proliferation similarly to *kismet,* related to Figure 5.

(A-B') Histone H3K27me3 marks (RED) were broadly distributed in cells of wild-type control (A, A') and kis^{10D26} mutant clones (B, B') 9 days AHS; (clones outlined in WHITE; GFP, GREEN; DAPI, BLUE). **(C-G)** Wild-type clones (C), and those expressing an *ash1* RNAi construct (D), trx^{E2} mutant clones (E), or expressing a *brm* RNAi construct (F) or a *set1* RNAi construct (G) at 9 days AHS (clones outlined in WHITE; GFP, GREEN; DAPI, BLUE; Delta, RED). No obvious *kismet*-like ISC accumulation phenotype was detected. **(H, I)** Quantification of cells per clone (H), and the Delta+ cells per clone (I) from (C, D, F). **(J)** Quantification of cells per clone and the Delta+ cells per clone from (K-L'). **(K-L')** Wild-type (K, K'), and trr^{B} mutant clones (L, L'), 9 days AHS MARCM clones; (Clones outlined in WHITE, in K', L'; GFP, GREEN; DAPI, BLUE; Delta, RED). **(M-N')** Histone H3K27ac marks (RED) were broadly distributed in cells of wild-type control (M, M') and kis^{10D26} mutant clones (N, N') 9 days AHS; (clones outlined in WHITE; GFP, GREEN; DAPI, BLUE). **(O-P', R-S')** ISC-specific expression of GFP (O, O'), *Cbl RNAi* (P, P'), *kis RNAi*

(BL34908) (R, R') and *trr RNAi* (S, S') for 3 days at 29°C. Arrows highlight ISC cells. **(Q, T)** Total EGFR fluorescence intensity in GFP+ ISCs (Q), and of the mean EGFR fluorescence intensity per GFP+ ISC (T) in control guts and knock-downs of *Cbl*, *kismet* and *trr* from (O-P', R-S'). Results were compared using a two-tailed Mann-Whitney statistical test. Mean values in red; error bars= SEM. Scale bars=20 μm.

Figure S7. Effects on Histone modifications, Kismet, and Trr COMPASS-like proteins in mutant contexts, related to Figure 7.

(A-B') Wild-type clones (A, A'), and expressing RNAi construct against *trr* (B, B') at 9 days AHS (clones outlined in WHITE; GFP, GREEN; DAPI, BLUE; dpERK, RED) showed an increase in EGFR pathway activity upon knock-down of *trr*. **(C-F)** A control wild-type clone (C), a kis^{10D26} mutant clone (D), a clone expressing *trr RNAi* (E), a kis^{10D26} mutant clone expressing *trr RNAi* (F) at 10 days AHS (GFP, GREEN; DAPI, BLUE; Delta, RED). **(G)** Quantification of clone size and number of Delta+ cells per clone from (C-F). **(H-I')** Kismet protein (RED) in wild-type control clones (H, H'), and *trr RNAi* construct expressing clones (I, I') (clones outlined in WHITE; GFP, GREEN; DAPI, BLUE). **(J-K')** Trr protein (RED) in wild-type control (J, J') and kis^{10D26} mutant clones (K, K'), 9 days AHS (clones are outlined in WHITE; GFP, GREEN; DAPI, BLUE). No changes were found in Kismet or Trr intensity from wild-type to mutant contexts. **(L-O')** Histone H3K4me1 marks (RED) were broadly distributed in wild-type control clones (L, L'), but greatly reduced in both *trr RNAi* (M, M') and *lpt RNAi* construct expressing clones (N, N'). In contrast, kis^{10D26} mutant clones (O, O') showed no obvious reduction in Histone H3K4me1 levels (9 days AHS; clones are outlined in WHITE; GFP, GREEN; DAPI, BLUE). Results were compared using a two-tailed Mann-Whitney statistical test. Mean values in RED; error bars= SEM. Scale bars=20 μm.

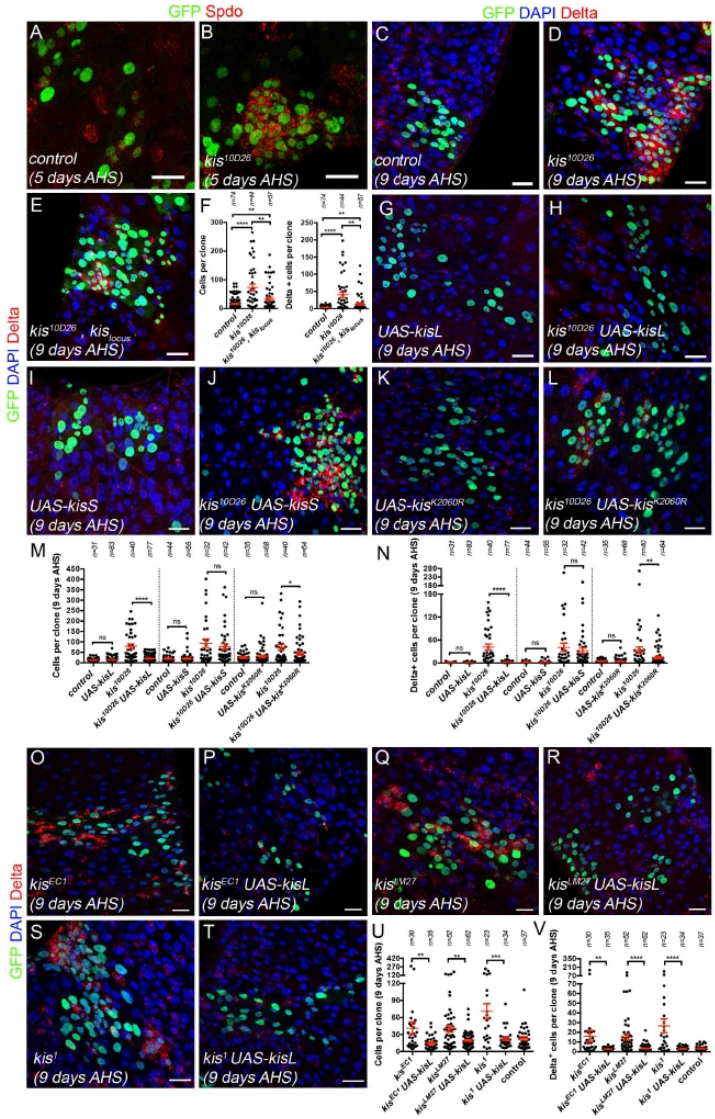

Gervais *et al.*, Fig. S1

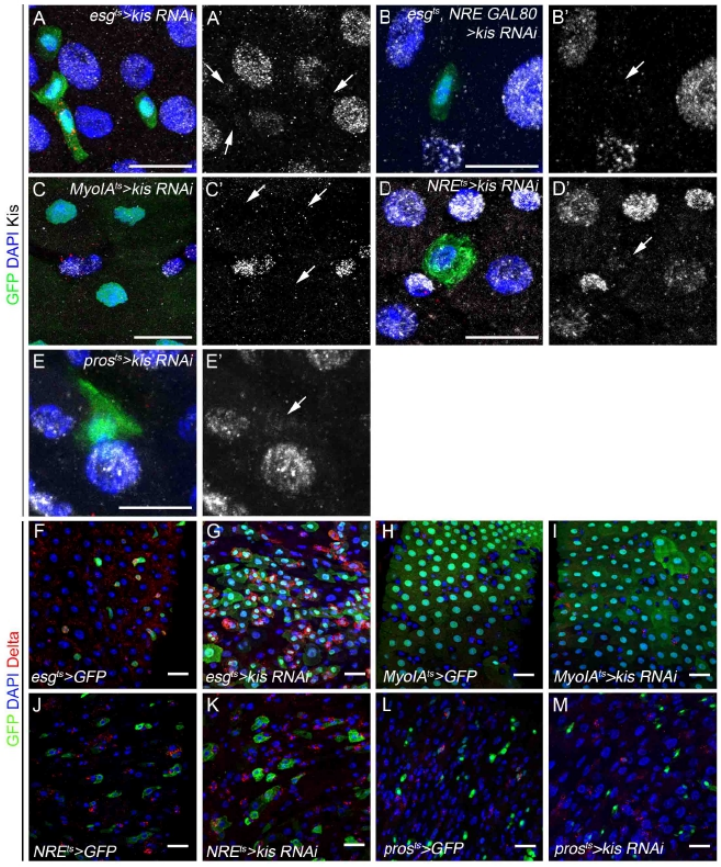

Gervais *et al*. Fig. S2

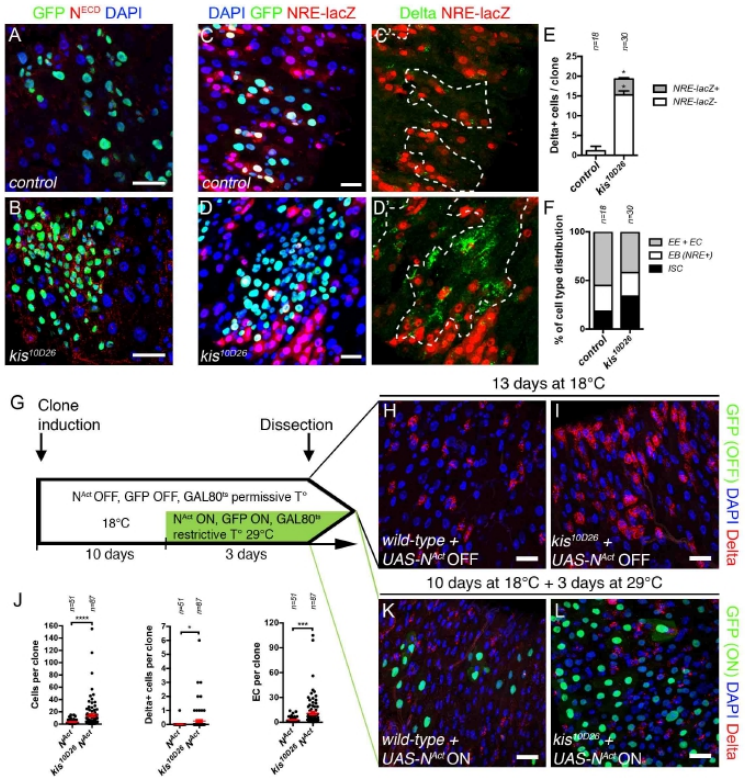

Gervais *et al.*, Fig.S3

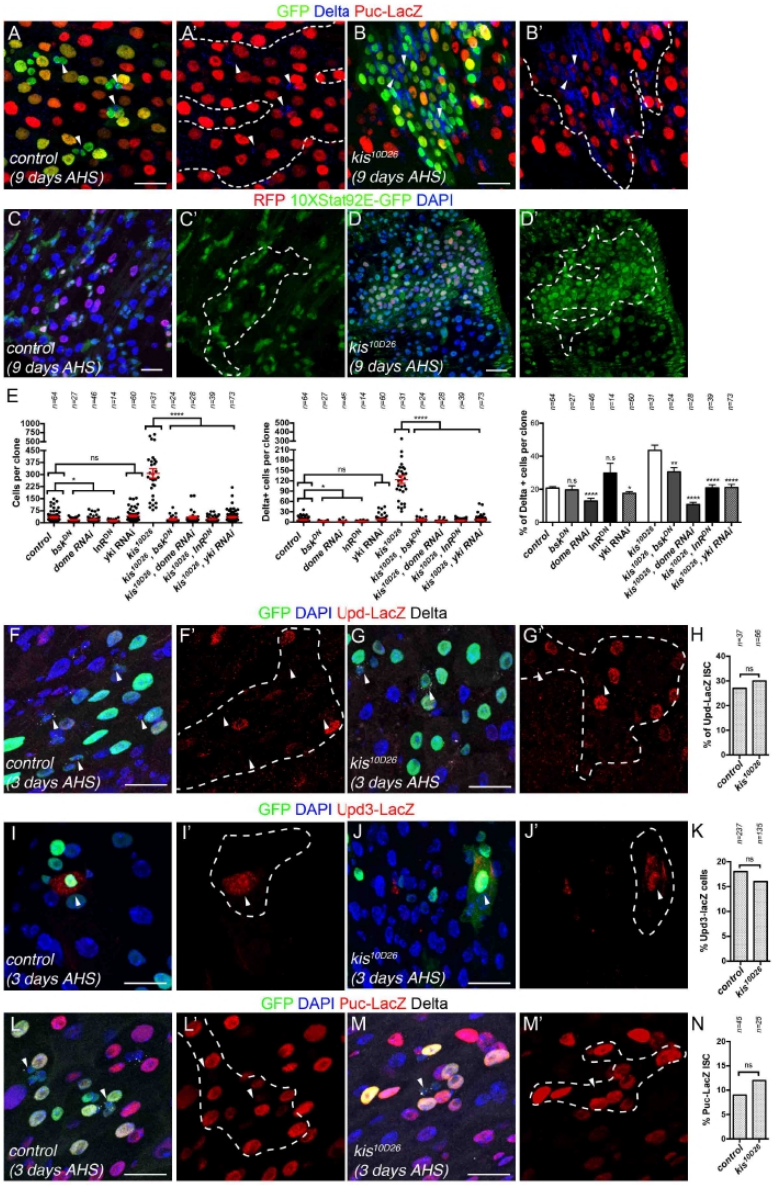

Gervais *et al.* Fig. S4

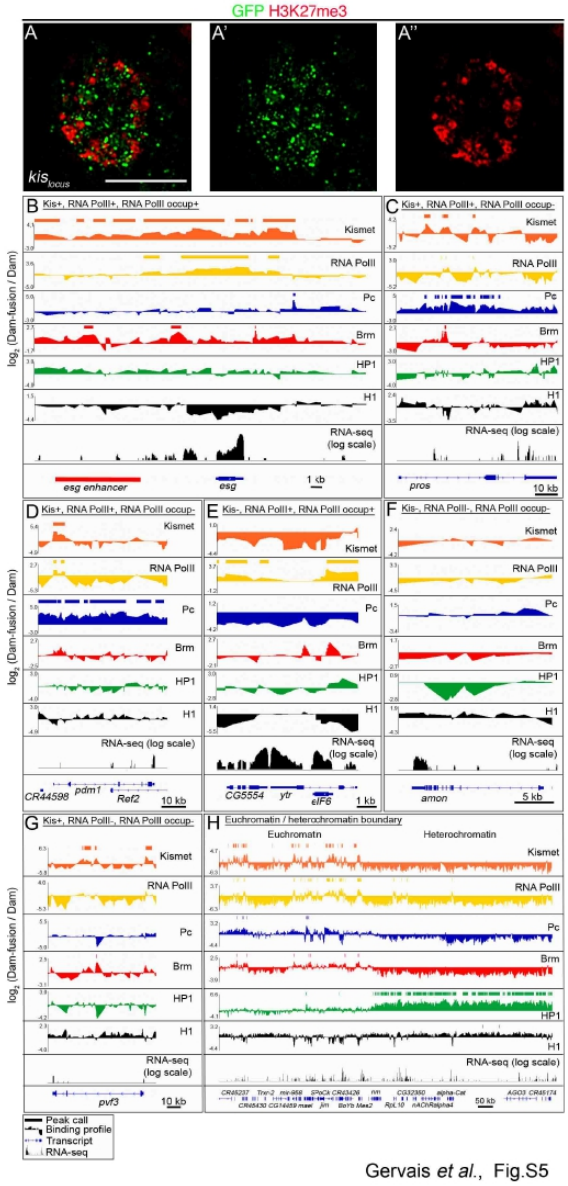

Gervais *et al.*, Fig.S5

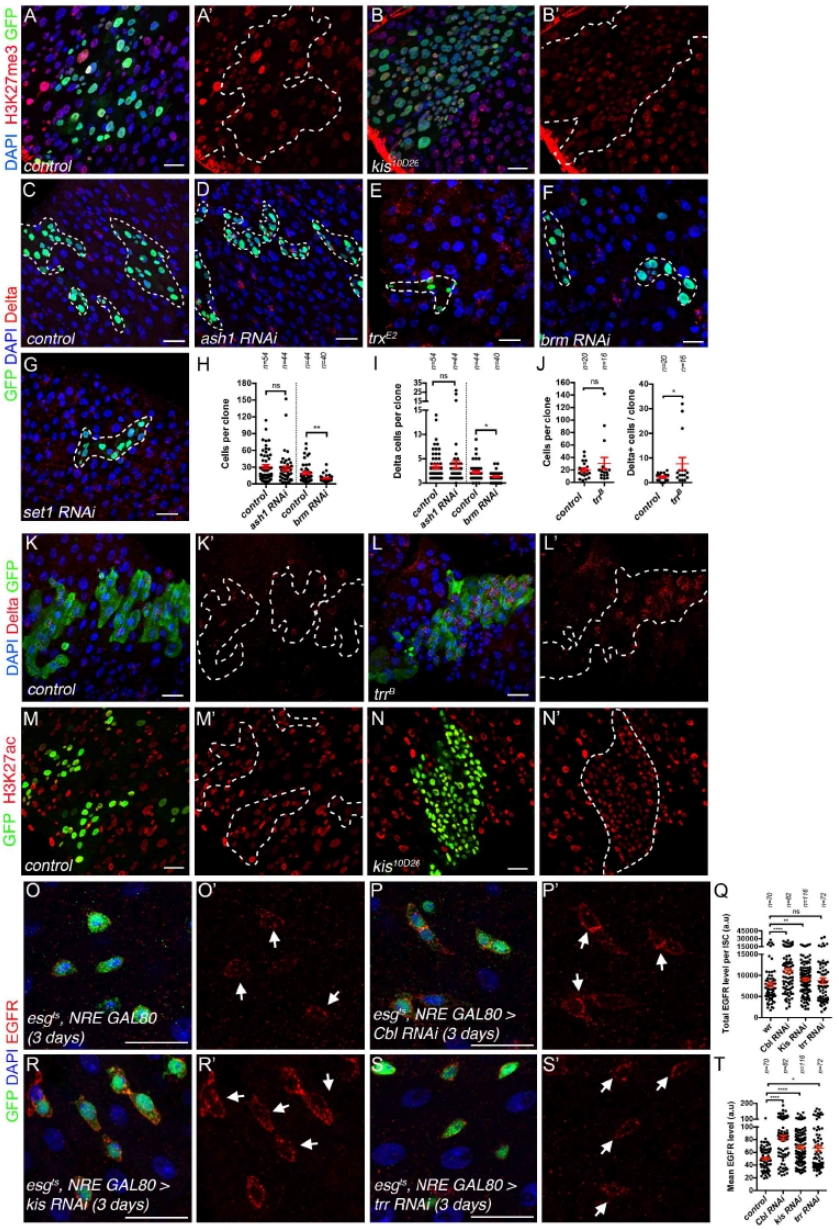

Gervais *et al.*, Fig.S6

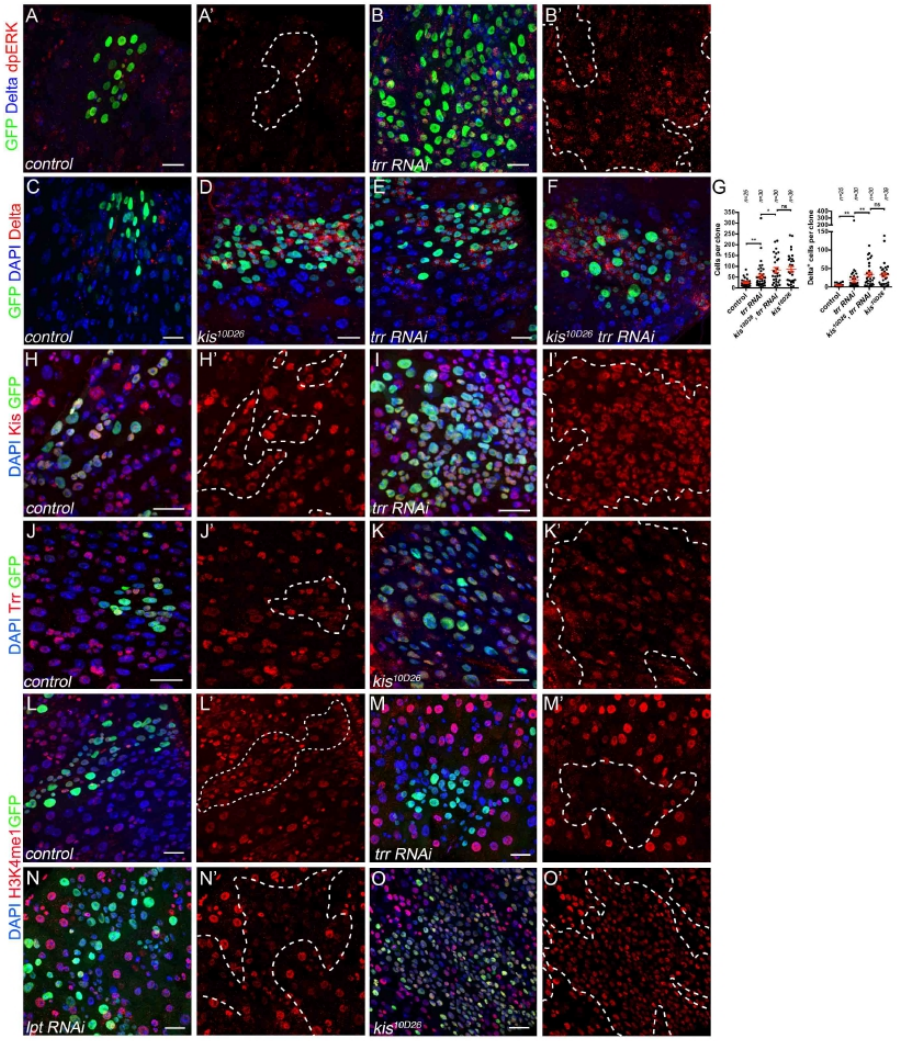

Gervais et al.,Fig. S7

RÉSUMÉ

Les cellules souches adultes s'auto-renouvellent et se différencient en un ou plusieurs types cellulaires, assurant ainsi l'homéostasie d'un tissu. Comprendre leur régulation est crucial pour mieux appréhender les mécanismes de prolifération incontrôlée et de défauts de différenciation observés lors de la tumorigenèse et du déclin fonctionnel des tissus pendant le vieillissement. Ma thèse avait pour but de mieux comprendre les états chromatiniens associés à l'activité des cellules souches adultes *in vivo*, dans un tissu homéostatique en utilisant l'intestin adulte de la drosophile comme modèle. Nous avons montré le rôle de facteurs de remodelage de la chromatine conservés dans le contrôle de la prolifération des cellules souches intestinales (CSI) (Gervais et al, 2019), soulignant leur importance dans la régulation du lignage intestinal. Ma thèse a prolongé ces travaux en étudiant les changements d'état de la chromatine associés à la différenciation des cellules souches à l'échelle du génome entier.

J'ai généré pour chaque type cellulaire des cartes de sites de fixation au génome de 5 protéines de chromatine (ARN Pol II, Brahma, Polycomb, Heterochromatin Protein 1 et Histone linker H1) en utilisant la technique de Targeted DamID. En effectuant un modèle de Markov caché pour définir les états chromatiniens, nous avons découvert que 7 états majeurs de la chromatine existent dans le lignage intestinal. Il s'agit de 2 états actifs ("Yellow" et "Red"), 3 états répressifs ("BlueR" enrichi en Polycomb, "Green" enrichi en HP1, "Black" enrichi en H1) et 2 états intermédiaires ("Yellow Weak" et "Blue Mixed"). L'étude de ces états au niveau des gènes a révélé que de nombreux gènes, dont les régulateurs clés de l'activité des CSI, subissent des transitions d'état chromatinien distinctes pour chaque lignage lors de la différenciation en entérocytes (EC) ou en cellules entéro-endocrines (EE), les deux types de cellules intestinales différenciées. Ces résultats indiquent que les différences d'organisation de la chromatine entre ECs et EEs pourraient être particulièrement importantes pour la détermination du destin cellulaire.

Nous avons aussi constaté que les gènes de différenciation suivent des changements chromatiniens spécifiques pendant la différenciation. Premièrement, les principaux régulateurs transcriptionnels de la spécification du lignage, incluant *prospero* et *nubbin*, passent de l'état «BlueR» vers des états chromatiniens actifs lors de la différenciation. Ces données suggèrent une fonction régulatrice de la chromatine marquée par Polycomb pour le contrôle de la hiérarchie transcriptionnelle au sein du lignage intestinal. D'autre part, les gènes liés à la physiologie et à l'activité métabolique des cellules différenciées suivent une transition de l'état «Black» dans les CSI vers des états chromatiniens actifs dans les ECs et EEs lors de leur activation, ce qui suggère un mode de régulation des gènes liés à la physiologie qui n'était pas encore caractérisé.

Nous avons ensuite étudié les effets de la perturbation génétique de HP1 et H1 sur l'accessibilité de la chromatine, la transcription et l'homéostasie du tissu intestinal. Bien que HP1 soit nécessaire pour maintenir l'hétérochromatine, nos résultats suggèrent que cette protéine régule aussi l'expression de gènes ayant des fonctions métaboliques cellulaires indépendamment de l'accessibilité de la chromatine. De plus, HP1 est nécessaire pour maintenir la proolifération des CSI. Enfin, nous avons observé que dans les CSI, H1 régule le programme transcriptionnel spécifique des EEs, suggérant que H1 pourrait jouer un rôle dans l'amorçage du destin cellulaire «EE» dans les CSI.

Globalement, notre caractérisation approfondie des changements d'état de la chromatine au cours de la différenciation fournit une ressource utile pour mieux comprendre les programmes de régulation qui contrôlent le destin et l'identité cellulaire ainsi que les fonctions physiologiques dans ce tissu homéostatique.

MOTS CLÉS

État de la chromatine – différenciation – cellules souche – intestin – Drosophile – séquençage

ABSTRACT

Adult stem cells self-renew and differentiate into one or several cell types, thus ensuring tissue homeostasis. Understanding their regulation is crucial to have a better comprehension of uncontrolled proliferation and altered differentiation mechanisms occurring during tumorigenesis and age-dependent functional decline of tissues. My thesis aimed to better understand what chromatin states are associated with adult stem cell activity *in vivo* in a homeostatic tissue using the *Drosophila* adult intestine as a model. We have previously provided evidence of roles of conserved chromatin remodeling factors in controlling intestinal stem cell (ISC) proliferation (Gervais et al, 2019), highlighting their importance in the regulation of the intestinal lineage. During my PhD, I expanded on these studies to investigate chromatin state changes associated with stem cell differentiation at the genome-wide scale.

By generating cell-type specific whole-genome binding maps of 5 chromatin proteins (RNA Pol II, Brahma, Polycomb, Heterochromatin Protein 1 and Histone linker H1) using Targeted DamID and performing subsequent Hidden Markov modelling to define chromatin states, we found that 7 major chromatin states exist in the intestinal lineage. These are 2 actives states ("Yellow" and "Red"), 3 repressive states (Polycomb-enriched "BlueR", HP1-enriched "Green", Histone H1-enriched "Black") and 2 intermediate states ("Yellow Weak" and "Blue Mixed"). Examining these states at genes revealed that many genes, including key regulators of ISC activity, undergo lineage-specific chromatin state transitions upon differentiation to enterocytes (ECs) or enteroendocrine cells (EEs), the two differentiated intestinal cell types. These results indicate that differences of chromatin organization between the EC and EE lineages might be critical for cell fate decisions.

We also found that differentiation genes follow specific chromatin state changes during differentiation. First, the key transcriptional regulators of lineage specification including *prospero* and *nubbin* undergo a transition from the BlueR state (Polycomb-enriched) to active states upon differentiation. These data suggest a potential regulatory function of Polycomb-marked chromatin for control of the transcriptional hierarchy within the ISC lineage. In contrast, we found that physiology and metabolic activity-related genes follow a transition from the Histone H1-enriched Black state in ISCs to active states in ECs and EEs upon their activation, suggesting a previously uncharacterized mode of regulation of physiology-related genes. Following this, we investigated the effect of genetic perturbation of HP1 and H1 on chromatin accessibility, transcription and tissue homeostasis. While HP1 is required to maintain heterochromatin, our results suggest that it also regulates the expression of genes with cellular metabolic functions independently of chromatin accessibility. Furthermore, HP1 is necessary to maintain ISC proliferation. Finally, we found a role for Histone H1 in regulating the EE transcriptional program in ISCs, suggesting that it could prime the ISCs towards the EE fate.

Overall, our extensive characterization of chromatin state changes during differentiation provides a valuable resource to better understand the regulatory programs that control cell fate and identity, as well as physiological functions in this homeostatic tissue.

KEYWORDS

Chromatin state – differentiation – stem cell – intestine – Drosophila – sequencing